The Quark Sector of the QCD Ground State in Coulomb Gauge

Dissertation

der Mathematisch-Naturwissenschaftlichen Fakultät
der Eberhard Karls Universität Tübingen
zur Erlangung des Grades eines
Doktors der Naturwissenschaften
(Dr. rer. nat.)

vorgelegt von
Markus Pak
aus Klagenfurt (Österreich)

Tübingen
2012

Tag der mündlichen Qualifikation:	23.10.2012
Dekan:	Prof. Dr. Wolfgang Rosenstiel
1. Berichterstatter:	Prof. Dr. Hugo Reinhardt
2. Berichterstatter:	Prof. Dr. Dr. h.c. mult. Amand Fäßler

Für Johann

Zusammenfassung

Diese Doktorarbeit ist in zwei Teile aufgespaltet, die sich jeweils mit den beiden ungelösten Hauptfragen der QCD beschäftigt. Im ersten Teil untersuchen wir chirale Symmetriebrechung. Wir konzentrieren uns auf den fermionischen Anteil der QCD-Lagrangefunktion, da die chirale Symmetrie eine Eigenschaft des Quarksektors ist. Im zweiten Teil wenden wir uns dem Problem des Farbeinschlusses zu und berechnen das Potential zwischen einem Paar unendlich schwerer Quarks aus dem sogenannten Wilsonloop. Hier befassen wir uns mit der reinen Gluodynamik, da der Farbeinschluss im gluonischen Sektor der QCD verschlüsselt ist.

Der erste Teil dieser Doktorarbeit behandelt die Einbeziehung dynamischer Fermionen in den Variationszugang zur QCD in Coulomb-Eichung. Es ist seit dreißig Jahren bekannt, dass ein Ansatz für das Quark-Vakuumwellenfunktional, der die BCS-Theorie imitiert, obwohl auf einem qualitativen Level erfolgreich, nicht ausreicht, um das richtige Maß an dynamischer chiraler Symmetriebrechung zu generieren, das für die dynamische Nukleonmasse benötigt wird – der Wert des chiralen Kondensates ist um einen Faktor zwei zu klein. Wir identifizieren den fehlenden Teil als die Kopplung der Quarks zu den transversalen Gluonen. Wir verallgemeinern den BCS-Ansatz und schließen die Kopplung der Quarks zum transversalen Eichfeld in das Quark-Wellenfunktional ein. Wir finden heraus, dass diese Kopplung das chirale Kondensat wesentlich erhöht und die dynamische Masse in den Bereich der experimentellen Daten bringt.

In Teil II der Arbeit wenden wir uns einer Methode zu, sich dem Wilsonloop in einer Kontinuumsformulierung zu nähern, die vor einigen Jahren für supersymmetrische Yang-Mills-Theorien vorgeschlagen und kürzlich auf die QCD in Landau-Eichung angewandt wurde. Alle planaren Leiterdiagramme, die zwei temporale Pfade des Wilsonloops verbinden, werden zu einer Dysongleichung summiert, die zumindest näherungsweise die Pfadordnung beinhaltet.

Die Dysongleichung wird kritisch überprüft, ihr Anwendungsbereich für nicht-supersymmetrische Theorien diskutiert, und auf Gluonpropagatoren in Coulomb-Eichung angewandt. Wir berechnen den Wilsonloop für den temporalen, sowie den räumlichen Gluonpropagator. Wir erkennen, dass die Ergebnisse für den räumlichen Wilsonloop qualitativ, aber nicht quantitativ aussagekräftig sind. Wir bekommen ein statisches Quarkpotential, das sowohl einen Coulombschen als auch eine farbeinschließenden Bereich aufweist; allerdings ist die Stringspannung, die man aus dem Anstieg des linearen Potentials extrahiert, zu groß verglichen mit der Stringspannung, die aus der Gitter-QCD bekannt ist.

Abstract

This thesis is divided into two parts concerning the two unresolved issues of QCD. In Part I we investigate chiral symmetry breaking. We concentrate on the fermionic content of the QCD Lagrangian, since chiral symmetry is a property of the quark sector. In Part II we turn to the issue of color confinement and compute the potential between a pair of infinitely heavy quarks from the so-called Wilson loop. Here we deal with pure gluodynamics, since color confinement is encoded in the gluon sector of QCD.

The first part of the thesis concerns the inclusion of dynamical quarks into the variational approach to QCD in Coulomb gauge. It has been known for thirty years that an ansatz for the quark vacuum wave functional mimicking BCS theory, although successful on a qualitative level, is not sufficient to generate the right amount of dynamical chiral symmetry breaking to account for the dynamical nucleon mass – the value of the chiral condensate is by a factor of two too low. We identify the missing piece as the coupling of the quarks to the transverse gluons. We generalize the BCS-ansatz and include the coupling of the quarks to the transverse gauge field into the quark vacuum wave functional. We find this coupling to increase the chiral condensate substantially and to bring the dynamical mass into the region of experiment.

In Part II we turn to a method to approach the Wilson loop in a continuum formulation which has been suggested years ago for supersymmetric theories and has recently been applied to QCD in Landau gauge. All planar ladder diagrams connecting the two temporal paths of the Wilson loop are summed to give a Dyson equation, which, at least in an approximate fashion, accounts for path ordering.

This Dyson equation is critically reviewed, its range of applicability in non-supersymmetric gauge theories discussed and applied to Coulomb gauge gluon propagators. We compute the Wilson loop for the temporal gluon propagator as well as the spatial gluon propagator. We find for the spatial Wilson loop results which are qualitatively, but not quantitatively, significant. We find a static quark potential which shows both a Coulombic as well as a confining region; however, the string tension extracted from the slope of the linear potential is too large compared to the string tension obtained in lattice QCD.

Acknowledgments

I would like to thank my supervisor Prof. Dr. Hugo Reinhardt, first of all, for working with me on the subject of quarks in the variational approach to QCD, which kept entertaining me for the last years, and for sharing his knowledge and expertise with me. Throughout all the projects we closely worked together and I appreciate the many blackboard discussions in this time. I am looking forward for many new and exciting research activities with him in the future.

The fact that the post-doc office doors stand always open creates a special and motivating working atmosphere in our group. I want to acknowledge special thanks to Dr. Wolfgang Schleifenbaum, who accompanied my first research attempts in my first months in Tübingen. I am indebted to Dr. Peter Watson for discussing and comparing new results with me, for helping me with numerical problems and especially for carefully reading and correcting my thesis. I am grateful to Dr. Giuseppe Burgio for discussions on the lattice results, for taking time to explain me topics of QCD beyond the scope of my thesis and for the group seminar on technicolor theories. I would like to thank Dr. Markus Quandt for the interesting lectures he gave in the last years.

Although it was great for me to have my own office, all the work would not have been possible without my office neighbors Dr. Markus Leder and Dr. Davide Campagnari. I very much profited from their knowledge of the Yang-Mills part of QCD and we often spent hours together looking for an answer to particular problems. Moreover, both of them had to read and correct nearly all my publication manuscripts in the last years. Particularly for correcting my thesis, I would like to thank them.

I am grateful to my part-time office colleague Stefan Haag for the nice time in the year we shared the office. I also like to mention Dipl.-Phys. Kai Hüwelmeyer for the discussions on scalar fields in the variational approach, and Dr. Andrey V. Zayakin for the discussions on the Wilson loop project.

I am grateful to the European Graduate School Basel-Graz-Tübingen "Hadronen im Vakuum, in Kernen und Sternen" as well as the Graduiertenkolleg "Kepler-Kolleg: Particles, Fields and Messengers of the Universe" for financial support, for the graduate days in Basel, Graz and Tübingen, for the workshops in Todtmoos, Blaubeuren and Hallstatt, and especially for the opportunity to come into contact with other interesting research activities in particle- and astrophysics. I like to thank Prof. Dr. Josef Jochum for the organization and Frau Gaby Behring who made the bureaucratic issues for me as easy as possible. I like to mention Dipl.-Phys. Kai Freund and Dr. Georg Maierhofer for many explanations on the subject of experimental neutrino physics and Dipl.-Phys. Hannah Tomczyk for the possibility to visit a quantum optics laboratory.

I thank the elementary particle physics group of the Institute for Theoretical Physics at the University of Graz for the opportunity to present my work in a seminar. I like to acknowledge many interesting discussions with Dr. Klaus Lichtenegger and Mag. Gernot Lassnig, who also worked in the quark sector of Coulomb gauge QCD. I also want to mention the numerous Schladming Winter Schools I attended in the last years, which offer a great possibility for a particle physics student to come into contact with the nowadays research activities.

I am grateful to the mathematical physics group of the Institute of Mathematics at the University of Tübingen for the possibility to join their monday evening football game.

I say thank you to my parents Johann and Ingrid, my sister Daniela and her husband Jeremy, and to my friends Andreas, Claudia, Sigrun, Gernot and Sabine, Hannah, Stefan, Eva, Simon, Wolfgang, Julia and Hannes.

Francisca, thank you for the first seven months and for returning to Tübingen.

Contents

List of Figures

Introduction

Quantum Chromodynamics (QCD) is the theory of the strong interaction. Its elementary degrees of freedom are quarks and gluons. The subject of this thesis is the low-energy sector of QCD, where the coupling constant becomes large and non-perturbative methods have to be applied.

Due to asymptotic freedom a weak-coupling expansion is valid for large energies. Perturbative QCD has been tested to successfully describe deep inelastic scattering processes. Pedagogical introductions are given in Refs. [1, 2].

The two cornerstones of non-perturbative QCD are color confinement and chiral symmetry breaking. Color confinement denotes the absence of free quark states in the physical spectrum and manifests itself in a linearly rising long-distance potential between two infinitely heavy quarks. Chiral symmetry breaking explains for example how the large nucleon mass is generated dynamically from the small up- and down-quark masses that appear in the QCD Lagrangian. The underlying mechanisms of both these phenomena and their interplay are the big unresolved challenges of QCD.

In the last decade lattice QCD as well as continuum methods — the variational approach and Dyson-Schwinger equations — could make important progress in both directions. A recent review on lattice QCD, Ref. [3], states that it is now possible to determine the nucleon mass within 3.5% on the lattice. Despite this success, for a detailed understanding of QCD it is equally well important to have continuum techniques at hand. Moreover, in contrast to lattice QCD calculations, the equations which are solved in the continuum are computationally inexpensive. Especially the small momentum region of QCD propagators are more easily accessible in the continuum. A review on Dyson-Schwinger results can be found in Ref. [4]. In particular the Hamiltonian formulation of QCD in Coulomb gauge has been tested in recent years to be an efficient method in describing the Yang-Mills sector of the theory, see Refs. [5–8].

The organization of Part I of the thesis is as follows: In Chapter 1 we introduce the Hamiltonian approach to QCD and derive all quantities needed for later work. In Chapter 2 we present the phenomenological consequences which follow from chiral symmetry breaking. In Chapter 3 we start our considerations on the inclusion of quarks into the variational approach and propose a quark vacuum wave functional which includes the interaction of quarks with transverse gluons. With this new quark wave functional and the Gaussian ansatz of the pure Yang-Mills sector on hand, we have a powerful technique to approach the full QCD system. We represent the quark fields in terms of a coherent fermion basis and set up the generating functional in order to compute the correlation functions of the theory.

In Chapters 4 and 5 we compute the various energy densities. By minimizing them with

respect to the variational kernels we get an estimate for the lowest energy eigenstate of the system. So-called gap equations which determine the kernels appearing in the vacuum wave functional are derived. We solve these equations analytically in the asymptotic momentum regions and numerically in the whole momentum range. We compute the low-energy chiral properties of the theory, like the chiral condensate and the constituent mass, and compare their values to the experimental data.

The explicit computations are performed in the Appendices: In Appendix A spinor identities are derived, in Appendix B the generating functional of quarks is evaluated, and in Appendix C the energy densities are computed. Finally, in Appendix D we explain how the non-linear integral equations were solved numerically.

In Part II of the thesis we turn to the issue of color confinement. A criterion for color confinement is to show a linearly rising long-distance interquark potential. This corresponds to demonstrating an area law for the Wilson loop. In the definition of the Wilson loop the so-called path ordering occurs, which is a prescription of how the gauge field is transported along a path. Path ordering in a continuum formulation is, however, difficult to implement. Therefore no analytic calculation of the Wilson loop could be given so far; the only reliable results come from lattice QCD.

In Chapter 6 we present a Dyson equation, which can, at least approximately, evaluate the expectation value of the Wilson loop in a continuum framework. The only quantity which enters this Dyson equation is the gluon propagator. The static quark potential is easily evaluated, since the Dyson equation can be rewritten into a Schrödinger equation to be solved for the lowest eigenvalue.

The explicit form of the Schrödinger potential as well as the numerical algorithm to solve the Schrödinger equation for the lowest eigenvalue are presented in Appendix E.

In the last chapter of the thesis we summarize our main findings and present an outlook on possible forthcoming studies.

Chapter 1

Hamiltonian Approach to QCD in Coulomb Gauge

This chapter presents a brief introduction to the Hamiltonian approach to QCD in Coulomb gauge, paying special attention to the quark sector of the theory, which will be the setting for the main part of the thesis.

In the first section, starting from the definition of the QCD Lagrangian density, we introduce the notion of gauge freedom and the concept of gauge fixing. After deriving the classical Hamiltonian we pass on to the quantum theory by demanding canonical quantization rules for the field operators. In Section 2 we collect the basic definitions and main properties of Dirac fermions. Section 3 is dedicated to Gauss' law, which is lost as a dynamical equation of motion during the canonical quantization procedure. After a short comment on the Schrödinger picture in Section 4, we arrive at the final form of the Coulomb gauge-fixed Hamiltonian in Section 5. In Section 6 we present the results gained in the variational approach to Yang-Mills theory, which is needed as input for the projects presented in this thesis.

1.1 Hamiltonian Formulation of QCD

Let us start with the classical Lagrangian density of N_{F} types of non-interacting fermion fields,

$$\mathcal{L} = \sum_{f=1}^{N_{\mathrm{F}}} \overline{\psi}_f(x) \left(i\gamma_\mu \partial^\mu - m\right) \psi_f(x) \ , \tag{1.1}$$

with $\psi_f(x)$ denoting the spinor-valued fermion field carrying a flavor index f. The Dirac conjugate field is $\overline{\psi}_f = \psi_f^\dagger \gamma_0$ and m is the mass of the fermion fields. The Dirac matrices obey the anti-commutation relation $\{\gamma^\mu, \gamma^\nu\} = 2g^{\mu\nu}$ with the metric convention for space-time $g^{\mu\nu} = \mathrm{diag}(1, -1, -1, -1)$. For later use we define the free massive Dirac operator

$$\mathcal{D} = i\gamma_\mu \partial^\mu - m \ . \tag{1.2}$$

We demand the flavored fermion fields to have an internal color degree of freedom and require the action $\mathcal{S} = \int d^4x \, \mathcal{L}$ to be invariant under local rotations in color space, i.e.,

at each space-time point a different color rotation is performed:

$$\psi(x) \to \psi'(x) = \Omega(x)\psi(x) \;, \tag{1.3}$$

$$\overline{\psi}(x) \to \overline{\psi}'(x) = \overline{\psi}(x)\Omega^\dagger(x) \;. \tag{1.4}$$

The matrices Ω belong to the group $SU(N_\mathrm{C})$, i.e., they are unitary and fulfill $\det[\Omega] = 1$. The standard group parametrization is the exponential representation, given as $\Omega(x) = e^{i\varepsilon^a(x)T^a}$ with T^a being the Hermitian generators of the gauge group. The sum index a runs over all generator elements, i.e., $a = 1 \ldots N_\mathrm{C}^2 - 1$ with the generators T^a satisfying

$$[T^a, T^b] = if^{abc}T^c \;, \tag{1.5}$$

where f^{abc} are the structure constants of the gauge group. Relation (1.5) defines the Lie algebra of the gauge group. We note that anti-Hermitian generators would avoid the factor of i appearing in the exponent of the exponential representation and in the commutation relation, Eq. (1.5). Setting the structure constants f^{abc} to zero, we recover the Abelian theory, such as electrodynamics, with the gauge group $U(1)$ being a simple phase. Although it is well known that quarks come in three colors, we will always keep the number of colors arbitrary until the last step of the calculation. The generator elements are normalized to

$$\mathrm{Tr}[T^aT^b] = \frac{1}{2}\delta^{ab} \;. \tag{1.6}$$

Let us list another important identity needed for later work,

$$\sum_m (T^m)^{ab}(T^m)^{bc} = \delta^{ac}C_F \;, \qquad C_F = \frac{N_\mathrm{C}^2 - 1}{2N_\mathrm{C}} \;, \tag{1.7}$$

with C_F denoting the quadratic Casimir invariant. Note, that here a, b run from 1 to N_C, whereas m runs from 1 to $N_\mathrm{C}^2 - 1$. Whenever appropriate, we will distinguish between fundamental $a, b, \ldots$ and adjoint $m, n \ldots$ indices. In all other cases, we will use the labels $a, b, \ldots$ for fundamental as well as adjoint color components.

The free fermion Lagrangian, Eq. (1.1), is made locally gauge invariant by replacing the derivative ∂_μ by the covariant derivative D_μ which we demand to transform as

$$D_\mu \to D'_\mu = \Omega(x)D_\mu\Omega^\dagger(x) \;, \tag{1.8}$$

so that $D_\mu\psi$ and ψ transform in the same way. Analogously to electrodynamics we introduce a gauge field via minimal substitution

$$\partial_\mu \to D_\mu = \partial_\mu + igA^a_\mu T^a \;, \tag{1.9}$$

where g is the coupling constant and $A_\mu(x) = A^a_\mu(x)T^a$ is a matrix-valued field, known as the gauge field, which transforms as

$$A_\mu(x) \to A'_\mu(x) = \Omega(x)A_\mu(x)\Omega^\dagger(x) - \frac{i}{g}\Omega(x)(\partial_\mu\Omega^\dagger(x)) \;, \tag{1.10}$$

and assumes values in $su(N_\mathrm{C})$, the algebra of the gauge group $SU(N_\mathrm{C})$. The color components A^a_μ of the gauge field are real-valued, carry a Lorentz index $\mu = 0, \ldots, 3$ and describe for the color group $SU(3)$ eight gluons. We arrive at the gauge-invariant Lagrangian of the form

$$\mathcal{L} = -\frac{1}{4} F^m_{\mu\nu} F^{m,\mu\nu} + \sum_{f=1}^{N_\mathrm{F}} \overline{\psi}^a_f \left(i\gamma_\mu D^\mu - m \right)^{ab} \psi^b_f \tag{1.11}$$

where we have made explicit the color and flavor degrees of freedom and suppressed the space-time argument. In order to make the gauge field dynamical, we have introduced a kinetic term, where

$$F^a_{\mu\nu} = \partial_\mu A^a_\nu - \partial_\nu A^a_\mu - g f^{abc} A^b_\mu A^c_\nu \ , \tag{1.12}$$

is the Yang-Mills field strength tensor, which transforms as $F'_{\mu\nu} = \Omega F_{\mu\nu} \Omega^\dagger$. Note, that $F_{\mu\nu} = F^a_{\mu\nu} T^a$ and that $\frac{1}{4} F^a_{\mu\nu} F^{a,\mu\nu} = \frac{1}{2} \mathrm{Tr}[F_{\mu\nu} F^{\mu\nu}]$. The last term on the right-hand side of Eq. (1.12), which is the commutator of two gauge fields, makes the non-Abelian pure gauge theory (i.e., the theory defined by the Lagrangian $\mathcal{L}$, Eq. (1.11), in the absence of fermion fields) highly non-trivial, because cubic and quartic terms in the gauge potential appear which give rise to self-interactions of the gluons. In these self-interactions new physical phenomena are encoded, which are not present in the Abelian theory, the most prominent one being the confinement of color, i.e., the absence of colored objects in the hadronic spectrum. Part II of the thesis deals with the issue of color confinement, which will be analyzed by computing the potential between two static color charges.

Now the issue of gauge fixing comes into play. Considering for a moment the Abelian $U(1)$ theory and ignoring the fermion degrees of freedom, the Lagrangian (1.11) can be rewritten, using integration by parts and discarding surface terms, as a bilinear expression in the gauge field

$$\mathcal{L} = \frac{1}{2} A^\mu \left(g_{\mu\nu} \Box - \partial_\mu \partial_\nu \right) A^\nu \ , \tag{1.13}$$

with $\Box = \partial^\mu \partial_\mu$ being the d'Alembertian operator. Taking a field configuration A^ν which is pure gauge $A^\nu = \partial^\nu \Lambda$, the operator $g_{\mu\nu} \Box - \partial_\mu \partial_\nu$ can be shown to have zero modes

$$(g_{\mu\nu} \Box - \partial_\mu \partial_\nu) \partial^\nu \Lambda = (\Box \partial_\mu - \partial_\mu \Box) \Lambda = 0 \ , \tag{1.14}$$

concluding that the photon propagator, being the inverse of this operator, is singular. Let us deepen this picture and define the generating functional of the Yang-Mills part of QCD

$$Z[j] = \frac{1}{Z[j=0]} \int DA_\mu \, e^{i S_\mathrm{G}[A_\mu] + i \int d^4x \, j^\mu A_\mu}, \qquad S_\mathrm{G} = \int d^4x \, \mathcal{L}_\mathrm{G} \ , \tag{1.15}$$

with j^μ the external current source, $\mathcal{L}_\mathrm{G}$ the Lagrangian (1.11) without fermion fields, and $Z[j=0]$ the normalization. From $Z[j]$ expectation values can be computed in the

standard fashion, see Ref. [9]. The integrands in $Z[j]$ take the same value for each gauge configuration related by a gauge transformation. This gives rise to a divergent integral $Z[j]$ and therefore the Green's functions of the theory cannot be evaluated.

We can resolve this problem by fixing the gauge. Let us stress that it is one of the main advantages of lattice Quantum Field Theory that it is not necessary to fix the gauge in order to make expectation values well defined[1]. Gauge fixing on the lattice is used, for instance, to compare gauge dependent quantities with continuum results.

We proceed with the Euler-Lagrange equations, which for the gluon fields divide into the non-Abelian generalizations of Gauss' law ($\nu = 0$) and Ampere's law ($\nu = i$),

$$\hat{D}^{ab}_{\mu} F^{b,\mu\nu} = g\overline{\psi}\gamma^{\nu} T^{a}\psi \;, \tag{1.16}$$

where we have defined the covariant derivative in the adjoint representation of the color group

$$\hat{D}^{ab}_{\mu} = \delta^{ab}\partial_{\mu} + g f^{abc} A^{c}_{\mu} \;. \tag{1.17}$$

On the right-hand side of equation (1.16) the color current of the quarks $j^{a,\mu} = g\overline{\psi}\gamma^{\mu}T^{a}\psi$ occurs, which can be shown to fulfill $\hat{D}^{ab}_{\nu} j^{\nu,b} = 0$. The equations (1.16) are non-linear in the gauge field, which is again a manifestation of the self-interaction contributions in the QCD Lagrangian (1.11). The quark Euler-Lagrange equation is the Dirac equation in an external field A_{μ}, given as

$$\left(i\gamma^{\mu} D_{\mu} - m\right)\psi = 0 \;. \tag{1.18}$$

The next step towards the Hamiltonian formulation of QCD is to derive the conjugate momenta

$$\Pi^{m,0}_{\mathrm{G}}(x) = \frac{\delta\mathcal{S}}{\delta(\partial_0 A^{m}_{0}(x))} = 0 \;, \tag{1.19}$$

$$\Pi^{m,i}_{\mathrm{G}}(x) = \frac{\delta\mathcal{S}}{\delta(\partial_0 A^{m}_{i}(x))} = F^{m,i0} \;, \tag{1.20}$$

$$\Pi^{a}_{\mathrm{F}}(x) = \frac{\delta\mathcal{S}}{\delta(\partial_0 \psi^{a})} = i\psi^{\dagger a} \;, \tag{1.21}$$

so that the total Hamiltonian, defined as the Legendre transform

$$H = \int d^3x \left(\Pi^{m,i}_{\mathrm{G}} \partial_0 A^{m}_{i} + \Pi^{a}_{\mathrm{F}} \partial_0 \psi^{a} - \mathcal{L}\right) , \tag{1.22}$$

[1] On the lattice the gauge field and fermion measures in the functional integral are products of a finite number of individual measures and therefore well defined.

consists of three different parts,

$$H = H_{\mathrm{G}} + H_{\mathrm{F}} + H_{\mathrm{GAUSS}} \ , \tag{1.23}$$

$$H_{\mathrm{G}} = \int d^3x \left(-\frac{1}{2}\Pi_{\mathrm{G}}^{m,i}\Pi_{\mathrm{G},i}^{m} + \frac{1}{4}F^{m,ij}F_{ij}^{m} \right) \ , \tag{1.24}$$

$$H_{\mathrm{F}} = \int d^3x\, d^3y\, \psi^{\dagger a}(\boldsymbol{x}) h^{ab}(\boldsymbol{x},\boldsymbol{y}) \psi^{b}(\boldsymbol{y}) \ , \tag{1.25}$$

$$H_{\mathrm{GAUSS}} = \int A_0^m \left(-\hat{D}_i^{mn}\Pi_{\mathrm{G}}^{n,i} + g\psi^{\dagger}T^m\psi \right) \ , \tag{1.26}$$

with

$$h^{ab}(\boldsymbol{x},\boldsymbol{y}) = \left(-i\alpha^i\partial_{\boldsymbol{x},i}\delta^{ab} + \beta m\delta^{ab} + g\alpha^i A_i^m(\boldsymbol{x})(T^m)^{ab} \right) \delta(\boldsymbol{x}-\boldsymbol{y}) \ . \tag{1.27}$$

Here H_{G}, Eq. (1.24), is the pure gluonic part of the Hamiltonian. H_{F}, Eq. (1.25), is the fermionic part, which includes also the interaction term coupling the quarks to the gluons and which we refer to as single-particle Hamiltonian. In the third part H_{GAUSS}, Eq. (1.26), we have explicitly separated the time component of the gauge field A_0^a, which gives Gauss' law (1.16) when deriving the Hamiltonian equation of motion for $\Pi_{\mathrm{G},0}^m$

$$\partial_0\Pi_{\mathrm{G},0}^m = -\frac{\delta H}{\delta A_0^m} \ . \tag{1.28}$$

In (1.24) and (1.26) we have omitted space-time arguments. In (1.27) we have introduced the matrices $\alpha_i = \gamma_0\gamma_i, \beta = \gamma_0$, which fulfill $\{\alpha_i,\alpha_j\} = \delta_{ij}$ and defined the Dirac matrix $h^{ab}(\boldsymbol{x},\boldsymbol{y})$, Eq. (1.27). In (1.26) we have performed an integration by parts in the $\hat{D}$-term. In addition, in all these expressions, Eqs. (1.19)-(1.28), we have distinguished between fundamental indices a,b and adjoint indices m,n.

Let us, at this stage, change notation. Since no temporal vector components occur anymore, it is not necessary to use a Minkowski metric notation any longer. We use contravariant vector components only, which we denote, for convenience, with a subscript. The gauge potential in Eq. (1.9) therefore changes sign (and correspondingly in Eq. (1.17)), however, the derivative operator $\partial_{\boldsymbol{x},i} = \frac{\partial}{\partial x^i}$, which already contains contravariant vector components, gets no additional sign. For instance, the Dirac matrix (1.27) becomes

$$h^{ab}(\boldsymbol{x},\boldsymbol{y}) = \left(-i\alpha_i\partial_{\boldsymbol{x},i}\delta^{ab} + \beta m\delta^{ab} - g\alpha_i A_i^m(\boldsymbol{x})(T^m)^{ab} \right) \delta(\boldsymbol{x}-\boldsymbol{y}) \ . \tag{1.29}$$

The quantum theory is imposed by the Lagrangian (1.11) or the Hamiltonian (1.23) and the equal-time commutation relations between the field variables. The fact that the momentum conjugate to the scalar potential, Eq. (1.19), vanishes, is a well-known problem of the canonical quantization of a gauge theory, which is overcome by switching to Weyl (temporal) gauge $A_0^a = 0$. The non-vanishing equal-time canonical commutation relations for the gauge field read

$$[A_i^a(\boldsymbol{x}), \Pi_j^b(\boldsymbol{y})] = i\delta^{ab}\delta_{ij}\delta(\boldsymbol{x}-\boldsymbol{y}) \ , \tag{1.30}$$

and the anti-commutation relations for the fermion fields are

$$\{\psi^a(\boldsymbol{x}), \psi^{\dagger b}(\boldsymbol{y})\} = \delta^{ab}\delta(\boldsymbol{x}-\boldsymbol{y}) \; . \tag{1.31}$$

During this procedure the field variables have become field operators.

1.2 Dirac Fermions

Let us turn to the fermionic part of the Weyl gauge-fixed Hamiltonian, Eq. (1.25), and collect basic definitions and main properties of the quark fields, which we will need throughout the thesis. Fourier-transforming the gauge-field independent part of the single-particle Hamiltonian (1.25) yields

$$H_{\mathrm{F}} = \int \text{đ}^3 p \, \psi^{\dagger a}(\boldsymbol{p}) h^{ab}(\boldsymbol{p}) \psi^b(\boldsymbol{p}) \; , \tag{1.32}$$

with $\text{đ}^3 p \equiv \frac{d^3 p}{(2\pi)^3}$ and the Dirac matrix $h^{ab}(\boldsymbol{p})$ given as

$$h^{ab}(\boldsymbol{p}) \; = \; \boldsymbol{\alpha} \cdot \boldsymbol{p} \, \delta^{ab} + \beta \, m \delta^{ab} \; , \tag{1.33}$$

which is Hermitian, i.e., $h^\dagger(\boldsymbol{p}) = h(\boldsymbol{p})$. For $m = 0$ it fulfills the identity

$$\{\gamma_5, h(\boldsymbol{p})\} = 0 \; , \tag{1.34}$$

with the chirality matrix γ_5 defined as $\gamma_5 = i\gamma_0\gamma_1\gamma_2\gamma_3$. In addition, the eigenfunctions φ_n of the Dirac matrix h and of $h\gamma_5$ given as

$$h\varphi_n = \lambda_n \varphi_n \; , \qquad h\gamma_5\varphi_n = -\lambda_n \gamma_5 \varphi_n \; , \tag{1.35}$$

are orthogonal, i.e., $(\varphi_n, \gamma_5 \varphi_m) = \delta_{mn}$, except for zero eigenvalue. This orthogonality relation follows from the anti-commutativity of h with γ_5, Eq. (1.34). In Chapter 2 the zero eigenvalues of the Dirac matrix h, Eq. (1.33), will be related to a quantity called the chiral condensate. Relation (1.34) will be of central importance for this construction.

We proceed with splitting up the Dirac field into positive and negative energy components

$$\psi^a(\boldsymbol{x}) = \psi^a_+(\boldsymbol{x}) + \psi^a_-(\boldsymbol{x}) \; , \tag{1.36}$$

which are defined with use of the orthogonal projectors to positive and negative energy states

$$\psi^a_\pm(\boldsymbol{x}) = \int d^3 y \, \Lambda_\pm(\boldsymbol{x}, \boldsymbol{y}) \, \psi^a(\boldsymbol{y}) \; , \tag{1.37}$$

$$\psi^{\dagger a}_\pm(\boldsymbol{x}) = \int d^3 y \, \psi^{\dagger a}(\boldsymbol{y}) \, \Lambda_\pm(\boldsymbol{y}, \boldsymbol{x}) \; , \tag{1.38}$$

where

$$\Lambda_\pm(\boldsymbol{x},\boldsymbol{y}) = \int đ^3p\, e^{i\boldsymbol{p}\cdot(\boldsymbol{x}-\boldsymbol{y})}\Lambda_\pm(\boldsymbol{p}), \qquad \Lambda_\pm(\boldsymbol{p}) = \frac{1}{2}\left(\mathbb{1} \pm \frac{h(\boldsymbol{p})}{E(\boldsymbol{p})}\right) , \tag{1.39}$$

with $E(\boldsymbol{p}) = \sqrt{\boldsymbol{p}^2 + m_{\rm F}^2}$. In later considerations we will work exclusively with massless fermions, i.e., $m_{\rm F} = 0$. The projectors are idempotent, i.e., $\Lambda_\pm^2 = \Lambda_\pm$, orthogonal, i.e., $\Lambda_\pm\Lambda_\mp = 0$, and complete, i.e., $\Lambda_\pm + \Lambda_\mp = \mathbb{1}$.

In Fourier-space the positive and negative energy components can be expanded in terms of eigenfunctions of the free Dirac Hamiltonian

$$\psi_+(\boldsymbol{x}) = \int đ^3p\, \frac{1}{\sqrt{2E(\boldsymbol{p})}} \sum_{s=\pm1} a^a(\boldsymbol{p},s)u(\boldsymbol{p},s)e^{i\boldsymbol{p}\cdot\boldsymbol{x}} , \tag{1.40}$$

$$\psi_-(\boldsymbol{x}) = \int đ^3p\, \frac{1}{\sqrt{2E(\boldsymbol{p})}} \sum_{s=\pm1} b^{\dagger a}(\boldsymbol{p},s)v(\boldsymbol{p},s)e^{-i\boldsymbol{p}\cdot\boldsymbol{x}} , \tag{1.41}$$

with the spinor solutions u and v chosen as eigenspinors of the helicity operator $\boldsymbol{\sigma}\cdot\hat{\boldsymbol{p}}$, Eq. (A.13), where the matrices $\boldsymbol{\sigma} = (\sigma_1,\sigma_2,\sigma_3)$ are the Pauli matrices, Eq. (A.12). An explicit realization of the eigenvectors u, v to the massless Dirac equation is given in Appendix A, see Eqs. (A.26), (A.28). Note that the pre-factors in Eqs. (1.40), (1.41) appear due to the normalization $u^\dagger(\boldsymbol{p},s)u(\boldsymbol{p},s) = v^\dagger(\boldsymbol{p},s)v(\boldsymbol{p},s) = 2E(\boldsymbol{p})$. The Hermitian conjugates of the time-zero quark fields then read

$$\psi_+^{\dagger a}(\boldsymbol{x}) = \int đ^3p\, \frac{1}{\sqrt{2E(\boldsymbol{p})}} \sum_{s=\pm1} a^{\dagger a}(\boldsymbol{p},s)u^\dagger(\boldsymbol{p},s)e^{-i\boldsymbol{p}\cdot\boldsymbol{x}} , \tag{1.42}$$

$$\psi_-^{\dagger a}(\boldsymbol{x}) = \int đ^3p\, \frac{1}{\sqrt{2E(\boldsymbol{p})}} \sum_{s=\pm1} b^a(\boldsymbol{p},s)v^\dagger(\boldsymbol{p},s)e^{i\boldsymbol{p}\cdot\boldsymbol{x}} . \tag{1.43}$$

The creation and annihilation operators $a^{\dagger a}(\boldsymbol{p},s)$, $a(\boldsymbol{p},s)$ and $b^{\dagger a}(\boldsymbol{p},s)$, $b(\boldsymbol{p},s)$ fulfill the anti-commutation relations

$$\{a^a(\boldsymbol{p},s), a^{\dagger a}(\boldsymbol{q},t)\} = \delta^{ab}\delta_{st}\delta(\boldsymbol{p}-\boldsymbol{q}) , \tag{1.44}$$

$$\{b^a(\boldsymbol{p},s), b^{\dagger b}(\boldsymbol{q},t)\} = \delta^{ab}\delta_{st}\delta(\boldsymbol{p}-\boldsymbol{q}) , \tag{1.45}$$

with all other anti-commutators vanishing. The bare vacuum is defined by

$$a^a(\boldsymbol{p},s)|0\rangle = 0, \qquad b^a(\boldsymbol{p},s)|0\rangle = 0 . \tag{1.46}$$

Finally, let us state the relation between the energy projectors and the spinor solutions

$$\Lambda_+(\boldsymbol{p}) = \frac{1}{2E(\boldsymbol{p})}\sum_s u(\boldsymbol{p},s)u^\dagger(\boldsymbol{p},s), \qquad \Lambda_-(\boldsymbol{p}) = \frac{1}{2E(\boldsymbol{p})}\sum_s v(-\boldsymbol{p},s)v^\dagger(-\boldsymbol{p},s) . \tag{1.47}$$

1.3 Gauss' Law

Due to Weyl gauge Gauss' law, Eq. (1.16) for $\nu = 0$, does no longer appear in the Hamiltonian equations of motion, but degenerates to a constraint equation, which, in order to select the (physical) gauge-invariant states, has to be fulfilled by the set of physical states

$$\mathcal{G}^a(\boldsymbol{x})|\psi\rangle = 0, \qquad \mathcal{G}^a(\boldsymbol{x}) = \hat{D}_i^{ab}\Pi_i^b(\boldsymbol{x}) + g\psi^\dagger(\boldsymbol{x})T^a\psi(\boldsymbol{x}) \;, \tag{1.48}$$

where we have defined the Gauss law operator $\mathcal{G}^a(\boldsymbol{x})$. The following relations hold (using the commutation relations (1.30), (1.31))

$$[\mathcal{G}^a(\boldsymbol{x}), \mathcal{G}^b(\boldsymbol{y})] = igf^{abc}\mathcal{G}^c(\boldsymbol{x})\delta(\boldsymbol{x}-\boldsymbol{y}) \;, \tag{1.49}$$

$$[\mathcal{G}^m(\boldsymbol{x}), \psi^a(\boldsymbol{y})] = -gT^m\psi^a(\boldsymbol{y})\delta(\boldsymbol{x}-\boldsymbol{y}) \;, \tag{1.50}$$

$$[\mathcal{G}^a(\boldsymbol{x}), \Pi_{\mathrm{G},i}^b(\boldsymbol{y})] = igf^{abc}\Pi_{\mathrm{G},i}^c(\boldsymbol{x})\delta(\boldsymbol{x}-\boldsymbol{y}) \;, \tag{1.51}$$

$$[\mathcal{G}^a(\boldsymbol{x}), A_i^b(\boldsymbol{y})] = igf^{abc}A_i^c(\boldsymbol{x})\delta(\boldsymbol{x}-\boldsymbol{y}) - \delta^{ab}\partial_i\delta(\boldsymbol{x}-\boldsymbol{y}) \;, \tag{1.52}$$

with the first commutator defining a Lie-algebra for the Gauss law operator. Notice that in the second commutator, Eq. (1.50), we have again used the index a for fundamental and the index m for adjoint fields. From

$$[H, \mathcal{G}^a(\boldsymbol{x})] = 0 \tag{1.53}$$

it follows that the Gauss law operator and the Hamiltonian can be diagonalized simultaneously and a state which satisfies Gauss' law at one time, does it for all other times.

Weyl gauge ($A_0^a = 0$) does not fix the gauge completely and the Hamiltonian, Eq. (1.23), is still invariant under spatial (local) gauge transformations $\Omega(\boldsymbol{x}) = e^{i\varepsilon^a(\boldsymbol{x})T^a}$. We now show that the fermion part of the Gauss law operator $\mathcal{G}^a$, Eq. (1.48), is the generator $\mathcal{U}$ of time-independent gauge transformations for the quark sector, for which we demand

$$\mathcal{U}\psi(\boldsymbol{x})\mathcal{U}^\dagger = \Omega(\boldsymbol{x})\psi(\boldsymbol{x}) = \psi'(\boldsymbol{x}) \;, \tag{1.54}$$

$$\mathcal{U}\psi^\dagger(\boldsymbol{x})\mathcal{U}^\dagger = \psi^\dagger(\boldsymbol{x})\Omega^\dagger(\boldsymbol{x}) = \psi^{\dagger\prime}(\boldsymbol{x}) \;. \tag{1.55}$$

Expanding the operator

$$\mathcal{U} = \exp\left(-i\int d^3x\, \psi^\dagger T^a\psi(\boldsymbol{x})\varepsilon^a(\boldsymbol{x})\right) \tag{1.56}$$

to first order in ε, the relations (1.54), (1.55) can be proven using the anti-commutation relation (1.31).

The Yang-Mills part of the Gauss law operator $\mathcal{G}^a$, Eq. (1.48), given as $\hat{D}_i^{ab}\Pi_i^b$, can be shown to generate time-independent gauge transformations for the gauge boson sector

$$\mathcal{U} = \exp\left(-i\int d^3x\, \hat{D}_i^{ab}\Pi_{\mathrm{G},i}^b(\boldsymbol{x})\varepsilon^a(\boldsymbol{x})\right) \tag{1.57}$$

fulfilling

$$\mathcal{U}A_i(\boldsymbol{x})\mathcal{U}^\dagger = \Omega(\boldsymbol{x})\left(A_i - \frac{i}{g}\partial_i\right)\Omega^\dagger(\boldsymbol{x}) = A'_i(\boldsymbol{x}) \;, \tag{1.58}$$

$$\mathcal{U}\Pi_i(\boldsymbol{x})\mathcal{U}^\dagger = \Omega(\boldsymbol{x})\Pi_{\mathrm{G},i}(\boldsymbol{x})\Omega^\dagger = \Pi'_{\mathrm{G},i}(\boldsymbol{x}) \;. \tag{1.59}$$

A wave functional satisfying Gauss' law (1.48) then obeys

$$\mathcal{U}|\psi\rangle = 0 \;, \tag{1.60}$$

which guarantees the gauge invariance of the wave functional with respect to time-independent spatial gauge transformations. This last statement marks the central meaning of Gauss' law: Violation of Gauss' law corresponds to violation of gauge invariance.

1.4 Schrödinger Picture

Solving the Schrödinger equation $H|\psi\rangle = E|\psi\rangle$ of a given Quantum Field Theory for the lowest eigenvalue would clarify the vacuum structure and from the correlation functions, which would then be known, all observables could be computed. For the Abelian $U(1)$-theory without coupling to matter we are able to find the exact ground state; however, for complicated interacting theories, such as QCD, it is hard to find the exact ground state and we will explore the vacuum structure by the variational principle.

To solve the QCD Schrödinger equation for the vacuum state we have to adopt a certain representation for the field operators, which we denote with a hat during this section, i.e., $\hat{A}^a_i, \hat{\Pi}^a_i, \hat{\psi}^a, \hat{\psi}^{\dagger a}$.

The basis vectors in the bosonic case are most conveniently chosen to be the eigenstates of the gauge field operator, which corresponds to the coordinate space representation in quantum mechanics, and the eigenvalue equation reads

$$\hat{A}^a_i(\boldsymbol{x})|A\rangle = A^a_i(\boldsymbol{x})|A\rangle \;. \tag{1.61}$$

The conjugate momentum $\hat{\Pi}^a_{\mathrm{G},i}$, Eq. (1.20), then acts as a derivative with respect to the gauge field

$$\hat{\Pi}^a_{\mathrm{G},i}(\boldsymbol{x})|A\rangle = \frac{\delta}{i\delta A^a_i(\boldsymbol{x})}|A\rangle \;. \tag{1.62}$$

Expectation values of field operators are then evaluated according to

$$\langle\mathcal{O}[A]\rangle = \int DA\,\psi^*[A]\mathcal{O}[A]\psi[A] \;, \tag{1.63}$$

which again shows the strong formal similarity of Quantum Field Theory in the Hamiltonian approach to ordinary quantum mechanics.

The Schrödinger equation restricted to the purely gluonic part of the Hamiltonian (1.24) is represented as

$$\int d^3x \left(-\frac{1}{2}\frac{\delta^2}{\delta A_k^a(\boldsymbol{x})^2} + \frac{1}{4}F_{ij}^a F_{ij}^a \right) \psi[A] = E\psi[A] \; , \tag{1.64}$$

which has to be solved together with the Gauss law constraint, Eq. (1.48), maintaining the state $\psi[A] = \langle A|\psi\rangle$ invariant under time-independent gauge transformations. Since the potential energy in QED is quadratic in the gauge field, the eigenvalue equation determining the QED wave functional has the same structure as the harmonic oscillator equation and is solved by a Gaussian state, which in momentum space reads

$$\psi[A] = \exp\left(-\frac{1}{2}\int đ^3p \, A_i(\boldsymbol{p}) \, |\boldsymbol{p}| \, A_i(-\boldsymbol{p}) \right) \; , \tag{1.65}$$

where $|\boldsymbol{p}|$ is the ground state energy of non-interacting photons. This result will become important when considering an ansatz for the Yang-Mills wave functional in the next section.

Due to the anti-commuting nature of fermion fields, extending this picture to the quark sector is not straightforward. In the literature several possibilities have been discussed, for example, representing the fermion field operators as in the case of bosonic fields, Eqs. (1.61), (1.62), by

$$\hat{\psi}^a(x) \to \eta^a(x) \; , \tag{1.66}$$

$$\hat{\psi}^{\dagger a}(x) \to \frac{\delta}{\delta\eta^a(x)} \; , \tag{1.67}$$

which was proposed in Refs. [10, 11] and can easily be shown to satisfy the anti-commutation relation (1.31). Note that η^a is a anti-commuting Grassmann variable. This representation, however, has the disadvantage that the Hermitian conjugate of η^a is given by $\eta^{\dagger a} = \frac{\delta}{\delta\eta^a}$, and the adjoint state is therefore not given by complex conjugation, but has a more complicated form. In Section 3.3 we will suggest a different and more convenient representation, introducing coherent fermion states as eigenfunctions of the annihilation operators a and b, Eqs. (1.40), (1.43).

1.5 Fixing to Coulomb Gauge

In principle, we could now work with QCD ground state wave functionals in Weyl gauge, as has been done in particular in $D = 2 + 1$ dimensions for pure Yang-Mills theory [12]. A more convenient way is to resolve Gauss' law explicitly by fixing the residual gauge freedom with respect to time-independent gauge transformations. We choose the Coulomb gauge condition

$$\boldsymbol{\partial} \cdot \boldsymbol{A}^a = 0 \; , \tag{1.68}$$

which eliminates the non-physical longitudinal component of the gauge potential. The independent degrees of freedom are the transverse gauge potential and the transverse part of the conjugate momentum, given as

$$A_i^{\perp a} = t_{ij} A_j^a, \qquad \Pi_i^{\perp a} = t_{ij} \Pi_j^a, \tag{1.69}$$

defined with use of the transverse projector

$$t_{ij}(\boldsymbol{x}) = \int đ^3p \, (\delta_{ij} - \hat{p}_i \hat{p}_j) \, e^{i\boldsymbol{p}\cdot\boldsymbol{x}}, \qquad \hat{p}_i = \frac{p_i}{|\boldsymbol{p}|} \, . \tag{1.70}$$

In addition, the non-vanishing equal-time commutation relations (1.30) in the subspace of transverse fields become

$$[A_i^{\perp a}(\boldsymbol{x}), \Pi_j^{\perp b}(\boldsymbol{y})] = i\delta^{ab} t_{ij}(\boldsymbol{x}) \delta(\boldsymbol{x} - \boldsymbol{y}) \, . \tag{1.71}$$

In the scalar product (1.63) Coulomb gauge is implemented in the standard way via the so-called Faddeev-Popov method [13]. Going over to Coulomb gauge corresponds to the transition from cartesian to curvilinear coordinates and the determinant $\mathcal{J}[A^\perp]$ of the Faddeev-Popov operator

$$(\hat{G}^{-1})^{ab}(\boldsymbol{x}, \boldsymbol{y}) = (-\partial_i \hat{D}_i^{ab}) \delta(\boldsymbol{x} - \boldsymbol{y}) \tag{1.72}$$

enters the scalar product in the Coulomb gauge-fixed configuration space

$$\langle \psi | \mathcal{O} | \phi \rangle = \int DA^\perp \mathcal{J}[A^\perp] \psi^*[A^\perp] \mathcal{O} \phi[A^\perp], \qquad \mathcal{J}[A^\perp] = \mathsf{Det}[\hat{G}^{-1}] \, , \tag{1.73}$$

representing the metric in the curved configuration space. In Eq. (1.72) $\hat{D}_i^{ab}$ is the covariant derivative in the adjoint representation, Eq. (1.17).

The Hamiltonian is now expressed entirely in terms of the transverse components of the gauge field, except for the kinetic part of the Yang-Mills Hamiltonian (which appears as the first part in H_G, Eq. (1.24)) where the momentum operator still has a longitudinal part. Following the derivations in Refs. [14], [15], Gauss' law (1.16) can explicitly be resolved, resulting in [16]

$$H = H_\mathrm{G} + H_\mathrm{C} \, , \tag{1.74}$$

$$H_\mathrm{G} = \frac{1}{2} \int d^3x \left(\frac{1}{2} \mathcal{J}^{-1}[A^\perp] \Pi_i^{\perp m} \mathcal{J}[A^\perp] \Pi_i^{\perp m} + \frac{1}{4} F_{ij} F_{ij} \right) \, , \tag{1.75}$$

$$H_\mathrm{C} = \frac{g^2}{2} \int d^3x \int d^3y \, \mathcal{J}^{-1}[A^\perp] \rho^m(\boldsymbol{x}) \mathcal{J}[A^\perp] \hat{F}^{mn}(\boldsymbol{x}, \boldsymbol{y}) \rho^n(\boldsymbol{y}) \, , \tag{1.76}$$

where the second term is the so-called Coulomb Hamiltonian H_C, describing the interaction of non-Abelian color charges with the densities

$$\rho^m(\boldsymbol{x}) = \psi^\dagger(\boldsymbol{x}) T^m \psi(\boldsymbol{x}) + f^{mno} A_i^{\perp n}(\boldsymbol{x}) \Pi_i^{\perp o}(\boldsymbol{x}) \equiv \rho_\mathrm{F}^m(\boldsymbol{x}) + \rho_\mathrm{G}^m(\boldsymbol{x}) \, , \tag{1.77}$$

through the non-Abelian Coulomb kernel

$$\hat{F}^{mn}(\boldsymbol{x},\boldsymbol{y}) = \int d^3z\, \hat{G}^{mo}(\boldsymbol{x},\boldsymbol{z})(-\partial_{\boldsymbol{z}}^2)\hat{G}^{on}(\boldsymbol{z},\boldsymbol{y}) \; . \tag{1.78}$$

In (1.77) the first term on the right-hand side is the matter charge of dynamical fermions and the second part is the dynamical charge density of the gauge field. Note that this second part is absent in an Abelian gauge theory. The operator $\hat{F}^{mn}$ involves the Green's function of the Faddeev-Popov kernel G^{-1}, Eq. (1.72), twice. In the Abelian theory Eq. (1.78) becomes the ordinary Coulomb kernel, the Green's function of the Laplacian, i.e., $\hat{F}(\boldsymbol{x},\boldsymbol{y}) = 1/(4\pi|\boldsymbol{x}-\boldsymbol{y}|)$.

We work entirely in Coulomb gauge and therefore omit for the rest of the thesis the transversality sign attached to the gauge field.

At the end of this section, let us shortly comment on the so-called Gribov problem which occurs when quantizing non-Abelian gauge theories. For a pedagogical introduction we refer to Ref. [17]. In Section 1.1 we have observed that gauge fixing is necessary in the continuum to make expectation values well defined. In the Faddeev-Popov method to implement the gauge condition Eq. (1.68) one has to assume that the gauge fixing condition has precisely one unique solution [18]. However, it was discovered by Gribov, Ref. [19], that there exist so-called gauge copies, also referred to as Gribov copies. These are gauge fields A_i and A_i' connected by a gauge transformation Eq. (1.10), which satisfy the same gauge condition,

$$\partial_i A_i = 0 = \partial_i A_i' \; . \tag{1.79}$$

These Gribov copies are connected to the existence of zero modes of the Faddeev-Popov operator, Eq. (1.72). In order to bypass this problem, it was proposed to restrict the functional integral, Eq. (1.73), to the so-called Gribov region, defined as

$$\Omega = \{A_i : \partial_i A_i = 0, \hat{G}^{-1} > 0\} \; , \tag{1.80}$$

allowing only for a positive definite Faddeev-Popov operator, Eq. (1.72). The boundary of this region, $\partial\Omega$, is the so-called (first) Gribov horizon. Here the Faddeev-Popov operator has zero eigenvalue. Unfortunately, the Gribov region still contains Gribov copies [20]. An even further restriction of the functional integral is the so-called fundamental modular region (FMR). Here one takes the absolute minimum of each gauge orbit (the set of all gauge fields A_i^a connected by a gauge transformation, Eq. (1.10)), i.e., of a given gauge orbit one gauge field A_i.

1.6 Variational Approach to Yang-Mills Theory in Coulomb Gauge

In this section we collect the results obtained in Refs. [7, 21] in the variational approach to pure Yang-Mills theory in Coulomb gauge, which will be used as input for the projects

presented in this thesis[2]. Two quantities are of special interest for later use, namely the gluon propagator,

$$D_{ij}^{ab}(\boldsymbol{p}) = \int d^3x\, e^{-i\boldsymbol{p}\cdot\boldsymbol{x}} \langle A_i^a(\boldsymbol{x}) A_j^b(\boldsymbol{0})\rangle \;, \tag{1.81}$$

and the so-called non-Abelian color Coulomb potential

$$V_{\mathrm{C}}^{ab}(\boldsymbol{p}) = g^2 \int d^3x\, e^{-i\boldsymbol{p}\cdot\boldsymbol{x}} \langle \hat{F}^{ab}(\boldsymbol{x},\boldsymbol{0})\rangle \;, \tag{1.82}$$

with the Coulomb kernel $\hat{F}^{ab}$ given in Eq. (1.78). The non-Abelian color Coulomb potential V_{C}^{ab} is derived by replacing the quark charge densities in Eq. (1.77) by static quark-antiquark color charge sources separated by a distance $|\boldsymbol{x}|$, and by computing the Coulomb energy density (1.76) for this charge distribution. The expectation value $\langle \hat{F}^{ab}(\boldsymbol{x},\boldsymbol{0})\rangle$ is called the Coulomb propagator.

In addition, we define the ghost propagator, given as the expectation value of the inverse Faddeev-Popov operator (1.72)

$$G^{ab}(\boldsymbol{p}) = \int d^3x\, e^{-i\boldsymbol{p}\cdot\boldsymbol{x}} \langle \hat{G}^{ab}(\boldsymbol{x},\boldsymbol{0})\rangle \;. \tag{1.83}$$

Moreover, we define the ghost and Coulomb form factors

$$G^{ab}(\boldsymbol{p}) = \frac{1}{\boldsymbol{p}^2}\frac{d(\boldsymbol{p})}{g}\delta^{ab} \;, \qquad V^{ab}(\boldsymbol{p}) = \frac{f(\boldsymbol{p})d^2(\boldsymbol{p})}{\boldsymbol{p}^2}\delta^{ab} \;, \tag{1.84}$$

measuring the deviation from their Abelian results, i.e., $gd(\boldsymbol{p}) = f(\boldsymbol{p}) = 1$.

In any variational calculation the first step is to choose a well-motivated ansatz for the vacuum wave functional, denoted as $\psi[A]$, which depends on one or more variational kernels. By computing the energy density

$$\langle\psi|H|\psi\rangle = \int DA\, \mathcal{J}[A]\, \psi^*(A)\, H\, \psi(A) \;, \tag{1.85}$$

and minimizing it with respect to the variational kernels entering the wave functional one gets an estimate for the ground state energy, which is the upper bound to the true ground state of the system.

In order to find a suitable ansatz for the Yang-Mills wave functional one uses the fact that for the high-momentum part, due to asymptotic freedom, the Yang-Mills wave functional is expected to approach the QED wave functional, Eq. (1.65). One therefore suggests a Yang-Mills ground state of the form [7]

$$\psi[A] = \langle A|\psi\rangle = \frac{\mathcal{N}_{\mathrm{G}}}{\sqrt{\mathcal{J}[A]}} \exp\left(-\frac{1}{2}\int \text{đ}^3p\, A_i^a(\boldsymbol{p})\, \omega_{ij}^{ab}(\boldsymbol{p})\, A_j^b(-\boldsymbol{p})\right) \;, \tag{1.86}$$

[2] All results in this chapter are obtained for (color) $SU(2)$ Yang-Mills theory.

with $\omega_{ij}^{ab}(\boldsymbol{p})$ the variational kernel chosen to be a color and Lorentz scalar, i.e., $\omega_{ij}^{ab}(\boldsymbol{p}) = \delta^{ab} t_{ij}(\boldsymbol{p})\omega(\boldsymbol{p})$. The fact that the Faddeev-Popov determinant $\mathcal{J}[A]$, Eq. (1.73), enters the wave functional is of central importance. At the Gribov horizon $\partial\Omega$ the Faddeev-Popov operator $\hat{G}^{-1}$, Eq. (1.72), has zero eigenvalue and the Faddeev-Popov determinant $\mathcal{J}[A]$, Eq. (1.73), vanishes. The wave functional $\psi[A]$, Eq. (1.86), becomes strongly peaked. This goes in hand with the conjecture that the dominant infrared configurations lie on the Gribov horizon [22–24]. In addition, the ansatz (1.86) has the technical advantage that the Faddeev-Popov determinant in the integration measure (1.73) cancels against the Faddeev-Popov determinant in the vacuum wave functional (1.86). The generating functional defined as

$$Z[j] = \left\langle \psi \right| \exp\left(\int đ^3 p \, j_i^a(\boldsymbol{p}) A_i^a(-\boldsymbol{p}) \right) \left| \psi \right\rangle \, , \tag{1.87}$$

can be performed analytically, yielding

$$\begin{aligned} Z[j] &= \mathcal{N}_{\mathrm{G}}^2 \int DA \, \exp\left(- \int đ^3 p \, A_i^a(\boldsymbol{p}) \, \omega_{ij}^{ab}(\boldsymbol{p}) \, A_j^b(-\boldsymbol{p}) + \int đ^3 p \, j_i^a(\boldsymbol{p}) A_i^a(-\boldsymbol{p}) \right) \\ &= \exp\left(\frac{1}{4} \int đ^3 p \, j_i^a(\boldsymbol{p}) (\omega_{ij}^{ab}(\boldsymbol{p}))^{-1} j_j^b(-\boldsymbol{p}) \right) \, . \end{aligned} \tag{1.88}$$

Here j_i^a is the gluonic source and the normalization constant $\mathcal{N}_{\mathrm{G}}$ is fixed by the condition $\langle 1 \rangle = 1$. Evaluating the gluon propagator (1.81) yields

$$\langle A_i^a(\boldsymbol{p}) A_j^b(\boldsymbol{q}) \rangle = (2\pi)^6 \frac{\delta^2 Z[j]}{\delta j_i^a(\boldsymbol{p}) \delta j_j^b(\boldsymbol{q})}\Big|_{j=0} = \delta^{ab} \frac{t_{ij}(\boldsymbol{p})}{2\omega(\boldsymbol{p})} (2\pi)^3 \delta(\boldsymbol{p} + \boldsymbol{q}) \, , \tag{1.89}$$

where we have assumed rotational invariance, i.e., $\omega(\boldsymbol{p}) = \omega(-\boldsymbol{p})$. We observe that the gluon propagator is the inverse of the operator appearing in the exponent of the wave functional, which is special for the ansatz (1.86) and no longer holds true for non-Gaussian wave functionals [25] and for Gaussian wave functionals with an arbitrary power α in the exponent of the Faddeev-Popov determinant, i.e., [21]

$$\psi[A] = \mathcal{J}^{-\alpha}[A] \, \mathcal{N}_{\mathrm{G}} \exp\left(-\frac{1}{2} \int đ^3 p \, A_i^a(\boldsymbol{p}) \, \omega_{ij}^{ab}(\boldsymbol{p}) \, A_j^b(-\boldsymbol{p}) \right) \, . \tag{1.90}$$

The (inverse) gluon propagator (1.81), now denoted as $D(\boldsymbol{p}) = \frac{1}{2\Omega(\boldsymbol{p})}$, and the wave functional kernel ω, Eq. (1.86), obey the relation [21]

$$\Omega(\boldsymbol{p}) = \omega(\boldsymbol{p}) + (1 - 2\alpha)\chi(\boldsymbol{p}) \, , \tag{1.91}$$

where

$$\chi_{ij}^{ab}(\boldsymbol{p}) = \frac{1}{2} \int d^3 x \, e^{i\boldsymbol{p}\cdot\boldsymbol{x}} \left\langle \frac{\delta^2 \ln \mathcal{J}}{\delta A_i^a(\boldsymbol{x}) A_j^b(\boldsymbol{0})} \right\rangle \, , \tag{1.92}$$

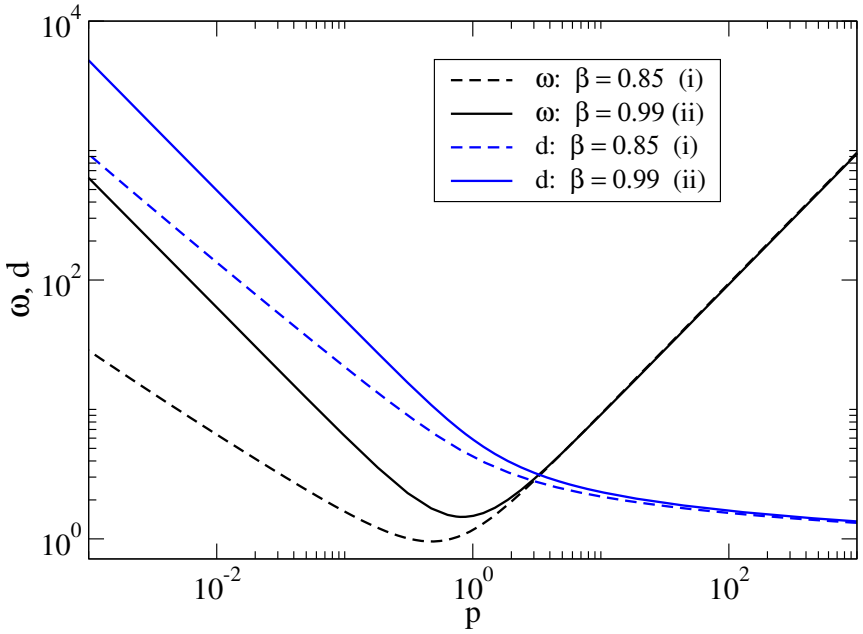

Figure 1.1: *Comparison of the gluon energy ω and the ghost form factor d for the two critical solutions $\beta = 0.99$ (full curve) and $\beta = 0.85$ (dashed curve).*

is the curvature of the gauge orbit in field space and $\chi^{ab}_{ij}(\boldsymbol{p}) = \delta^{ab} t_{ij}(\boldsymbol{p})\chi(\boldsymbol{p})$. For the choice $\alpha = 1/2$ the inverse gluon propagator Ω is then identical with the wave functional kernel ω.

In the standard procedure the energy density of the gluon part $E[A] = \langle H_{\rm G}\rangle$ (with $H_{\rm G}$ given in Eq. (1.75)) is computed and then varied with respect to the kernel ω to yield a coupled system of integral equations, found in Refs. [7], [8], determining the gluon propagator (1.81), the Coulomb propagator (1.82), and the ghost propagator (1.83).

It can be shown analytically [26] that the infrared exponents of the gluon propagator $\omega(p \to 0) \sim p^{-\alpha}$ and ghost form factor $d(p \to 0) \sim p^{-\beta}$ obey the sum rule $\alpha = 2\beta - 1$ and have two possible solutions[3]

$$i) \quad \beta \simeq 0.796\,(0.85), \qquad ii) \quad \beta = 1.0\,(0.99)\,, \tag{1.93}$$

which can also be found numerically, see Fig. 1.1. The values in the brackets denote the numerically determined values, which were obtained in Refs. [7, 8]. Both solutions have in common that at small momenta the variational kernel ω diverges and from Eq. (1.89) we can read off that the gluon propagator vanishes. Moreover, for both solutions the ghost form factor d, Eq. (1.84), diverges for small momenta. For large momenta both solutions go over into the photon energy $\omega(\boldsymbol{p} \to \infty) \sim \boldsymbol{p}$, which can also be seen in Fig. 1.1.

Before we come to discuss the form of the static non-Abelian color Coulomb potential $V_{\rm C}$, Eq. (1.82), within the variational approach, let us comment on this quantity. An inequality relates the color Coulomb confinement potential $V_{\rm C}(r)$, Eq. (1.82), and the

[3] There also exist so-called subcritical solutions [27], for which $d^{-1}(0) \neq 0$.

static potential extracted from the Wilson loop (see Part II of the thesis), denoted as $V_{\mathrm{W}}(r)$ and reads [28]

$$V_{\mathrm{C}}(r) \geq V_{\mathrm{W}}(r) \; . \tag{1.94}$$

From this inequality we can deduce that in a confining theory there always must be a confining non-Abelian Coulomb potential $V_{\mathrm{C}}(r)$. The slope of the linear potential, referred to as the *Coulomb string tension* σ_{C}, is the upper bound for the gauge invariant string tension extracted from the expectation value of the Wilson loop, known as the *Wilsonian string tension* σ_{W}. The evaluation of the Wilsonian string tension within the Hamiltonian approach will be subject of the second project presented in Part II of this thesis. Although difficult to compute, lattice measurements for $SU(2)$ as well as $SU(3)$ suggest for σ_{C} a value which is two to three times larger than the Wilsonian string tension σ_{W}, see Refs. [23, 29–32]. In Ref. [30], calculating V_{C}, Eq. (1.82), directly via Monte-Carlo simulations, a value of $\sigma_{\mathrm{C}} \approx 1.6\sigma_{\mathrm{W}}$ has been estimated. Throughout this thesis we will use values $\sigma_{\mathrm{C}} = (2 \ldots 3)\sigma_{\mathrm{W}}$ in order to set the scale.

Let us return to the evaluation of the color Coulomb potential in the variational approach to QCD[4]. Numerical investigations show that in Eq. (1.93) solution $i)$ is more stable. However, the color Coulomb potential $V_{\mathrm{C}}(r)$ extracted from (1.82) is not rising linearly for large distances. On the other hand, solution $ii)$ in Eq. (1.93) allows for a strictly linearly rising non-Abelian color Coulomb-potential $V_{\mathrm{C}}(r)$, Eq. (1.82), which can be seen analytically by plugging $d(\boldsymbol{p}) \sim 1/p$ into Eq. (1.84), to give $V(\boldsymbol{p} \to 0) \sim 1/\boldsymbol{p}^4$. We note that in the equation determining the Coulomb form factor f the ghost form factor d is set to its bare value, $d(\boldsymbol{p}) = g$, see Ref. [7].

Finally, let us compare the results for the gluon propagator obtained in the Hamiltonian approach with lattice calculations, see Fig. 1.2. For a review of gauge fixing on the lattice we refer to Ref. [35]. The lattice data for the kernel ω can be nicely fitted by Gribov's formula [19] over the whole momentum range

$$\omega(\boldsymbol{p}) = \sqrt{\boldsymbol{p}^2 + \frac{M_{\mathrm{G}}^4}{\boldsymbol{p}^2}} \; , \tag{1.95}$$

where M_{G} is a mass scale referred to as Gribov mass, which is determined on the lattice in Ref. [36] in terms of the Wilsonian string tension σ_{W} and has the value

$$M_{\mathrm{G}} \approx 880\,\mathrm{MeV} \approx 2\sqrt{\sigma_{\mathrm{W}}} \; . \tag{1.96}$$

In the asymptotic momentum regions the variational result using the ansatz (1.86) and the lattice data agree excellently. In the mid-momentum regime, however, the lattice data signal a more pronounced maximum. The Gaussian ansatz (1.86) is extended to non-Gaussian wave functions including up to quartic terms in the gauge field [25],

$$|\psi[A]|^2 = \exp(-S[A]), \qquad S[A] = \int \omega A^2 + \frac{1}{3!}\int \gamma^{(3)} A^3 + \frac{1}{4!}\int \gamma^{(4)} A^4 \; , \tag{1.97}$$

[4] In the functional integral approach, where Weyl gauge is not imposed, the static non-Abelian color Coulomb potential V_{C}, Eq. (1.82), is essentially the instantaneous part of the temporal gluon propagator $D_{00} = \langle A_0 A_0 \rangle$, see Refs. [33, 34] and Section 6.3.

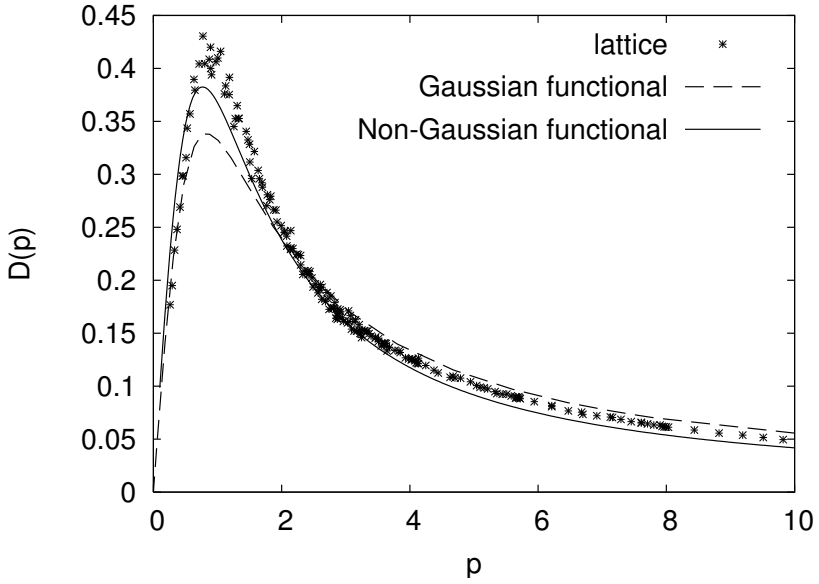

Figure 1.2: *Comparison of the gluon propagator obtained on the lattice (data points) with the variational solution for the Gaussian ansatz (dashed curve) and non-Gaussian ansatz for the wave functional (full curve). Plot taken from Ref. [25].*

suspecting that these deviation stems from ignoring the three-gluon and higher-order vertices in the Gaussian ansatz. In fact, from Fig. 1.2 one observes that with the non-Gaussian ansatz (1.97) the maximum moves towards the lattice result.

Let us shortly summarize the main findings of this chapter. Starting from the definition of the QCD Lagrangian, the corresponding Hamiltonian in a Coulomb gauge fixed scheme has been presented. We have shown that the so-called Faddeev-Popov determinant, which essentially describes the Jacobian in the curved space, enters the Hamiltonian and the scalar product. Moreover, in the construction of the Yang-Mills vacuum wave functional it plays an important role. In the last section we have studied the pure Yang-Mills sector and collected the most important quantities for later work, i.e., the gluon propagator and the non-Abelian color Coulomb potential.

All these results offer a rich variety of applications[5]: for instance, the Gaussian Yang-Mills vacuum wave functional $\psi[A]$, Eq. (1.90), can be applied to obtain a perimeter law in the 't Hooft loop, Ref. [40], or to show that the inverse ghost form factor $d^{-1}(\boldsymbol{p})$, Eq. (1.84), has the meaning of the dielectric function of the Yang-Mills vacuum, Ref. [41]. In addition, the topological susceptibility, Ref. [42], has been successfully computed using the Gaussian ansatz and currently the finite temperature case in pure Yang-Mills theory is investigated, Refs. [43, 44]. Moreover, the above described formalism can be used to extract information about lower dimensional QCD as well. The Gaussian vacuum has been applied to Yang-Mills theory in $D = 1 + 1$ dimensions, Ref. [45], and in $D = 2 + 1$

[5] A collection of all results gained in recent years in the Hamiltonian approach to Yang-Mills theory can be found in Refs. [37–39].

dimensions, Ref. [46]. However, the ultimate goal is, at last, to approach hadron physics and to compute hadron observables from the elementary degrees of freedom, the quarks and gluons.

In Part I of the work we therefore extend the variational approach and include quark fields into the ansatz for the vacuum wave functional.

In Part II we show how the area law for spatial Wilson loops can be obtained from the results presented in this section.

Finally, let us shortly mention other approaches to non-perturbative Yang-Mills theory in Coulomb gauge. Although most work in recent years in Coulomb gauge has been performed in the Hamiltonian approach, also the Dyson-Schwinger approach within the first order formalism has become quite popular, Ref. [47]. In this framework the Slavnov-Taylor identities are studied in Ref. [48]. In Ref. [49] a non-perturbative constraint on the total color charge is derived. Heavy quarks are explored in Refs. [50–52]. A one-loop perturbative analysis of propagators is performed in Refs. [53–55]. Besides the Dyson-Schwinger approach, there exists another powerful functional method to explore the non-perturbative sector, the Functional Renormalization Group, Ref. [56]. Transferring this formalism to the Hamiltonianian formalism in Coulomb gauge, Ref. [57], flow equations for the ghost and gluon propagators are derived and solved in Ref. [58]. Moreover, in Ref. [59] a flow equation for the static non-Abelian color Coulomb potential is presented. Another method is lattice QCD in Coulomb gauge. A key issue on the lattice in Coulomb gauge is the renormalizability of Greeen's functions. It has been discovered that for static correlation functions a non-perturbative renormalization procedure can be defined, see Refs. [36, 60, 61]. Recent calculations of lattice Yang-Mills propagators are reported in Ref. [62]. It is a remarkable fact that most results gained in all these different approaches to Coulomb gauge QCD agree quantitatively.

Part I

Inclusion of Quarks into the Hamiltonian Formalism

Chapter 2

Chiral Symmetry Breaking and Dynamical Mass Generation

The aim of the first project presented in this thesis is to formulate a vacuum wave functional for the quark sector of QCD. In this chapter we introduce the theoretical concept which is essential for this construction: the spontaneous breakdown of chiral symmetry. Important low-energy phenomena follow from this concept, like the small pion masses and the non-existence of degenerate masses of parity partners.

In the first section we introduce the notion of a *constituent* quark mass and motivate, in a simple physical picture, how a constituent mass evolves from a small or even vanishing bare quark mass. In Section 2 we put these observations on a theoretical foundation. Starting from the definition of a general flavor symmetry transformation, we discuss the symmetry group of QCD and introduce chiral flavor rotations. Section 3 is devoted to the phenomenological hints for chiral symmetry to be broken spontaneously. We then discuss the resulting ground state properties and invoke the Goldstone theorem, which explains the small pion masses.

2.1 Bare and Constituent Quark Masses

The masses of the lightest quark flavors m_{U}, m_{D} and m_{S} are small compared to the typical QCD scale, which is of order 1 GeV, e.g., the mass of the proton. These *bare* or *Lagrangian quark masses* are fixed in a certain renormalization scheme, for instance, the $\overline{MS}$ scheme, and take values of about [63]

$$m_{\mathrm{U}} \approx 2\,\mathrm{MeV}, \qquad m_{\mathrm{D}} \approx 4\,\mathrm{MeV}, \qquad m_{\mathrm{S}} \approx 100\,\mathrm{MeV}. \tag{2.1}$$

The fact that the proton mass, $M_{\mathsf{proton}} \approx 940$ MeV, differs from the sum of the masses of its building blocks (two up-quarks and one down-quark) by almost two orders of magnitude, motivates the introduction of a *constituent quark mass*. It consists of the bare quark mass m_{F}, with F denoting flavor, and the contribution from binding effects of QCD. Since three constituent quarks form a nucleon, the mass of a constituent quark is about $M_{\mathsf{constituent}} = M_{\mathsf{proton}}/3 \approx 300$ MeV. Many bound-state models use this value as input.

Starting from the bare mass m_{F} the constituent mass $M_{\mathsf{constituent}}$ is generated dynamically, which can be illustrated in the following way [64]: As the bare quark moves

through the hadron, due to QCD interactions it acquires more and more mass until it freezes out and becomes a heavy constituent quark at large distances (around 1 fm). In momentum space we can therefore define the constituent mass as the dynamically generated mass, denoted as $M(p)$, at zero momentum and the current quark mass as its limit for large momenta[1]:

$$M(p \to 0) = M_{\text{constituent}}, \qquad M(p \to \infty) = m_{\text{F}} \ . \tag{2.2}$$

We can conclude that due to the large difference between constituent and bare quark mass nearly the whole proton mass arises from the strong interaction. To compare, the Higgs field, from which should follow the bare quark masses, only accounts for one or two percent of the proton mass, Ref. [65].

Theoretically also with vanishing quark mass a non-vanishing constituent mass can be obtained, which leads to the statement that quark mass is generated *from nothing* [66]. This reveals that mass generation must be non-perturbative in nature, since in perturbation theory the mass of a particle is proportional to its bare mass at every order in the coupling. Hence, in order to describe the emergence of the constituent quark mass from QCD, we clearly have to rely on non-perturbative methods. Such a method, outlined in Chapter 1, is the variational approach to QCD in Coulomb gauge.

A puzzle, which arises at this stage, comes from the pion, composed of an up- and a down anti-quark. Sticking to the constituent representation, we would expect a pion mass of about $M_{\text{pion}} = 2 \times M_{\text{constituent}} \approx 600$ MeV. However, the experimental value is much smaller, $M_{\text{pion}} \approx 140$ MeV. We therefore have to clarify how a light composite particle, the pion, is formed from two massive constituent quarks.

2.2 Chiral Symmetry

Considering fermion fields that carry a flavor index running from 1 to N_{F}, Eq. (1.1), we define a general symmetry transformation of the form

$$\psi(x) \to \psi'(x) = e^{i\varepsilon X_a}\psi(x) \ , \tag{2.3}$$

$$\overline{\psi}(x) \to \overline{\psi}'(x) = \overline{\psi}(x)e^{i\varepsilon \overline{X}_a} \ , \tag{2.4}$$

with $X_a, \overline{X}_a$ being the symmetry generators in flavor space and the index a runs from $a = 1$ to N_{F}^2. Expanding the fermion Lagrangian, Eq. (1.1), to first order in the parameter ε, the invariance with respect to the general symmetry (2.3), (2.4) can be formulated as

$$\overline{X}_a \mathcal{D} + \mathcal{D} X_a = 0 \ , \tag{2.5}$$

[1] Let us emphasize that the non-trivial behavior of QCD under a scale transformation leads to the fact that physical quantities become momentum dependent, which means that all quark masses become running masses.

with $\mathcal{D}$, Eq. (1.2), denoting the massive Dirac operator. From the general symmetry transformations we build up $N_{\rm F}^2$ vector transformations $X_a^{\rm V}$ and $N_{\rm F}^2$ axial-vector (chiral) transformations $X_a^{\rm A}$ as

$$X_a^{\rm V} = \{T_a, \mathbb{1}\}, \qquad X_a^{\rm A} = \{\gamma_5 T_a, \gamma_5\} \; . \tag{2.6}$$

We find both to be symmetries of the massless QCD action. Note that $\overline{X}_a^{\rm V}$ gets an additional sign, i.e., $\overline{X}_a^{\rm V} = \{-T_a, -\mathbb{1}\}$. The invariance with respect to axial transformations can directly be seen from the anti-commutativity of the massless Dirac operator with γ_5, i.e., $\{\mathcal{D}, \gamma_5\} = 0$. The invariance with respect to vector transformations extends to the case of degenerate masses $m_{\rm F} = m$. The QCD action, however, is chirally symmetric for massless quark fields only. A mass term explicitly breaks chiral symmetry, as can be seen by inserting the transformations $X_a^{\rm A}$ in (2.5) with $\mathcal{D} = m$. Therefore, setting the quark masses to zero, i.e., $m_{\rm U} = m_{\rm D} = m_{\rm S} = 0$, is called *chiral limit*.

From now on, to the rest of this thesis, we deal with massless quarks only. The symmetry group of massless QCD is

$$SU_{\rm V}(N_{\rm F}) \times SU_{\rm A}(N_{\rm F}) \times U_{\rm V}(1) \times U_{\rm A}(1) \; . \tag{2.7}$$

Noether's theorem connects a continuous symmetry with a conserved current, which reads for the symmetry transformations quoted above

$$J_\mu^{a,{\rm V}} = \overline{\psi} T^a \gamma_\mu \psi \; , a = 1, \ldots, N_{\rm F}^2 - 1 \qquad J_\mu^{a,{\rm V}} = \overline{\psi} \gamma_\mu \psi \; , a = N_{\rm F}^2 \; , \tag{2.8}$$

$$J_\mu^{a,{\rm A}} = \overline{\psi} T^a \gamma_\mu \gamma_5 \psi \; , a = 1, \ldots, N_{\rm F}^2 - 1 \qquad J_\mu^{a,{\rm A}} = \overline{\psi} \gamma_\mu \gamma_5 \psi \; , a = N_{\rm F}^2 \; , \tag{2.9}$$

where we identify the conserved vector currents $J_\mu^{a,{\rm V}}$ to give isospin and baryon number conservation. The axial current $J_\mu^{N_{\rm F}^2,{\rm A}}$ is conserved at the classical level only. In the quantized theory the $U_{\rm A}(1)$ symmetry is violated, leading to a non-zero operator occurring on the right-hand side of the divergence

$$\partial^\mu \left(\overline{\psi} \gamma_\mu \gamma_5 \psi \right) \neq 0 \; . \tag{2.10}$$

This so-called *axial anomaly* can be demonstrated in an elegant manner using the Fujikawa method [67] which starts from the observation that the fermion measure in the fermionic path integral is *not* invariant under a chiral rotation[2].

Finally, we define the orthogonal projectors $\mathcal{P}_\pm = \frac{\mathbb{1} \pm \gamma_5}{2}$ on right-handed and left-handed components

$$\psi_R = \mathcal{P}_+ \psi, \qquad \psi_L = \mathcal{P}_- \psi \; , \tag{2.11}$$

such that we can decouple the massless fermion Lagrangian as

$$\mathcal{L} = \overline{\psi}_L \mathcal{D} \psi_L + \overline{\psi}_R \mathcal{D} \psi_R \; . \tag{2.12}$$

[2] The *explicit* chiral $U_{\rm A}(1)$ symmetry breaking by the axial anomaly gives mass to the η' particle. In this thesis we do not consider the axial anomaly, which has been already calculated in the Hamiltonian approach in Ref. [42].

Chiral symmetry manifests itself in the possibility to decouple the Lagrangian into a left-handed and right-handed part, which can again be related to the fact that γ_5 anti-commutes with the massless Dirac operator $\mathcal{D}$ or correspondingly with the Dirac Hamiltonian h, see Eqs. (1.33), (1.34) and the discussion which follows these equations. The explicit chiral symmetry breaking by a mass term then leads to a mixing between left- and right-handed components, i.e., $\overline{\psi}_L\psi_R + \overline{\psi}_R\psi_L$. Moreover, left- and right-handed currents can be constructed as sum and difference of Eqs. (2.8), (2.9) to give

$$J^L_\mu = \frac{1}{2}\left(J^{\mathrm{V}}_\mu - J^{\mathrm{A}}_\mu\right) \ , \tag{2.13}$$

$$J^R_\mu = \frac{1}{2}\left(J^{\mathrm{V}}_\mu + J^{\mathrm{A}}_\mu\right) \ . \tag{2.14}$$

Both currents are conserved separately implying that the fermion numbers of ψ_L and ψ_R are separately conserved. In addition, we can construct left- and right-handed transformations and end up with the following isomorphic symmetry groups

$$SU_{\mathrm{V}}(N_{\mathrm{F}}) \times SU_{\mathrm{A}}(N_{\mathrm{F}}) \times U_{\mathrm{V}}(1) \times U_{\mathrm{A}}(1) \cong SU_{\mathrm{L}}(N_{\mathrm{F}}) \times SU_{\mathrm{R}}(N_{\mathrm{F}}) \times U_{\mathrm{L}}(1) \times U_{\mathrm{R}}(1) \ . \tag{2.15}$$

Let us emphasize that ψ_R and ψ_L are eigenfunctions to the chirality matrix γ_5 with eigenvalues ± 1, i.e.,

$$\gamma_5\psi_R = \psi_R, \qquad \gamma_5\psi_L = -\psi_L \ . \tag{2.16}$$

This observation will become important for the considerations below.

2.3 Spontaneous Breaking of Chiral Symmetry

We now motivate the fact that the axial-vector symmetry $SU_{\mathrm{A}}(N_{\mathrm{F}})$ is not realized in nature. We start from the observation that left- and right-handed particles are at the same time helicity eigenstates (in the chiral limit)

$$\boldsymbol{\sigma}\cdot\hat{\boldsymbol{p}}\ \psi_R \ = \ \psi_R, \qquad \boldsymbol{\sigma}\cdot\hat{\boldsymbol{p}}\ \psi_L \ = \ -\psi_L, \tag{2.17}$$

where we have used the definition of the helicity matrix $\boldsymbol{\sigma}\cdot\hat{\boldsymbol{p}}$, Eq. (A.14). Right-handed massless fermions ψ_R have helicity $+1$ and left-handed fermions ψ_L have helicity -1. For massless fermions helicity eigenstates are at the same time chirality eigenstates. To see this compare Eq. (2.16) with Eq. (2.17). Acting with a parity operator a particle with positive helicity transforms into a particle with negative helicity and vice versa. We therefore expect hadrons to occur in nearly degenerate parity doublets, i.e., parity partners should have nearly degenerate masses. For instance, the nucleon N and its parity partner N^* should have nearly equal masses. However, while the nucleon N has a mass of 940 MeV, its parity partner N^* is about 600 MeV heavier. Hence, no such degeneracy occurs in the hadron spectrum. We can conclude that the ground

state of QCD does not obey the symmetry of the action, Eq. (2.15), i.e., axial-vector transformations $SU_{\mathrm{A}}(N_{\mathrm{F}})$ are broken *spontaneously*.

The true vacuum of QCD, denoted as $|\Phi\rangle$, is not chirally invariant:

$$e^{i\varepsilon X_a^{\mathrm{A}}}|\Phi\rangle \neq |\Phi\rangle \ , \tag{2.18}$$

where we have used the definition (2.6). This argumentation can further be supported by the fact that the flavor-singlet vacuum expectation value

$$\langle\Phi|\overline{\psi}\psi|\Phi\rangle = \langle\Phi|\overline{\psi}_R\psi_L|\Phi\rangle + \langle\Phi|\overline{\psi}_L\psi_R|\Phi\rangle \ , \tag{2.19}$$

referred to as *chiral condensate*, acquires a non-zero value. This non-zero expectation value signals the mixing of left- and right-handed quarks. In this picture the QCD ground state, being populated by quark-antiquark states, is responsible for giving mass to the hadrons. We stress that the relation (2.18) will become important in later considerations. We speak of such a symmetry to be realized in the Nambu-Goldstone mode as opposed to the Wigner-Weyl mode, in which the vacuum possesses the same symmetry as the action of the system.

In the chiral limit the value of the chiral condensate is given as $\langle\overline{\psi}\psi\rangle = -(235 \pm 15\,\mathrm{MeV})^3$, Ref. [68]. In recent years lattice measurements[3] could confirm this value [70–72].

We are now able to solve the puzzle of the small pion mass. For a spontaneously broken continuous global symmetry the Goldstone theorem applies, leading to the existence of massless and spinless particles, the Goldstone bosons. If the broken symmetry is a vector symmetry then the associated Goldstone particle is a massless scalar particle, whereas a broken axial-vector symmetry leads to pseudoscalar massless particles. The number of Goldstone particles corresponds to the number of generators of the broken symmetry, i.e., for $SU_{\mathrm{A}}(N_{\mathrm{F}})$ there are $N_{\mathrm{F}}^2 - 1$ Goldstone particles. The eight lightest hadrons $\pi^{\pm}, \pi^0, K^{\pm}, K^0, \overline{K}^0, \eta$ are therefore the pseudoscalar Goldstone bosons associated with the eight generators of $SU_{\mathrm{A}}(3)$. Since the lightest quark flavors are only approximately massless, the Goldstone modes also acquire a small non-vanishing mass, but are still much lighter than the other hadrons.

In the quantized theory the symmetry (2.7) is broken to the remaining symmetry

$$SU_{\mathrm{V}}(N_{\mathrm{F}}) \times U_V(1) \ , \tag{2.22}$$

[3] On the lattice the quark condensate, Eq. (2.19), is given via the Banks-Casher relation [69]

$$\langle\Phi|\overline{\psi}\psi|\Phi\rangle = -\lim_{V\to\infty} \pi\rho(0) \ , \tag{2.20}$$

with the spectral density $\rho(\lambda)$ of the Dirac operator defined by

$$\rho(\lambda) = \frac{1}{V}\sum_n \langle\delta(\lambda - \lambda_n)\rangle \ , \tag{2.21}$$

and $\rho(0)$ the zero-eigenvalue density of the Dirac operator, see Eq. (1.35). Here V is the volume and λ denotes the eigenvalue of the Dirac operator.

which is realized in nature. Since no light scalar particles appear in the spectrum, baryon number is conserved and hadrons form multiplets of $SU_{\mathrm{V}}(3)$. Moreover, there exists a general theorem [73], which states that in vector-like theories[4] vector symmetries cannot be spontaneously broken. The independent left- and right-handed symmetries, Eq. (2.15), are spontaneously broken to a group of simultaneous transformations

$$SU_{\mathrm{L}}(N_{\mathrm{F}}) \times SU_{\mathrm{R}}(N_{\mathrm{F}}) \cong SU_{\mathrm{L+R}}(N_{\mathrm{F}}) \; . \tag{2.23}$$

In the next chapter we will make use of the concepts presented in this chapter in order to construct a vacuum wave functional for the quark sector of QCD.

[4] These are theories in which the gauge field only couples to vector currents, as opposed to chiral gauge theories, in which gauge fields couple to axial-vector currents as well. A famous example for vector-like theories is QCD and for a chiral gauge theory the $U(1) \times SU(2)$ gauge theory of the electroweak sector.

Chapter 3

Variational Approach to the Quark Sector of QCD

In this chapter we introduce quark fields into the variational approach to QCD in Coulomb gauge.

In the first section we motivate the choice of BCS-like trial states containing quark-antiquark pairs, which we generalize to include the coupling of the quarks to transverse spatial gluons. In Section 2 we represent the quark fields in a coherent fermion basis, and in section 3 we establish the generating functional in terms of Grassmann fields and evaluate fermionic n-point functions. In Section 4 we discuss the evaluation of the gluonic expectation values which, due to the presence of the quark fields, can no longer be done exactly. Section 5 exploits the low energy chiral properties of the theory, like the quark condensate and the constituent mass and connects the solutions obtained in the variational approach to the quark propagator dressing functions.

All results are given in the chiral limit, but it is straightforward to reformulate the system to non-zero quark masses.

Explicit calculations and technical details are postponed to Appendix B. Some of the results presented in the following chapters have been published in Ref. [74].

3.1 Motivation

Let us start with the microscopic theory of superconductivity, the BCS theory. Below a critical temperature electron-hole pairs, so-called *Cooper pairs* form and signal the transition to the BCS phase. The ground state of a superconductor can therefore be represented in terms of Cooper pairs [75]

$$|\mathrm{BCS}\rangle = e^{-\sum_{k,l} C_{kl} a_k^\dagger b_l^\dagger} |0\rangle \ , \tag{3.1}$$

with C_{kl} denoting the amplitudes, where the variational kernels denoting the occupation probabilities for the different single-particle states are hidden. The creation operators $a^\dagger$ and $b^\dagger$ for electrons and holes are defined according to Eqs. (1.41), (1.42). Varying the BCS-Hamiltonian with respect to the variational functions results in the so-called *gap equation* [75], which is a self-consistent equation for the energy gap Δ. The Nambu–Jona-Lasinio model (NJL-model) transports this picture to quark physics. Cooper pairs

become quark-antiquark pairs, the critical temperature becomes the critical coupling and the energy gap Δ becomes the mass gap M [76, 77]. The first attempts to construct a quark vacuum wave functional within QCD make use of this analogy. In the pioneering works of Finger and Mandula [78], Yaouanc et al. [79], and Adler and Davis [80] a BCS-like ground state is considered

$$|\phi\rangle = \mathcal{N}_{\mathrm{F}} \exp\left[- \int đ^3p \sum_{s,t} S(\boldsymbol{p}) \overline{u}(\boldsymbol{p},s) v(-\boldsymbol{p},t) a^{\dagger a}(\boldsymbol{p},s) b^{\dagger a}(-\boldsymbol{p},t) \right] \Big|0\Big\rangle \,, \tag{3.2}$$

where $\mathcal{N}_{\mathrm{F}}$ is the normalization, $S(\boldsymbol{p})$ is the variational kernel, $\overline{u}(\boldsymbol{p},s)$, $v(-\boldsymbol{p},t)$ the spinor solutions, Eqs. (A.26), (A.28), and $a^{\dagger a}(\boldsymbol{p},s)$, $b^{\dagger a}(\boldsymbol{p},t)$ the creation operators for massless quarks and anti-quarks of momentum $\boldsymbol{p}$, color a and helicities s,t, Eqs. (1.41), (1.42). The flavor index is suppressed and can straightforwardly be attached to the creation operators. However, to the present approximation the result is independent on the number of flavors used, so that we will drop the flavor index.

The vacuum state (3.2) has zero total momentum, zero angular momentum and is a color singlet. Employing Bogoliubov transformations generalized creation and annihilation operators can be constructed, from which the expectation value of the Hamiltonian is evaluated. After variation with respect to the variational kernel S a non-linear equation determining S, the so-called *quark gap equation* is derived [78–80]. The construction of Bogoliubov quasi-particles can be seen as a realization of the BCS formalism within QCD.

However, this ansatz has certain limitations. Since the wave functional (3.2) does not take a coupling to transverse gluon fields into account, the part of the single-particle Hamiltonian H_{F}, Eq. (1.25), which couples the quarks to the transverse gluon fields - the last term in Eq. (1.29) - cannot be accessed: the corresponding expectation value is zero. As a consequence, chiral parameters of the theory result too small [80].

In this work we improve the BCS-type wave functional (3.2) and explicitly take the coupling to gluons into account. We suggest the following general ansatz for the quark vacuum wave functional,

$$|\phi\rangle = \mathcal{N}_{\mathrm{F}} \exp\left[- \int đ^3p\, đ^3q \sum_{s,t} K^{ab}(\boldsymbol{p},s;\boldsymbol{q},t) a^{\dagger a}(\boldsymbol{p},s) b^{\dagger b}(\boldsymbol{q},t) \right] \Big|0\Big\rangle \,, \tag{3.3}$$

where the kernel K will be specified below to consist of two parts: the BCS part, Eq. (3.2), and a part which couples the transverse gauge field to the quark-antiquark pairs. For the following considerations we give the adjoint vacuum state

$$\langle\phi| = \mathcal{N}_{\mathrm{F}}^* \Big\langle 0\Big| \exp\left[- \int đ^3p\, đ^3q \sum_{s,t} \overline{K}^{ba}(\boldsymbol{q},t;\boldsymbol{p},s) b^b(\boldsymbol{q},t) a^a(\boldsymbol{p},s) \right] \,, \tag{3.4}$$

where $\overline{K}$ denotes the complex-conjugate kernel. The coordinate-space representation of the wave functional (3.3) is

$$|\phi\rangle = \mathcal{N}_{\mathrm{F}} \exp\left[- \int d^3x\, d^3y\, \psi_+^{\dagger a}(\boldsymbol{x}) K^{ab}(\boldsymbol{x},\boldsymbol{y}) \psi_-^b(\boldsymbol{y}) \right] \Big|0\Big\rangle \,, \tag{3.5}$$

where we have used the definitions (1.41) and (1.42).

It is natural to consider the full QCD vacuum as a direct product of gluon and fermion wave functionals

$$|\Phi\rangle = \mathcal{N}\left(|\phi\rangle_{\mathrm{F}} \otimes |\psi\rangle_{\mathrm{G}}\right) \ , \tag{3.6}$$

where for the Yang-Mills vacuum $|\psi\rangle_{\mathrm{G}}$ we use the Gaussian-type wave functional, Eq. (1.86), and $\mathcal{N}$ is an overall normalization. With this ansatz, Eq. (3.6), we can, in principle, explore the full QCD system, i.e., all parts of the Coulomb gauge-fixed Hamiltonian, Eqs. (1.25),(1.75),(1.76), can be accessed. However, in the variational analysis in Chapters 4 and 5 we will keep the gluon kernel fixed and vary with respect to the quark kernels only.

3.2 Representation in Terms of Coherent Fermion States

In principle we could follow the framework of Refs. [78, 80] and extend the BCS quasiparticle picture by using generalized Bogoliubov transformations, which can be found in Ref. [75]. However, we will follow here Ref. [81] and use a more elegant way introducing coherent fermion states, which allow us to construct a generating functional in terms of Grassmann fields and to apply the Dyson-Schwinger technique to the correlation functions of the theory.

We start with defining coherent fermion states as eigenstates of the annihilation operators

$$a^a(\boldsymbol{p},s)|\xi_+,\xi_-^*\rangle = \xi_+^a(\boldsymbol{p},s)|\xi_+,\xi_-^*\rangle \ , \tag{3.7}$$
$$b^a(\boldsymbol{p},s)|\xi_+,\xi_-^*\rangle = \xi_-^{*a}(\boldsymbol{p},s)|\xi_+,\xi_-^*\rangle \ , \tag{3.8}$$

with the coherent fermion states being of the form

$$|\xi\rangle \equiv |\xi_+,\xi_-^*\rangle = \exp\left(\int \bar{d}^3p \sum_s \left[a^{\dagger a}(\boldsymbol{p},s)\xi_+^a(\boldsymbol{p},s) + b^{\dagger a}(\boldsymbol{p},s)\xi_-^{*a}(\boldsymbol{p},s)\right]\right)\Big|0\Big\rangle \ , \tag{3.9}$$

which can be easily proven by expanding the exponential using the nilpotency condition of Grassmann fields. The adjoint coherent state reads

$$\langle\xi| \equiv \langle\xi_+^*,\xi_-| = \Big\langle 0\Big|\exp\left(\int \bar{d}^3p \sum_s \left[\xi_+^{*a}(\boldsymbol{p},s)a^a(\boldsymbol{p},s) + \xi_-^a(\boldsymbol{p},s)b^a(\boldsymbol{p},s)\right]\right) \ , \tag{3.10}$$

satisfying

$$\langle\xi|a^{\dagger a}(\boldsymbol{p},s) = \langle\xi|\xi_+^{*a}(\boldsymbol{p},s) \ , \tag{3.11}$$
$$\langle\xi|b^{\dagger a}(\boldsymbol{p},s) = \langle\xi|\xi_-^a(\boldsymbol{p},s) \ . \tag{3.12}$$

In the basis of the coherent fermion states the vacuum wave functional (3.3) and its adjoint (3.4) are represented as

$$\phi[\xi] = \langle \xi | \phi \rangle = \exp\left[- \int đ^3p \, đ^3q \sum_{s,t} \left(K(\boldsymbol{p}, s; \boldsymbol{q}, t) \right)^{ab} \xi_+^{*a}(\boldsymbol{p}, s) \xi_-^b(\boldsymbol{q}, t) \right] , \quad (3.13)$$

$$\phi^*[\xi] = \langle \phi | \xi \rangle = \exp\left[- \int đ^3q \, đ^3p \sum_{t,s} \left(\overline{K}(\boldsymbol{q}, t; \boldsymbol{p}, s) \right)^{ba} \xi_-^{*b}(\boldsymbol{q}, t) \, \xi_+^a(\boldsymbol{p}, s) \right] , \quad (3.14)$$

with the bare vacuum being $\langle \xi | 0 \rangle = 1$.

3.3 Generating Functional for Fermion Fields

In order to evaluate various n-point functions as derivatives with respect to fermion sources, which we denote as η, we define the generating functional of fermion fields by

$$Z[\eta] \equiv Z[\eta_+^*, \eta_-^*; \eta_+, \eta_-] = \mathcal{N}_{\mathrm{F}}^2 \langle \phi | e^{\left(\eta_+^* a + \eta_- b \right)} \, e^{\left(a^\dagger \eta_+ + b^\dagger \eta_-^* \right)} | \phi \rangle , \quad (3.15)$$

where all occuring indices are implicitly summed over. From this key definition we derive a functional integral representation of the generating functional in terms of Grassmann fields (3.15) using the coherent fermion basis, see Appendix B. Here we quote the result (B.7),

$$Z[\Lambda^\dagger, \Lambda] = \mathcal{N}_{\mathrm{F}}^2 \, \mathsf{Det}[\Omega[A]] \, e^{\Lambda^\dagger \Omega^{-1} \Lambda} . \quad (3.16)$$

where we have used a compact matrix notation for the source terms

$$\Lambda = \begin{pmatrix} \eta_+ \\ -\eta_- \end{pmatrix} , \quad (3.17)$$

and the kernels $\Omega[A]$ and $\Omega^{-1}[A]$ are explicitly given as

$$\Omega[A] = \begin{pmatrix} \mathbb{1} & K[A] \\ \overline{K}[A] & -\mathbb{1} \end{pmatrix} , \quad \Omega^{-1}[A] = \begin{pmatrix} \left[\mathbb{1} + K\overline{K} \right]^{-1} & \left[\mathbb{1} + K\overline{K} \right]^{-1} K \\ \left[\mathbb{1} + \overline{K}K \right]^{-1} \overline{K} & -\left[\mathbb{1} + \overline{K}K \right]^{-1} \end{pmatrix} . \quad (3.18)$$

From the definition of the full QCD generating functional

$$Z[j, \eta] = \mathcal{N}^2 \langle \Phi | e^{j_i A_i} e^{\left(\eta_+^* a + \eta_- b \right)} \, e^{\left(a^\dagger \eta_+ + b^\dagger \eta_-^* \right)} | \Phi \rangle , \quad (3.19)$$

where $\mathcal{N}$ is the overall normalization and j_i denote the bosonic sources, we then are left with an integral over the transverse gauge field, reading

$$Z[j, \Lambda^\dagger, \Lambda] = \int DA \, \mathcal{J}[A] |\psi(A)|^2 \, \exp\left[j_i A_i \right] \, \mathcal{N}_{\mathrm{F}}^2 \, \mathsf{Det}[\Omega[A]] \, \exp\left[\Lambda^\dagger \Omega^{-1}[A] \Lambda \right] . \quad (3.20)$$

Lorentz indices are explicitly, and all other indices are implicitly understood. Using the Gaussian ansatz (1.86) for the Yang-Mills ground state, the Faddeev-Popov determinant $\mathcal{J}[A]$, Eq. (1.73), entering the functional integral cancels. However, due to the presence of the gauge-field dependent determinant $\mathsf{Det}[\Omega[A]]$ and the inverse kernel $\Omega^{-1}[A]$, Eq. (3.18), the gluonic path integral can no longer be performed exactly and we have to resort to certain approximations.

We turn to the issue of normalization. As a first approximation we demand that $\langle 1\rangle_{\rm F} = 1$ and $\langle 1\rangle_{\rm G} = 1$, so that we have

$$\mathcal{N}|\Phi\rangle = \mathcal{N}_{\rm F}|\phi\rangle \otimes \mathcal{N}_{\rm G}|\psi\rangle \ , \tag{3.21}$$

with

$$\mathcal{N}_{\rm F}^{-2}[A] = \mathsf{Det}[\Omega[A]], \qquad \mathcal{N}_{\rm G}^{2} = \sqrt{\mathsf{Det}[\omega]} \ , \tag{3.22}$$

where we have used Gaussian integration for fermion and boson fields. Below we show that this approximation corresponds to what is called in lattice gauge theory quenched approximation. We will clarify the physical interpretation of this approximation. When investigating the back-reaction of fermions on the gluon sector we will have to weaken the assumption (3.21) and expand the fermion determinant in powers of the gauge field. This is currently under investigation. Note, however, that although the determinant $\mathsf{Det}[\Omega[A]]$ in (3.20) now cancels, the path integral over the gauge field can not be performed exactly, due to the inverse kernel $\Omega^{-1}[A]$, Eq. (3.18). We are left with

$$Z[j,\Lambda^\dagger,\Lambda] = \int DA \, \exp\left[-A_i\omega_{ij}A_j + j_iA_i\right] \exp\left[\Lambda^\dagger\Omega^{-1}[A]\Lambda\right] \ . \tag{3.23}$$

The approximations in order to evaluate the gluon path integral are part of Sect. 3.5.

In order to clarify the meaning of Eq. (3.21), let us set the Hamiltonian approach in correspondence with the usual Lagrangian euclidean path integral approach, in which correlation functions of field operators are computed via

$$\langle \mathcal{O}[\psi^\dagger,\psi,A]\rangle = \frac{1}{Z}\int DA e^{-S_{\rm G}[A]} \int D\psi^\dagger D\psi e^{-S_{\rm F}[\psi^\dagger,\psi,A]}\mathcal{O}[\psi^\dagger,\psi,A] \ , \tag{3.24}$$

with $Z = \int DA\, e^{-S_{\rm G}[A]} \int D\psi^\dagger D\psi\, e^{-S_{\rm F}[\psi^\dagger,\psi,A]}$ denoting the normalization. The fermion part of the partition function

$$Z_{\rm F} = \int D\psi^\dagger D\psi e^{-S_{\rm F}[\psi^\dagger,\psi,A]} = \mathsf{Det}[\mathcal{D}] \ , \tag{3.25}$$

yields the determinant of the (Euclidean) Dirac operator $\mathcal{D} = \gamma_\mu\partial_\mu$, referred to as *fermion determinant*, and corresponds to $\mathsf{Det}[\Omega[A]]$ in Ref. (3.20). From this it follows that the normalization (3.22) corresponds to setting $\mathsf{Det}[\mathcal{D}] = 1$ in Eq. (3.24), which is in lattice field theory called quenched approximation[1]. It can be considered as the limit,

[1] On the lattice it means that, for instance, the quark propagator is evaluated on gauge configurations of pure Yang-Mills theory [82]. In the Dyson-Schwinger approach unquenching is implemented by adding a quark loop in the gluon Dyson-Schwinger equation [83].

in which the sea quarks (i.e., quarks which are created and annihilated in the vacuum), are infinitely heavy and cannot be generated from the vacuum, see Ref. [82]. Recent Dyson-Schwinger studies, Ref. [84], indicate that the effect of such virtual pairs of quarks and anti-quarks from the vacuum on hadronic observables is small[2].

From Eqs. (3.20) and (3.24) we can identify

$$e^{-S_{\mathrm{G}}[A]} = \mathcal{J}^{-1}[A]\,|\psi[A]|^2 \ , \tag{3.26}$$

$$e^{-S_{\mathrm{F}}[\psi^\dagger,\psi,A]} = |\phi[\xi^*,\xi,A]|^2 \ . \tag{3.27}$$

The action of the bosonic and fermionic part of the theory in coordinate space reads

$$S_{\mathrm{G}}[A] = \int d^3x d^3y\, A_i^a(\boldsymbol{x})\omega(\boldsymbol{x},\boldsymbol{y})A_i^a(\boldsymbol{y}) \ , \tag{3.28}$$

$$S_{\mathrm{F}}[\psi^\dagger,\psi,A] = \int d^3x d^3y\, \psi_+^\dagger(\boldsymbol{x})\Omega[A](\boldsymbol{x},\boldsymbol{y})\psi_-(\boldsymbol{y}) \ . \tag{3.29}$$

For later use we separate the fermionic and gauge field part of the expectation value and write

$$\langle \ldots \rangle = \langle \langle \ldots \rangle_{\mathrm{F}} \rangle_{\mathrm{G}} \ , \tag{3.30}$$

which means that we first of all take the expectation value in the fermion sector and subsequently in the Yang-Mills sector.

We go ahead with identifying expectation values in the fermion sector $\langle \ldots \rangle_{\mathrm{F}}$ as derivatives of the sources η. As an example we compute the expectation value $\langle aa^\dagger \rangle$. In Eq. (3.15) we identify the derivatives η_+^* and η_+ to belong to the fermion operators a and $a^\dagger$, respectively. In Eq. (3.16), or correspondingly Eq. (B.9), we identify the first entry in $\Omega^{-1}[A]$, Eq. (3.18) to belong to these derivatives. We arrive at

$$\langle a^a(\boldsymbol{p},s)a^{\dagger b}(\boldsymbol{q},t)\,\rangle_{\mathrm{F}} = -\frac{\delta^2 Z[\eta]}{\delta\eta_+^{*a}(\boldsymbol{p},s)\,\delta\eta_+^b(\boldsymbol{q},t)}\Big|_{\eta=0} = \left(\left[\mathbb{1} + K\overline{K}\right]^{-1}\right)^{ab}(\boldsymbol{p},s;\boldsymbol{q},t) \ . \tag{3.31}$$

A list of all occurring two-point functions is given in Eqs. (B.10) to (B.15). We are going to use these expectation values extensively throughout the next chapters.

In the end, we stress that Ω, as well as Ω^{-1}, Eq. (3.18), can be shown to be manifestly Hermitian, see Appendix B. The eigenvalues come in complex conjugate pairs and the determinants are real.

3.4 Wave Functional Kernels

Up to now we have considered a general interaction kernel K, see Eq. (3.3). As already mentioned in Section 3.1 we specify the kernel K to consist of two parts

$$K(A) = K_0 + K_1(A) \ , \tag{3.32}$$

[2]Note, however, that unquenching has some impact on the intermediate momentum region of the gluon propagator, Ref. [83], which can be related to the color screening effect of the sea quarks, as opposed to color anti-screening, which comes from the gluon self-energy.

with the first part K_0 being the BCS-part, Eq. (3.2), and the second part K_1 containing the transverse gluon field. Moreover, we assume the kernels K_0 and K_1 to have precisely the color- and Dirac structure of the single-particle Hamiltonian H_{F}, Eq. (1.25). For the field operators $a^\dagger(\boldsymbol{p}), b^\dagger(\boldsymbol{p})$ appearing in the vacuum wave functional, Eq. (3.3), the single-particle Hamiltonian H_{F} can be expressed as

$$\int d^3x\, \psi_+^{\dagger a}(\boldsymbol{x}) h^{ab}(\boldsymbol{x}) \psi_-^b(\boldsymbol{x}) = \int đ^3p\, đ^3q \frac{1}{2\sqrt{|\boldsymbol{p}||\boldsymbol{q}|}} \sum_{s,t} a^{\dagger a}(\boldsymbol{p},s) u^\dagger(\boldsymbol{p},s) h^{ab}(\boldsymbol{p}+\boldsymbol{q}) b^{\dagger b}(\boldsymbol{q},t) v(\boldsymbol{q},t)\ , \tag{3.33}$$

with the Dirac matrix $h(\boldsymbol{p}+\boldsymbol{q})$ taking into account the interaction with transverse gluons, Eq. (1.29), is explicitly given as

$$h^{ab}(\boldsymbol{p}+\boldsymbol{q}) = \beta\, m\, \delta(\boldsymbol{p}+\boldsymbol{q}) \delta^{ab} - \alpha_i A_i^m(\boldsymbol{p}+\boldsymbol{q})\, (T^m)^{ab}\ . \tag{3.34}$$

Here we ignored the kinetic part of the quarks, i.e., the first term in Eq. (1.29), which is chirally symmetric and will not enter the variational wave functional (3.3).

The BCS part K_0 in Eq. (3.32) has the Dirac- and color structure of the mass term in Eq. (3.34). The choice is clear: A mass term in the wave functional, Eq. (3.3), breaks chiral symmetry, which goes in hand with the notion of dynamical symmetry breaking. The vacuum state (3.3) does not share the (chiral) symmetry of the Hamiltonian and fulfills the condition (2.18). With this choice the kernel K_0 assumes the form

$$K_0^{ab}(\boldsymbol{p},s;\boldsymbol{q},t) = \frac{1}{2\sqrt{|\boldsymbol{p}||\boldsymbol{q}|}} S(\boldsymbol{p})\, u^\dagger(\boldsymbol{p},s) \beta v(\boldsymbol{q},t) (2\pi)^3 \delta(\boldsymbol{p}+\boldsymbol{q}) \delta_{st}\, \delta^{ab}\ . \tag{3.35}$$

Plugging in this ansatz into Eq. (3.3) we arrive at the BCS type wave functional (3.2). We refer to the dimensionless variational function S as *scalar* variational function. Using the spinor relation (A.38), the BCS-type of wave functional (3.2) can be rewritten as [78, 80]

$$|\phi\rangle = \mathcal{N} \exp\left[- \int đ^3p \sum_s s\, S(\boldsymbol{p}) a^{\dagger a}(\boldsymbol{p},s) b^{\dagger a}(-\boldsymbol{p},s) \right] \Big| 0 \Big\rangle\ , \tag{3.36}$$

with s denoting the helicity eigenvalue.

We proceed with determining the part K_1 in Eq. (3.32) which couples the fermion fields to the transverse gluon field. From the Dirac matrix $h^{ab}(\boldsymbol{p}+\boldsymbol{q})$, Eq. (3.34), we read off the Dirac and color structure of the term coupling the quarks to the transverse gluons. We choose the quark-gluon vertex in the wave functional to be of the form[3]

$$K_1^{ab}(\boldsymbol{p},s;\boldsymbol{q},t) = (K_i^m)^{ab}\, (\boldsymbol{p},s;\boldsymbol{q},t) A_i^m(\boldsymbol{p}+\boldsymbol{q}) = = \frac{1}{2\sqrt{|\boldsymbol{p}||\boldsymbol{q}|}} V(\boldsymbol{p},\boldsymbol{q}) u^\dagger(\boldsymbol{p},s) \alpha_i\, (T^m)^{ab}\, v(\boldsymbol{q},t) A_i^m(\boldsymbol{p}+\boldsymbol{q})\ . \tag{3.37}$$

[3] In general, we could include more complex Dirac tensor structures in the ansatz for the quark-gluon vertex. This has been done in three-dimensional QED in Landau gauge, Ref. [85], and in four-dimensional QCD in Landau gauge, Ref. [86].

We name the variational function $V(\boldsymbol{p},\boldsymbol{q})$ *vectorial* variational function and clearly distinguish from the spinor solution $v(\boldsymbol{q},t)$ whenever appropriate. It has dimension of inverse momentum, i.e., $[V(\boldsymbol{p},\boldsymbol{q})] = \mathrm{GeV}^{-1}$, see Appendix B.4 for a detailed dimensional analysis.

The adjoint kernels are given as

$$\overline{K}_0^{ba}(\boldsymbol{q},t;\boldsymbol{p},s) = \frac{1}{2\sqrt{|\boldsymbol{p}||\boldsymbol{q}|}} S^*(\boldsymbol{q})\, v^\dagger(\boldsymbol{q},t)\beta u(\boldsymbol{p},s)(2\pi)^3\delta(\boldsymbol{q}+\boldsymbol{p})\delta_{ts}\,\delta^{ba} \tag{3.38}$$

$$\begin{aligned}\overline{K}_1^{ba}(\boldsymbol{q},t;\boldsymbol{p},s) &= \left(\overline{K}_i^m\right)^{ba}(\boldsymbol{q},t;\boldsymbol{p},s)A_i^m(-\boldsymbol{q}-\boldsymbol{p}) = \\ &= \frac{1}{2\sqrt{|\boldsymbol{p}||\boldsymbol{q}|}} V^*(\boldsymbol{q},\boldsymbol{p})v^\dagger(\boldsymbol{q},t)\alpha_i\,(T^m)^{ba}\,u(\boldsymbol{p},s)A_i^m(-\boldsymbol{q}-\boldsymbol{p})\;,\end{aligned} \tag{3.39}$$

where we have used $(\overline{u}v)^\dagger = \overline{v}u$, $(\overline{u}\gamma_i v)^\dagger = \overline{v}\gamma_i u$, and $A^*(\boldsymbol{k}) = A(-\boldsymbol{k})$.

3.5 Expectation Value in the Gluon Sector

As already discussed in Section 3.3, due to the presence of the inverse kernel $\Omega^{-1}[A]$, Eq. (3.18), the gluonic path integral (3.23)

$$Z[j,\Lambda^\dagger,\Lambda] = \int DA\, \exp\left[-A_i\omega_{ij}A_j + j_iA_i\right] \exp\left[\Lambda^\dagger\Omega^{-1}[A]\Lambda\right] \tag{3.40}$$

can not be performed exactly. As a first approximation in the gluon sector we ignore this gauge-field dependence and evaluate the QCD generating functional as

$$Z[j,\Lambda^\dagger,\Lambda] \approx \exp\left[\frac{1}{4}\int đ^3p\, j_i^a(\boldsymbol{p})t_{ij}(\boldsymbol{p})\delta^{ab}\omega^{-1}(\boldsymbol{p})j_j^b(-\boldsymbol{p})\right] \exp\left[\Lambda^\dagger\Omega^{-1}\Lambda\right]\;, \tag{3.41}$$

where we have used Eq. (1.88). This approximation is again consistent with the quenched approximation, i.e., we ignore the back-reaction of quarks on the Yang-Mills vacuum. Now we assume that we have evaluated the fermionic part of a given expectation value using Eqs. (B.10)-(B.15). Such an expectation value is, in general, of the form

$$\langle\ldots\rangle = \langle\ldots(1+\overline{K}K)^{-1}\ldots\rangle_{\mathrm{G}}\;, \tag{3.42}$$

which can, due to the inverse kernels K and $\overline{K}$ not be performed according to Eq. (3.41). We therefore use the following approximation to handle the gluon expectation values

$$\langle\ldots(1+\overline{K}K)^{-1}\ldots\rangle_{\mathrm{G}} \approx \langle\ldots(1+\langle\overline{K}K\rangle_{\mathrm{G}})^{-1}\ldots\rangle_{\mathrm{G}}\,. \tag{3.43}$$

Hence, we replace the denominators in the expressions (B.10)-(B.15) by their expectation values in the gluon vacuum.

Throughout the next chapters we extensively need expectation values of the form $\langle\overline{K}K\rangle$ and $\langle K\overline{K}\rangle$, which appear in the denominator of all occurring two-point functions

(B.10)-(B.15). From the key definitions (3.35) and (3.37) we find

$$\begin{aligned}\left\langle \left(\overline{K}K\right)^{ab}(\boldsymbol{p},s;\boldsymbol{q},t)\right\rangle &= \left\langle \left(\left(\overline{K}_0+\overline{K}_1\right)\left(K_0+K_1\right)\right)^{ab}(\boldsymbol{p},s;\boldsymbol{q},t)\right\rangle \\ &= \left[S^*(\boldsymbol{p})S(-\boldsymbol{p})+R(\boldsymbol{p})\right]\delta(\boldsymbol{p}-\boldsymbol{q})\delta^{ab}\delta_{st}\ , \qquad (3.44)\\ \left\langle \left(K\overline{K}\right)^{ab}(\boldsymbol{p},s;\boldsymbol{q},t)\right\rangle &= \left\langle \left(\left(K_0+K_1\right)\left(\overline{K}_0+\overline{K}_1\right)\right)^{ab}(\boldsymbol{p},s;\boldsymbol{q},t)\right\rangle \\ &= \left[S(\boldsymbol{p})S^*(-\boldsymbol{p})+\overline{R}(\boldsymbol{p})\right]\delta(\boldsymbol{p}-\boldsymbol{q})\delta^{ab}\delta_{st}\ , \qquad (3.45)\end{aligned}$$

with $R(\boldsymbol{p}),\overline{R}(\boldsymbol{p})$ specified below. The contributions $\langle\overline{K}_0K_0\rangle$ and $\langle K_0\overline{K}_0\rangle$ can immediately be read off from the basic definition (3.35) and (3.38). Terms of the form $\langle K_0K_i\rangle$ vanish, since $\langle A\rangle_{\rm G}=0$. The contribution $\langle K_1\overline{K}_1\rangle$ is computed in Appendix B.2 to give (using the definitions (B.30), (B.31))

$$R(\boldsymbol{p}) = C_F\int đ^3q\, V^*(\boldsymbol{p},\boldsymbol{q})V(\boldsymbol{q},\boldsymbol{p})\,D(\boldsymbol{\ell})\left[1+(\hat{\boldsymbol{p}}\cdot\hat{\boldsymbol{\ell}})\,(\hat{\boldsymbol{q}}\cdot\hat{\boldsymbol{\ell}})\right]\ , \qquad (3.46)$$

$$\overline{R}(\boldsymbol{p}) = C_F\int đ^3q\, V(\boldsymbol{p},\boldsymbol{q})V^*(\boldsymbol{q},\boldsymbol{p})\,D(\boldsymbol{\ell})\left[1+(\hat{\boldsymbol{p}}\cdot\hat{\boldsymbol{\ell}})\,(\hat{\boldsymbol{q}}\cdot\hat{\boldsymbol{\ell}})\right]\ , \qquad (3.47)$$

with $\boldsymbol{\ell}=\boldsymbol{p}-\boldsymbol{q}$, $D(\boldsymbol{\ell})=1/(2\omega(\boldsymbol{\ell}))$ the spatial gluon propagator, Eq. (1.89), and the Casimir factor $C_F=(N_{\rm C}^2-1)/(2N_{\rm C})$, Eq. (1.7), coming from the trace in color space. We stress that the quantity $R(\boldsymbol{p})$ will enter the definition of the chiral condensate and the dynamical mass, see Section 3.7.

For later use we quote the derivative of (3.46) with respect to the vectorial variational function V

$$R'(\boldsymbol{p};\boldsymbol{k},\boldsymbol{k}') \equiv \frac{\delta R(\boldsymbol{p})}{\delta V(\boldsymbol{k},\boldsymbol{k}')} = V^*(\boldsymbol{k},\boldsymbol{k}')X(\boldsymbol{k},\boldsymbol{k}')\delta(\boldsymbol{p}-\boldsymbol{k})\ , \qquad (3.48)$$

having used the definition

$$X(\boldsymbol{k},\boldsymbol{k}') = C_F\,\frac{D(\boldsymbol{\ell})}{(2\pi)^3}\left[1+(\hat{\boldsymbol{k}}\cdot\hat{\boldsymbol{\ell}})\,(\hat{\boldsymbol{k}}'\cdot\hat{\boldsymbol{\ell}})\right]\ ,\quad \boldsymbol{\ell}=\boldsymbol{k}-\boldsymbol{k}'\ . \qquad (3.49)$$

In Appendix B.3 we show that the approximation in the gluonic expectation value, Eq. (3.43), leads to the following assumptions on the variational kernels

$$S(\boldsymbol{p})=S(-\boldsymbol{p})\ ,\quad V(\boldsymbol{p},\boldsymbol{q})=V(\boldsymbol{q},\boldsymbol{p})\ ,\quad \overline{R}(\boldsymbol{p})=R(\boldsymbol{p})\ ,\quad R(-\boldsymbol{p})=R(\boldsymbol{p})\ . \qquad (3.50)$$

At the end, let us make a comment on performing the path integrals (3.20). Instead of taking the expectation value in the fermionic part first, we could, in principle, carry out the bosonic integral (explicitly denoting Lorentz indices)

$$\begin{aligned}Z[j,\Lambda,\Lambda^\dagger] = \mathcal{N}_{\rm G}^2\int DA\exp\left[-A_i^a\omega_{ij}^{ab}A_j^b+j_i^aA_i^a\right]& \\ \int D\Psi^\dagger D\Psi\mathcal{N}_{\rm F}^2\exp\left[-\Psi^\dagger\Omega\Psi+\Psi^\dagger\Lambda+\Lambda^\dagger\Psi\right]\ ,& \qquad (3.51)\end{aligned}$$

and end up with a purely fermionic path integral

$$Z[j,\Lambda,\Lambda^\dagger] = \int D\Psi^\dagger D\Psi\, \mathcal{N}_{\mathrm{F}}^2 \exp\left[\frac{1}{4}(j_i^a - \Psi^\dagger\Omega_i^a\Psi)\left(\omega_{ij}^{ab}\right)^{-1}(j_j^b - \Psi^\dagger\Omega_j^b\Psi)\right]\times \\ \times \exp\left[-\Psi^\dagger\Omega_0\Psi + \Psi^\dagger\Lambda + \Lambda^\dagger\Psi\right], \tag{3.52}$$

where we have used the matrix notation (B.6), explicitly separated the gauge field dependent terms and used the normalization (3.22) in the Yang-Mills sector. We end up with a fermionic path integral, which again can not be performed exactly. We would have to use an approximation scheme according to Eq. (3.43) in order to evaluate the fermion expectation values. This is somewhat more difficult, since in the expression (3.52) a term appears, which is quartic in the fermion fields.

3.6 Coordinate Space Representation

As outlined in the introduction, Section 3.1, the vacuum state can be dressed in terms of coordinate-space fermion fields (3.5). In this section we set the link between coordinate-space and momentum-space kernels K. Defining the coordinate-space coherent fermion states following (3.7), (3.8) by (Ref. [81])

$$\psi_+^a(\boldsymbol{x})|\xi\rangle = \xi_+^a(\boldsymbol{x})|\xi\rangle\,, \tag{3.53}$$
$$\psi_-^{\dagger a}(\boldsymbol{x})|\xi\rangle = \xi_-^{*a}(\boldsymbol{x})|\xi\rangle\,, \tag{3.54}$$

and

$$Z[\eta] \equiv Z[\eta_+^*,\eta_-^*;\eta_+,\eta_-] = \mathcal{N}_{\mathrm{F}}^2\langle\phi|e^{\left(\eta_+^*\psi_+ + \eta_-\psi_-^\dagger\right)}\, e^{\left(\psi_+^\dagger\eta_+ + \psi_-\eta_-^*\right)}|\phi\rangle\,, \tag{3.55}$$

it is straightforward to repeat the steps from Eq. (3.9) to Eq. (3.14) and to derive the generating functional following Eqs. (B.4)-(B.7).

Next we express the projectors onto positive and negative energy components in coordinate space according to Eqs. (1.37), (1.38), (1.39) and write the exponent of the vacuum wave functional (3.5) as

$$\int d^3x \int d^3y\, \psi_+^{\dagger a}(\boldsymbol{x})K^{ab}(\boldsymbol{x},\boldsymbol{y})\psi_-^b(\boldsymbol{y}) = \\ = \int d^3x \int d^3y \int d^3z \int d^3z' \psi_+^{\dagger a}(\boldsymbol{x})\Lambda_+(\boldsymbol{x},\boldsymbol{z})K^{ab}(\boldsymbol{z},\boldsymbol{z}')\Lambda_-(\boldsymbol{z}',\boldsymbol{y})\psi_-^b(\boldsymbol{y})\,, \tag{3.56}$$

where we have used $\psi_+^\dagger = \psi_+^\dagger\Lambda_+, \psi_- = \Lambda_-\psi_-$, and correspondingly

$$\int d^3x \int d^3y\, \psi_-^{\dagger a}(\boldsymbol{x})\overline{K}^{ab}(\boldsymbol{x},\boldsymbol{y})\psi^b(\boldsymbol{y}) = \\ = \int d^3x \int d^3y \int d^3z \int d^3z' \psi_-^{\dagger a}(\boldsymbol{x})\Lambda_-(\boldsymbol{x},\boldsymbol{z})\overline{K}^{ab}(\boldsymbol{z},\boldsymbol{z}')\Lambda_+(\boldsymbol{z}',\boldsymbol{y})\psi_+^b(\boldsymbol{y})\,. \tag{3.57}$$

Without loss of generality we can assume the kernel to be of the form

$$K^{ab}(\boldsymbol{x},\boldsymbol{y}) = \int d^3z \int d^3z' \Lambda_+(\boldsymbol{x},\boldsymbol{z})\Gamma^{ab}(\boldsymbol{z},\boldsymbol{z}')\Lambda_-(\boldsymbol{z}',\boldsymbol{y}) \;, \tag{3.58}$$

with the kernel Γ consisting of two parts,

$$\Gamma^{ab}(\boldsymbol{z},\boldsymbol{z}') = \Gamma_0^{ab}(\boldsymbol{z},\boldsymbol{z}') + \int d^3z'' (\Gamma_i^m)^{ab}(\boldsymbol{z},\boldsymbol{z}';\boldsymbol{z}'') A_i^m(\boldsymbol{z}'') \;, \tag{3.59}$$

in agreement with Eq. (3.35) and Eq. (3.37). We can then set up the link to the momentum space kernels, Eqs. (3.35), (3.37) via (with the Dirac and color structure as discussed in Section 3.4)

$$\Gamma_0^{ab}(\boldsymbol{z},\boldsymbol{z}') = \delta^{ab} \int đ^3p \, e^{i\boldsymbol{p}\cdot(\boldsymbol{z}-\boldsymbol{z}')} \beta S(\boldsymbol{p}) \;, \tag{3.60}$$

$$(\Gamma_i^m)^{ab}(\boldsymbol{z},\boldsymbol{z}',\boldsymbol{z}'') = \int đ^3p \, đ^3q \, e^{i\boldsymbol{p}\cdot(\boldsymbol{z}-\boldsymbol{z}')} e^{i\boldsymbol{q}\cdot(\boldsymbol{z}''-\boldsymbol{z}')} (\Gamma_i^m)^{ab}(\boldsymbol{p},\boldsymbol{q}) \tag{3.61}$$

and obtain the interaction kernels to be of the form

$$K_0^{ab}(\boldsymbol{x},\boldsymbol{y}) = \delta^{ab} \int đ^3p \, e^{i\boldsymbol{p}\cdot(\boldsymbol{x}-\boldsymbol{y})} \Lambda_+(\boldsymbol{p}) \beta S(\boldsymbol{p}) \Lambda_-(\boldsymbol{p}) \;, \tag{3.62}$$

$$(K_i^m)^{ab}(\boldsymbol{x},\boldsymbol{y};\boldsymbol{z}) = (T^m)^{ab} \int đ^3p \, đ^3q \, e^{i\boldsymbol{p}\cdot(\boldsymbol{x}-\boldsymbol{y})} e^{iq(\boldsymbol{z}-\boldsymbol{y})} \Lambda_+(\boldsymbol{p}) \alpha_i V(\boldsymbol{p},\boldsymbol{p}+\boldsymbol{q}) \Lambda_-(\boldsymbol{p}+\boldsymbol{q}) \;, \tag{3.63}$$

with

$$K_1(\boldsymbol{x},\boldsymbol{y}) = \int d^3z \, K_i^m(\boldsymbol{x},\boldsymbol{y};\boldsymbol{z}) A_i^m(\boldsymbol{z}) \;. \tag{3.64}$$

The adjoint kernels read

$$\overline{K}_0^{ab}(\boldsymbol{x},\boldsymbol{y}) = \delta^{ab} \int đ^3p \, e^{i\boldsymbol{p}\cdot(\boldsymbol{x}-\boldsymbol{y})} \Lambda_-(\boldsymbol{p}) \beta S^*(\boldsymbol{p}) \Lambda_+(\boldsymbol{p}) \;, \tag{3.65}$$

$$\overline{K}_i^{ab}(\boldsymbol{x},\boldsymbol{y};\boldsymbol{z}) = (T^m)^{ab} \int đ^3p \, đ^3q \, e^{i\boldsymbol{p}\cdot(\boldsymbol{x}-\boldsymbol{y})} e^{-i\boldsymbol{q}(\boldsymbol{z}-\boldsymbol{x})} \Lambda_-(\boldsymbol{p}+\boldsymbol{q}) \alpha_i V^*(\boldsymbol{p}+\boldsymbol{q},\boldsymbol{p}) \Lambda_+(\boldsymbol{p}) \;. \tag{3.66}$$

3.7 Quark Propagator and Chiral Properties

We can now, as a first application, derive the physical properties of the theory – the constituent quark mass and the chiral condensate – in terms of the quark variational functions. Since the constituent quark mass is defined in terms of the dressing functions of the static quark propagator, denoted as $S^{(3)}(\boldsymbol{p})$, we first of all have to evaluate the static quark propagator in terms of the variational functions S and V, in order to

establish the connection between the dressing functions and the variational functions. In the Dyson-Schwinger approach one usually derives integral equations for the dressing functions, for an introduction to the formalism see Ref. [87]. The quark propagator thus also serves as the link between the results obtained in the variational approach and in the Dyson-Schwinger calculation.

We then put the notion of a constituent quark on theoretical foundations, defining the dynamical quark mass in terms of the dressing functions of the quark propagator. At last, we evaluate the chiral condensate $\langle\overline{\psi}\psi\rangle$ in terms of the dressing functions.

We emphasize that all results gained in this section become important throughout the work, connecting the results from the variational calculation with phenomenological predictions.

Quark Propagator

To gain insight into the formulation of the dynamical quark mass in terms of the static quark propagator[4] we start with considering the static tree-level quark propagator $S^{(3)}(\boldsymbol{p})$. It can either be evaluated in terms of the quark fields at time zero,

$$(S^{(3)})^{ab}(\boldsymbol{x}-\boldsymbol{y}) \;=\; \left\langle \Phi \left| \frac{1}{2} \left[\psi^a(\boldsymbol{x}), \overline{\psi}^b(\boldsymbol{y}) \right] \right| \Phi \right\rangle \;, \tag{3.67}$$

and explicitly making use of the bare vacuum ($|\Phi\rangle = |0\rangle$), or via the p^0-integral of the dynamical propagator $S^{(4)}(p_0,\boldsymbol{p})$, which is the inverse of the Dirac operator $\mathcal{D}(\boldsymbol{p})$, Eq. (1.1), yielding

$$\begin{aligned} S^{(3)}(\boldsymbol{p}) \;&=\; i\int \frac{dp^0}{2\pi} S^{(4)}(p_0,\boldsymbol{p}) = i\int \frac{dp^0}{2\pi} \frac{\gamma^0 p_0 - \boldsymbol{\gamma}\cdot\boldsymbol{p} + m_{\mathrm{F}}}{p_0^2 - \boldsymbol{p}^2 - m_{\mathrm{F}}^2} \\ &= \frac{1}{2}\left[\frac{m_{\mathrm{F}}}{\sqrt{m_{\mathrm{F}}^2+\boldsymbol{p}^2}}\mathbb{1} - \frac{1}{\sqrt{m_{\mathrm{F}}^2+\boldsymbol{p}^2}}\boldsymbol{\gamma}\cdot\boldsymbol{p} \right] . \end{aligned} \tag{3.68}$$

We observe that the bare static quark propagator $S^{(3)}(\boldsymbol{p})$ can be decomposed into two irreducible Lorentz tensors, the scalar mass part ($\mathbb{1}$) and the vector part ($\boldsymbol{\gamma}\cdot\boldsymbol{p}$). For chiral fermions the scalar part vanishes, and we are left with only the vector Dirac component. In terms of the quark propagator chiral symmetry breaking can be understood in the following manner: A vanishing scalar part at tree-level becomes non-vanishing for the non-perturbative propagator, thus generating the scalar mass term dynamically. The scalar part is therefore used as an order parameter of dynamical chiral symmetry breaking, Ref. [83].

We now work out the same calculation for the non-perturbative vacuum wave functional $|\Phi\rangle$, Eq. (3.6), and ask if additional Dirac components occur. We set the current

[4] Most recently lattice calculations of the quark propagator and the dynamical quark mass in Coulomb gauge have been performed, Ref. [88]. It has been shown that the static lattice quark propagator is non-perturbatively renormalizable. Moreover, it has been observed that the full four-dimensional quark propagator has a trivial energy dependence, which allows for the definition of a quark effective energy.

quark mass to zero. In order to evaluate Eq. (3.67) we Fourier-decompose the chiral quark fields, Eqs. (1.40)-(1.43), and arrive at the following momentum-space expectation values

$$\left\langle \left[a^a(\boldsymbol{p},s),a^{\dagger a}(\boldsymbol{q},t)\right]+\left[b^{\dagger a}(\boldsymbol{p},s),a^{\dagger a}(\boldsymbol{q},t)\right]+\left[a^a(\boldsymbol{p},s),b^b(\boldsymbol{q},t)\right]+\left[b^{\dagger a}(\boldsymbol{p},s),b^b(\boldsymbol{q},t)\right]\right\rangle , \tag{3.69}$$

which are easily evaluated by means of the correlation functions (B.10)-(B.15). We arrive at

$$\left\langle \left[a^a(\boldsymbol{p},s),a^{\dagger b}(\boldsymbol{q},t)\right]\right\rangle = \delta^{ab}\delta_{st}(2\pi)^3\delta(\boldsymbol{p}-\boldsymbol{q})\,\frac{1-S^*(\boldsymbol{p})S(\boldsymbol{p})-R(\boldsymbol{p})}{1+S^*(\boldsymbol{p})S(\boldsymbol{p})+R(\boldsymbol{p})}\,, \tag{3.70}$$

$$\left\langle \left[b^{\dagger a}(\boldsymbol{p},s),a^{\dagger b}(\boldsymbol{q},t)\right]\right\rangle = 2\,\delta^{ab}\delta_{st}(2\pi)^3\delta(\boldsymbol{p}+\boldsymbol{q})\frac{sS^*(\boldsymbol{p})}{1+S^*(\boldsymbol{p})S(\boldsymbol{p})+R(\boldsymbol{p})}\,, \tag{3.71}$$

$$\left\langle \left[a^a(\boldsymbol{p},s),b^b(\boldsymbol{q},t)\right]\right\rangle = 2\,\delta^{ab}\delta_{st}(2\pi)^3\delta(\boldsymbol{p}+\boldsymbol{q})\frac{sS(\boldsymbol{p})}{1+S^*(\boldsymbol{p})S(\boldsymbol{p})+R(\boldsymbol{p})}\,, \tag{3.72}$$

$$\left\langle \left[b^{\dagger a}(\boldsymbol{p},s),b^b(\boldsymbol{q},t)\right]\right\rangle = \delta^{ab}\delta_{st}(2\pi)^3\delta(\boldsymbol{p}-\boldsymbol{q})\,\frac{S^*(\boldsymbol{p})S(\boldsymbol{p})+R(\boldsymbol{p})-1}{1+S^*(\boldsymbol{p})S(\boldsymbol{p})+R(\boldsymbol{p})}\,. \tag{3.73}$$

Here we have employed the anti-commuting nature of Grassmann fields, leading to the additional factor of 2 in Eqs. (3.71) and (3.72). All expectation values are diagonal in color and spin space. Employing the spinor solutions (A.26), (A.27) and taking the variational functions to be real (which will be justified in Chapter 5), we obtain for the static quark propagator

$$\begin{aligned}(S^{(3)})^{ab}(\boldsymbol{x}-\boldsymbol{y}) =& \frac{1}{2}\delta^{ab}\int đ^3p\, e^{i\boldsymbol{p}\cdot(\boldsymbol{x}-\boldsymbol{y})}\times \\ &\times\left[\frac{2S(\boldsymbol{p})}{1+S^2(\boldsymbol{p})+R(\boldsymbol{p})}\mathbb{1}-\frac{1-S^2(\boldsymbol{p})-R(\boldsymbol{p})}{1+S^2(\boldsymbol{p})+R(\boldsymbol{p})}\boldsymbol{\gamma}\cdot\hat{\boldsymbol{p}}\right]\,.\end{aligned} \tag{3.74}$$

Like the bare quark propagator, Eq. 3.68, the dressed static quark propagator consists of a scalar ($\mathbb{1}$) and a vector Dirac component ($\boldsymbol{\gamma}\cdot\hat{\boldsymbol{p}}$). The expectation values (3.70) and (3.73) lead to the vector tensor component of the static quark propagator $S^{(3)}(\boldsymbol{p})$, and the parts (3.71), (3.72) provide the scalar piece, which is also obtained at tree-level. Setting the vector kernel in the quark vacuum wave functional to zero, i.e., $V=0$, then the gluon loop integral R, Eq. (3.46), vanishes and the result simplifies to the formula obtained in Ref. [80]. For free particles, i.e., setting $S=0$ and $V=0$ the quark propagator reduces to its bare form (3.68) in the chiral limit.

Dynamical Mass

According to the result (3.74) two irreducible Dirac components occur for the static quark propagator $S^{(3)}(\boldsymbol{p})$. We therefore use two dressing functions as an ansatz for the inverse static quark propagator

$$\left(S^{(3)}(\boldsymbol{p})\right)^{-1} = B(\boldsymbol{p})\,\mathbb{1}-A(\boldsymbol{p})\,\boldsymbol{\gamma}\cdot\hat{\boldsymbol{p}}\,, \tag{3.75}$$

with B called scalar and A vectorial dressing function, both dimensionless. The expression is easily inverted, yielding

$$S^{(3)}(\boldsymbol{p}) = \frac{B(\boldsymbol{p})\mathbb{1} + A(\boldsymbol{p})\boldsymbol{\gamma}\cdot\hat{\boldsymbol{p}}}{B^2(\boldsymbol{p}) + A^2(\boldsymbol{p})} \,. \tag{3.76}$$

The signs of the dressing functions are chosen such that for the bare static propagator (3.68) the following identification holds,

$$B(\boldsymbol{p}) \,=\, \frac{m_{\mathrm{F}}}{\sqrt{m_{\mathrm{F}}^2 + \boldsymbol{p}^2}} \,, \quad A(\boldsymbol{p}) \,=\, \frac{p}{\sqrt{m_{\mathrm{F}}^2 + \boldsymbol{p}^2}} \,. \tag{3.77}$$

We define the dynamical mass as the ratio of the scalar part to the vector part

$$M(\boldsymbol{p}) \,=\, |\boldsymbol{p}|\, \frac{B(\boldsymbol{p})}{A(\boldsymbol{p})} \,. \tag{3.78}$$

For large momenta the dynamical mass should approach the bare quark mass $M(\boldsymbol{p} \to \infty) = m_{\mathrm{F}}$, which is shown by plugging the tree-level results (3.77) into (3.78). A Dyson-Schwinger analysis in Coulomb gauge, taking into account only the instantaneous part of the temporal gluon propagator, shows that the dressing functions A and B diverge for small momenta, whereas the dynamical mass M approaches a finite result, Refs. [34, 89].

Comparing the static quark propagator $S^{(3)}(\boldsymbol{p})$ in terms of the variational functions (3.74) with the result (3.76) enables us to obtain the following identifications[5]

$$\frac{S(\boldsymbol{p})}{1 + S^2(\boldsymbol{p}) + R(\boldsymbol{p})} \,=\, \frac{B(\boldsymbol{p})}{B^2(\boldsymbol{p}) + A^2(\boldsymbol{p})} \,, \tag{3.80}$$

$$\frac{1}{2}\frac{1 - S^2(\boldsymbol{p}) - R(\boldsymbol{p})}{1 + S^2(\boldsymbol{p}) + R(\boldsymbol{p})} \,=\, \frac{A(\boldsymbol{p})}{B^2(\boldsymbol{p}) + A^2(\boldsymbol{p})} \,. \tag{3.81}$$

In terms of the variational functions the dynamically generated quark mass M, Eq. (3.78), becomes

$$M(\boldsymbol{p}) \,=\, |\boldsymbol{p}|\, \frac{2S(\boldsymbol{p})}{1 - S^2(\boldsymbol{p}) - R(\boldsymbol{p})} \,. \tag{3.82}$$

The vectorial variational function, coupling the quarks to the transverse gluons, enters this equation via $R(\boldsymbol{p})$, Eq. (3.46). Neglecting the coupling of the quarks to the transverse gluons $V = 0$, the integral $R(\boldsymbol{p})$ vanishes and the result simplifies to

$$M(\boldsymbol{p}) \,=\, |\boldsymbol{p}|\, \frac{2S(\boldsymbol{p})}{1 - S^2(\boldsymbol{p})} \,, \tag{3.83}$$

[5] For vanishing vector kernel V the relations (3.80), (3.81), yields the constraint $A^2(\boldsymbol{p}) + B^2(\boldsymbol{p}) = 4$. However, with the vector coupling V this constraint no longer holds true. With an additional gluon loop integral R in the expression (3.80)

$$\frac{S(\boldsymbol{p}) + R(\boldsymbol{p})}{1 + S^2(\boldsymbol{p}) + R(\boldsymbol{p})} \,=\, \frac{B(\boldsymbol{p})}{B^2(\boldsymbol{p}) + A^2(\boldsymbol{p})} \,, \tag{3.79}$$

we would recover the constraint $A^2(\boldsymbol{p}) + B^2(\boldsymbol{p}) = 4$.

which agrees with the formula obtained in Ref. [89].

Chiral Condensate

Finally, we consider the chiral condensate, which was introduced for a single quark flavor in Eq. (2.19) and serves as an order parameter of chiral symmetry breaking. It can either be expressed via the static quark propagator

$$\left\langle \Phi \middle| \overline{\psi}^a(\boldsymbol{x})\psi^a(\boldsymbol{x}) \middle| \Phi \right\rangle = -N_{\mathrm{C}} \int đ^3p \, \mathsf{Tr}_{\mathrm{D}} \left[S^{(3)}(\boldsymbol{p}) \right] \, , \tag{3.84}$$

where the trace is taken over Dirac indices, or by Fourier-decomposing the quark field, explicitly using the vacuum wave functional $|\Phi\rangle$, Eq. (3.3). The actual computation is straightforward and detailed in Appendix B. We quote the result

$$\left\langle \Phi \middle| \overline{\psi}^a(\boldsymbol{x})\psi^a(\boldsymbol{x}) \middle| \Phi \right\rangle = -N_{\mathrm{C}}\, 2 \int đ^3p \frac{2S(\boldsymbol{p})}{1 + S^2(\boldsymbol{p}) + R(\boldsymbol{p})} \, , \tag{3.85}$$

and stress again that the result is understood in the chiral limit.

Neglecting the coupling of the quarks to the gluons, i.e., $V = 0$, this expression reduces to

$$\left\langle \Phi \middle| \overline{\psi}^a(\boldsymbol{x})\psi^a(\boldsymbol{x}) \middle| \Phi \right\rangle = -N_{\mathrm{C}}\, 4 \int đ^3p \frac{S(\boldsymbol{p})}{1 + S^2(\boldsymbol{p})} \, , \tag{3.86}$$

which agrees with the result in Ref. [80]. In this case the chiral condensate can be expressed entirely in terms of the dynamical mass function $M(\boldsymbol{p})$, Eq. (3.82), yielding

$$\left\langle \Phi \middle| \overline{\psi}^a(\boldsymbol{x})\psi^a(\boldsymbol{x}) \middle| \Phi \right\rangle \, = \, -N_{\mathrm{C}}\, 2 \int đ^3p \, \frac{M(\boldsymbol{p})}{\sqrt{\boldsymbol{p}^2 + M^2(\boldsymbol{p})}} \, . \tag{3.87}$$

For the case with non-vanishing vectorial kernel V, no closed expression for Eq. (3.85) in terms of the dynamical mass function $M(\boldsymbol{p})$, Eq. (3.82), can be found. In the limit of the bare vacuum the gap kernels S and V are zero and the condensate vanishes.

Let us make a comment on the form of the dynamical mass, Eq. (3.82), and the chiral condensate, Eq. (3.85). The vector kernel V appears only in the denominator of the expressions (3.82) and (3.85). Moreover, the vector kernel V enters the formulae (3.82) and (3.85) only indirectly via the loop integral $R(\boldsymbol{p})$, Eq. (3.46). This could be a consequence of the approximation outlined in Eq. (3.43).

Chapter 4

Single-Particle Hamiltonian

With the new QCD vacuum wave functional, proposed in the last chapter, at hand, which goes beyond the typical BCS-type approximation and explicitly contains the coupling of the quark-antiquark pairs to the transverse spatial gluons, we can access all parts of the Coulomb gauge-fixed Hamiltonian. As a first step towards a full solution we explore the pure transverse gluon interaction in the Hamiltonian and investigate the possibility of a vacuum state realized in the Nambu-Goldstone mode.

In the first section we derive the expectation value of the single-particle Hamiltonian, i.e., the kinetic energy of the quarks and the interaction energy of transverse gluons with the color current of the quarks. In Section 2 we employ the variational principle to determine the gap equation, which we refer to as *single-particle gap equation*. In Section 3 we solve the gap equation for the unknown kernels S and V and discuss the phenomenological implications thereof.

Much of the actual computation of this chapter, especially the evaluation of the energy density, is performed in great detail in Appendix C.

4.1 Energy Densities

In the chiral limit the single-particle Hamiltonian H_{F}, Eq. (1.25), has the form

$$H_{\mathrm{F}} = \int d^3x \, \left(-i\psi^{\dagger a}(\boldsymbol{x})\boldsymbol{\alpha}\cdot\boldsymbol{\partial}\psi^{a}(\boldsymbol{x}) - g\psi^{\dagger a}(\boldsymbol{x})\boldsymbol{\alpha}\cdot\boldsymbol{A}^{ab}(\boldsymbol{x})\psi^{b}(\boldsymbol{x})\right) \equiv H_{\mathrm{D}} + H_{\mathrm{QGC}} \, , \tag{4.1}$$

with H_{D} and H_{QGC} denoting the gauge-field independent and gauge-field dependent part, respectively. The coupling g is referred to as the quark-gluon coupling constant and is the only parameter of the Hamiltonian. It will be specified at the end of the calculation. The color indices are explicitly denoted as $\boldsymbol{A}^{ab} = \boldsymbol{A}^{m}\,(T^{m})^{ab}$.

We take the expectation value of the Hamiltonian (4.1) with respect to the QCD vacuum wave functional $|\Phi\rangle$, Eq. (3.6), for both parts separately and employ the strategy outlined in the last chapter: First we take the expectation value in the fermionic state $|\phi\rangle_{\mathrm{F}}$, Eq. (3.3), and subsequently in the Yang-Mills vacuum state $|\psi\rangle_{\mathrm{G}}$, Eq. (1.86).

Dressing the quark fields in the terms of the momentum-helicity representation, Eqs. (1.40)-(1.43), results in the well-known expression for the kinetic energy of chiral

quarks

$$\langle H_{\rm D}\rangle \;=\; \left\langle \Phi\right| \int đ^3p\,|\boldsymbol{p}| \sum_s \left(a^{\dagger a}(\boldsymbol{p},s)a^a(\boldsymbol{p},s) + b^{\dagger a}(\boldsymbol{p},s)b^a(\boldsymbol{p},s)\right) \left|\Phi\right\rangle \;, \tag{4.2}$$

leading to a trace in momentum-, spin-, and color space. The evaluation of the expectation values is straightforward. Using (B.11), (B.13) for the fermionic and (3.44), (3.46) for the gluonic part and the properties (3.50) of the kernels, yields

$$\begin{aligned}\left\langle \Phi\right| a^{\dagger a}(\boldsymbol{p},s)a^a(\boldsymbol{p},s) + b^{\dagger a}(\boldsymbol{p},s)b^a(\boldsymbol{p},s) \left|\Phi\right\rangle \;=& \\ = 2\,\frac{S^*(\boldsymbol{p})S(\boldsymbol{p}) + R(\boldsymbol{p})}{1 + S^*(\boldsymbol{p})S(\boldsymbol{p}) + R(\boldsymbol{p})} \delta_{ss}\,\delta^{aa}(2\pi)^3\delta(\boldsymbol{p}-\boldsymbol{p})\;,&\end{aligned} \tag{4.3}$$

where the δ-function is the volume of space. The kinetic energy density of interaction-free quarks becomes

$$\frac{\langle\Phi|H_{\rm D}|\Phi\rangle}{\delta^3(0)} \;=\; 4\,N_{\rm C} \int d^3p\,|\boldsymbol{p}|\,\frac{S^*(\boldsymbol{p})S(\boldsymbol{p}) + R(\boldsymbol{p})}{1 + S^*(\boldsymbol{p})S(\boldsymbol{p}) + R(\boldsymbol{p})}\;. \tag{4.4}$$

The result is symmetric in the variational functions S^*, S and V^*, V, which means that replacing S by S^* or V by V^* does not alter the energy density. The factor $N_{\rm C}$ comes from the color trace and a factor of two stems from the trace in Dirac space. We underline that for the kinetic energy density only the terms $\langle\psi_+^{\dagger a}(\boldsymbol{x})\psi_+^a(\boldsymbol{x})\rangle$ and $\langle\psi_-^{\dagger a}(\boldsymbol{x})\psi_-^a(\boldsymbol{x})\rangle$ contribute. This is different for the interaction of the transverse gluons with the color current of the quarks, which is explicitly shown in Appendix C.1.

We take the expectation value $\langle H_{\rm QGC}\rangle$, Eq. (4.1), decompose the Hamiltonian in terms of its Fourier-modes and obtain two non-vanishing contributions

$$\left\langle \Phi\right| a^{\dagger a}(\boldsymbol{p},s)b^{\dagger b}(\boldsymbol{q},t)A_i^m(\boldsymbol{k}) \left|\Phi\right\rangle \;=\; \left\langle \psi\right| - \left(\left[\mathbb{1} + \overline{K}K\right]^{-1}\overline{K}\right)^{ba}(\boldsymbol{q},t;\boldsymbol{p},s)\,A_i^m(\boldsymbol{k}) \left|\psi\right\rangle_{\rm G}, \tag{4.5}$$

$$\left\langle \Phi\right| b^a(\boldsymbol{p},s)\,a^b(\boldsymbol{q},t)A_i^m(\boldsymbol{k}) \left|\Phi\right\rangle = \left\langle \psi\right| - \left(\left[\mathbb{1} + K\overline{K}\right]^{-1}K\right)^{ba}(\boldsymbol{q},t;\boldsymbol{p},s)\,A_i^m(\boldsymbol{k}) \left|\psi\right\rangle_{\rm G}, \tag{4.6}$$

which correspond to the terms $\langle\psi_+^{\dagger a}(\boldsymbol{x})\psi_-^b(\boldsymbol{x})\rangle$ and $\langle\psi_-^{\dagger a}(\boldsymbol{x})\psi_+^b(\boldsymbol{x})\rangle$ in coordinate space. The expectation values in the gluon sector are approximated according to Eq. (3.43), yielding for Eq. (4.5)

$$\left\langle \psi\right| \left(-\left[\mathbb{1} + \overline{K}K\right]^{-1}\overline{K}A\right) \left|\psi\right\rangle_{\rm G} \approx \left\langle \psi\right| \left(-\left[\mathbb{1} + \overline{K}K\right]^{-1}\right) \left|\psi\right\rangle_{\rm G} \left\langle \psi\right| \overline{K}A \left|\psi\right\rangle_{\rm G}\;. \tag{4.7}$$

The explicit computation of these expectation values is performed in Appendix C and we quote the final result for the energy density of the interaction between the quarks

and the transverse gluons

$$\frac{\langle H_{\rm QGC}\rangle}{\delta^3(0)} = \\ = 2\,g\,N_{\rm C}\,C_F\,(2\pi)^3 \int đ^3p \int đ^3q \frac{V^*(\boldsymbol{p},\boldsymbol{q})+V(\boldsymbol{p},\boldsymbol{q})}{1+S^*(\boldsymbol{p})S(\boldsymbol{p})+R(\boldsymbol{p})} D(\boldsymbol{\ell}) \left[1+(\hat{\boldsymbol{p}}\cdot\hat{\boldsymbol{\ell}})(\hat{\boldsymbol{q}}\cdot\hat{\boldsymbol{\ell}})\right] , \tag{4.8}$$

with $\boldsymbol{\ell} = \boldsymbol{p} - \boldsymbol{q}$. The expectation value is again symmetric in the variational functions S^*, S and V^*, V. In Chapter 5 we will observe that this also holds true for the Coulomb energy density. The Casimir invariant $C_F = (N_{\rm C}^2 - 1)/2N_{\rm C}$, Eq. (1.7), comes from the trace in color space and the factor of two from the trace in Dirac space. Moreover, we point out that the angular dependence of the integrand in Eq. (4.8) is typical for transverse fields.

As a consistency check we set the kernel V coupling the quarks to transverse gluons to zero, so the wave functional (3.3) becomes of BCS-type and the energy density (4.8) vanishes.

4.2 Single-Particle Quark Gap Equations

Varying the expectation values of the quark kinetic energy density (4.4) with respect to the gap functions $S(\boldsymbol{k})$ (and analogously for $S^*(\boldsymbol{k})$), yields

$$\frac{\delta}{\delta S(\boldsymbol{k})}\frac{\langle H_{\rm D}\rangle}{\delta^3(0)} = 4N_{\rm C}|\boldsymbol{k}|\frac{S^*(\boldsymbol{k})}{(1+S^*(\boldsymbol{k})S(\boldsymbol{k})+R(\boldsymbol{k}))^2} , \tag{4.9}$$

and with respect to the vectorial gap function $V(\boldsymbol{k},\boldsymbol{k}')$ we obtain (employing (3.48))

$$\begin{aligned}\frac{\delta}{\delta V(\boldsymbol{k},\boldsymbol{k}')}\frac{\langle H_{\rm D}\rangle}{\delta^3(0)} &= 4N_{\rm C}\int d^3p\,|\boldsymbol{p}|\frac{R'(\boldsymbol{p};\boldsymbol{k},\boldsymbol{k}')}{1+S^*(\boldsymbol{p})S(\boldsymbol{p})+R(\boldsymbol{p})} \\ &= 4N_{\rm C}|\boldsymbol{k}|\frac{V^*(\boldsymbol{k},\boldsymbol{k}')X(\boldsymbol{k},\boldsymbol{k}')}{(1+S^*(\boldsymbol{k})S(\boldsymbol{k})+R(\boldsymbol{k}))^2} ,\end{aligned} \tag{4.10}$$

where we have used (3.48), (3.49) and $\boldsymbol{\ell} = \boldsymbol{k} - \boldsymbol{k}'$. It is interesting to note that for the variation with respect to $V(\boldsymbol{k},\boldsymbol{k}')$, Eq. (4.10), the energy dispersion $E(\boldsymbol{k}) = |\boldsymbol{k}|$ of only one momentum occurs, and the denominator in (4.10) also depends on only one momentum, which will become important when solving the coupled integral equations. Both expressions (4.9) and (4.10) have in common that the variational functions S^* (in Eq. (4.9)) and V^* (in Eq. (4.10)) appear linearly in the numerator. Free non-interacting fermions therefore possess the trivial solutions $S(\boldsymbol{k}) = S^*(\boldsymbol{k}) = 0$ and $V(\boldsymbol{k},\boldsymbol{k}') = V^*(\boldsymbol{k},\boldsymbol{k}') = 0$. The fermion vacuum wave functional (3.3) then degenerates to the bare vacuum, i.e., $|\phi\rangle_{\rm F} = |0\rangle_{\rm F}$.

Variation of the interaction part (4.8) with respect to the scalar wave function $S(\boldsymbol{k})$ yields

$$\begin{aligned}\frac{\delta}{\delta S(\boldsymbol{k})}\frac{\langle H_{\mathrm{QGC}}\rangle}{\delta^3(0)} &= -2\,gN_{\mathrm{C}}\,C_F\,\frac{S^*(\boldsymbol{k})}{(1+S^*(\boldsymbol{k})S(\boldsymbol{k})+R(\boldsymbol{k}))^2}\times \\ &\quad\times\int đ^3q\,(V^*(\boldsymbol{k},\boldsymbol{q})+V(\boldsymbol{k},\boldsymbol{q}))\,D(\boldsymbol{\ell})\left[1+(\hat{\boldsymbol{k}}\cdot\hat{\boldsymbol{\ell}})(\hat{\boldsymbol{q}}\cdot\hat{\boldsymbol{\ell}})\right] = \\ &= -2\,g\,N_{\mathrm{C}}C_F\,\frac{S^*(\boldsymbol{k})}{(1+S^*(\boldsymbol{k})S(\boldsymbol{k})+R(\boldsymbol{k}))^2}I_\omega(\boldsymbol{k})\,, \end{aligned} \tag{4.11}$$

with $\boldsymbol{\ell}=\boldsymbol{k}-\boldsymbol{q}$. After the second equality sign we have defined the loop integral

$$I_\omega(\boldsymbol{k}) \;=\; \int đ^3q\,(V^*(\boldsymbol{k},\boldsymbol{q})+V(\boldsymbol{k},\boldsymbol{q}))\,D(\boldsymbol{\ell})\left[1+(\hat{\boldsymbol{k}}\cdot\hat{\boldsymbol{\ell}})\,(\hat{\boldsymbol{q}}\cdot\hat{\boldsymbol{\ell}})\right]\,. \tag{4.12}$$

Performing the variation of the expectation value (4.8) with respect to $V(\boldsymbol{k},\boldsymbol{k}')$ results in

$$\begin{aligned}&\frac{\delta}{\delta V(\boldsymbol{k},\boldsymbol{k}')}\frac{\langle H_{\mathrm{QGC}}\rangle}{\delta^3(0)} = \\ &= -2gN_{\mathrm{C}}C_F\frac{V^*(\boldsymbol{k},\boldsymbol{k}')X(\boldsymbol{k},\boldsymbol{k}')}{(1+S^*(\boldsymbol{k})S(\boldsymbol{k})+R(\boldsymbol{k}))^2}I_\omega(\boldsymbol{k})+2gN_{\mathrm{C}}\,\frac{X(\boldsymbol{k},\boldsymbol{k}')}{1+S^*(\boldsymbol{k})S(\boldsymbol{k})+R(\boldsymbol{k})}\,. \end{aligned} \tag{4.13}$$

The first term, emerging from the variation of the denominator in (4.8) with respect to V, has the same structure as the kinetic part (4.10). It is the second term, emerging from the variation of the nominator in (4.8) with respect to V, which establishes the non-trivial structure. Moreover, it is a remarkable fact that the terms subsumed in $X(\boldsymbol{k},\boldsymbol{k}')$, Eq. (3.49), enter the second non-trivial term, which will simplify the evaluation of the solution function a lot. Note that the Casimir invariant C_F entering (4.8) has been absorbed in the definition of $X(\boldsymbol{k},\boldsymbol{k}')$ for this term. Again, the result for the complex conjugate variational function V^* is analogous.

Now we have all ingredients to set up the coupled equations, which we refer to as *single-particle gap equations*.

4.3 Solving the Single-Particle Quark Gap Equations

Since for the single-particle Hamiltonian (4.1) the variations for S and S^* and V and V^* are analogous, we set in this section $S=S^*$ and $V=V^*$. In Chapter 5 we will show that this assumption holds true for the Coulomb interaction H_{C}, Eq. (1.76), as well.

Collecting the variations with respect to the scalar function S, Eqs. (4.9) and (4.11), we obtain the following integral equation for the variational parameter S

$$\frac{S(\boldsymbol{k})}{(1+S^2(\boldsymbol{k})+R(\boldsymbol{k}))^2}\,(8N_{\mathrm{C}}|\boldsymbol{k}|-4\,N_{\mathrm{C}}\,C_F\,gI_\omega(\boldsymbol{k}))\;=\;0\,. \tag{4.14}$$

We note that the quark-gluon vertex V, Eq. (3.37), is hidden in $I_\omega(\boldsymbol{k})$, Eq. (4.12). The equation admits the trivial solution $S(\boldsymbol{k}) = 0$, which is by no means surprising: In the case of vanishing vector kernel V the variational equation allows for the scalar variational function S the trivial solution only. The transverse gluon interaction does not provide the scalar form factor with a non-trivial part. A non-trivial solution, i.e., $S(\boldsymbol{k}) \neq 0$, leads to the constraint equation

$$8\,|\boldsymbol{k}| - 4\,C_F\,g\,I_\omega(\boldsymbol{k}) \;=\; 0\;. \tag{4.15}$$

Using (4.10) and (4.13) we attain the gap equation for the vector variational function

$$\frac{V(\boldsymbol{k},\boldsymbol{k}')X(\boldsymbol{k},\boldsymbol{k}')}{(1+S^2(\boldsymbol{k})+R(\boldsymbol{k}))^2}\,(8N_{\mathrm{C}}|\boldsymbol{k}| - 4\,g\,N_{\mathrm{C}}\,C_F\,I_\omega(\boldsymbol{k})) \;=\; -4g\,N_{\mathrm{C}}\,\frac{X(\boldsymbol{k},\boldsymbol{k}')}{1+S^2(\boldsymbol{k})+R(\boldsymbol{k})}\;, \tag{4.16}$$

which, due to the right-hand side of the equation, does not possess the trivial solution $V(\boldsymbol{k},\boldsymbol{k}') = 0$.

The pair of equations, determining the gap functions $S(\boldsymbol{k})$ and $V(\boldsymbol{k},\boldsymbol{k}')$ finally becomes

$$\frac{S(\boldsymbol{k})}{(1+S^2(\boldsymbol{k})+R(\boldsymbol{k}))^2}\,(2|\boldsymbol{k}| - g\,C_F I_\omega(\boldsymbol{k})\,) = 0\,, \tag{4.17}$$

$$\frac{V(\boldsymbol{k},\boldsymbol{k}')}{(1+S^2(\boldsymbol{k})+R(\boldsymbol{k}))^2}\,(2|\boldsymbol{k}| - g\,C_F I_\omega(\boldsymbol{k})) = -g\,\frac{1}{1+S^2(\boldsymbol{k})+R(\boldsymbol{k})}\;. \tag{4.18}$$

The term $X(\boldsymbol{k},\boldsymbol{k}')$ cancels from Eq. (4.16). Using the constraint equation (4.17) the left-hand side of (4.18) vanishes. *Consequently, no non-trivial solution for the scalar variational function $S \neq 0$ exists, as long as we neglect the Coulomb interaction.* The coupled equations (4.17) and (4.18) for the interacting theory ($g \neq 0$) cannot be solved for $S \neq 0$ and $V \neq 0$. The coupled system (4.17), (4.18) is solved with $S = 0$ only, which has important consequences on the chiral parameters of the theory. Since S appears in the numerator of the formula for the chiral condensate (3.85), this quantity vanishes. The same conclusion holds true for the dynamical quark mass, Eq. (3.82). We conclude, that a purely transverse gluon interaction does not account for a dynamically generated mass and a non-vanishing chiral condensate. This indicates that the instantaneous Coulomb interaction must be essential for the formation of a chirally non-symmetric solution, which will be verified in Chapter 5. This result is confirmed in a recent Functional Renormalization Group Flow (FRG) equation calculation, Ref. [57].

Since it is not possible to solve the coupled equations (4.17) and (4.18) for both variational functions non-trivially, we explore the possibility of a solution $S = 0, V \neq 0$. Setting $S(\boldsymbol{k}) = 0$ in Eq. (4.18) yields the following single-particle gap equation

$$V(\boldsymbol{k},\boldsymbol{k}') \;=\; -g\frac{1+R(\boldsymbol{k})}{2\,|\boldsymbol{k}| - g\,C_F\,I_\omega(\boldsymbol{k})}\;. \tag{4.19}$$

The right-hand side of the equation is independent of the momentum $\boldsymbol{k}'$. The vector kernel $V(\boldsymbol{k},\boldsymbol{k}')$ can therefore be simplified to $V(\boldsymbol{k},\boldsymbol{k}') = V(\boldsymbol{k})$. The loop integrals $I_\omega(\boldsymbol{k})$, Eq. (4.12), and $R(\boldsymbol{k})$, Eq. (3.46), become

$$I_\omega(\boldsymbol{k}) = 2\,V(\boldsymbol{k})\,I(\boldsymbol{k}), \qquad R(\boldsymbol{k}) = C_F V^2(\boldsymbol{k}) I(\boldsymbol{k}) \tag{4.20}$$

with

$$I(\boldsymbol{k}) = \int \text{đ}^3 q\, D(\boldsymbol{\ell}) \left[1 + (\hat{\boldsymbol{k}}\cdot\hat{\boldsymbol{\ell}})\,(\hat{\boldsymbol{q}}\cdot\hat{\boldsymbol{\ell}})\right], \qquad \boldsymbol{\ell} = \boldsymbol{k} - \boldsymbol{q}\,. \tag{4.21}$$

We note that the momentum $\boldsymbol{k}'$ is conjugate to the coordinate $\boldsymbol{z}''-\boldsymbol{z}'$, which can directly be seen in Eq. (3.61). In a current investigation taking the kinetic part of the Yang-Mills Hamiltonian, Eq. (1.75), into account, this simplification does not seem to hold true any longer. Hence, this simplification most likely comes from taking only certain parts of the Coulomb gauge Hamiltonian into account and ignoring, for instance, the pure Yang-Mills part H_{G}, Eq. (1.75), in the variational analysis.

Loop Integral of the Static Spatial Gluon Propagator

In principle, the gluon variational kernel $\omega(\boldsymbol{k})$, which enters the Gaussian ansatz for the Yang-Mills vacuum $\psi[A]$, Eq. (1.86), should be varied as well. However, we ignore the back-reaction of the gluon sector on the quark fields and take for $\omega(\boldsymbol{k})$ the solution found by minimizing the Yang-Mills vacuum energy, which is in good agreement with the lattice data fitted by Gribov's formula (1.95). The Gribov mass M_{G}, Eq. (1.96), sets the scale in the gap equation (4.19). For more details on the comparison between variational results and lattice measurements we refer to Section 1.6.

Plugging the Gribov formula, Eq. (1.95), into the gluon loop integral $I(\boldsymbol{k})$, Eq. (4.21), we find the integral to diverge for large momenta. Hence, before we proceed with solving the single-particle gap equation, we have to find a regularization prescription to make the integral finite in the large-momentum region.

We start with identifying the divergent terms. Taking only the UV-tail of the Gribov formula (1.95) into account, $\omega(\boldsymbol{k}) = \omega_{\mathrm{UV}}(\boldsymbol{k}) = |\boldsymbol{k}|$, the integral $I(\boldsymbol{k})$, Eq. (4.21), can be analytically performed, yielding

$$I_{\mathsf{UV}}(k) = \frac{1}{2}\frac{1}{(2\pi)^2}\left[\underbrace{\Lambda_{\mathrm{UV}}^2 - \frac{2}{3}\Lambda_{\mathrm{UV}}\,k}_{\text{divergent}} + \frac{1}{6}k^2\right] \;=\; I_{\mathsf{UV}}^{\mathsf{DIV}}(k) + I_{\mathsf{UV}}^{\mathsf{REG}}(k)\,, \tag{4.22}$$

with the momentum cut-off Λ_{UV}. After the second equality sign we have identified the divergent terms, which we omit and only take the regular part $I_{\mathsf{UV}}^{\mathsf{REG}}(k) = \frac{1}{2}\frac{1}{(2\pi)^2}\frac{1}{6}k^2$ into account.

The infrared part of the static spatial gluon propagator is incorporated as follows,

$$I_{\mathsf{IR}}(k) = \int \text{đ}^3 q \left|D(\boldsymbol{\ell}) - D_{\mathrm{UV}}(\boldsymbol{\ell})\right| \left[1 + (\hat{\boldsymbol{k}}\cdot\widehat{\boldsymbol{\ell}})\,(\hat{\boldsymbol{q}}\cdot\widehat{\boldsymbol{\ell}})\right]\,, \tag{4.23}$$

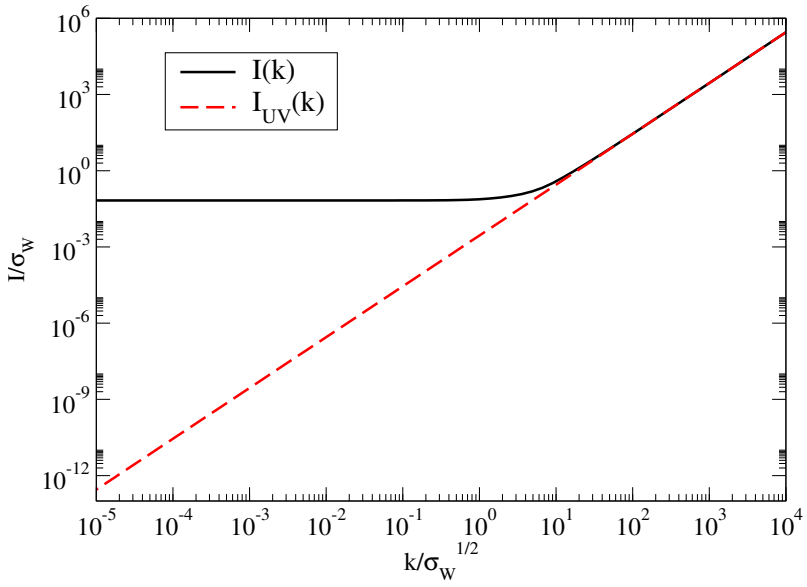

Figure 4.1: *Regularized loop integral with IR part (full line) and without (dashed line).*

with $\boldsymbol{\ell} = \boldsymbol{k} - \boldsymbol{q}$. The regularized gluon loop integral writes

$$I(k) = I_{\mathrm{IR}}(k) + I_{\mathrm{UV}}^{\mathrm{REG}}(k) \; . \tag{4.24}$$

Numerically evaluating this integral results in the following asymptotic behavior

$$k \to 0 : \qquad I(k) = \frac{1}{2}\frac{1}{(2\pi)^2} M^2 \; , \tag{4.25}$$

$$k \to \infty : \qquad I(k) = \frac{1}{2}\frac{1}{(2\pi)^2}\frac{1}{6} k^2 \; . \tag{4.26}$$

For small momenta the gluon loop integral $I(k)$ approaches a constant, essentially the Gribov mass squared M_{G}^2. In the ultraviolet region the integral $I(k)$ behaves as k^2. The full gluon loop integral is plotted in Fig. 4.1. The scale at which the constant solution builds up is set by the Gribov mass M_{G}, see Figs. 4.1, 4.2. This observation will become important when analyzing the gap equation (4.19).

We return to the gap equation (4.19), plug in the result (4.21) and set $V(\boldsymbol{k}) \to -V(\boldsymbol{k})$, so that we arrive at

$$V(\boldsymbol{k}) \; = \; \frac{g}{2}\frac{1 + C_F V^2(\boldsymbol{k}) I(\boldsymbol{k})}{|\boldsymbol{k}| + C_F g V(\boldsymbol{k}) I(\boldsymbol{k})} \; , \tag{4.27}$$

with all quantities being positive definite[1]. This gap equation has a very simple form with the gap function $V(\boldsymbol{k})$ appearing only with external momentum, which is due to

[1]We emphasize, that setting $V(\boldsymbol{k}) \to -V(\boldsymbol{k})$ changes the sign of the vector kernel V, Eq. (3.37), in the vacuum wave functional (3.3), which is then given as

$$|\Phi\rangle_{\mathrm{F}} \sim e^{-a^\dagger K_0 b^\dagger + a^\dagger K_i A_i b^\dagger} \; , \tag{4.28}$$

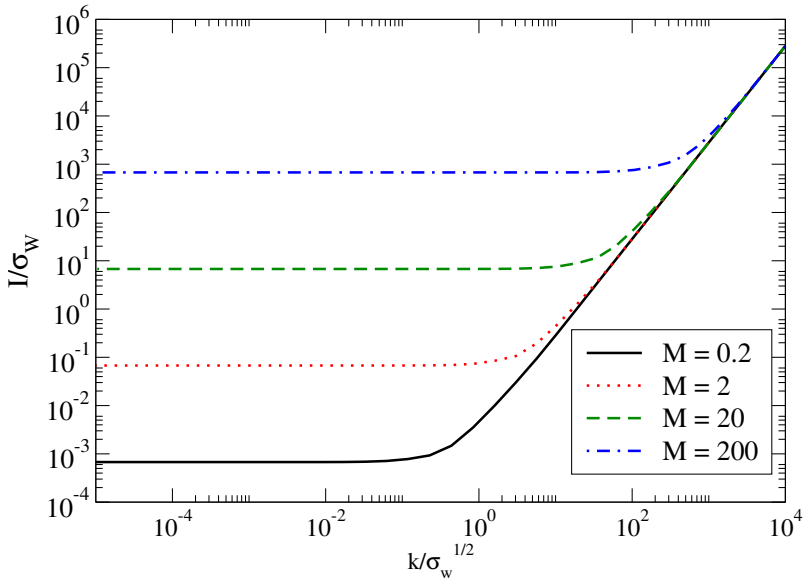

Figure 4.2: *Regularized loop integral for different Gribov mass scales* M_{G}.

the simplification $V(\boldsymbol{k},\boldsymbol{k}') = V(\boldsymbol{k})$. Numerically, the integral equation (4.27) can be rewritten as a quadratic equation and easily be solved.

Before we go ahead with studying the equation analytically and numerically, we identify the constants which appear in the gap equation. For the Casimir invariant C_F, Eq. (1.7), we take the $SU(3)$ value $C_F = 4/3$. Moreover, we replace the (running) coupling g, which was calculated in the Hamiltonian approach in Ref. [8] from the ghost-gluon vertex, by its infrared value $g \equiv g(k=0) = 8\pi/\sqrt{3N_{\mathrm{C}}}$. We stress that at first sight two scales enter the equation, the IR limit of the running coupling $g(k=0)$ and the Gribov mass M_{G}, which appears in the loop integral $I(k)$, Eq. (4.21). However, it is only the (Wilsonian) string tension, which fixes the scale and is given as $\sqrt{\sigma_{\mathrm{W}}} = 440$ MeV. The Gribov mass M_{G} is determined by the string tension, see Eq. (1.96). On the other hand, the infrared value of the running coupling $g(k=0)$ is independent of the scale.

Next we analyze the properties of the gap equation in the asymptotic regions. We start with the small momentum region, i.e., setting $k \to 0$. We assume the gap function $V(k)$ to be analytic and expand $V(k)$ as well as $I(k)$ around zero. We find the following value for the vectorial solution function V at $k = 0$,

$$V(k\to 0) \;=\; \frac{1}{2}\,\frac{1 + C_F I(k\to 0) V^2(k\to 0)}{C_F I(k\to 0) V(k\to 0)}\;, \tag{4.30}$$

where all indices are implicitly summed. We have split up the kernel K in two parts according to Eq. (3.32). Starting the variational analysis with a vector kernel K_1 of the form

$$K_1^{ab}(\boldsymbol{p},s;\boldsymbol{q},t) = -\frac{1}{2\sqrt{|\boldsymbol{p}||\boldsymbol{q}|}} V(\boldsymbol{p},\boldsymbol{q}) u^\dagger(\boldsymbol{p},s)\alpha_i \left(T^m\right)^{ab} v(\boldsymbol{q},t) A_i^m(\boldsymbol{p}+\boldsymbol{q})\;, \tag{4.29}$$

we would have ended up with the gap equation (4.27) without changing sign.

from which we obtain

$$V(k \to 0) \;=\; \pm \sqrt{\frac{1}{C_F\, I(k \to 0)}}\;, \tag{4.31}$$

where I denotes the regularized integral, Eq. (4.24). We find $V(0) = \pm 3.84765/\sqrt{\sigma_{\rm W}}$. The infrared value $V(0)$ depends on the Gribov mass $M_{\rm G}$ and the Casimir invariant C_F, but is independent of the quark-gluon coupling g. We find, for the present case of a purely transverse gluon interaction, the kernel V, coupling the quarks to the transverse gluons, to become constant in the infrared region.

We turn to the large momentum behavior of the gap equation setting $k \to \infty$. The solution of the quadratic equation can be given analytically as

$$V(k) \;=\; \frac{1}{k}\left(\frac{\sqrt{(1+Gg^2C_F)}-1}{GgC_F}\right) \approx \frac{4}{k} \qquad \text{with} \qquad G = \frac{1}{2}\frac{1}{(2\pi)^2}\frac{1}{6}\,. \tag{4.32}$$

Comparing the large-momentum behavior of V with the result obtained from perturbation theory [14] the single-particle gap equation yields the correct $1/k$ perturbative behavior. This statement will also hold true for the full solution, i.e., with taking into account the Coulomb energy density as well, from which we will conclude that the large-momentum behavior of the vectorial gap function V is driven by the transverse-gluon interaction, see Chapter 5.

Next we present the results of the numerical evaluation of the gap equation determining $V(k)$, Eq. (4.27). Note that all plots are given in units of $\sqrt{\sigma_{\rm W}}$. The asymptotic behavior (4.31), (4.32) is confirmed in the numerical evaluation. The vectorial solution function $V(k)$ freezes out for small momenta and vanishes as $1/k$ for large momenta, see Fig. 4.3. In addition, we find that the infrared constant solution builds up around the Gribov mass $M_{\rm G}$, see Figs. 4.3, 4.4. We also investigate the dependence of the solution function $V(k)$ on the coupling g, see Fig. 4.5. For decreasing g the range, in which the infrared constant value builds up, moves to smaller momenta. However, the infrared constant value $V(0)$ is independent of the coupling g, which is also observed analytically, Eq. (4.31).

In the end, let us summarize the main results of this chapter. Due to its very simple form, the single-particle gap equation (4.27) serves as a laboratory to gain insight into the behavior of the vectorial variational function, which incorporates the effect of transverse gluon fields on chiral symmetry breaking. It yields an infrared constant behavior and the power-law decrease for large momenta which agrees with perturbation theory [14]. We note that it is the Gribov mass $M_{\rm G}$, Eq. (1.96), which sets the scale at which the solution assumes the infrared plateau value.

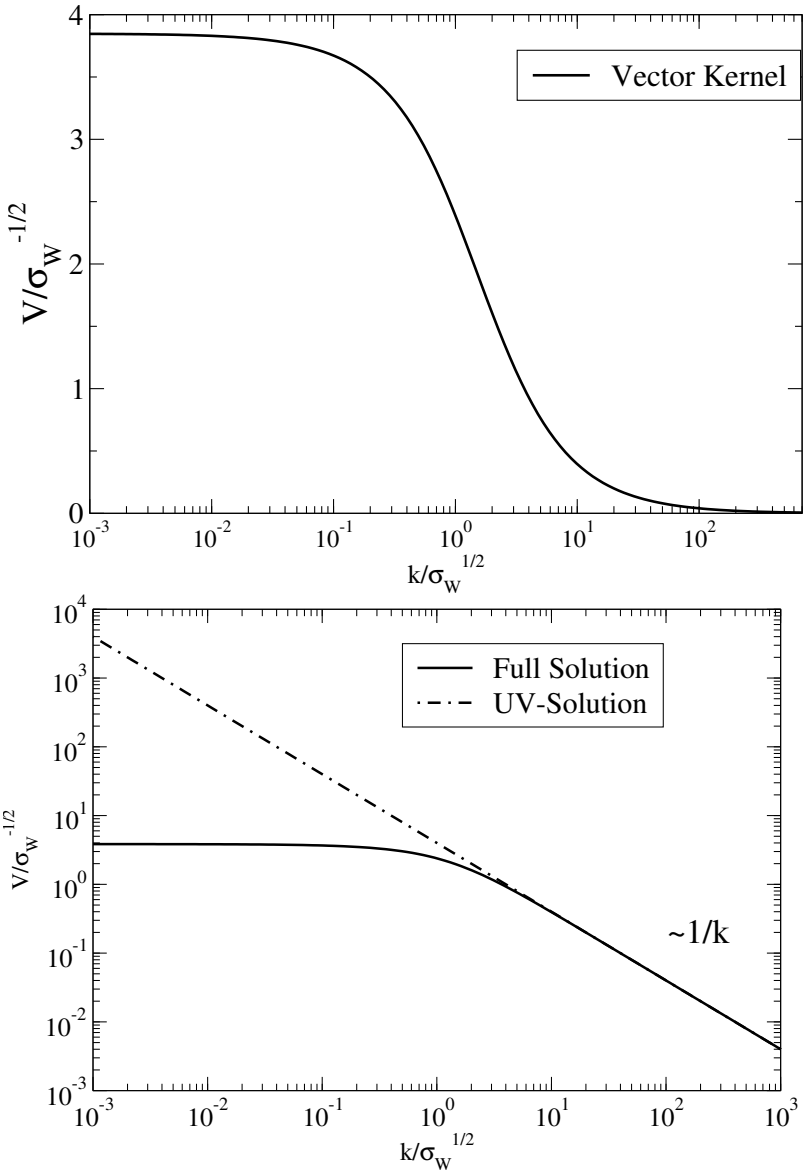

Figure 4.3: *Upper panel: Semi-logarithmic plot of the vectorial solution function $V(k)$ for the single-particle gap equation (4.27). Lower Panel: Double-logarithmic plot of the vectorial solution function $V(k)$ with (full line) and without (dash-dotted line) the IR part of the gluon loop integral $I(k)$.*

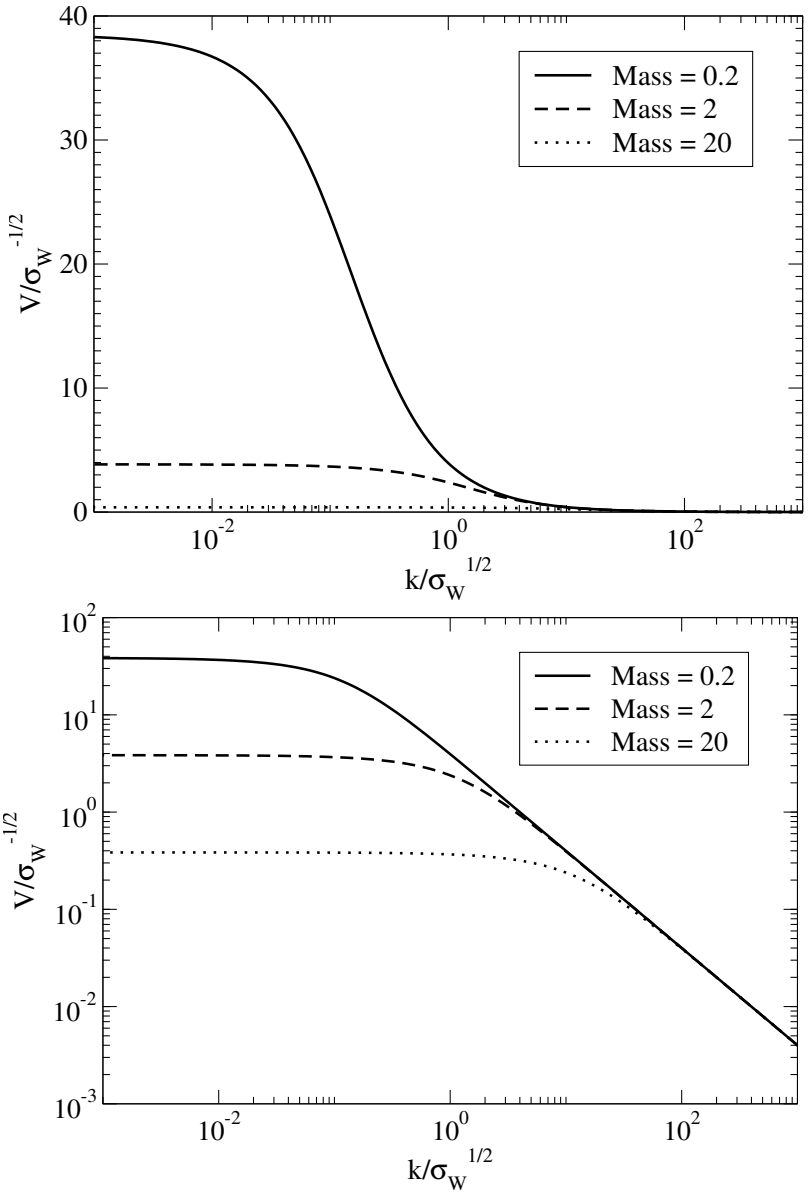

Figure 4.4: *Upper panel: Semi-logarithmic plot of vectorial solution function $V(k)$ for different values of the Gribov mass M_{G}. Lower panel: Double-logarithmic plot of vectorial solution function $V(k)$ for different values of the Gribov mass M_{G}.*

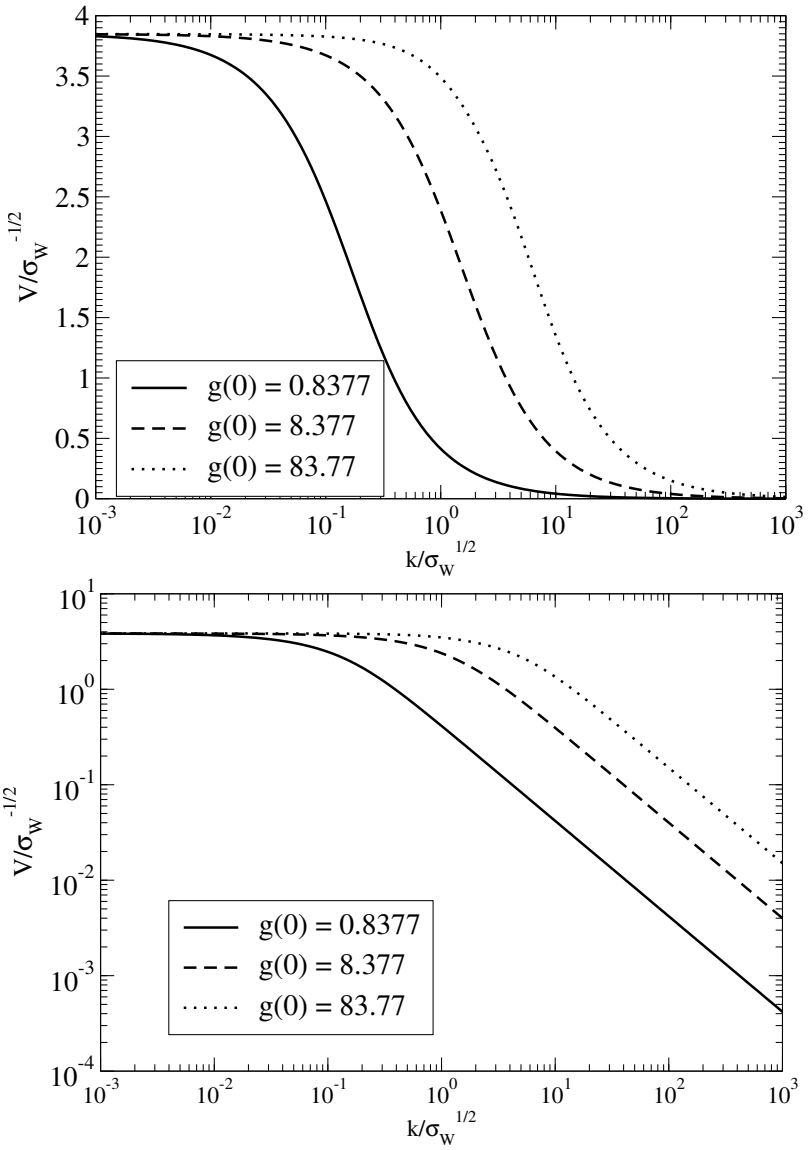

Figure 4.5: *Upper panel: Semi-logarithmic plot of vectorial solution function $V(k)$ for different values of the coupling g. Lower panel: Double-logarithmic plot of vectorial solution function $V(k)$ for different values of the coupling g.*

Chapter 5

Coulomb Hamiltonian

After having incorporated the interaction energy of transverse gluons into the variational calculation, which did not provide a non-vanishing chiral condensate, the next logical step is to include the Coulomb Hamiltonian, which describes the interaction of color charges mediated by the Coulomb kernel and which is expected to account for the main part of the symmetry breaking.

This chapter follows the same steps as the previous chapter. After a short introduction in Section 1, we derive the Coulomb energy density in Section 2, subsequently determine the gap equations in Section 3 and combine the result with the single-particle pieces to give the full coupled gap equations. In Section 4 we study the coupled system analytically and numerically for a confining non-Abelian color Coulomb potential and compare it to the case with vanishing quark-gluon vertex in the ansatz for the quark wave functional. Lastly, in order to understand the role of the infrared part of the static spatial gluon propagator for the solution functions, we compare the result to the case with a one-loop (perturbative) gluon propagator.

The lengthy evaluation of the Coulomb energy density is placed in Appendix C.

5.1 Introduction

Ignoring the purely gluonic contributions, the Coulomb Hamiltonian, Eq. (1.76), can be split up in three different parts

$$H_{\mathrm{C}} = \frac{g^2}{2}\int d^3x d^3y\, \psi^{\dagger a}(\boldsymbol{x})\,(T^m)^{ab}\,\psi^b(\boldsymbol{x})\hat{F}^{mn}(\boldsymbol{x},\boldsymbol{y})\psi^{\dagger c}(\boldsymbol{y})\,(T^n)^{cd}\,\psi^d(\boldsymbol{y}) \tag{5.1}$$

$$+\frac{g^2}{2}\int d^3x d^3y\, \mathcal{J}^{-1}[A]\rho^m_{\mathrm{G}}(\boldsymbol{x})\mathcal{J}(A)\hat{F}^{mn}(\boldsymbol{x},\boldsymbol{y})\psi^{\dagger c}(\boldsymbol{y})\,(T^n)^{cd}\,\psi^d(\boldsymbol{y}) \tag{5.2}$$

$$+\frac{g^2}{2}\int d^3x d^3y\, \psi^{\dagger a}(\boldsymbol{x})\,(T^m)^{ab}\,\psi^b(\boldsymbol{x})\hat{F}^{mn}(\boldsymbol{x},\boldsymbol{y})\rho^n_{\mathrm{G}}(\boldsymbol{y})\,. \tag{5.3}$$

where we have made explicit the quark charge densities ρ^m_{F}, Eq. (1.77). The gluon charge densities are $\rho^m_{\mathrm{G}}(\boldsymbol{x}) = f^{mno}A^n_i(\boldsymbol{x})\Pi^o_i(\boldsymbol{x})$, Eq. (1.77). We use the same conventions for the color indices as in the previous chapters: To distinguish fundamental from adjoint indices we label the fundamental fields with $a, b, \ldots$ and the adjoint fields with $m, n, \ldots$. The first term, Eq. (5.1), describes the interaction between quark charge densities and

the other two terms, Eqs. (5.2), (5.3), between gluon and quark charge densities, where for the last term we have used that the quark fields commute with the Faddeev-Popov determinant $\mathcal{J}[A]$, Eq. (1.73). Due to its four-fermion structure, the first part, Eq. (5.1), is assumed to be most important for studying the effect of dynamical chiral symmetry breaking. As an approximation we concentrate on the interaction between the color charge densities of the quarks only, Eq. (5.1). The additional contributions, Eqs. (5.2), (5.3), as well as taking into account the pure Yang-Mills part, Eq. (1.75), are currently, at the time of writing the thesis, under investigation.

As a further approximation we replace the Coulomb kernel $\hat{F}^{ab}$, Eq. (1.78), by its expectation value in the Yang-Mills sector

$$g^2\langle\hat{F}^{ab}(\boldsymbol{x},\boldsymbol{y})\rangle_{\mathrm{G}} = \delta^{ab}V_{\mathrm{C}}(\boldsymbol{x},\boldsymbol{y}) \;, \tag{5.4}$$

with the non-Abelian color Coulomb potential V_{C} given in Eq. (1.82). This approximation is consistent with the quenched approximation discussed in Section 3.3, since here we ignore the effect of the quark vacuum on the Coulomb kernel $\hat{F}^{ab}$, Eq. (1.78). The Coulomb energy density is then given as

$$\langle H_{\mathrm{C}}\rangle = \frac{1}{2}\int d^3x\, d^3y\, V_{\mathrm{C}}(\boldsymbol{x},\boldsymbol{y})\langle\psi^{\dagger a}(\boldsymbol{x})\,(T^m)^{ab}\,\psi^b(\boldsymbol{x})\psi^{\dagger c}(\boldsymbol{y})\,(T^m)^{cd}\,\psi^d(\boldsymbol{y})\rangle \;. \tag{5.5}$$

The non-Abelian color Coulomb potential $V_{\mathrm{C}}(r)$ with $r = |\boldsymbol{x}-\boldsymbol{y}|$ describes the interaction potential between two static color charge densities (see Section 1.6) and it can be split up into two parts

$$V_{\mathrm{C}}(r) = \sigma_{\mathrm{C}} r - \frac{\alpha_{\mathrm{S}}}{r} \;, \tag{5.6}$$

with a long-range linear potential $\sigma_{\mathrm{C}} r$ and a short-range Coulomb potential α_{S}/r. The slope of the linear potential, referred to as color Coulomb string tension σ_{C}, sets the scale in our approach (for more details, see the discussion after Eq. (1.94)).

5.2 Coulomb Energy Density

The four-fermion terms appearing in the Coulomb Hamiltonian (5.1) make the evaluation of the energy density tedious. Here we only present some general arguments useful for the derivation. A detailed computation of the occurring expectation values is carried out in Appendix C.2.

We expand the quark fields in Eq. (5.1) in terms of Fourier modes, Eqs. (1.40)-(1.43), ending up with a lengthy expression, see Eq. (C.47). These sixteen contributions are evaluated applying Wick's Theorem, which for a general four-fermion expectation value means

$$\left\langle\psi_A^\dagger\,\psi_B\,\psi_C^\dagger\,\psi_D\right\rangle = \left\langle\psi_A^\dagger\,\psi_B\right\rangle\left\langle\psi_C^\dagger\,\psi_D\right\rangle - \left\langle\psi_A^\dagger\psi_C^\dagger\right\rangle\left\langle\psi_B\,\psi_D\right\rangle + \left\langle\psi_A^\dagger\,\psi_D\right\rangle\left\langle\psi_B\,\psi_C^\dagger\right\rangle \;. \tag{5.7}$$

We have used $\psi \sim ua + vb^\dagger$, Eqs. (1.40), (1.41), and a condensed index denoting momentum, color and spin indices. Since all expectation values on the right-hand side give a unit matrix in color space, the first term on the right-hand side vanishes due to

$$\delta^{ab}\,(T^m)^{ab}\,\delta^{cd}\,(T^m)^{cd} \;=\; \mathsf{Tr}_{\rm C}[T^m]\mathsf{Tr}_{\rm C}[T^m] = 0\;. \tag{5.8}$$

The second two-point expectation values in (5.7) vanish as well, see Eqs. (B.16), (B.17). Moreover, we can show that only terms with a symmetric number of fermions and anti-fermions contribute and for all other terms the spin sums vanish, which is explicitly demonstrated in Appendix C.2.

We quote the final form of the Coulomb energy density

$$\frac{\langle H_C\rangle}{\delta^3(0)} \;=\; \frac{1}{2}N_{\rm C}C_F(2\pi)^3\int \text{đ}^3p\,\text{đ}^3q\,V_{\rm C}(\boldsymbol{p}-\boldsymbol{q})\;[Y(\boldsymbol{p},\boldsymbol{q}) + Z(\boldsymbol{p},\boldsymbol{q})\hat{\boldsymbol{p}}\cdot\hat{\boldsymbol{q}}]\;, \tag{5.9}$$

with the definitions

$$Y(\boldsymbol{p},\boldsymbol{q}) \;=\; 1 - \frac{S^*(\boldsymbol{p})S(\boldsymbol{q}) + S(\boldsymbol{p})S^*(\boldsymbol{q}) + S(\boldsymbol{p})S(\boldsymbol{q}) + S^*(\boldsymbol{p})S^*(\boldsymbol{q})}{(1+S^*(\boldsymbol{p})S(\boldsymbol{p}) + R(\boldsymbol{p}))(1+S^*(\boldsymbol{q})S(\boldsymbol{q}) + R(\boldsymbol{q}))}\;, \tag{5.10}$$

$$\begin{aligned} Z(\boldsymbol{p},\boldsymbol{q}) \;=\; &-\frac{(1-S^*(\boldsymbol{p})S(\boldsymbol{p}) - R(\boldsymbol{p}))(1-S^*(\boldsymbol{q})S(\boldsymbol{q}) - R(\boldsymbol{q}))}{(1+S^*(\boldsymbol{p})S(\boldsymbol{p}) + R(\boldsymbol{p}))(1+S^*(\boldsymbol{q})S(\boldsymbol{q}) + R(\boldsymbol{q}))} + \\ &+\;\frac{-S^*(\boldsymbol{p})S(\boldsymbol{q}) - S(\boldsymbol{p})S^*(\boldsymbol{q}) + S(\boldsymbol{p})S(\boldsymbol{q}) + S^*(\boldsymbol{p})S^*(\boldsymbol{q})}{(1+S^*(\boldsymbol{p})S(\boldsymbol{p}) + R(\boldsymbol{p}))(1+S^*(\boldsymbol{q})S(\boldsymbol{q}) + R(\boldsymbol{q}))}\;. \end{aligned} \tag{5.11}$$

Both parts Y and Z (and therefore the Coulomb energy density, Eq. (5.9)) are symmetric in the variational functions, i.e., replacing S by S^* or V by V^* does not alter the quantities Y and Z. This observation holds true for *all* parts of the energy density, which we have taken into account, see Eqs. (4.4),(4.8). As shown in the last chapter for the single-particle energy density, Section 4.2, due to this symmetry the variations with respect to S and S^* (or V and V^*) lead to identical gap equations and we can set

$$S = S^*, \qquad V = V^*\;. \tag{5.12}$$

The second term in Z, Eq. (5.11), then cancels.

We note, that the vector kernel V enters in Y, Eq. (5.10), and Z, Eq. (5.11), only indirectly via the loop integral $R(\boldsymbol{p})$, Eq. (3.46).

We investigate two limits: Switching off the scalar variational function, i.e., $S = 0$, the part denoted as Y, Eq. (5.10), simplifies to unity. On the other hand, setting the vectorial gap function to zero, i.e., $V = 0$, the loop integral $R(\boldsymbol{p})$, Eq. (3.46), vanishes and the energy density (5.9) reduces to its form determined in Ref. [80].

Next we perform the variations and incorporate the Coulomb interaction, Eq. (5.9), into the coupled system (4.17), (4.18). We emphasize that we now work with the variational functions S and V to be real, Eq. (5.12).

5.3 Full Coupled Quark Gap Equations

The variation of the energy density (5.9) with respect to $S(\boldsymbol{k})$ yields

$$\frac{\delta}{\delta S(\boldsymbol{k})}\frac{\langle H_{\rm C}\rangle}{\delta^3(0)} \;=\; -\frac{1}{2}N_{\rm C}C_F\,8\,\frac{I_{\rm C}^{(1)}(\boldsymbol{k})}{(1+S^2(\boldsymbol{k})+R(\boldsymbol{k}))^2}\;, \tag{5.13}$$

with

$$\begin{aligned} I_{\rm C}^{(1)}(\boldsymbol{k}) \;=& \int đ^3q \frac{V_{\rm C}(\boldsymbol{k}-\boldsymbol{q})}{1+S^2(\boldsymbol{q})+R(\boldsymbol{q})}\times \\ &\times\Big[S(\boldsymbol{q})(1-S^2(\boldsymbol{k})+R(\boldsymbol{k}))-(\hat{\boldsymbol{k}}\cdot\hat{\boldsymbol{q}})S(\boldsymbol{k})\left(1-S^2(\boldsymbol{q})-R(\boldsymbol{q})\right)\Big]\;. \end{aligned} \tag{5.14}$$

In contrast to the variation of the single-particle energy densities (4.9) and (4.11) with respect to $S(\boldsymbol{k})$, here the scalar variational function $S(\boldsymbol{k})$ does *not* appear as a factor in the numerator on the right-hand side of Eq. (5.13), but only in the integral $I_{\rm C}^{(1)}(\boldsymbol{k})$, Eq. (5.14). This has important consequences on the structure of the resulting gap equation

$$\frac{\delta}{\delta S(\boldsymbol{k})}\langle H_{\rm D}+H_{\rm QGC}+H_{\rm C}\rangle = 0\;, \tag{5.15}$$

where we have used the definitions $H_{\rm D}$, Eq. (4.1), and $H_{\rm QGC}$, Eq. (5.1). With the inclusion of the Coulomb energy density, Eq. (5.9), the constraint equation (4.14) becomes a non-linear integral equation (using Eqs. (4.9), (4.11), (5.13))

$$S(\boldsymbol{k})\left(|\boldsymbol{k}|-\frac{1}{2}gC_FI_\omega(\boldsymbol{k})\right)=\frac{1}{2}C_FI_{\rm C}^{(1)}(\boldsymbol{k})\;. \tag{5.16}$$

We can draw the conclusion that the Coulomb interaction, Eq. (5.1), provides the non-trivial part for the gap function S.

For the variation of the energy density (5.9) with respect to $V(\boldsymbol{k},\boldsymbol{k}')$ we obtain

$$\frac{\delta}{\delta V(\boldsymbol{k},\boldsymbol{k}')}\frac{\langle H_{\rm C}\rangle}{\delta^3(0)} \;=\frac{1}{2}N_{\rm C}C_F\,8\,\frac{V(\boldsymbol{k},\boldsymbol{k}')X(\boldsymbol{k},\boldsymbol{k}')}{(1+S^2(\boldsymbol{k})+R(\boldsymbol{k}))^2}I_{\rm C}^{(2)}(\boldsymbol{k})\;, \tag{5.17}$$

with

$$I_{\rm C}^{(2)}(\boldsymbol{k}) \;=\; \int đ^3q\frac{V_{\rm C}(\boldsymbol{k}-\boldsymbol{q})}{1+S^2(\boldsymbol{q})+R(\boldsymbol{q})}\left[2S(\boldsymbol{k})S(\boldsymbol{q})+(\hat{\boldsymbol{k}}\cdot\hat{\boldsymbol{q}})\left(1-S^2(\boldsymbol{q})-R(\boldsymbol{q})\right)\right]\;, \tag{5.18}$$

and $X(\boldsymbol{k},\boldsymbol{k}')$ defined in (3.49). However, the variation with respect to V leads for the Coulomb part $H_{\rm C}$, Eq. (5.17), to the same structure as for the kinetic part $H_{\rm D}$, Eq. (4.10). When ignoring the interaction with transverse gluons $H_{\rm QGC}$, Eq. (4.13), we arrive at a constraint equation of the form

$$V(\boldsymbol{k},\boldsymbol{k}')\left(|\boldsymbol{k}|+\frac{1}{2}C_F\,I_{\rm C}^{(2)}(\boldsymbol{k})\right)=0\;. \tag{5.19}$$

This equation together with the equation determining S, Eq. (5.16), has the non-trivial solution $V = 0$ and $S \neq 0$. (Note that the opposite case, ignoring the Coulomb interaction $H_{\rm C}$, Eq. (5.17), and using the transverse gluon exchange only, i.e., $H_{\rm QGC}$, Eq. (4.13), was studied in the previous chapter in Section 4.3 and could be solved with $V \neq 0$ and $S = 0$.) Hence, the transverse gluon interaction $H_{\rm QGC}$, Eq. (4.8), more precisely the variation of the nominator term in (4.8) with respect to V (which is the second part on the right-hand side of Eq. (4.13)), supplies us with the non-trivial contribution for the gap function V.

Collecting Eq. (5.16) and the variations with respect to the vector function V (Eqs. (4.10), (4.13), (5.17)) we arrive at the following system of coupled integral equations,

$$S(\boldsymbol{k}) = \frac{\frac{1}{2}C_F I_{\rm C}^{(1)}(\boldsymbol{k})}{|\boldsymbol{k}| - \frac{1}{2}gC_F I_\omega(\boldsymbol{k})} \,, \tag{5.20}$$

$$V(\boldsymbol{k},\boldsymbol{k}') = -g\frac{1 + S^2(\boldsymbol{k}) + R(\boldsymbol{k})}{2|\boldsymbol{k}| - gC_F I_\omega(\boldsymbol{k}) + \frac{1}{2}C_F\, 2\, I_{\rm C}^{(2)}(\boldsymbol{k})} \,, \tag{5.21}$$

where we have used the definitions $R(\boldsymbol{k})$, Eq. (3.46), $I_\omega(\boldsymbol{k})$, Eq. (4.12), and $I_{\rm C}^{(1)}(\boldsymbol{k})$, Eq. (5.14), $I_{\rm C}^{(2)}(\boldsymbol{k})$, Eq. (5.18). As for the case of a pure transverse gluon interaction $H_{\rm QGC}$, Eq. (4.19), the gap equation (5.21) determines the variational function V to depend only on one momentum, $V(\boldsymbol{k},\boldsymbol{k}') = V(\boldsymbol{k})$, since the right-hand side of Eq. (5.21) depends on only $\boldsymbol{k}$. As discussed in Section 4.3 this is an artifact of our approximations. However, it significantly simplifies the numerical evaluation of the coupled system Eq. (5.20), (5.21). Employing Eq. (4.21) and setting $V(\boldsymbol{k}) \to -V(\boldsymbol{k})$ we can rewrite the coupled equations as

$$S(\boldsymbol{k}) = \frac{\frac{1}{2}C_F I_{\rm C}^{(1)}(\boldsymbol{k})}{|\boldsymbol{k}| + gC_F V(\boldsymbol{k}) I(\boldsymbol{k})} \,, \tag{5.22}$$

$$V(\boldsymbol{k}) = \frac{g}{2}\frac{1 + S^2(\boldsymbol{k}) + R(\boldsymbol{k})}{|\boldsymbol{k}| + gC_F V(\boldsymbol{k}) I(\boldsymbol{k}) + \frac{1}{2}C_F\, I_{\rm C}^{(2)}(\boldsymbol{k})} \,, \tag{5.23}$$

with the regularized integral $I(\boldsymbol{k})$ defined in Eq. (4.24). The meaning of the replacement $V(\boldsymbol{k}) \to -V(\boldsymbol{k})$ has already been discussed in Section 4.3, see Eq. (4.28).

Now we have all the ingredients to study the coupled system analytically and numerically. We are going to observe how these two equations, Eq. (5.22) and Eq. (5.23), interact to give the solution functions S and V. A special role will be played by the infrared part of the static spatial gluon propagator $D(\boldsymbol{k})$, Eq.(1.81).

Let us, at this point, summarize the main outcome of the variational calculation performed in the last two chapters. The Coulomb energy density, Eq. (5.9), is the non-trivial part of the gap equation determining S, Eq. (5.22), whereas the transverse gluon interaction, Eq. (4.8), is the non-trivial piece for determining V, Eq. (5.23).

Before we go ahead with studying the coupled system in an analytical and numerical framework, we make a short comment on strong-coupling electrodynamics.

Strong-Coupling Electrodynamics

Quantum Electrodynamics (QED) without coupling to matter fields can be rewritten as a system of uncoupled harmonic oscillators and solved by means of a Gaussian ansatz, see Section 1.4. Resolving the Gauss law and switching on dynamical fermion fields yields the Coulomb Hamiltonian of the form

$$H_{\mathrm{C}} = \frac{e^2}{2} \int d^3x d^3y \, \psi^\dagger(\boldsymbol{x})\psi(\boldsymbol{x})\hat{F}(\boldsymbol{x},\boldsymbol{y})\psi^\dagger(\boldsymbol{y})\psi(\boldsymbol{y}) \; . \tag{5.24}$$

with $\hat{F}$ denoting the ordinary Coulomb potential, i.e., $\hat{F}(\boldsymbol{x},\boldsymbol{y}) = 1/(4\pi|\boldsymbol{x}-\boldsymbol{y}|)$. In contrast to QCD the QED color charge densities are independent of the gauge field. Chiral symmetry is dynamically broken when the coupling exceeds a critical coupling and the (massless) electrons become massive. Instead of $\alpha = 1/137$ (with $\alpha = e^2/(4\pi)$) the ground state properties are studied with $\alpha > 1$. Such a system serves as a laboratory to investigate strong interaction phenomena in the simplest possible gauge theory, Refs. [66, 90–95].

The evaluation of expectation values works analogously to the QCD case, however, with additional terms occurring, since terms vanishing in QCD due to the trace in color space give non-zero contributions in QED, see Eqs. (5.7), (5.8). It is remarkable that all these additional contributions can be summed to give a divergent term of the form

$$\langle H_{\mathrm{DIV}} \rangle = \frac{e^2}{2} 4 \int đ^3p \, đ^3q \int đ^3k \, V_{\mathrm{C}}(\boldsymbol{k}) \; (\delta(\boldsymbol{k}))^2 \; , \tag{5.25}$$

which is independent of the variational functions and therefore just an irrelevant divergent constant. When varying Eq. (5.25) with respect to the variational parameters S and V this term vanishes and we are left with the equations (5.22), (5.23) with the color factors N_{C}, C_F set to unity. We can conclude, that the equations determining S and V in QED are the same as in QCD, Eqs. (5.22), (5.23). Clearly, the Coulomb kernel $\hat{F}$ in QED has no confining piece.

5.4 Solving the Quark Gap Equations

Now we have everything in place to investigate the gap equations, Eqs. (5.22) and (5.23), analytically in the asymptotic momentum regime and numerically in the whole momentum region. For the non-Abelian color Coulomb potential V_{C}, Eq. (5.6), we take in a first study only the confining part $\sigma_{\mathrm{C}} r$ into account, which reads in momentum space

$$V_{\mathrm{C}}(\boldsymbol{k}-\boldsymbol{q}) = \frac{8\pi\sigma_{\mathrm{C}}}{|\boldsymbol{k}-\boldsymbol{q}|^4} \; . \tag{5.26}$$

This has the advantage that we can compare our results with Ref. [80], where the gap equation for the $V = 0$ case has been solved. Moreover, the spatial gluon loop integral

$I(k)$, Eq. (4.21), enters the gap equations, Eqs. (5.22) and (5.23). We will use two types of gluon propagators $D(k)$, Eq. (1.81), in the loop integral $I(k)$: the purely perturbative gluon propagator and the full non-perturbative gluon propagator, Eq. (1.95),

$$\omega(\boldsymbol{k}) = |\boldsymbol{k}| \Longrightarrow \quad I(k) = C_F \frac{1}{2} \frac{1}{2\pi^2} \frac{1}{6} k^2 \,, \tag{5.27}$$

$$\omega(\boldsymbol{k}) = \sqrt{\boldsymbol{k}^2 + \frac{M_{\mathrm{G}}^4}{\boldsymbol{k}^2}} \Longrightarrow \quad I(k) \text{ given in Eq. (4.24)} \,. \tag{5.28}$$

Since the Gribov mass M_{G} sets the scale for the non-perturbative gluon propagator, we will often refer to $M_{\mathrm{G}} = 0$ as the perturbative gluon propagator, Eq. (5.27) and to $M_{\mathrm{G}} \neq 0$ as the non-perturbative gluon propagator, Eq. (5.28).

We analyze three different situations analytically and numerically:

1. with the vector kernel V set to zero, known as Adler-Davis gap equation
2. with the vector kernel V switched on, but the Gribov mass M_{G}, Eq. (5.27), set to zero
3. with the vector kernel V and the Gribov mass M_{G}, Eq. (5.28), switched on.

Situation 1 takes only the BCS part in the quark vacuum wave functional ansatz, Eq. (3.35), into account, which has already been computed in Ref. [80]. We reproduce this result in order to compare it to the result with non-vanishing vector kernel V, Eq. (3.37), and to clarify if the additional coupling V influences the chiral properties of the theory. Moreover, reproducing the result in Ref. [80] is a good way to check our code and algorithm.

Situations 2 and 3 take into account either the tree-level static gluon propagator, Eq. (5.27) or the non-perturbative gluon propagator, Eq. (5.28), as input into the gap equations. Comparing both these situations will unfold the influence of the non-perturbative part of the spatial gluon propagator, Eq. (5.28), on chiral symmetry breaking.

5.4.1 Asymptotic Analysis

Before solving the gap equations, Eqs. (5.22), (5.23), by iteration, we start with an analysis of the gap equations in the asymptotic momentum regions $k \to 0$ and $k \to \infty$, analogous to Section 4.3. First of all, we explore the asymptotics of the Coulomb integrals $I_{\mathrm{C}}^{(1)}(\boldsymbol{k})$, Eq. (5.14), and $I_{\mathrm{C}}^{(2)}(\boldsymbol{k})$, Eq. (5.18). We evaluate the angular integrals and expand the resulting functions for small and large momenta. We note that only the non-Abelian color Coulomb potential V_{C}, Eq. (5.6), has to be evaluated at the difference of the two momenta $\boldsymbol{k} - \boldsymbol{q}$, which simplifies the computation a lot. We then examine the three different settings listed above in the small and large momentum regions.

Angular Integration

In the Coulomb integrals $I_{\rm C}^{(1)}$ and $I_{\rm C}^{(2)}$, (5.14) and (5.18), two types of angular integrals occur, namely

$$\int đ^3q\, V_{\rm C}(\boldsymbol{k}-\boldsymbol{q}), \qquad \int đ^3q\, V_{\rm C}(\boldsymbol{k}-\boldsymbol{q})\, \hat{\boldsymbol{k}}\cdot\hat{\boldsymbol{q}}\ , \tag{5.29}$$

which can be performed analytically, yielding

$$L(k,q) = \int_{-1}^{1} dz\, \frac{1}{(k^2-2kqz+q^2)^2} \;=\; \frac{2}{(k^2-q^2)^2}\ , \tag{5.30}$$

$$K(k,q) = \int_{-1}^{1} dz\, \frac{z}{(k^2-2kqz+q^2)^2} \;=\; \frac{k^2+q^2}{kq(k^2-q^2)^2} + \frac{1}{2}\frac{1}{k^2q^2}\ln\left|\frac{k-q}{k+q}\right|\ , \tag{5.31}$$

where we have ignored for simplicity the pre-factors of the non-Abelian static color Coulomb potential $V_{\rm C}(\boldsymbol{k}-\boldsymbol{q})$. Eq. (5.26), and shifted the angular integrals according to $\int_0^\pi d\theta \sin\theta = \int_{-1}^1 dz$ with $z=\cos\theta$. In order to make the divergent integrals at $p=q$ finite, when setting up the numerical evaluation in the next section, we are going to introduce a regulator ε, according to Ref. [79]. For the time being, we assume that the integrals are properly regularized at $p=q$.

We expand the kernels $L(k,q)$, Eq. (5.30), and $K(k,q)$, Eq. (5.31), around $k=0$, and end up with

$$L(k,q) = \frac{2}{(k^2-q^2)^2} = \frac{2}{q^4} + \frac{4k^2}{q^6} + \mathcal{O}(k^4)\ , \tag{5.32}$$

$$\begin{aligned} K(k,q) &= \frac{k^2+q^2}{kq(k^2-q^2)^2} + \frac{1}{2}\frac{1}{k^2q^2}\ln\left|\frac{k-q}{k+q}\right| = \\ &= \left[\frac{1}{kq^3} + \frac{3k}{q^5} + \mathcal{O}(k^3)\right] - \left[\frac{1}{kq^3} + \frac{k}{3q^5} + \mathcal{O}(k^3)\right] = \\ &= \frac{8}{3}\frac{k}{q^5} + \mathcal{O}(k^3)\ . \end{aligned} \tag{5.33}$$

For $k\to 0$ the leading contribution comes from the kernel $L(k,q)$, which approaches a constant for vanishing k. For $k\to\infty$ the kernels $L(k,q)$ and $K(k,q)$ behave as

$$L(k,q) = \frac{2}{k^4} + \mathcal{O}\left(\frac{1}{k^6}\right)\ , \tag{5.34}$$

$$K(k,q) = \frac{8q}{3k^5} + \mathcal{O}\left(\frac{1}{k^7}\right)\ , \tag{5.35}$$

where again the kernel $L(k,q)$ is the leading order term, since the kernel $K(k,q)$ approaches zero more rapidly. Both these observations will become important throughout this section.

1. Adler-Davis Gap Equation

Setting the coupling of the quarks to the transverse gluons to zero, $V = 0$, the gap equation determining the scalar variational function (5.22) simplifies to

$$S(\boldsymbol{k})|\boldsymbol{k}| = \frac{g^2}{2} C_F \int đ^3 q \, V_{\mathrm{C}}(\boldsymbol{k}-\boldsymbol{q}) \frac{S(\boldsymbol{q})[1-S^2(\boldsymbol{k})] - S(\boldsymbol{k})[1-S^2(\boldsymbol{q})]\hat{\boldsymbol{k}}\cdot\hat{\boldsymbol{q}}}{1+S^2(\boldsymbol{q})} \,, \quad (5.36)$$

which is known in the literature as *Coulomb gauge paring model*, and which we refer to as *Adler-Davis gap equation*. In Ref. [80], starting from the renormalized gap equation, Adler and Davis found a numerical solution for the scalar kernel S with the confining non-Abelian color Coulomb potential, Eq. (5.26).

This integral equation[1], first derived in Ref. [78] and correctly renormalized in Ref. [80], has been analyzed in great detail in Ref. [79], showing analytically that chirally non-invariant solutions S for power-law potentials $r^\alpha (0 < \alpha < 3)$ exist independently of the strength of the coupling constant. It offers many applications, for instance when generalizing it to non-zero quark masses, Ref. [89], taking into account the Coulomb potential, Refs. [89, 96–98], and studying finite temperatures, Ref. [99] and finite densities, Ref. [100]. The massless pions are described within this approach by the so-called Bethe-Salpeter equation, which follows directly from the gap equation, Ref. [101]. Phenomenological consequences from the Bethe-Salpeter equation are analyzed in Ref. [102].

The first attempts to include transverse gluons were started in Ref. [103] and taken up in Ref. [89] using the so-called Breit approximation, which is also used in Ref. [104]. In Ref. [105] the so-called "expontential-S" method is applied to study the influence of transverse gluons, however, without solving the underlying eigenvalue problem. The influence of transverse gluons on chiral symmetry breaking could not be clarified until now. This missing piece clearly goes in hand with the fact that up to now only BCS type wave functionals, Eq. (3.2), were used as an ansatz for the QCD vacuum and transverse gluons could only be included in an approximate fashion.

We now recall the most important characteristics of the Adler-Davis gap equation, Eq. (5.36), in order to compare it with the solution of the full coupled equations (5.22), (5.23), i.e., when switching on the vector coupling V in the vacuum wave functional (3.3).

Let us start with the analysis for small momenta k and rewrite the gap equation (5.36) with use of the angular integrals (5.30), (5.31) as a one-dimensional integral equation,

$$S(k)\, k \;=\; G \int dq\, q^2 \left(L(k,q) \frac{S(q)}{1+S^2(q)} [1-S^2(k)] - K(k,q) \frac{1-S^2(q)}{1+S^2(q)} S(k) \right) \,, \quad (5.37)$$

[1] The gap equation (5.36) is equivalent to a rainbow-ladder Dyson-Schwinger equation, where only the instantaneous part of the temporal gluon propagator is taken into account, see Ref. [80]. Moreover, in a recent article, Ref. [34], it is shown how the gap equation (5.36) is derived from a leading order truncation of the quark Dyson-Schwinger equations in Coulomb gauge within the first order formalism.

where $G = 8\pi\sigma_C C_F/(2(2\pi)^2)$. Expanding S around $k = 0$, the gap equation in the small momentum region reads

$$\begin{aligned}
&[S(0) + kS'(0)]\, k + \mathcal{O}(k^3) = \\
&G \int dq\, q^2 \frac{S(q)}{1+S^2(q)} \left(\frac{2}{q^4} + \frac{4k^2}{q^6} + \mathcal{O}(k^4) \right) \left[(1 - S^2(0)) - 2kS(0)S'(0) \right] - \\
&- G \int dq\, q^2 \frac{1-S^2(q)}{1+S^2(q)} \left(\frac{8}{3} \frac{k}{q^5} + \mathcal{O}(k^3) \right) (S(0) + \mathcal{O}(k)) \ ,
\end{aligned} \tag{5.38}$$

so that for $k = 0$ the equation simplifies to

$$0 = G \int dq \frac{2}{q^2} \frac{S(q)}{1+S^2(q)} \left[1 - S^2(k \to 0) \right] \equiv I_C^{(1)}(k \to 0) \left[1 - S^2(k \to 0) \right] \ , \tag{5.39}$$

which is solved for $S(0) = \pm 1$. We have to keep in mind that the integral $I_C^{(1)}(k \to 0)$ on the right-hand side of the equation is finite, when the (infrared) regulator ε is introduced. This is an important result: The gap equations (5.22), (5.23) for vanishing vector kernel V constrain the scalar kernel S for small momenta to approach unity.

This result has important impact on the evaluation of the constituent quark mass $M(0)$, defined in Eq. (3.82). To see this, we derive the quark gap equation (5.36) in terms of the dynamical mass function $M(p)$.

With use of the definition (3.82) we can derive the relations

$$\frac{M(\boldsymbol{k})}{\sqrt{\boldsymbol{k}^2 + M^2(\boldsymbol{k})}} = \frac{2S(\boldsymbol{k})}{1+S^2(\boldsymbol{k})} \ , \quad \frac{|\boldsymbol{k}|}{|\boldsymbol{q}|} \frac{2S(\boldsymbol{k})}{1-S^2(\boldsymbol{q})} \frac{1-S^2(\boldsymbol{q})}{1+S^2(\boldsymbol{q})} = \frac{M(\boldsymbol{k})}{\sqrt{\boldsymbol{q}^2 + M^2(\boldsymbol{q})}} \ , \tag{5.40}$$

and with the angular integrals (5.30) and (5.31) the Adler-Davis gap equation (5.36) can be rewritten as

$$M(k) \ = \ G \int dq\, q^2 \left(L(k,q) \frac{M(q)}{\sqrt{q^2 + M^2(q)}} - K(k,q) \frac{q}{k} \frac{M(k)}{\sqrt{q^2 + M^2(q)}} \right) \ , \tag{5.41}$$

or in a quotient form as (which is particularly convenient for a numerical analysis)

$$M(k) = \frac{G \int dq\, q^2\, L(k,q) M(q) [q^2 + M^2(q)]^{-\frac{1}{2}}}{1 + G \int dq\, q^2\, K(k,q) \frac{q}{k} [q^2 + M^2(q)]^{-\frac{1}{2}}} \ . \tag{5.42}$$

In order to test our numerics, we are going to evaluate equation (5.42) as well. We note that it is no longer possible to express the gap equations (5.22) and (5.23) entirely in terms of the dynamical mass function $M(p)$, Eq. (3.82), when the coupling part V of the vacuum wave functional is taken into account.

Expanding the expression for the dynamical mass $M(k)$, Eq. (3.82), around zero and keeping the leading order only, the constituent quark mass $M(0)$ and the infrared part of the condensate wave function S are connected via

$$M(0) = k \frac{2S(0) + \mathcal{O}(k)}{1 - S^2(0) - 2kS(0)S'(0) + \mathcal{O}(k^2)} = -\frac{1}{S'(0)} + \mathcal{O}(k) \ . \tag{5.43}$$

Consequently, the constituent mass can be read off from the slope of the scalar wave function S at zero momentum.

We turn to the large momentum region of the variational function $S(k)$. Since condensation is a low-momentum effect, we expect the gap function to vanish as $k \to \infty$. The condition that for large momenta the integral $L(k,q)$, Eq. (5.34), is the leading order term translates into

$$S(k \to \infty)k = \frac{2}{k^4}\left[1 - S^2(k \to \infty)\right] \ . \tag{5.44}$$

Assuming a power-law solution in the ultraviolet region, $S(k) = A/k^\alpha$, the gap function $S(k)$ vanishes as

$$S(k \to \infty) \sim \frac{1}{k^5} \ . \tag{5.45}$$

Correspondingly, the mass function $M(k)$, Eq.(3.82), goes to zero as

$$M(k \to \infty) \sim \frac{1}{k^4} \ , \tag{5.46}$$

and in general $M(k \to \infty) \sim 1/V_{\rm C}(k)$. Both behaviors are confirmed in the numerical computation in Section 5.4.2. With the result (5.45) it can be shown that the expression for the chiral condensate (3.85) is a convergent integral.

2. Gap Equation with Vector Kernel V and with Tree-Level Gluon Propagator

At next we switch on the vector kernel V and study the full coupled equations (5.22), (5.23) with the gluon loop integral $I(k)$ given in Eq. (5.27) as input, which takes only the large momentum part of the static spatial gluon propagator (1.95) into account.

We explore the infrared region of the gap equation determining the scalar part S, Eq. (5.22), rewrite it as

$$\left[k + gC_F V(k) I(k)\right] S(k) = \frac{1}{2} C_F I_{\rm C}^{(1)}(k) \ . \tag{5.47}$$

and ask how the kernel V alters the asymptotic behavior of the scalar gap function S. We use the expansion of the Coulomb integral $I_{\rm C}^{(1)}(k)$ around zero in Eq. (5.39) (with the additional loop integral $R(k)$, Eq. (3.46), in the denominator), abbreviate $I(k) = Ck^2$ with $C = C_F \frac{1}{2} \frac{1}{(2\pi)^2} \frac{1}{6}$ and arrive at

$$\left[k + gC_F V(k \to 0) C k^2\right] S(k \to 0) = I_C^{(1)}(k \to 0)\left[1 - S^2(k \to 0) + V^2(k \to 0) C k^2\right] . \tag{5.48}$$

Assuming that $V(k)$ does not diverge for small momenta we find to lowest order

$$0 = I_C^{(1)}(k \to 0)\left[1 - S^2(k \to 0)\right] \ , \tag{5.49}$$

which yields, as for the case of switching off the coupling of quarks to the transverse gluons $V = 0$, the constraint $S(0) = \pm 1$. The small momentum behavior of S is therefore governed by the Coulomb part of the interaction, Eq. (5.9) and the vector kernel V does *not* alter the infrared behavior of S since the loop integral $I(k)$, Eq. (4.22), using the tree-level gluon propagator as input vanishes as k^2.

We turn to the integral equation for the vectorial part Eq. (5.23), which is after angular integration given as

$$\left[k + gC_F V(k) I(k) + \frac{1}{2} C_F I_C^{(2)}(k)\right] V(k) \;=\; \frac{g}{2}\left[1 + S^2(k) + R(k)\right] \;. \tag{5.50}$$

The small momentum behavior of V is determined both by the infrared value of the Coulomb-integral $I_C^{(2)}(k)$ on the left-hand side of Eq. (5.50) as well as the term on the right-hand side of Eq. (5.50), which comes from the interaction of the quarks with the transverse gluons, Eq. (4.8). The second term on the left-hand side of Eq. (5.50) as well as the last term on the right-hand side of Eq. (5.50), namely $R(k)$, vanish due to $I(k \to 0) \sim k^2$. The infrared value of the vector variational function V is therefore determined as

$$V(k \to 0) = \frac{\frac{g}{2}(1 + S^2(k \to 0))}{\frac{1}{2} C_F I_{\mathrm{C}}^{(2)}(k \to 0)} \;. \tag{5.51}$$

With the result $S(k \to 0) = 1$ and the Coulomb integral $I_C^{(2)}(k \to 0)$ becoming constant, the vector kernel V approaches a constant for small momenta.

Let us again take a look at the dynamical mass function $M(k)$, Eq. (3.82). Now the loop integral $R(k)$, Eq. (3.46), enters its definition, which, however, vanishes as $k \to 0$ (under the assumption that V does not diverge). As a result, the evaluation of the constituent mass $M(0)$ according to (5.43) holds true.

We turn to the ultraviolet behavior of the gap functions S and V. We again start with analyzing the gap equation for the scalar variational function (5.22) and use the large-momentum behavior of the Coulomb integrals, Eq. (5.34), so that the loop integral $I_{\mathrm{C}}^{(1)}(k)$ approaches

$$I_C^{(1)}(k \to \infty) \sim \left(\frac{2}{k^4} + \mathcal{O}\left(\frac{1}{k^6}\right)\right)\left(1 - S^2(k) + C_F V^2(k) I(k)\right) \;, \tag{5.52}$$

and with $I(k \to \infty) = Ck^2$ the gap equation reads

$$\begin{aligned} S(k \to \infty)k + gV(k \to \infty)Ck^2 S(k \to \infty) = \\ = \frac{1}{2}\frac{2}{k^4} C_F \left(1 - S^2(k \to \infty) + C_F V^2(k) Ck^2\right) \;. \end{aligned} \tag{5.53}$$

Assuming a power-law behavior for $S(k \to \infty)$ and $V(k \to \infty)$ and comparing both sides of the equation we find $S(k \to \infty) \sim 1/k^5$, which was also obtained when solving

the Adler-Davis gap equation, Eq. (5.45). Moreover, we find $V(k) \sim 1/k$, which is confirmed when analyzing the gap equation for V, Eq. (5.23), which reads

$$\left[k + g(0)V(k)I(k) + \frac{1}{2}C_F I_C^{(2)}(k)\right] V(k) = \frac{g}{2}\left[1 + S^2(k) + C_F V^2(k) I(k)\right] \ , \quad (5.54)$$

using the fact that the Coulomb integral $I^{(2)}(k)$ approaches

$$I_C^{(2)}(k \to \infty) \sim \left(\frac{1}{k^4} + \mathcal{O}\left(\frac{1}{k^6}\right)\right) S(k) \ . \quad (5.55)$$

We conclude that the Coulomb integral $I_C^{(1)}(k)$, Eq. (5.14) governs the asymptotic regions of the scalar gap function. However, for the ultraviolet behavior of V the transverse gluon interaction, Eq. (4.8) is the leading piece. All these findings agree with a recent perturbative analysis, Ref. [14].

We note that the preceding ultraviolet analysis obviously also holds true when using the non-perturbative gluon propagator, Eq. (5.28), since it approaches the tree-level propagator for large momenta. In the last part we therefore perform only the small momenta analysis of the gap equations, Eqs. (5.22), (5.23), with a non-perturbative gluon propagator, Eq. (5.28), as input.

3. Gap Equation with Vector Kernel V and with Non-Perturbative Gluon Propagator

We now switch on the Gribov mass (thus take the infrared constant part of the loop integral I, Eq. (4.24), into account), use $I(k \to 0) = \frac{1}{2}\frac{1}{(2\pi)^2}M^2$ and rewrite Eq. (5.22) as

$$\begin{aligned} &\left[k + gC_F V(k \to 0) I(k \to 0)\right] S(k) = \\ &= I_C^{(1)}(k \to 0)\left[1 - S^2(k \to 0) + C_F V^2(k \to 0) I(k \to 0)\right] \ . \end{aligned} \quad (5.56)$$

This is a quadratic equation and can be solved as

$$S(k \to 0) = \frac{-gC_F V(0) I(0) \pm \sqrt{g^2 C_F^2 V^2(0) I^2(0) + 4\left(I_C^{(1)}(0)\right)^2 (1 + C_F V^2(0) I^2(0))}}{2 I_C^{(1)}(0)} . \quad (5.57)$$

Now all parts of the gap equation are combined to give the infrared value of the scalar gap function S, which is no longer constrained to approach unity. The infrared value of $V(k)$, determined from the equation (5.23), given as

$$\begin{aligned} &\left[k + gC_F V(k \to 0) I(k \to 0) + \frac{1}{2} I_C^{(2)}(k \to 0)\right] V(k \to 0) = \\ &= \frac{g}{2}\left[1 + S^2(k \to 0) + C_F V^2(k \to 0) I(k \to 0)\right] \ , \end{aligned} \quad (5.58)$$

is solved as

$$V(k\to 0) = -\frac{GI_C^{(2)}(0) \pm \sqrt{(GI_C^{(2)}(0))^2 + 4\frac{g}{2}C_F I(0)\frac{g}{2}(1+S^2(0))}}{2\frac{g}{2}C_F I(0)} \,, \tag{5.59}$$

which is again infrared constant. However, in contrast to the infrared value of V using the perturbative gluon propagator (5.51), here V is connected non-trivially with S. All different parts of the energy density are combined to give the zero-momentum value of the vector kernel V.

However, as a side-effect of these results, the constituent quark mass can, in principle, no longer be extracted as the slope of the scalar wave function $S'(0)$, Eq. (5.43). Expanding the expression for the dynamical mass (3.82) around zero, we arrive at

$$M(k\to 0) = k\frac{2S(k\to 0)+\mathcal{O}(k)}{1-S^2(k\to 0)+\mathcal{O}(k)-(R(k\to 0)+\mathcal{O}(k))} \,, \tag{5.60}$$

and the identification $M(0) = -1/S'(0)$ only holds true if

$$S^2(k\to 0) + C_F V^2(k\to 0) I(k\to 0) = 1 \,. \tag{5.61}$$

For instance, if S approaches a value larger than unity then Eq. (5.61) cannot be fulfilled (since the loop integral $I(k) \geq 0$) and we would end up with $M(k\to 0) \sim -k\mathcal{C}$, with $\mathcal{C}$ a constant. It will be interesting to observe, if the solution functions S and V fulfill Eq. (5.61) and thus allow for an infrared constant quark mass $M(0)$.

However, before we start with the numerical evaluation, we summarize the most important findings for the three different situations studied in this section:

1. Adler-Davis gap equation, i.e., setting $V = 0$

$$S(k\to 0) = 1, \quad S(k\to\infty) = \frac{1}{k^5} \tag{5.62}$$

2. Gap equation with perturbative spatial gluon propagator, i.e., $V \neq 0, M_{\rm G} = 0$

$$S(k\to 0) = 1 \,, \quad S(k\to\infty) = \frac{1}{k^5} \tag{5.63}$$

$$V(k\to 0) = \frac{\frac{g}{2}(1+S^2(k\to 0))}{\frac{1}{2}C_F I_{\rm C}^{(2)}(k\to 0)} \,, \quad V(k\to\infty) = \frac{1}{k} \tag{5.64}$$

3. Gap equation with non-perturbative spatial gluon propagator, i.e.,$V \neq 0, M_{\rm G} \neq 0$

$$S(k\to 0) = f(I(k\to 0), I_{\rm C}^{(1)}(k\to 0), V(k\to 0)) \,, \quad S(k\to\infty) = \frac{1}{k^5} \tag{5.65}$$

$$V(k\to 0) = g(I(k\to 0), I_{\rm C}^{(2)}(k\to 0), S(k\to 0)) \,, \quad V(k\to\infty) = \frac{1}{k} \tag{5.66}$$

Switching off the vector kernel constrains the scalar gap function S to unity in the infrared, Eq. (5.62), and the dynamical mass $M(p)$, Eq. (3.82), can be evaluated from the slope of S around zero, Eq. (5.43). The same conclusion holds true for a perturbative static spatial gluon propagator, Eq. (5.63). However, the infrared value of S becomes a non-trivial expression of *all* terms appearing in the gap equation, when switching on the infrared part of the spatial gluon propagator, Eq. (5.65). This indicates that the infrared part of the gluon propagator (5.28) is essential, in order that the solution functions S and V start to interact. The vector kernel V, is constrained for a perturbative gluon propagator, Eq. (5.27), by the infrared value of the scalar kernel S as well as the Coulomb integral $I_{\mathrm{C}}^{(2)}$, Eq (5.64). For the non-perturbative gluon propagator, Eq. (5.28), it becomes an expression of all parts contributing to the energy density, Eq. (5.66).

In the ultraviolet we find power-law solutions, Eqs. (5.65) (5.66), with the scalar variational kernel S being governed by the Coulomb energy, Eq. (5.9), and the vector variational function V driven by the transverse gluon exchange, Eq. (4.8).

5.4.2 Numerical Analysis

All quantities appearing in the coupled system, Eqs. (5.22), (5.23), are expressed in units of the Coulomb string tension σ_{C}, which enters the static quark potential V_{C}, Eq. (5.26). We use values $\sigma_{\mathrm{C}} = (2 \ldots 3)\sigma_{\mathrm{W}}$ with $\sqrt{\sigma_{\mathrm{W}}} = 440$ MeV the Wilson string tension determined on the lattice (for a discussion of this quantity see Section 1.6). The Gribov mass $M_{\mathrm{G}} = 880$ MeV is then determined by the Coulomb string tension σ_{C}. The coupling g, which is fixed as in Section 4.3 at the infrared value $g(0)$ calculated in Ref. [8] from the ghost-gluon vertex, is, in contrast to $\alpha(k)$ at finite k, independent of the scale. We will introduce physical units when evaluating the phenomenological quantities, i.e., the chiral condensate $\langle\overline{\psi}\psi\rangle$, Eq. (3.85), and the dynamical mass $M(k)$, Eq. (3.82).

We have to regularize the kernels $L(k,q)$ and $K(k,q)$, Eqs. (5.30), (5.31), which are both divergent for $k = q$. In order to make the integrals in the gap equations well-defined we introduce a regulator ε as [79]

$$V_{\mathrm{C}}(\boldsymbol{k}) \to V_{\mathrm{C}}(\boldsymbol{k},\varepsilon) \;=\; \frac{8\pi\sigma_{\mathrm{C}}}{\boldsymbol{k}^2(\boldsymbol{k}^2+\varepsilon^2)} \;. \tag{5.67}$$

The kernels $L(k,q,\varepsilon)$ and $K(k,q,\varepsilon)$ then read

$$L(k,q,\varepsilon) = \frac{1}{kq\varepsilon^2}\ln\left|\frac{k+q}{k-q}\right| + \frac{1}{2kq\varepsilon^2}\ln\left[\frac{(k-q)^2+\varepsilon^2}{(k+q)^2+\varepsilon^2}\right] \;, \tag{5.68}$$

$$K(k,q,\varepsilon) = \frac{1}{2}\left(\frac{k^2+q^2}{k^2q^2\varepsilon^2}\ln\left|\frac{k+q}{k-q}\right| + \frac{\varepsilon^2+k^2+q^2}{2k^2q^2\varepsilon^2}\ln\left[\frac{(k-q)^2+\varepsilon^2}{(k+q)^2+\varepsilon^2}\right]\right) \;. \tag{5.69}$$

The variational function and consequently all physical observables become ε-dependent, however, with setting $\varepsilon \to 0$, the functions converge onto a final result

$$\lim_{\varepsilon\to 0} S(k,\varepsilon) = S(k) \;, \quad \lim_{\varepsilon\to 0} V(k,\varepsilon) = V(k) \;. \tag{5.70}$$

We note that there are plenty of possible infrared regularizations, for a different realization see Ref. [102].

The coupled one-dimensional integral equations which we compute numerically then read

$$S(k) = \frac{G\int dq\,(L(k,q;\varepsilon)\Xi_1(q)(1-S^2(k)+C_FV^2(k)I(k))-K(k,q;\varepsilon)\Xi_2(q)S(k))}{k+g(0)C_FV(k)I(k)}\,, \tag{5.71}$$

$$V(k) = \frac{\frac{g(0)}{2}\,(1+S^2(k)+C_FV^2(k)I(k))}{k+g(0)C_FV(k)I(k)+G\int dq\,(L(k,q;\varepsilon)2\Xi_1(q)S(k)+K(k,q;\varepsilon)\Xi_2(q))}\,, \tag{5.72}$$

where we have used

$$\Xi_1(q) \;=\; \frac{S(q)}{1+S^2(q)+C_FV^2(q)I(q)}\,, \tag{5.73}$$

$$\Xi_2(q) \;=\; \frac{1-S^2(q)-C_FV^2(q)I(q)}{1+S^2(q)+C_FV^2(q)I(q)}\,. \tag{5.74}$$

The constants $G = \frac{1}{2}8\pi C_F\frac{1}{(2\pi)^2}$ (in units of the string tension $\sigma_{\rm C}$) and $g(0) = \frac{8\pi}{\sqrt{3N_{\rm C}}}$ then read for $SU(3)$ and for $SU(2)$

$$SU(3): \quad G\approx 0.4244, \qquad \text{and} \quad g(0)\approx 8.37758, \tag{5.75}$$

$$SU(2): \quad G\approx 0.2387, \qquad \text{and} \quad g(0)\approx 10.2604\,. \tag{5.76}$$

We mostly work with the color group $N_{\rm C}=3$.

Let us again emphasize the dimensions of the gap functions. The scalar part S is dimensionless and V has dimension of $(\text{GeV})^{-1}$, see Appendix B.4. We can work with either dimensionfull $V(k)$ or the dimensionless quantity $\hat{V}(k)=V(k)/k$.

The three equations, studied in the previous section in an an analytic framework, will now be analyzed numerically.

1. Adler-Davis Gap Equation

We start with the numerical evaluation of Eq. (5.36), where the vector wave function V is set to zero. We solve the equation for the condensate wave function S, Eq. (5.37), as well as for the dynamical mass M, Eq. (5.42), numerically, in order to test the stability of our numerics. Using the definition of the dynamical mass, Eq. (3.82), we can crosscheck the solutions. We emphasize that the results derived in this subsection were already obtained in Ref. [80].

Before turning to the evaluation of the phenomenological quantities, we list the main numerical investigations:

1. As a first test on the asymptotic analysis, we set the kernel $K(k,q;\varepsilon)=0$ and solve the gap equations for S and the dynamical mass M. The solution is plotted

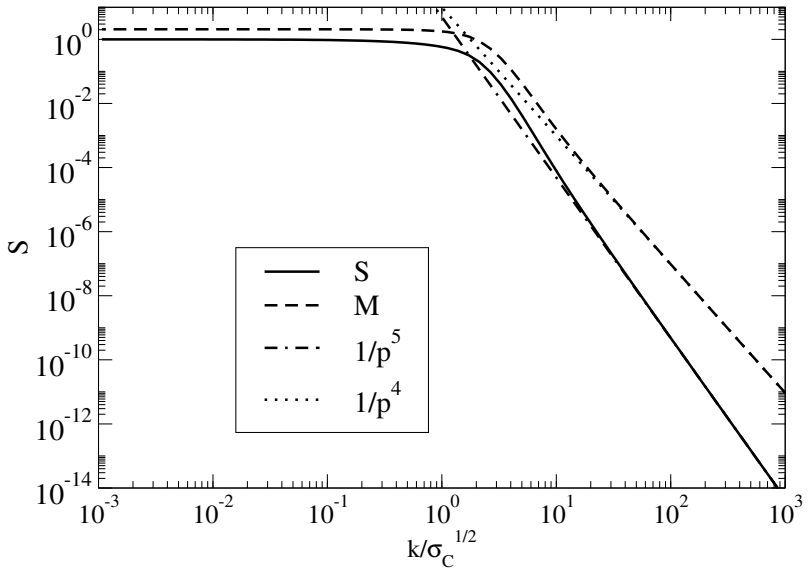

Figure 5.1: *Scalar gap function S and dynamical mass M with $K(k,q;\varepsilon)=0$. The coupling is set to $G=1$ and the (infrared) regulator is $\varepsilon=1$. The dashed-dotted curve indicates the UV-power law behavior of the scalar kernel S and the dotted curve indicates the power-law of the dynamical mass M.*

in Fig. 5.1. The infrared cut-off is fixed at $\varepsilon = 1$. The value of $S(0)$ is constrained by the non-linear equation to be unity. For large momenta the solution function shows the characteristic power-law behavior $S(k \to \infty) \sim 1/k^5$. This confirms that the asymptotic regions of the gap equation, Eq. (5.36), are driven by the integral $L(k,q)$, Eq. (5.30).

2. When taking into account the integral kernel $K(k,q;\varepsilon)$, Eq. (5.69), we have to be careful, since function values over a wide range of magnitudes of the momenta k and q have to be evaluated. For instance, with the outer momentum k becoming very small (around the lower boundary $k \sim \Lambda_{\mathrm{IR}}$) and the loop momentum reaching values at the upper boundary $q \sim \Lambda_{\mathrm{UV}}$, the contributions of the form $\frac{q^2}{k^2} \sim \frac{\Lambda_{\mathrm{UV}}^2}{\Lambda_{\mathrm{IR}}^2}$ become very large and lead to an oscillating behavior of the solution function for small external momenta k. We therefore represent the function $K(k,q;\varepsilon)$ for momenta $k^2 \ll (q^2+\varepsilon^2)$ around $k=0$ by its Taylor series

$$K(k,q;\varepsilon) = \frac{8(\varepsilon^2+2q^2)k}{3q^3(\varepsilon^2+q^2)^2} + \frac{16(\varepsilon^6+4\varepsilon^4q^2+6\varepsilon^2q^4+9q^6)k^3}{15q^5(\varepsilon^2+q^2)^4} + \mathcal{O}(k^4)\ . \quad (5.77)$$

This procedure will be performed for the coupled equation as well, i.e., with switching on the vector coupling V.

3. From a numerical point of view it is easier to solve the equation for the dynamical mass M, Eq. (5.42). Due to the momentum k appearing on the left-hand side of the gap equation determining S, Eq. (5.36), we have to introduce a relaxation

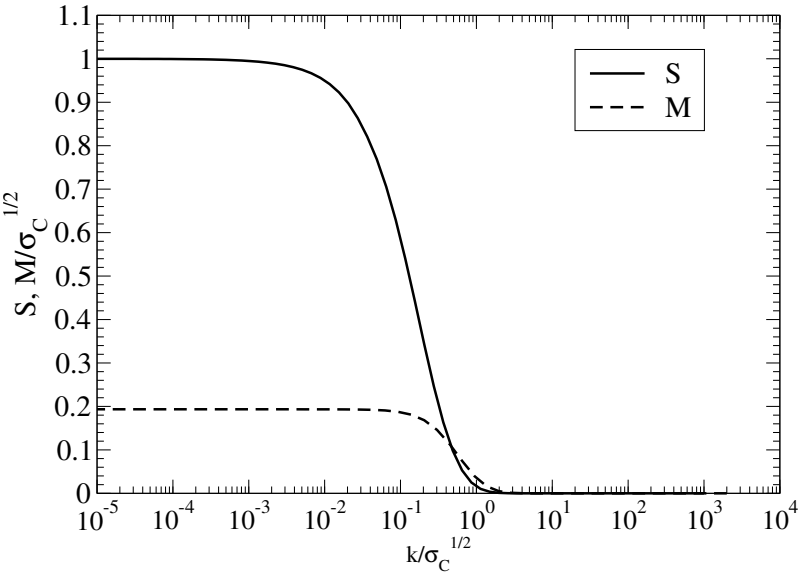

Figure 5.2: *Scalar gap function S and dynamical mass M for the Adler-Davis gap equation using the gauge group $SU(3)$ and the infrared regulator fixed at $\varepsilon = 0.01$.*

prescription in order to get a stable solution (for more details, see Appendix D). Such a relaxation method is not necessary for the dynamical mass equation (5.42). Hence, the equation for S, Eq. (5.36), converges much slower than the equation for the dynamical mass M, Eq. (5.42).

However, both solution functions show the characteristic behavior: In the small momentum regime the dynamical mass function $M(p)$ freezes out and S approaches unity as predicted by the analytic calculation. Moreover, via Eq. (5.43) both results are crosschecked and confirmed to be equal. In the large momentum regime the power-law behavior extracted from the asymptotic analysis, Eq. (5.45), is confirmed. The corresponding plot is shown in Fig. 5.2.

4. Next, we lower the infrared-regulator ε, see Figs. 5.3, 5.4 5.5. The number of iteration steps to reach a stable solution increases with decreasing ε. Due to numerical uncertainties we cannot approach arbitrary small values of ε. The solution functions S_ε converge onto a stable solution S at about $\varepsilon \approx 10^{-3}$.

We now turn to the chiral parameters of the theory, the dynamical mass (3.82) and the chiral condensate (3.85). Extracting the linear decrease of S for small momenta $S'(0) \approx 5.2$ or plugging the result for S in formula (3.82) we arrive at a value for the constituent mass of about

$$M(0) \approx 84\,\text{MeV}\,\sqrt{\sigma_\text{C}/\sigma_\text{W}}\,, \tag{5.78}$$

which is, using values of the Coulomb string tension of about $\sigma_\text{C} = (2\ldots3)\sigma_\text{W}$

$$M(0) \approx (120\ldots150)\,\text{MeV}\,. \tag{5.79}$$

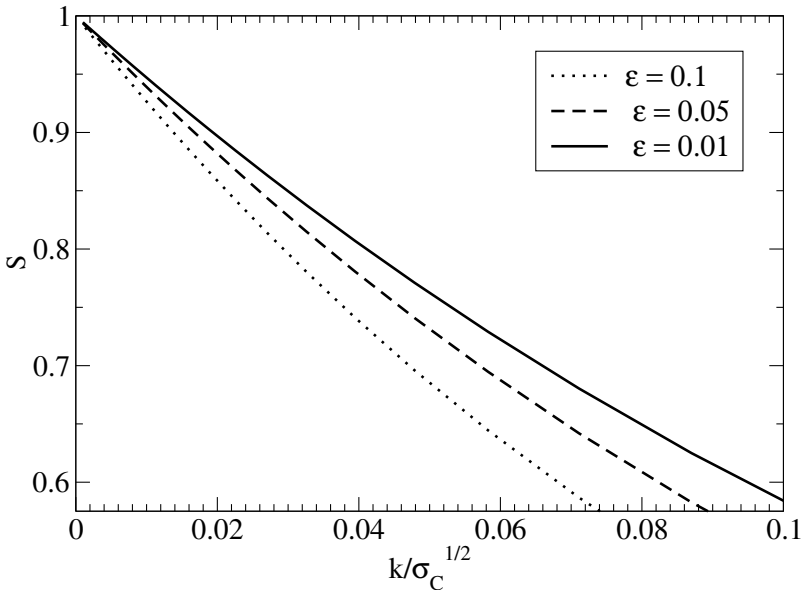

Figure 5.3: *Scalar solution function S for decreasing values of the cut-off ε. The constituent mass $M(0)$ manifests itself in the slope $S'(0)$. For decreasing ε the slope at $k = 0$ becomes smaller, which goes in hand with the observation that the constituent mass $M(0)$ increases for decreasing ε.*

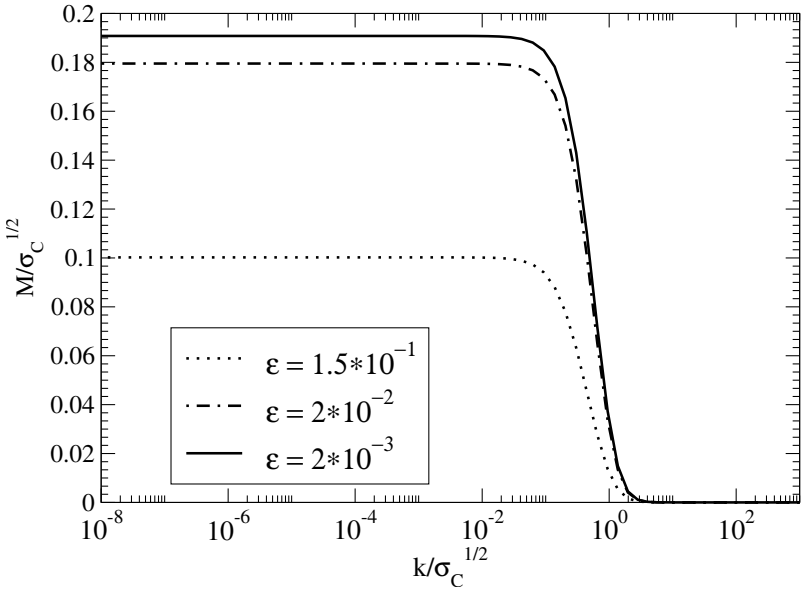

Figure 5.4: *The dependence of the dynamical mass on the infrared regulator ε. For decreasing infrared regulator ε the value $M(0)$ enlarges, converging onto a final curve.*

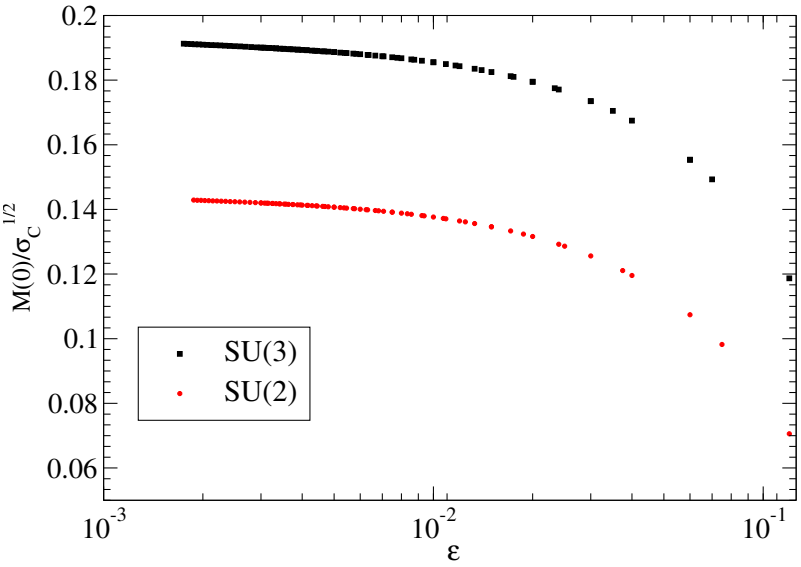

Figure 5.5: *The infrared value of the dynamical mass $M(0)$ for the color groups $SU(2)$ and $SU(3)$ plotted against the infrared regulator ε.*

Comparing with the phenomenological value $M(0) \approx 300$ MeV shows that even if we use values of the string tension at the upper limit, i.e., $\sigma_{\mathrm{C}} = 3\sigma_{\mathrm{W}}$ we reach values which are too small by a factor of (at least) two. For the gauge group $SU(2)$ we get $M(0) \approx 63\,\mathrm{MeV}\sqrt{\sigma_{\mathrm{C}}/\sigma_{\mathrm{W}}}$, which gives values around $M(0) \approx (90 - 110)\,\mathrm{MeV}$.

We compute the chiral condensate via Eq. (3.85) and arrive for $SU(3)$ at

$$\langle\overline{\psi}\psi\rangle \approx -\left(113\,\mathrm{MeV}\sqrt{\sigma_{\mathrm{C}}/\sigma_{\mathrm{W}}}\right)^3 . \tag{5.80}$$

Using the values of σ_{C} quoted above yields

$$\langle\overline{\psi}\psi\rangle \approx -\left(160 \ldots 196\,\mathrm{MeV}\right)^3 . \tag{5.81}$$

Comparing again with the phenomenological value $\langle\overline{\psi}\psi\rangle \approx -(235\,\mathrm{MeV})^3$, Ref. [68], we end up with values which are consistently smaller than the experimental ones.

We can conclude that the phenomenological quantities evaluated from the Adler-Davis gap equation (5.36) are too low, indicating that some important physical components are still missing. These shortcomings are clear: the ordinary Coulomb potential α_{S}/r in $V_{\mathrm{C}}(r)$, Eq. (5.6), and most importantly the transverse gluon exchange are not accounted for by the Adler-Davis gap equation.

2. Gap Equation with Vector Kernel V and with Tree-Level Gluon Propagator

We turn to the coupled equations (5.22) (5.23) and take the tree-level gluon propagator, Eq. (5.27), into account. We list the most important numerical findings:

1. To approach a convergent result we use a relaxation parameter (for details, see Appendix D). The number of iteration steps to reach a stable solution lies in

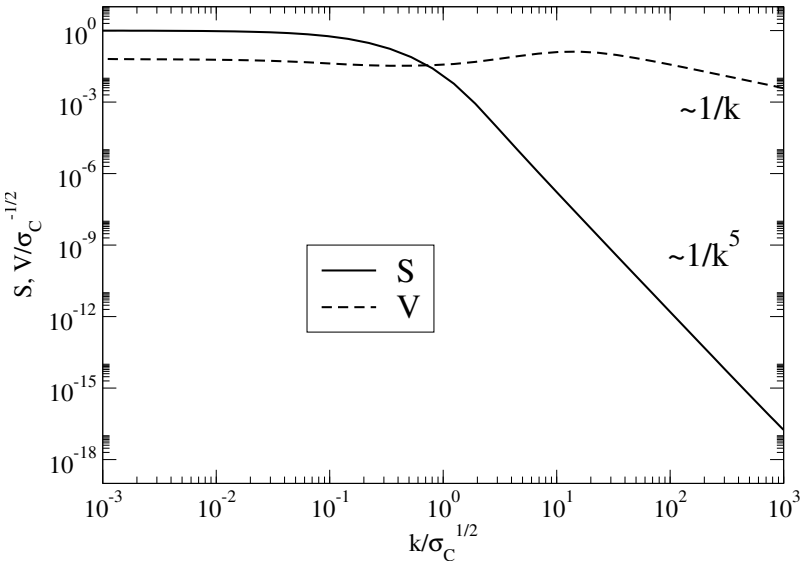

Figure 5.6: *Variational kernels S and V using the large momentum behavior of the static spatial gluon propagator as input. Both kernels become constant for small momenta and vanish for large momenta. The scalar solution S extends to a much larger range of magnitudes than the vectorial solution function V.*

the region of the Adler-Davis gap equation, Eq. (5.36). Taking different starting functions and altering the number of integration points and Chebyshev points, the coupled system is tested to be robust.

The results for the joint solution S and V are presented in Fig. 5.6, which confirm the asymptotic analysis, Eqs. (5.63), (5.64). The vectorial variational function V tends to a constant in the infrared and the scalar gap function S becomes unity. For large momenta the power-law behavior $S(k) \sim 1/k^5$, $V \sim 1/k$ is obtained.

2. We lower the infrared regulator ε. The value constraining the vector gap function V at zero momentum is related to the Coulomb integral $I_C^{(2)}(k)$, Eq. (5.51). As ε goes to zero, $I_C^{(2)}(k)$ approaches larger values, so that the infrared value of V becomes smaller.

3. We now compare the result for the scalar solution function S with the Adler-Davis result, Fig. 5.7. We observe that both functions are nearly identical and also the chiral parameters *do not increase* towards phenomenological values. For the dynamical mass, Eq. (3.82), as well as for the chiral condensate, Eq. (3.85), the vector coupling V gives only negligible corrections. The values for $M(0)$ and $\langle\overline{\psi}\psi\rangle$ are therefore given in Eq. (5.78) and Eq. (5.80).

4. Changing the value of the coupling $g(0)$ fixed at the infrared value, i.e., setting $g(0) = 83.77$ and $g(0) = 0.8377$ does not alter the scalar gap function $S(k)$. The infrared value of V is shifted upwards with increasing g, which can be understood from the asymptotic analysis, Eq. (5.51). We conclude that with the use of a

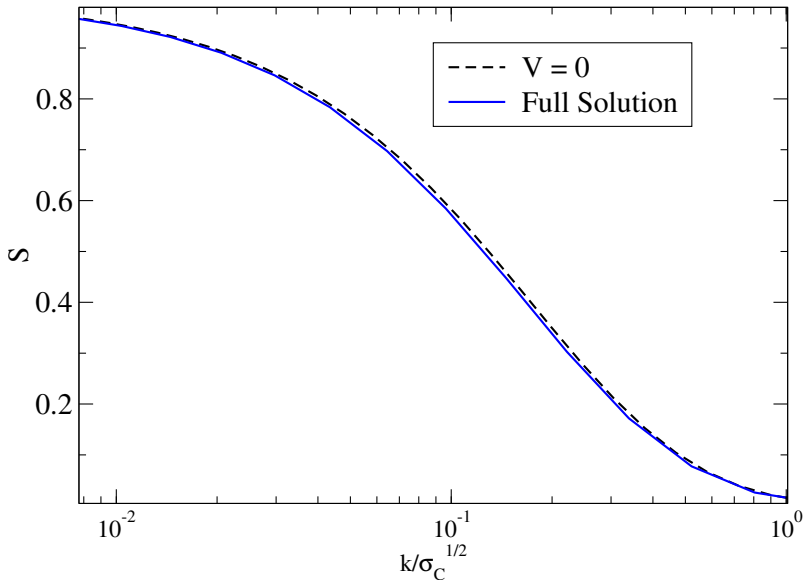

Figure 5.7: *Scalar variational functions $S(k)$ with and without the coupling to transverse gluons. The perturbative gluon propagator is used as input into the gap equations.*

perturbative propagator physical values are *insensitive* to the infrared value of the coupling $g(0)$. The chiral condensate as well as the dynamical mass, dominated by $S(k)$, are unaffected by the change of $g(0)$. This gives us a first hint that with use of a perturbative static gluon propagator the gap functions S and V *do not communicate*: Although the vector kernel V changes with the value of the coupling $g(0)$, the scalar gap function is unaffected.

5. It is interesting to take a different pre-factor for the Coulomb integral $I_C^{(2)}(k)$, Eq. (5.18), since it alters the infrared behavior of the vectorial part V, see Eq. (5.51). We use $0.1I_C^{(2)}(k)$ and $10I_C^{(2)}(k)$. The solution function S is *not* affected by the change of this pre-factor. The vectorial solution functions forms a decreasing infrared constant value for increasing values of the pre-factor, which can be understood in terms of the infrared analysis (5.51). Lowering the pre-factor of $I_C^{(2)}$ has the same effect as increasing g. However, what we can conclude from changing $g(0)$ and the pre-factor of $I_C^{(2)}$ is that the two variational functions S and V are not *fully* coupled. We will observe that this coupling is supplied by the infrared part of the static spatial gluon propagator, Eq. (5.28).

6. Lowering the infrared cut-off ε increases the solution function $S(k)$ in the same manner as it does for the Adler-Davis solution. The corresponding plot is in accordance with Fig. 5.3. The values of the solution function $S(k)$ become slightly larger with decreasing ε, which leads to increasing values of the constituent mass. We again reach a stable solution at $\varepsilon \approx 10^{-3}$.

The outcome of the numerical study is at first glance rather discouraging because physical values are not increased by the additional kernel V in the quark vacuum wave functional,

Eq. (3.3). Analyzing the equations for different couplings $g(0)$ and different pre-factors of $I_C^{(2)}$ Eq. (5.18), we observe that the scalar variational function S *does not feel* the vectorial solution function V. In the numerical analysis of the gap equations using the full non-perturbative gluon propagator, Eq. (5.28), we will observe that it is the Gribov mass M_{G}, Eq. (1.96), which plays the mediator between scalar part S and vectorial part V and which increases the scalar solution function S with increasing $g(0)$ and decreasing pre-factor of $I_C^{(2)}$, Eq. (5.18).

3. Gap Equation with Vector Kernel V and with Non-Perturbative Gluon Propagator

From the analytic framework, see Eqs. (5.65), (5.66) we have derived two important insights into the coupled system, Eqs. (5.22), (5.23). First of all, with the use of the non-perturbative gluon propagator, Eq. (5.28), the scalar gap function S is no longer constrained to approach unity for small momenta. Secondly, with the infrared constant loop integral $I(k)$, Eq. (4.23), all components appearing in the gap equations (5.22), (5.23) are combined to give a non-trivial relation between the infrared values of S and V.

We now clarify these findings in a numerical evaluation and establish further insights into the interplay between scalar and vector interaction kernels S and V. We again list the most important numerical findings:

1. The number of iteration steps to reach a stable solution is comparable to the Adler-Davis solution and the solution using the perturbative gluon propagator. Moreover, lowering the infrared cut-off ε we reach stable results at $\varepsilon \approx 10^{-3}$. As in the case using the perturbative propagator, with decreasing infrared regulator ε the infrared value of V becomes smaller.

2. The coupled solutions have the same characteristic features as the solutions using the perturbative gluon propagator. Both variational functions become constant in the infrared and show a power-law in the ultraviolet, see Fig. 5.8. The infrared value of the vector kernel V is enhanced in comparison to the case using the perturbative propagator. Moreover, in comparison to the result with vanishing quark-gluon vertex V in the wave functional, the scalar kernel S is *larger* in the mid-momentum region and the slope around zero is *smaller*. These two results have crucial impact on the chiral properties of the theory. Numerical investigations show that the mid-momentum region is closely connected to the chiral condensate, Eq. (3.85). The slope around unity is related to the constituent mass, Eq. (5.60). The plot comparing the Adler-Davis and the new result is shown in Fig. 5.9.

3. Altering the coupling $g(0)$ to larger values, shifts the scalar gap function S to larger values for intermediate momenta and also affects the infrared value, see Fig. 5.10. Comparing with the result for the perturbative gluon propagator, where altering the coupling $g(0)$ has no effect on S, we can conclude that the Gribov scale M_{G},

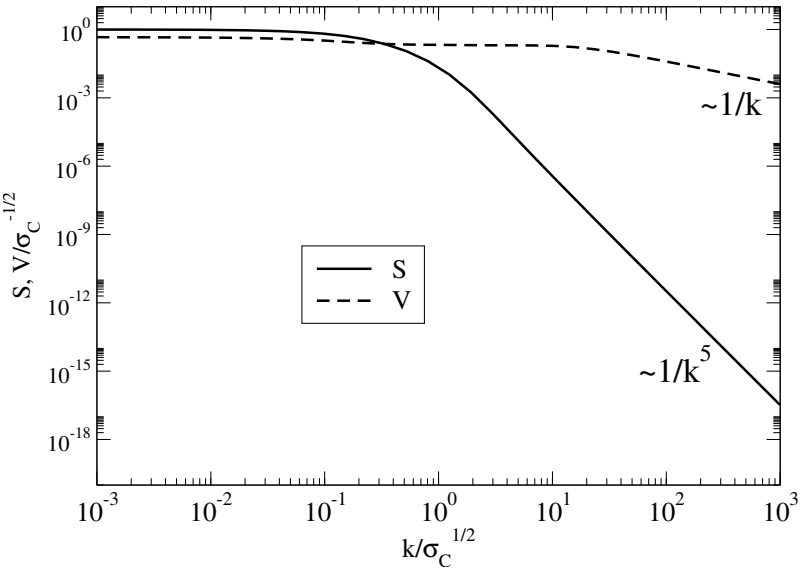

Figure 5.8: *Variational kernels S (full curve) and V (dashed curve) using the non-perturbative gluon propagator as input.*

Eq. (1.96), and therefore the infrared part of the gluon propagator, Eq. (5.28), is essential for the interplay between the coupled equations, Eqs. (5.22), (5.23).

4. As for the case of the perturbative propagator, we change the value of the pre-factor of $I_C^{(2)}$, Eq. (5.18), in Eq. (5.23). The corresponding plot is shown in Fig. 5.11. Smaller values of $I_C^{(2)}$ lead to larger values of S. At a certain value we find $S'(0) > 0$ and the scalar function S forms a maximum. In this case the dynamical mass becomes negative, see the discussion after Eq. (5.60). Note, however, that changing the pre-factor of $I_C^{(2)}$, Eq. (5.18), has no physical meaning and is only performed to test the coupled equations, Eqs. (5.22), (5.23). Moreover, for smaller values of the pre-factor the infrared constant value becomes shifted away from unity towards larger values. The value of V becomes larger for decreasing pre-factor, which was also true for the case using a perturbative gluon propagator.

Now we have everything in place to study the effect of these results on the phenomenological parameters of the theory. We begin with the expression for the chiral condensate, Eq. (3.85). Compared to the Adler-Davis condensate (5.80), with the additional quark-gluon coupling the value for the quark condensate is shifted to

$$\langle\overline{\psi}\psi\rangle \approx -\left(135\,\mathrm{MeV}\sqrt{\sigma_{\mathrm{C}}/\sigma_{\mathrm{W}}}\right)^3 , \tag{5.82}$$

which is a 20% increase of the figure in the bracket. We observe that this increase comes from the additional contributions in the mid-momentum regime of S, see Fig. 5.9. Moroever, we find that the gluon loop integral $R(k)$, Eq. (3.46), which enters the expression Eq. (3.85), gives negligible corrections to the value of the condensate. Setting

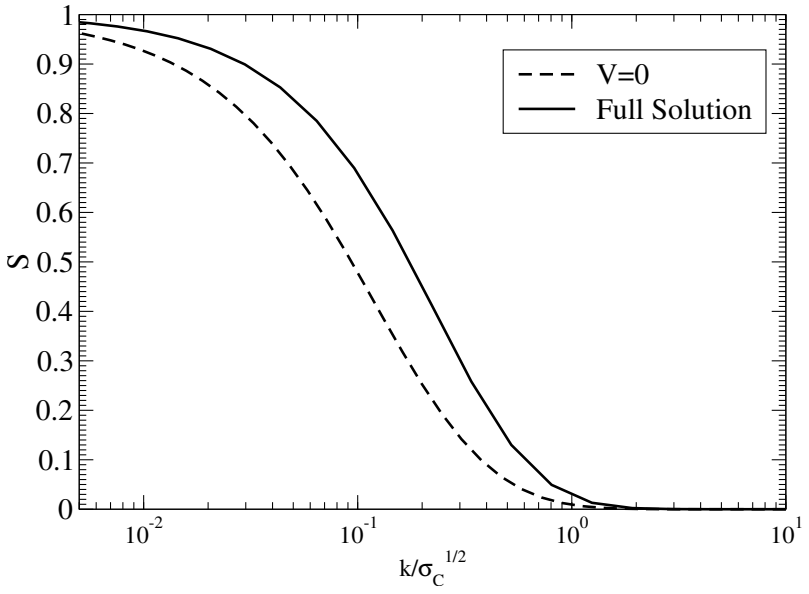

Figure 5.9: *Variational kernels S comparing the solutions with $V = 0$ (Adler-Davis solution) and $V \neq 0$ using the non-perturbative gluon propagator as input.*

the scale at $\sigma_{\rm C} = (2 \ldots 3)\sigma_{\rm W}$, we obtain physical values

$$\langle\overline{\psi}\psi\rangle \approx -\left(191 \ldots 234\,\text{MeV}\right)^3 , \tag{5.83}$$

and we can conclude that the coupling of the quarks to the transverse gluons shifts the quark condensate significantly towards the phenomenological value of about $\langle\overline{\psi}\psi\rangle = -(235\text{MeV})^3$, Ref. [68].

Before we extract the dynamical mass via Eq. (3.82) we note that the small-momentum slope of the scalar variational function S is given as $S'(0) \approx 3.36$ as opposed to the Adler-Davis value $S'(0) \approx 5.2$. We find that Eq. (5.61) approximately holds true, so that we can evaluate the constituent mass via Eq. (5.60). We get

$$M \approx 132\,\text{MeV}\sqrt{\sigma_{\rm C}/\sigma_{\rm W}}\,, \tag{5.84}$$

which is, compared to the Adler-Davis value, Eq. (5.78), an increase of 57%. Finally, using the values for $\sigma_{\rm C}$ quoted above we obtain

$$M \approx (186 \ldots 230)\,\text{MeV}\,, \tag{5.85}$$

which shows that also for the constituent quark mass the quark-gluon coupling V in the quark wave functional provides an essential enhancement and leads to fairly reasonable phenomenological values. The corresponding plot of the dynamical quark mass $M(k)$ with the scale fixed at $\sigma_{\rm C} = 2\sigma_{\rm W}$ is shown in Fig. 5.12.

Let us shortly summarize the main outcome of the numerical study to the coupled gap equations (5.22), (5.23). First of all, we evaluated the gap equation with vanishing

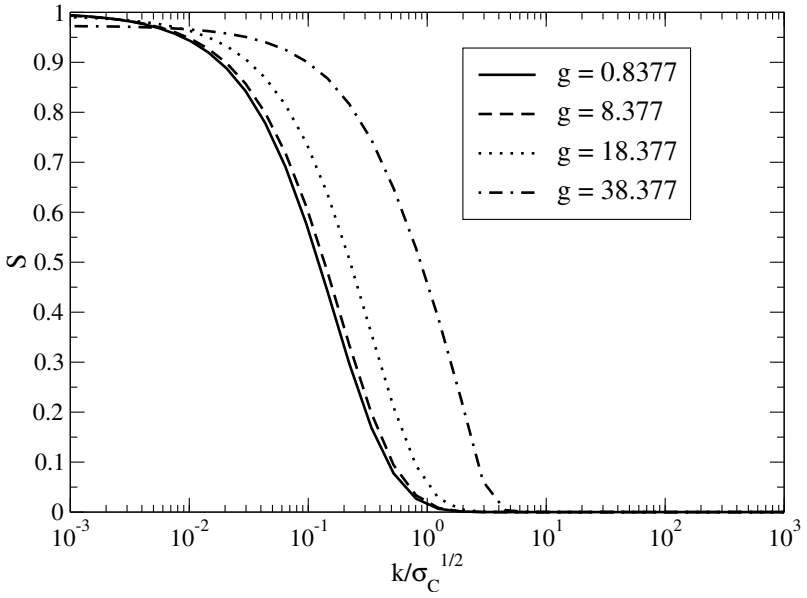

Figure 5.10: *Scalar variational kernel S for different values of the coupling $g(0)$ of quarks to transverse gluons.*

vector kernel $V = 0$, known as Adler-Davis gap equation. We found the scalar variational function S to agree with the result obtained in Ref. [80]. However, with setting the scale at the Coulomb string tension σ_{C} the physical values are slightly larger than in Ref. [80], where the scale is set at $\sqrt{\sigma_{\mathrm{W}}} = 350$ MeV. Nevertheless, the low energy chiral properties of the theory come out significantly too small. We then turned to the coupled system with non-vanishing vector kernel V. We could demonstrate that the small momentum part of the static spatial gluon propagator, Eq. (1.95), has a special role. It couples the gap functions S and V non-trivially. In comparison to the result with vanishing vector kernel the scalar kernel S becomes larger in the mid-momentum regime and the slope around unity is smaller. We could show that these features lead to increasing phenomenological values. The effect of the additional vector kernel V is in the range between $20 - 60\%$. For the chiral condensate we come into the right region of experiment. For the dynamical quark mass there is still a certain contribution missing, which can result from neglecting certain parts of the Hamiltonian (1.23) in the variational analysis. These additional contributions are currently under investigation. Moreover, to make more accurate predictions on the low energy properties of the theory, a more precise lattice measurement of the Coulomb string tension σ_{C} is required.

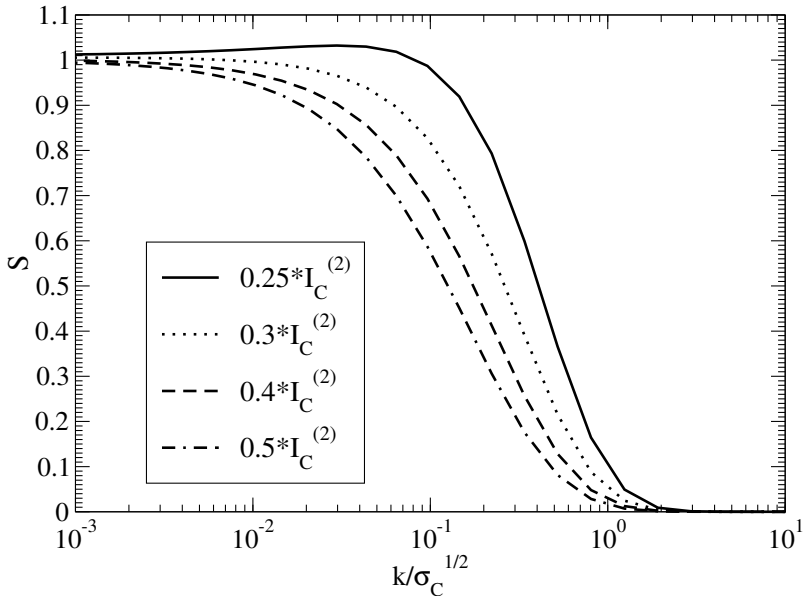

Figure 5.11: *Variational kernel S for different pre-factors of the integral $I_C^{(2)}(k)$. For explanations, see text.*

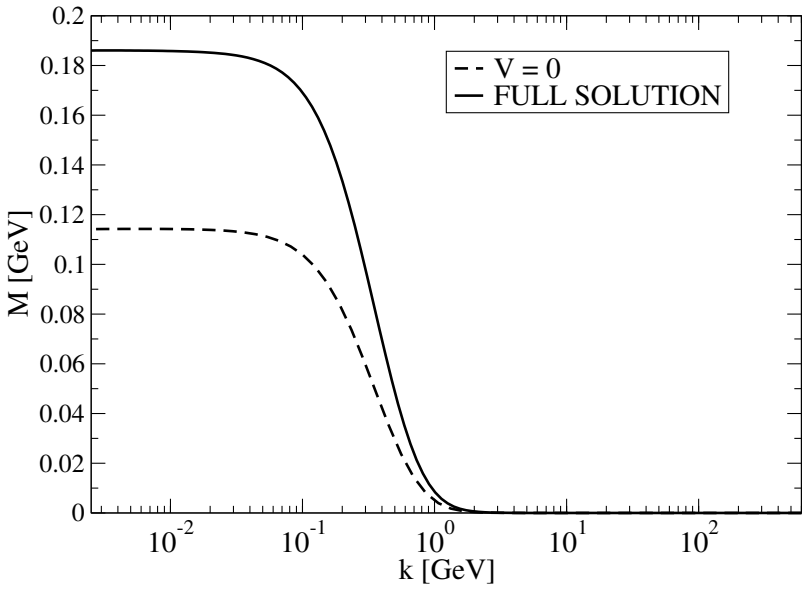

Figure 5.12: *Dynamical quark mass for the Adler-Davis (dashed curve) and coupled solution (full curve).*

Part II

Wilson Loop in the Hamiltonian Approach to QCD

Chapter 6

Wilson Loop from a Dyson Equation

The second part of the thesis concerns another distinctive property of QCD: the confinement of color, i.e., the phenomenon that in the hadron spectrum only color-singlet combinations, the hadrons, of color non-singlet objects, the quarks, appear. The potential between two static quark sources keeps rising linearly as one tries to isolate a single quark. Via the expectation value of the so-called Wilson loop the static quark-antiquark potential can be accessed. The Wilson loop, being the path-ordered exponential of a gauge field transported along a closed loop, serves as an order parameter of confinement. In a confining theory, the inter-quark potential extracted from the Wilson loop gives an area law, signalling that the interaction energy between the static sources is rising linearly. Nearly all information about the Wilson loop in non-perturbative QCD so far comes from the lattice. The computation of the Wilson loop in a continuum formulation is difficult due to the path ordering prescription, which enters the definition of the Wilson loop. One missing piece in the variational approach to Yang-Mills theory is to show the emergence of the area law from the Wilson loop.

A way to attempt the Wilson loop in the continuum comes from a Dyson equation, originally proposed in the context of supersymmetric theories and recently applied to Yang-Mills theory in Landau gauge. In this work we critically analyze this equation and apply it to Coulomb gauge Yang-Mills theory. We emphasize that in this part of the thesis we switch off the quark fields and work with pure gluodynamics.

In Section 1 we report on the Wilson loop, give a detailed description of path ordering, prove the gauge invariance of the Wilson loop and show how to extract the static quark-antiquark potential. In Section 2 we present the derivation of the Dyson-type integral equation, which sums all planar ladder diagrams and only needs the gluon propagator as its input. We discuss the approximations involved and work out its limitations. In Section 3 we apply the formalism to the temporal Wilson loop in Coulomb gauge. In Section 4 we show how to extract the static quark potential from the Dyson equation by solving a one-dimensional Schrödinger equation for the lowest eigenvalue. In Section 5 we calculate the spatial Wilson loop with the gluon propagator obtained from the variational approach to Yang-Mills theory as input.

An explicit realization of the paths along the Wilson loop as well as the computation of the gluon propagator contracted with the temporal paths is performed in Appendix E; the numerical technique used throughout this chapter is also presented there.

The results presented in this chapter are published in Ref. [106] and a summary of

these results can be found in Ref. [107].

6.1 Introduction

In Chapter 1, after Eq. (1.12) we have shortly raised the issue of color confinement: In the pure gluonic part of the QCD Lagrangian, Eq. (1.11), cubic and quartic terms in the gauge field A_μ^a appear, which give rise to self-interactions of the gluons. It is commonly accepted that confinement is a consequence of this non-Abelian nature of the gauge interaction.

Let us, in order to clarify this picture, compare the field lines which connect a pair of opposite charges in the non-Abelian and Abelian case. In QED the field lines connecting the static color sources are allowed to spread. In QCD, however, the field lines are believed to be concentrated within a narrow string, Ref. [112]. The potential between these color sources increases with the separation and at infinite distance one would need an infinite amount of energy to pull two quarks apart. In the full theory with dynamical quark fields the energy stored in the string would grow until the creation of quark-antiquark pairs is energetically favorable. This phenomenon is known as string breaking, Ref. [108], which can be observed on the lattice, see Refs. [3, 109–111].

Let us return to the pure Yang-Mills sector of QCD and formulate a criterion for confinement: Every theory of confinement should be able to explain the linearly rising potential between two static color sources [108].

We show how this quark-antiquark potential can be extracted by studying the Wilson loop, denoted as $\hat{W}(\mathcal{C})$. In Euclidean space-time the Wilson loop is defined by

$$\hat{W}(\mathcal{C}) \;=\; \frac{1}{d_{\mathrm{R}}} \mathsf{Tr}\, \mathcal{P}\, \exp\left[ig \oint\limits_{\mathcal{C}} dx_\mu A_\mu(x) \right] , \qquad A_\mu(x) = A_\mu^a(x) T^a \,. \tag{6.1}$$

Here d_{R} is the dimension of the representation of the gauge group and gives N_{C} for the fundamental representation of $SU(N_{\mathrm{C}})$. The quantity $\mathcal{P}$ denotes path ordering along this loop which will be described in detail below. The line integral in $\hat{W}(\mathcal{C})$, Eq. (6.1), is carried out along a closed loop $\mathcal{C}$, which is most conveniently taken to be of rectangular shape of length T and width L. The expectation value of this Wilson loop is then defined as

$$W(T;L) = \langle \hat{W}(\mathcal{C}) \rangle = \frac{\int DA_\mu \, \hat{W}(\mathcal{C})\, e^{-S[A]}}{\int DA_\mu e^{-S[A]}} \,. \tag{6.2}$$

The path ordering prescription $\mathcal{P}$ is defined as follows [112]: consider a path $\mathcal{C}$ with starting point x and divide the path into n infinitesimal segments. The intermediate points are $x_1, x_2, \ldots x_{n-1}$, $dx_m = x_m - x_{m-1}$ and x_0 is identified with the starting point and endpoint x. On each of the infinitesimal paths the exponential can be approximated

by the first term in the Taylor series. Then the expression Eq. (6.1) reads

$$W(\mathcal{C}) = \frac{1}{d_{\mathrm{R}}}\mathsf{Tr}\left[\lim_{dx_m\to 0}[1+igA_\mu(x_0)(x_1-x_0)]\dots[1+igA_\mu(x_{n-1})(x_n-x_{n-1})]\right] , \tag{6.3}$$

which is a product of non-commuting expressions. The path ordering $\mathcal{P}$ renders an evaluation of the Wilson loop in a continuum formulation of QCD complicated. In the Abelian case, however, path ordering is irrelevant. This last statement will become important below, when constructing the Dyson equation for the Wilson loop in Section 6.2.

Let us shortly report on the evaluation of the Wilson loop on the lattice[1]. On the lattice the algebra-valued gauge fields A_μ are replaced by the group-valued link variables U_μ. The link variables U_μ connect two space-time points on the lattice. The path ordered exponential (6.1) is then just the product of link variables along a path connecting the lattice sites

$$\hat{W}(\mathcal{C}) \;=\; \mathsf{Tr}\left[\prod_{(n,\mu)\in\mathcal{C}} U_\mu(n)\right] , \tag{6.4}$$

with n denoting the lattice sites. The most reliable evidence about the static inter-quark potential comes from lattice simulations, Ref. [113].

Before we come to discuss the connection of the Wilson loop with the static quark potential, let us discuss the properties of a Wilson loop under a gauge transformation. We define the so-called gauge transporter

$$\widetilde{W}(x,y) = \mathcal{P}\,\exp\left[ig\int_{\mathcal{C}_{xy}} dx_\mu A_\mu(x)\right] , \tag{6.5}$$

which connects two points x and y on the curve $\mathcal{C}_{xy}$ and can be seen as the continuum analogue to the lattice link variable U_μ. It has the following property under a gauge transformation, Eqs. (1.3), (1.4),

$$\widetilde{W}(x,y) \to \widetilde{W}'(x,y) = \Omega(x)\widetilde{W}(x,y)\Omega^\dagger(y) . \tag{6.6}$$

A quark-antiquark pair has the transformation property

$$\overline{\psi}(x)\psi(y) \to \overline{\psi}'(x)\psi'(y) = \overline{\psi}(x)\Omega^\dagger(x)\Omega(y)\psi(y) , \tag{6.7}$$

which can easily be verified with the use of Eqs. (1.3), (1.4). From this it follows that $\overline{\psi}(y)\widetilde{W}(y,x)\psi(x)$ is gauge invariant, which will be used below. Moreover, it is easy to see that the gauge rotations for a product of gauge transporters cancel for all but for the end-points

$$\Omega(x)\widetilde{W}(x,x_1)\underbrace{\Omega^\dagger(x_1)\,\Omega(x_1)}_{\mathbb{1}}\widetilde{W}(x,x_1)\Omega^\dagger(x_1)\dots \tag{6.8}$$

[1]For a pedagogical introduction to lattice QCD we refer to Ref. [82].

Taking now the trace of a closed loop the matrices Ω cancel against each other. The Wilson loop, being the trace of the parallel transporter along a closed contour $\mathcal{C}$, is then gauge invariant. The static quark potential derived from the behavior of the Wilson loop for large Euclidean times is therefore gauge invariant, too.

We come to discuss how to extract the quark-antiquark potential from the Wilson loop, $\hat{W}(\mathcal{C})$, Eq. (6.1). For the discussion we use the temporal gauge $A_0 = 0$, where the temporal gauge transporters become trivial. We consider the following quantity [114]

$$Q(t) = \overline{\psi}(\mathbf{0}, t)\widetilde{W}(\mathbf{0}, t; \boldsymbol{R}, t)\psi(\boldsymbol{R}, t) \; , \tag{6.9}$$

which can be interpreted as the creation operator of a state with an infinitely heavy quark at position $\mathbf{0}$ and an infinitely heavy anti-quark at position $\boldsymbol{R}$ at time t. The gauge transporter $\widetilde{W}$, Eq. (6.5), ensures gauge invariance of this quantity. We are interested in the quantity $Q^\dagger(T)Q(0)$. Computing the expectation value of this quantity for full QCD the quark fields can be integrated out, since quark loops can be neglected for infinitely heavy quarks. The quark fields in the expression (6.9) therefore do not have any influence and the expectation value of $Q^\dagger(T)Q(0)$ essentially becomes the Wilson loop average [114]

$$\langle Q^\dagger(T)Q(0)\rangle \sim W(T, L) \; . \tag{6.10}$$

We take the expectation value of the correlation function in pure gluodynamics,

$$\begin{aligned}\langle Q^\dagger(T)Q(0)\rangle &= \frac{1}{Z}\int DA\, e^{-S_{\mathrm{G}}[A]} Q^\dagger(T)Q(0) = \\ &= \sum_n \langle\psi|Q^\dagger(T)|n\rangle\langle n|Q(0)|\psi\rangle e^{-E_n T} = \sum_n |\langle\psi|Q^\dagger(T)|n\rangle|^2 e^{-E_n T} \; .\end{aligned} \tag{6.11}$$

Here we have expressed the correlator as a sum over eigenstates of the Hamiltonian operator. The Yang-Mills vacuum is denoted as $|\psi\rangle$, the excitation energy of the energy eigenstate $|n\rangle$ as E_n. We observe that for large times T the expectation value (6.11) is dominated by the lowest eigenvalue E_0. The behavior of the Wilson loop $\hat{W}(\mathcal{C})$, Eq. (6.1), for large Euclidean times T then is given as

$$\langle\hat{W}(\mathcal{C})\rangle \underset{T\longrightarrow\infty}{\longrightarrow} e^{-E_0(L)T} \; , \tag{6.12}$$

where $E_0(L)$ is the interaction energy of the static quark-antiquark pair separated by the distance L, known as static quark potential $V_{\mathrm{W}}(L)$ and sometimes referred to as Wilsonian potential. The energy of a quark-antiquark pair separated by a distance L is therefore computed as

$$E_0(L) = V_{\mathrm{W}}(L) = -\lim_{T\to\infty}\frac{1}{T}\ln\langle\hat{W}(\mathcal{C})\rangle \; . \tag{6.13}$$

At the present state of the art the inter-quark potential can only be determined in the lattice framework. In the next section we derive an equation where, at least in an approximate fashion, the Wilson loop can be computed using analytic methods[2].

[2] In a recent article, Ref. [115], the temporal Wilson loop in the continuum Hamiltonian approach is computed without resorting to the Dyson equation.

6.2 Derivation of the Dyson Equation

We now discuss in Euclidean space-time a Dyson-type integral equation, first derived in supersymmetric theories Refs. [116, 117]. Recently this equation has been applied to Yang-Mills theory in Landau gauge, Ref. [118].

We start from the observation that to leading order perturbation theory, i.e., at weak coupling $g \ll 1$, the gluonic part of the QCD Lagrangian can be written as

$$\mathcal{L} \;=\; -\frac{1}{4} F^a_{\mu\nu} F^{a;\mu\nu} \approx \mathcal{L} = -\frac{1}{2} A^a_\mu(x) D^{-1}_{\mu\nu} \delta^{ab} A^b(x) + \mathcal{O}(g) \;, \tag{6.14}$$

with the kernel $D^{-1}_{\mu\nu} = \delta_{\mu\nu}\Box - \partial_\mu\partial_\nu$. This formula has already been derived in Eq. (1.13). In the weak-coupling limit the Yang-Mills part of the action $S_{\rm G}[A]$ becomes of Gaussian type. However, from the discussion which follows Eq. (1.13) we know that in the present form the Wilson loop average $\langle \hat{W}(\mathcal{C}) \rangle$, Eq. (6.2), cannot be performed, since the inverse of $D^{-1}_{\mu\nu}$ does not exist. To give expectation values a meaning we have to fix the gauge. This gauge fixing is implicitly understood in the next equations. For weak coupling g the path ordering prescription $\mathcal{P}$ in Eq. (6.1) can be ignored and the expectation value of the Wilson loop reads

$$\langle \hat{W}(\mathcal{C}) \rangle = \frac{1}{Z} \frac{1}{d_{\rm R}} \mathsf{Tr} \left[\int DA \, \exp\left(-\frac{1}{2} \int d^4x \, A^a_\mu D^{-1}_{\mu\nu} A^a_\nu + ig \oint\limits_{\mathcal{C}} dx_\mu A^a_\mu(x) T^a \right) \right] \;. \tag{6.15}$$

Using the abbreviation

$$J^a_\mu(x) = ig \int ds_\mu \, \delta(x-s) \, T^a \;, \tag{6.16}$$

the Gaussian integration in Eq. (6.15) can be performed immediately and we obtain

$$\begin{aligned} \langle W(\mathcal{C}) \rangle &= \frac{1}{d_{\rm R}} \, \mathsf{Tr} \left[\exp\left(\frac{1}{2} \int d^4x \int d^4y \, J^a_\mu(x) D_{\mu\nu}(x,y) \delta^{ab} J^b_\nu(y) \right) \right] = \\ &= \exp\left[-\frac{g^2}{2} C_F I(\mathcal{C}) \right] \;, \end{aligned} \tag{6.17}$$

where, after gauge fixing, $D_{\mu\nu}$ is the Green's function of the operator $D^{-1}_{\mu\nu}$. After the second equality sign we have used the definition

$$I(\mathcal{C}) = \oint\limits_{\mathcal{C}} dx_\mu \oint\limits_{\mathcal{C}} dy_\nu D_{\mu\nu}(x,y) \;, \tag{6.18}$$

and evaluated the color trace with use of Eq. (1.7). The quadratic Casimir invariant C_F appears in the final form of the equation. Equation (6.17) can be understood as the line element dx_μ interacting with the line element dy_ν through the perturbative gluon

propagator $D_{\mu\nu}$. As an example we now take Feynman gauge, where the inverse gluon kernel in Eq. (6.14) reads $D^{-1}_{\mu\nu} = \delta_{\mu\nu}\Box$ and the gluon propagator

$$D_{\mu\nu}(x^2) = -\frac{1}{4\pi^2}\frac{1}{x^2}\delta_{\mu\nu} \ . \tag{6.19}$$

Consider now a rectangular contour $\mathcal{C}$ with temporal extent T and spatial extent L. We evaluate a graph where two different temporal paths interact, which for a large temporal extension T of the Wilson loop should be the leading graph. Moreover, we ignore the diagrams where the gluon lines run along the same temporal path. Using

$$D_{\mu\nu}(x(s)-x(t)) = -\frac{1}{4\pi^2}\frac{1}{(x(s)-x(t))^2}\delta_{\mu\nu} = -\frac{1}{4\pi^2}\frac{1}{(s-t)^2+L^2}\delta_{\mu\nu} \ , \tag{6.20}$$

the integral $I(\mathcal{C})$, Eq. (6.18), is evaluated as

$$\begin{aligned} I(\mathcal{C}) &= \oint\limits_{\mathcal{C}} dx_\mu \oint\limits_{\mathcal{C}} dy_\nu D_{\mu\nu}(x,y) = -\frac{2}{4\pi^2}\int_0^T ds \int_0^T dt\, \frac{1}{L^2+(s-t)^2} = \\ &= -\frac{1}{\pi^2}\left(\frac{T}{L}\arctan\left[\frac{T}{L}\right] - \frac{1}{2}\ln\left[1+\frac{T^2}{L^2}\right]\right) \ , \end{aligned} \tag{6.21}$$

where we have used

$$\oint\limits_{\mathcal{C}} dx_\mu \oint\limits_{\mathcal{C}} dy_\nu D_{\mu\nu}(x,y) = \int ds\, \dot{x}_\mu(s) \int dt\, \dot{x}_\nu(t)\, D_{\mu\nu}((x(s)-x(t)) \ . \tag{6.22}$$

Here $x_\mu(s), x_\nu(t)$ denote parameterizations of the paths on the rectangular loop, for more details see Appendix E. We evaluate the behavior of Eq. (6.21) for large temporal extents T and end up with [112, 119]

$$\langle W(\mathcal{C})\rangle = \exp\left[-\frac{g^2}{2}C_F I(\mathcal{C})\right] = \exp\left[\frac{g^2}{4\pi L}T\, f(T,L)\right] \ , \tag{6.23}$$

where we have used Eq. (6.21) and defined

$$f(T,L) = \frac{2}{\pi}\left(\arctan\left[\frac{T}{L}\right] - \frac{L}{2T}\ln\left[1+\frac{T^2}{L^2}\right]\right) \ . \tag{6.24}$$

For the limit $T\to\infty$ we have $f(T,L)\to 1$, Ref. [112], and therefore

$$\langle W(\mathcal{C})\rangle \underset{T\to\infty}{\longrightarrow} e^{\frac{g^2}{4\pi L}T} = e^{-V_{\mathrm{W}}(L)T} \ . \tag{6.25}$$

This result comes with no surprise: In the weak-coupling case the interaction is governed by perturbative one-gluon exchange and the Wilsonian potential $V_{\mathrm{W}}(L)$, Eq. (6.13), is the usual Coulomb potential.

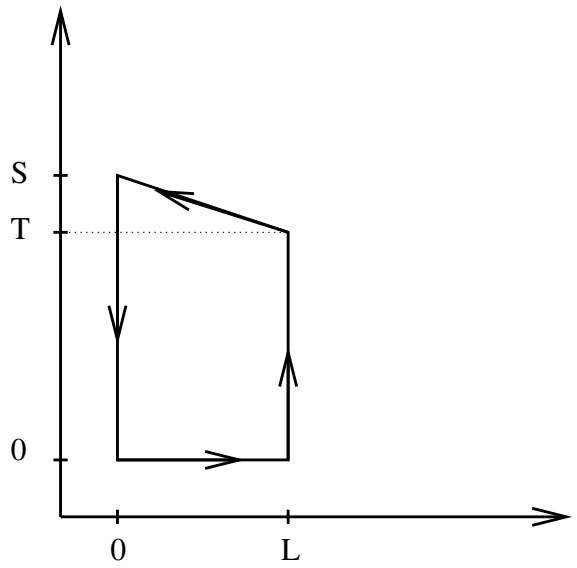

Figure 6.1: *Trapezoidal Wilson loop with temporal extents S and T and spatial extent L.*

We now proceed with deriving the Dyson equation for the Wilson loop. We consider trapezoidal Wilson loops, with two temporal extents S and T, separated by a distance L, see Fig. 6.1. We expand the Wilson loop average in Eq. (6.17), to order g^2 and get

$$W(S,T;L) = 1 + \frac{g^2}{2} \oint_C dx_\mu \oint_C dy_\nu D_{\mu\nu}(x,y) \; . \tag{6.26}$$

In order to extract the Wilsonian potential we are interested in large temporal extensions $S, T \gg L$ of the trapezoidal loop. Under the assumption that $S-T$ does not exceed the order of L the leading contributions clearly come from the diagrams shown in Fig. 6.2a, i.e., the gluon line connecting the two temporal paths, which was also assumed in the previous calculation. Note that again the diagram where the gluon line runs along the same temporal path is ignored. Moreover, we neglect the contribution from sets of interacting lines. From the 16 contributions in the line integral $I(\mathrm{C})$, Eq. (6.18), we therefore end up with only two remaining integrals. To arrive at a Dyson-type equation, we now sum up all ladder diagrams with the gluon exchange connecting the temporal paths, diagrammatically shown in Fig. 6.3a. The recursion relation is analytically given as [116, 117]

$$W(S,T;L) = 1 + g^2 C_F \int_0^S ds \int_0^T dt D\left((x(s) - s(t))^2\right) W(s,t;L) \; , \tag{6.27}$$

where

$$D\left((x(s) - x(t))^2\right) = \dot{x}_\mu^-(s) D_{\mu\nu}\left(x(s), x(t)\right) \dot{x}_\nu^+(t) \tag{6.28}$$

and $x_\mu^\pm(s)$ denotes a parametrization of the two temporal paths of the Wilson loop. We refer to Appendix E for an explicit realization of these paths for the trapezoidal loop.

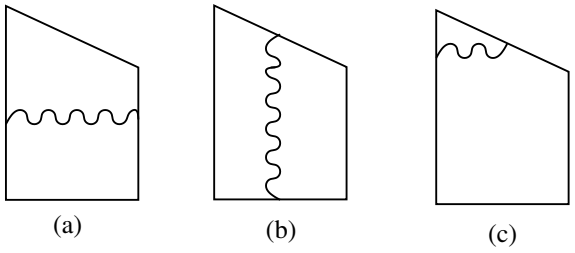

Figure 6.2: *Diagrams contributing (a) and diagrams ignored (b), (c) in the Dyson equation (6.27).*

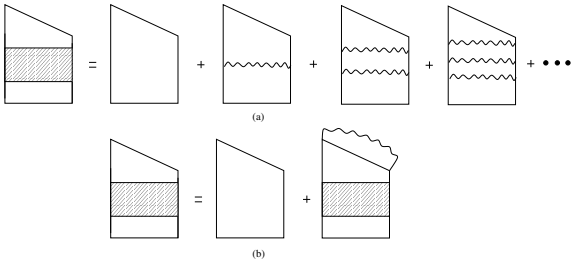

Figure 6.3: *Graphical illustration to the summation of the ladder diagrams (a) and the Dyson equation (b).*

After summation of the ladder diagrams the Dyson equation can now be applied to a non-perturbative gluon propagator $D_{\mu\nu}$ as well. A graphical illustration of the Dyson equation (6.27) is given in Fig. 6.3b.

Before we proceed with applying this equation (6.27) to Coulomb gauge gluon propagators we come to discuss its limitations:

1. Since we only include diagrams with gluon lines connecting the temporal paths, the Dyson equation (6.27) is restricted to strongly asymmetric loops consisting of two opposite long temporal paths S, T and two opposite short spatial paths. Otherwise it does not make sense to include one pair of paths, Fig. 6.2a in the integral (6.18) while neglecting the integrals of the other pair of paths (Fig. 6.2b) and their ladders. Therefore, the Dyson equation (6.27) is restricted to spatial distances $L \ll S, T$. As a consequence, the limit $L \to \infty$ cannot be accessed.

2. Let us turn to the boundary conditions of the integral equation (6.27). Setting one of the two temporal paths to zero, the trapezoidal loop degenerates to a triangle-shaped loop and the Dyson equation reads

$$W(S, T = 0; L) = 1, \qquad W(S = 0, T; L) = 1 \; . \tag{6.29}$$

   However, this boundary condition is in general not fulfilled for triangle-shaped contours. Moreover, such boundary conditions contradict one of the fundamental assumptions in the derivation of the Dyson equation (6.27): The temporal extensions S and T must be much larger than the spatial extent L.

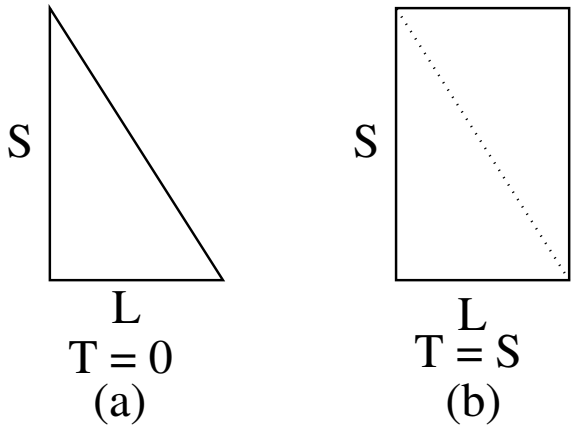

Figure 6.4: *(a) Triangle and (b) rectangular shaped contours representing the Wilson loop* $W(S, T = 0; L)$ *and* $W(S, T = S; L)$.

3. In the Dyson equation (6.27) the gauge group $SU(N_{\mathrm{C}})$ enters only via the quadratic Casimir invariant C_F. It is argued [108, 120, 121] and observed in lattice simulations [122–124] that the potential between the static quark sources $V_{\mathrm{W}}(L)$, Eq. (6.13), is proportional to the value of the quadratic Casimir operator C_F, Eq. (1.7), only in an intermediate distance regime. This phenomenon is known as the so-called *Casimir-scaling hypothesis*, Ref. [125]. Since the only remnant of the gauge group in the Dyson equation (6.27) is the Casimir invariant C_F, it should show strict Casimir scaling for the whole distance range. We can therefore conclude, that the Dyson equation (6.27) can be applied to an intermediate distance regime L only.

4. Another limitation concerns gauge invariance. The left-hand side of the Dyson equation (6.27) is clearly gauge invariant, as shown in Eq. (6.8). However, on the right-hand side a gauge dependent quantity, namely the gluon propagator $D_{\mu\nu}$ occurs. Consequently, it is expected that the Dyson equation (6.27) yields different results for different gauges. This observation is confirmed by comparing the Coulomb and Landau gauge results.

5. Besides gauge invariance, the Wilson loop is also renormalization group invariant. However, the gluon propagator on the right-hand side of the Dyson equation (6.27) is not, except for the temporal Wilson loop, which will be considered below.

From all the above listed limitations and approximations we can conclude that the Dyson equation (6.27) is only applicable to strongly asymmetric loops with the length scale L restricted from above to intermediate distances. This will be confirmed in Section 6.5 by a numerical evaluation. We now discuss a special case, where the Dyson equation (6.27) is exact and yields the correct result.

6.3 Temporal Wilson Loop in Coulomb Gauge

A remarkable property of Coulomb gauge, not shared by any Lorenz gauge, is that the time component of the gauge field A_0 is invariant under renormalization, Ref. [126],

$$g_0 A_0^{(0)} = g_r A_0^{(r)} \; . \tag{6.30}$$

Here the superscripts denote unrenormalized (0) and renormalized (r) quantities. As a consequence the temporal gluon propagator

$$\langle g A_0^a(x) g A_0^b(y) \rangle \; = \; g^2 D_{00}(x-y) \; = \; -\delta^{ab} V_{\rm C}(\boldsymbol{x}-\boldsymbol{y}) \delta(x^0-y^0) + P^{ab}(x-y) \tag{6.31}$$

is renormalization group invariant. Here we have decomposed the temporal gluon propagator into two parts [33]: The first part is the instantaneous non-Abelian Coulomb potential $V_{\rm C}(\boldsymbol{x}-\boldsymbol{y})$ which describes anti-screening of color charges and has been discussed in detail in Section 1.6. The second part $P(x-y)$ is the so-called vacuum polarization term, which describes ordinary screening. This second part is assumed to lower the Coulomb string tension $\sigma_{\rm C}$ towards the Wilson string tension $\sigma_{\rm W}$. The non-Abelian color Coulomb potential $V_{\rm C}(\boldsymbol{x}-\boldsymbol{y})$ is computed in the Hamiltonian approach according to Eq. (1.82). It consists of a long-range, linearly rising potential and a short-range Coulomb potential, Eq. (5.6),

$$V_{\rm C}(L) \; = \; \sigma_{\rm C} L - \frac{\alpha_{\rm S}}{L} \; . \tag{6.32}$$

We now ignore the screening part in Eq. (6.31) and plug in the instantaneous part of the gluon propagator $D_{00}(x-y)$ into the Dyson equation (6.27). Apparently, we expect to end up with a potential which rises linearly with $\sigma_{\rm C} r$, which is now explicitly worked out. Due to the δ-function appearing in the first part of the temporal propagator, Eq. (6.31), we have to apply the Dyson equation (6.27) to a rectangular shaped Wilson loop. We have

$$W(S=T,T;L) \equiv W(T;L) \; , \tag{6.33}$$

for which the Dyson equation (6.27) reduces to

$$W(T;L) = 1 - C_F V_{\rm C}(L) \int_0^T dt \, W(t;L) \; . \tag{6.34}$$

We note that for rectangular loops, i.e., $S=T$, neighboring edges do not interact, since in this case $dx_\mu dy_\nu = 0$. Therefore processes shown in Fig. 6.2c vanish identically.

Equation (6.34) can be converted into the differential equation

$$\frac{d}{dT} W(T;L) = -C_F V_{\rm C}(L) W(T,L) \tag{6.35}$$

with the boundary condition

$$W(T=0;L) = 1 \; , \tag{6.36}$$

which is, contrary to the boundary condition of the general case (6.29), indeed the correct one: The area enclosed by the loop vanishes for $T = 0$. Equation (6.35) can be solved analytically and yields

$$W(T; L) = \exp\left(-C_F V_{\mathrm{C}}(L) T\right) , \tag{6.37}$$

which is the expected result for large temporal Wilson loops. We thus have correctly obtained an area law. It is clear why in this case the Dyson equation (6.27) produces the correct result. First of all, the boundary condition (6.36) is exact for the rectangular Wilson loop. Moreover, processes shown in Fig. 6.2c vanish for rectangular loops. In addition, the processes shown in Fig. 6.2b, which connect the two spatial paths, and which are neglected in the Dyson equation (6.27) do not exist for an instantaneous propagator. Next we show how to extract the static quark potential $V_{\mathrm{W}}(L)$ for a general trapezoidal Wilson loop.

6.4 Extracting the Static Quark Potential

We now show that the Dyson equation (6.27) can be reduced to a one-dimensional Schrödinger equation, Refs. [116, 117], and the Wilsonian potential $V_{\mathrm{W}}(L)$, Eq. (6.13), can be extracted from its ground state energy.

First of all, we differentiate (6.27) with respect to the temporal extensions S and T, which yields the following differential equation

$$\frac{\partial^2 W(S,T;L)}{\partial S \partial T} \;=\; g^2 C_F \, D(L^2 + (S-T)^2) \, W(S,T;L) \; . \tag{6.38}$$

We have used the parametrization of the temporal paths with $(x(S) - x(T))^2 = L^2 + (S-T)^2$, Eq. (E.4). We introduce the following dimensionless variables

$$r \;=\; \frac{S-T}{L} \; , \qquad R \;=\; \frac{S+T}{L} \; . \tag{6.39}$$

With use of the relations

$$\frac{\partial}{\partial S} = \frac{1}{L}\left(\frac{\partial}{\partial r} + \frac{\partial}{\partial R}\right) , \qquad \frac{\partial}{\partial T} = \frac{1}{L}\left(\frac{\partial}{\partial R} - \frac{\partial}{\partial r}\right) \; , \tag{6.40}$$

the differential operator in Eq. (6.38) becomes

$$\frac{\partial^2}{\partial S \partial T} \;=\; \frac{1}{L^2}\left(\frac{\partial^2}{\partial R^2} - \frac{\partial^2}{\partial r^2}\right) \; . \tag{6.41}$$

One can then show that the Dyson equation, Eq. (6.38), is separable in the variables R and r [116, 117]

$$\frac{1}{L^2}\left(\frac{\partial^2}{\partial R^2} - \frac{\partial^2}{\partial r^2}\right) W(r,R) = g^2 C_F D(L^2(1+r^2)) \, W(r,R) \; . \tag{6.42}$$

Here we have used the notation $W(r,R) = W(S,T;L)$. With the following ansatz, Refs. [116, 117],

$$W(r,R) \;=\; \sum_n \varphi_n(r) c_n \, \exp\left(\Omega_n R/2\right) , \tag{6.43}$$

the differential equation (6.42) can be rewritten as

$$\left[\frac{\Omega_n^2}{4} - \frac{\partial^2}{\partial r^2}\right] \varphi_n(r) = L^2 g^2 C_F D(L^2(1+r^2))\, \varphi_n(r) , \tag{6.44}$$

which is a one-dimensional Schrödinger equation of the form

$$\left[-\frac{d^2}{dr^2} + U(r;L)\right] \varphi_n(r) \;=\; -\frac{\Omega_n^2}{4}\, \varphi_n(r) , \tag{6.45}$$

with the Schrödinger potential given as

$$U(r;L) = -L^2 g^2 C_F D(L^2(1+r^2)) . \tag{6.46}$$

The constants c_n in the ansatz (6.43) have to be chosen such that the boundary condition (6.29) is fulfilled. In the new variables r and R the boundary condition (6.29) reads

$$W(r=R,R) = W(r=-R,R) = 1 . \tag{6.47}$$

From Eq. (6.46) we find that the Schrödinger potential is symmetric, i.e., $U(r) = U(-r)$. In the new variables r and R approaching large Euclidean times means setting $r = 0$ and $R \to \infty$. For fixed r and large R the dominant contribution in the sum, Eq. (6.43), clearly comes from the largest eigenvalue Ω_n. From the condition $r = 0$ it follows that the largest eigenfunction φ_n in Eq. (6.45) has no nodes, i.e., $\varphi_n(0) \neq 0$. Since the ground state eigenfunction $\varphi_0(r)$ has no nodes it is the dominant contribution. Plugging in this result into the ansatz (6.43) the large-T behavior of the Wilson loop corresponds to

$$W(R\to\infty, r\to 0) \sim \varphi_0(r\to 0) e^{\frac{\Omega_0 R}{2}} . \tag{6.48}$$

Hence, to extract the static quark potential $V_{\rm W}(L)$, Eq. (6.13), we have to find the lowest eigenvalue $\Omega_0(L)$ of the Schrödinger equation (6.45). An area law for the Wilson loop for large separations $S = T \gg L$ requires

$$V_{\rm W}(L) \;=\; -\lim_{T\to\infty} \frac{1}{T} \ln W(S, T=S; L) \;=\; -\frac{\Omega_0(L)}{L} + \text{const.} . \tag{6.49}$$

Consequently, in order to extract the static quark potential $V_{\rm W}(L)$ from the Dyson equation (6.27) we have to solve the Schrödinger equation (6.45) for its ground state as a function of L. From the discussions in Section 6.2 we expect that the procedure is applicable to separations L not too large. How this limitation manifests itself in the numerical evaluation of the ground state energy of the Schrödinger equation (6.45) will explicitly be seen below.

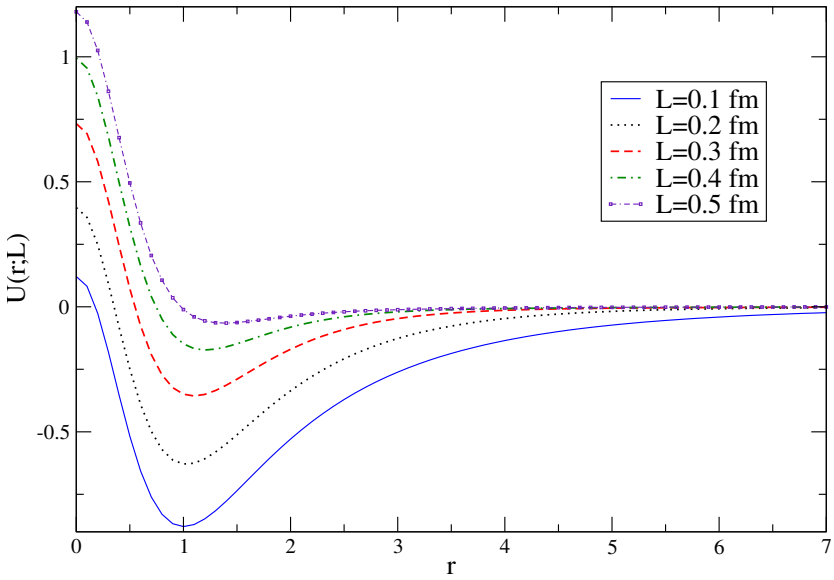

Figure 6.5: *The Schrödinger potential $U(r;L)$, Eq. (6.46), for several spatial distances L.*

6.5 Spatial Wilson Loop in Coulomb Gauge

We now apply the above formalism to the results obtained in the variational approach to QCD. In this procedure the temporal extents S, T become spatial extents: In the Hamiltonian approach the spatial Wilson loop is more easily derived, since for the temporal Wilson loop we would need to know the time evolution of the Yang-Mills vacuum wave functional $|\psi\rangle$, Eq. (1.86). We use as input the spatial gluon propagator defined in the Hamiltonian approach, Eq. (1.81), which can nicely be expressed by the Gribov formula, Eq. (1.95). In Appendix E we show, however, that the large momentum part of the gluon propagator leads to an ultraviolet divergent expression for $D((x(s)-x(t))^2)$, see Eq. (E.37). To overcome this problem we introduce the so-called anomalous dimension of the gluon propagator, denoted as γ. It is an additional term in the ultraviolet region of the gluon propagator [127]

$$D(p) \sim \frac{1}{p(1+\ln^{\gamma}[\frac{p^2}{\mu^2}])} \, . \tag{6.50}$$

Hence, the exponent γ of an additional logarithmic term in the ultraviolet part of the gluon propagator is the anomalous dimension. The quantity μ denotes some renormalization scale. Note that the anomalous dimension escapes the lattice calculation as well as the variational approach. On the lattice an anomalous dimension is difficult to observe. In the variational approach, however, it probably escapes due to the Gaussian ansatz in the wave functional. In Ref. [127] it has been analyzed with use of the ghost Dyson-Schwinger equation. In our analysis the only necessity to take the anomalous dimension into account is to make the divergent expression, Eq. (E.31), UV finite. The anomalous

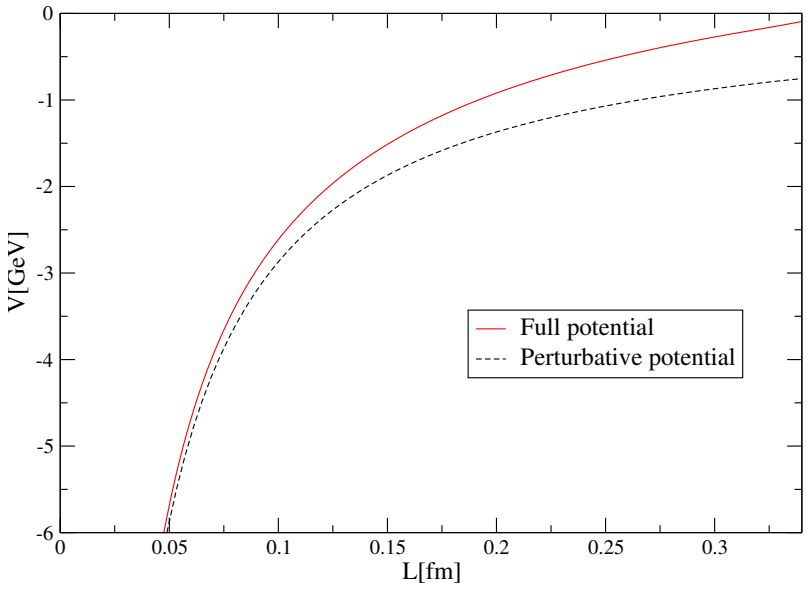

Figure 6.6: *The Wilsonian quark potential $V_{\mathrm{W}}(L)$ obtained from the non-perturbative gluon propagator (6.51) and the perturbative potential $V_{\mathrm{PERT}}(L)$ obtained from the ultraviolet part of the gluon propagator (6.53).*

dimension γ modifies the kernel ω in the Yang-Mills vacuum, Eq. (1.95), as

$$\omega(p) = \sqrt{p^2 \left(1 + a \ln^{\gamma}\left(\frac{p}{M_{\mathrm{G}}}\right)\right)^2 + \frac{M_{\mathrm{G}}^4}{p^2}} \,. \tag{6.51}$$

Here the anomalous dimension is given by $\gamma = \frac{3}{11}$, Ref. [127]. A parameter a depending on the Gribov mass scale M_{G}, Eq. (1.96), enters the gluon kernel ω. Since in our case the anomalous dimension enters only to make the integral (E.31) UV-convergent, we will use a small value of $a = 0.1$. Moreover, the infrared behavior of the gluon propagator is independent of the anomalous dimension γ and therefore also the long-range part of the Wilson loop should be unaffected. This has been confirmed in a numerical evaluation. Fig. 6.5 shows the potential $U(r; L)$, Eq. (6.46), calculated from the static propagator in Coulomb gauge with $\omega(k)$ given by Eq. (6.51) for various spatial distances L. The potential $U(r; L)$ has the form of a double well centered at $r = 0$. The dip in the potential, necessary for the formation of a bound state, flattens as L increases and vanishes for $L \geq 0.5$ fm. The bound state disappears for $L \approx 0.35$ fm. The Wilson potential $V_{\mathrm{W}}(L)$, Eq. (6.13), can then no longer be extracted from the "ground state energy" $\Omega_0(L)$. This limits the use of the Schrödinger equation (6.45) to an intermediate distance regime. We emphasize that already when discussing the limitations of the Dyson equation (6.27) we drew the conclusion that this equation is only applicable to intermediate distances.

The ground state eigenvalue $\Omega_0(L)$ is computed numerically with use of the so-called shooting method, a widely used method to solve one-dimensional Schrödinger equations for arbitrary potentials. It is described in Appendix E.5 and evaluates the Schrödinger

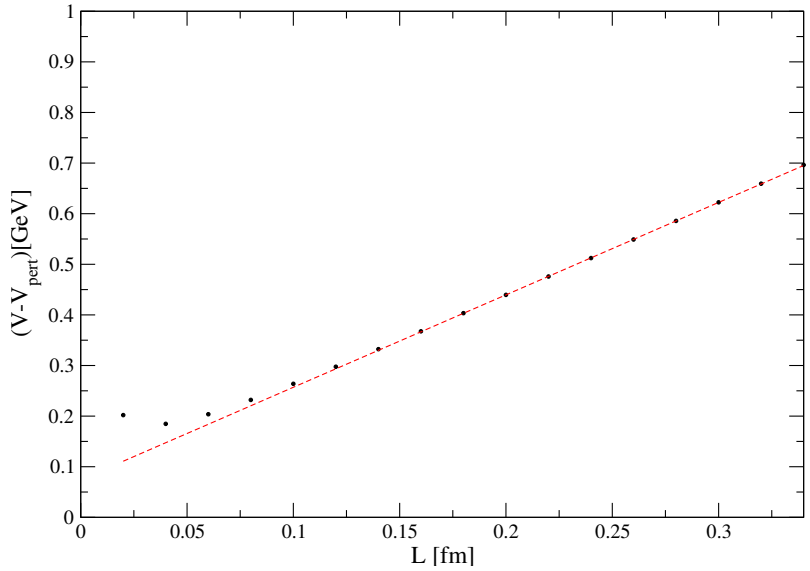

Figure 6.7: *Subtraction of the perturbative potential $V_{\mathrm{PERT}}(L)$ from the non-perturbative potential $V_W(L)$.*

equation (6.45) according to

$$\varphi_0'' + 2(E_0 - U(r))\varphi_0 = 0, \qquad V_{\mathrm{W}}(L) = -\frac{\sqrt{-4E_0}}{L} \,. \tag{6.52}$$

Although the resulting string tension could be used to fix the scale, we here fix the scale a priori. This has the advantage that we can check the reliability of the result by simply comparing the string tension which we obtain with the input string tension. We use as input the string tension obtained on the lattice, $\sqrt{\sigma_{\mathrm{W}}} = 440$ MeV. It enters the gluon kernel ω, Eq. (6.51), and therefore the Schrödinger potential $U(r;L)$, Eq. (6.46).

Let us turn to the results for the Wilsonian potential $V_{\mathrm{W}}(L)$, Fig. 6.6. It clearly shows the two regions: the Coulombic region up to 0.15 fm and a linear rising potential, up to the limit at 0.35 fm. We also compute the static quark potential $V_{\mathrm{PERT}}(L)$ with only the ultraviolet part of the gluon propagator[3] (again with taking into account the anomalous term) which is given as

$$\omega_{\mathrm{PERT}}(p) = p\left(1 + a\ln^{\gamma}\frac{p}{M_{\mathrm{G}}}\right) \,, \tag{6.53}$$

and observe that it only has a Coulombic behavior, as predicted by the analytic framework, Eq. (6.23). Both potentials $V_{\mathrm{W}}(L)$ and $V_{\mathrm{PERT}}(L)$ are plotted in Fig. 6.6. Moreover, in Fig. 6.7 we subtract the perturbative potential $V_{\mathrm{PERT}}(L)$ from the non-perturbative potential $V_{\mathrm{W}}(L)$ and observe an excellent linear behavior in the intermediate distance

[3]We also analyzed so-called decoupling solutions for the non-perturbative gluon propagator. Here the gluon propagator tends to a constant for small momenta. We observed that the Wilsonian potential $V_{\mathrm{W}}(L)$, Eq. (6.13), for such propagators only shows a Coulombic region.

regime. Note that for small distances, up to 0.1 fm, the subtraction shows numerical inaccuracies. From the fit

$$V_{\mathrm{W}}(L) - V_{\mathrm{Pert}}(L) = c + \sigma_{\mathrm{W}} L \,, \tag{6.54}$$

we can extract the string tension, yielding

$$\sigma_{\mathrm{W}} \approx (600\,\mathrm{MeV})^2 \ . \tag{6.55}$$

Comparing the string tension to its input value of $\sigma_{\mathrm{W}} = (440\,\mathrm{MeV})^2$ we end up with a value which is too large.

We can conclude that the results obtained from the Dyson equation (6.27) are not quantitatively significant. However, on a qualitative level, the results give the correct physical picture. We find the Wilsonian potential to have a Coulombic region as well as a strictly linearly rising region, see Fig. 6.6. This long-range linear behavior can be seen quite impressively after subtracting the perturbative part, see Fig. 6.7.

Conclusions and Outlook

In this thesis two projects were presented, each one covering one of the two main features of non-perturbative QCD: chiral symmetry breaking and color confinement.

In the first part of this thesis we investigated chiral symmetry breaking and were able to include quark fields into the variational approach to QCD. We could make important progress on the thirty-year old problem of the phenomenological quantities, which are too low in Coulomb gauge [103].

We started our considerations with a brief introduction to the Hamiltonian approach in Chapter 1. We collected the main results gained in recent years within the variational approach to pure Yang-Mills theory, with the most prominent ones being the spatial gluon propagator and the static non-Abelian color Coulomb potential.

In Chapter 2 a short discussion of spontaneous chiral symmetry breaking in QCD followed and we introduced the phenomenological quantities, which we later on computed by means of a variational calculation: the chiral condensate, which is the order parameter of chiral symmetry breaking, and the constituent quark mass, which is the dynamical quark mass at zero momentum.

In Chapter 3 we identified the missing piece in past studies of quarks in Coulomb gauge QCD: the interaction of quarks with transverse gluons. We generalized the BCS-like quark vacuum wave functional ansatz of Finger and Mandula, Ref. [78], in order to include the interaction of quarks with transverse gluons. Combining this quark wave functional with the Gaussian wave functional of pure Yang-Mills theory proposed in Ref. [7], we gained a powerful technique to approach the full QCD system by means of a variational calculation. The Finger-Mandula wave functional, Ref. [78], is limited in its applicability to those parts of the Coulomb gauge Hamiltonian which do not depend on the gauge field. Our ansatz, however, has no such limitations and can be used to explore the full QCD system. Within this new approach three variational kernels determine the different parts of QCD. The kernel in the Gaussian ansatz characterizes the pure Yang-Mills part of the theory. The two kernels entering the quark vacuum wave functional divide into a scalar part, which breaks chiral symmetry explicitly, and a vectorial part, which includes the interaction of quarks with the transverse gluons. We then, in the basis of coherent fermion states, formulated a generating functional for the quark sector, from which all fermion two-point functions were derived. Once the quark fields in the functional integral are integrated out, however, it is in general not possible to integrate out the gauge field as well. We bypassed this difficulty by resorting to the so-called quenched approximation, in which the back-reaction of the quarks on the gluon vacuum is ignored. Lattice calculations, Ref. [128], as well as Dyson-Schwinger results, Ref. [84], in Landau gauge indicate that the influence of unquenching on observable quantities is small. Moreover, this approximation is in accordance with the aim of our

first study: We want to understand the role of the vectorial part of the quark vacuum wave functional for chiral symmetry breaking. Hence, we keep the gluon sector and thus the kernel in the Yang-Mills Gaussian vacuum fixed.

In Chapter 4 we evaluated the so-called single-particle energy density, i.e., the energy density of free quarks and the interaction energy of quarks with transverse gluons. On the way towards the final form of the gap equations, we had to regulate the gluon loop integral, in which the static spatial gluon propagator enters. We then showed that for the gap equations with a purely transverse gluon interaction as input a non-zero solution for both variational kernels cannot be found. We concluded that the Coulomb interaction must be essential for chiral symmetry breaking, which was confirmed in the subsequent chapter.

In Chapter 5 the Coulomb energy density, which is the interaction energy of two quark charges mediated by the static non-Abelian color Coulomb potential, was derived. The gap equations with the transverse gluon interaction as well as the Coulomb interaction as input were set up. Taking for the non-Abelian color Coulomb potential only its long-range linear part into account, the final gap equations could be shown to be UV-finite. We then solved the coupled system analytically and numerically. The analytic investigation gave us first hints about the behavior of the variational kernels for small and large momenta: For small momenta both quark variational kernels tend to a constant, signalling that the scalar kernel as well as the vector kernel coupling the quarks to the transverse gluons are important for infrared physics. For large momenta the kernels show a power-law behavior, whose exponents are in agreement with a recent perturbative analysis, Ref. [14]. All analytic results were confirmed in a numerical investigation of the coupled system. Moreover, we were able to show that the infrared part of the static spatial gluon propagator is of central importance in order that the two integral equations determining the variational kernels start to interact. We solved the gap equations for different coupling constants as well as for different Gribov mass scales.

The results for the variational kernels then enabled us to obtain values for the chiral condensate and the constituent quark mass. By comparing these values to the result obtained with vanishing vector kernel, Ref. [80], we could conclude that it is indeed the coupling of the quarks to the transverse gluons which produces an increasing chiral condensate as well as a larger value for the constituent quark mass. However, while for the chiral condensate we come into the range of experiment, for the dynamical mass there is still a certain contribution missing which can result from neglecting the ordinary Coulomb potential as well as from ignoring certain parts of the Coulomb gauge Hamiltonian.

In the various Appendices we performed the explicit calculations: In Appendix A we computed, with the use of helicity eigenstates, the explicit spinor solutions for massless fermions. In Appendix B we showed how to integrate out the quark fields in the QCD generating functional. We derived several restrictions for the wave functional kernels and determined the dimension of these kernels. In Appendix C we calculated the energy densities of the Coulomb gauge-fixed Hamiltonian and in Appendix D we presented the algorithm how to solve numerically non-linear integral equations.

Most of the results gained in Part I of this thesis have already been published in [74]

and a summary can be found in [44].

All these results are very encouraging and call for further studies with use of this new QCD vacuum wave functional. There is enough room for extending the investigations in several directions. Clearly, the next step should be to take the parts of the Coulomb gauge-fixed Hamiltonian into account which have been neglected so far. These contributions are the kinetic gluon energy and the parts of the Coulomb Hamiltonian, where quark sources interact with gluon sources. Although these contributions are considered to be subleading, they could increase the constituent quark mass, which is so far about 100 MeV too small. Moreover, it is an interesting question if with these additional contributions the vector kernel in the quark vacuum wave functional starts to depend on *both* external momenta. Preliminary results indicate that this is indeed the case. An important source of uncertainty are the approximations used to compute the gluon expectation values. In order to test and get further insights into these approximations a recently proposed Dyson-Schwinger technique in the Hamiltonian approach, Ref. [25], which was only applied to the pure Yang-Mills sector so far, should be applied to the quark sector as well. The ordinary Coulomb potential should be included into the quark gap equations. Current investigations show that this results in logarithmically UV-divergent expressions, which have to be correctly renormalized, for instance, by adding counter-terms to the Hamiltonian. Another question concerns the form of the vector kernel in the quark wave functional: How would additional Dirac tensor components affect the phenomenological values? Clearly, the final step should be to evaluate the full QCD system, i.e., varying the energy densities with respect to *all* variational kernels. To approach realistic QCD, we should include finite quark masses as well. Moreover, for hadron phenomenology the pion form factor is an essential ingredient. *With only the BCS kind wave functional it is too small by a factor of five*, Ref. [80]. Since the coupling of quarks to transverse gluons in the quark vacuum wave functional increases the chiral condensate as well as the dynamical mass towards the experimental values, such an increase is also suspected for the pion form factor. Furthermore, in recent years much effort was spent into exploring new numerical methods for solving Coulomb gauge quark Dyson-Schwinger equations, especially to handle the infrared divergent static non-Abelian color Coulomb potential, Ref. [129]. From a numerical point of view it would be interesting to apply these methods to the integral equations presented in this work.

Another important line of QCD research explores the QCD phase diagram. Consequently, an extension of the framework to finite temperatures and finite densities is desirable. Since the wave functional suggested in this work couples the quarks to the transverse gluon fields, it is expected to be a good quantity to test the interplay between confinement and chiral symmetry breaking. In addition, our results may be of importance for investigations beyond QCD, for instance, technicolor theories. The techniques developed in this work could also be applied to non-QCD theories, like graphene description, which has most recently become popular, Ref. [130].

Let us turn to the project presented in Part II of this thesis. Its aim was to calculate the expectation value of the Wilson loop in the variational approach to QCD. The Wilson loop is related to the static quark-antiquark potential and therefore an order

parameter for confinement. However, the continuum evaluation of the Wilson loop has been rendered difficult so far, due to the path ordering problem. We applied a method, which has been proposed for Wilson loops in the context of supersymmetric Yang-Mills theories, see Refs. [116, 117].

In Section 6.1 we defined the Wilson loop and discussed the problem of path ordering. We set the link to lattice QCD and argued why the Wilson loop is more easily accessible on the lattice. We proved gauge invariance of the Wilson loop and derived the relation between the static quark potential and the Wilson loop average.

In Section 6.2 we briefly sketched the derivation of the Dyson equation: Starting from a weak-coupling expansion a recursion relation for a trapezoidal Wilson loop is derived, which sums all planar ladder diagrams in which gluon lines interact between the temporal paths. This equation is fully determined by the gluon propagator. However, in this procedure diagrams are neglected and assumptions on the form of the Wilson loops are made. We critically analyzed this Dyson equation. Among other limitations we showed that the boundary conditions can in general not be fulfilled. Moreover, we argued that the Dyson equation can be applied only to an intermediate distance regime.

In Section 6.3 we applied this Dyson equation to the instantaneous part of the temporal gluon propagator in Coulomb gauge. We showed the area law with the string tension being the Coulomb string tension.

In Section 6.4 we outlined how to derive the static quark potential from solving a one-dimensional Schrödinger equation for the lowest eigenvalue.

In Section 6.5 we applied the formalism to the spatial Wilson loop in $3+1$ dimensions in Coulomb gauge. We used the spatial gluon propagator obtained in the variational approach and on the lattice as input. We ended up with a static quark potential, which shows the characteristic short-range Coulomb potential and the long-range linear confinement potential. When subtracting the perturbative potential a strictly linearly rising confinement potential was obtained. However, on a quantitative level, the string tension extracted from this confinement potential was found to be much larger than the string tension obtained on the lattice.

In Appendix E we obtained an explicit parametrization of the temporal paths of the trapezoidal Wilson loop and derived an expression for the gluon propagator contracted with the temporal paths. We explained the so-called shooting method, from which the energy eigenvalues for general one-dimensional Schrödinger potentials can be obtained numerically.

This project has been published in Ref. [106] and a summary was given in Ref. [107]. Most recently, the temporal Wilson loop using the Hamiltonian approach to Yang-Mills theory has also been explored in Ref. [115].

Appendix A

Explicit Spinor Solutions

In this Appendix we give an explicit realization of eigenvectors to the massless Dirac equation, which are used for computing the various energy densities in Appendix C.

In Section 1 we derive, starting from the free massless Dirac equation, the defining eigenvalue equations for positive and negative energy eigenvalues. In Section 2 we introduce the helicity operator and solve the corresponding helicity eigenvalue equation. In Section 3 we give an explicit realization of the spinor solutions with use of these helicity eigenvectors. Finally, we list useful properties and relations of the spinor solutions.

A.1 Eigenvalue Equations

We set the scene in Minkowski space and use the standard Dirac representation for the Dirac matrices, which can be found in Ref. [9]. We start from the free Dirac equation for massless fermion fields (Eq. (1.18) with setting $A_\mu = 0$ and $m = 0$)

$$i\gamma^\mu \partial_\mu \, \psi(x) \; = \; 0 \; , \tag{A.1}$$

and take the time derivative to the right-hand side of the equation

$$i\gamma^i \partial_i \, \psi(x) \; = \; -i\gamma^0 \partial_0 \, \psi(x) \; . \tag{A.2}$$

With the following ansatz

$$\psi(\boldsymbol{x}, t) = w(\boldsymbol{p}, s) e^{-ip\cdot x} \; , \tag{A.3}$$

where s is an additional parameter, which will which will be introduced below, we can rewrite Eq. (A.2) as the eigenvalue equation for massless fermions (using $\alpha_i = \beta\gamma_i$)

$$\boldsymbol{\alpha} \cdot \boldsymbol{p} \, w(\boldsymbol{p}, s) \; = \; E(\boldsymbol{p}) \, w(\boldsymbol{p}, s) \; . \tag{A.4}$$

In matrix language the eigenvalue equation (A.4) reads

$$\begin{pmatrix} 0 & \sigma_i \\ \sigma_i & 0 \end{pmatrix} p_i \, w(\boldsymbol{p}, s) \; = \; E(\boldsymbol{p}) \, w(\boldsymbol{p}, s) \; , \tag{A.5}$$

which could be decoupled into separate equations for the left- and the right-handed particles, called the Weyl equations.

Solving the characteristic polynomial we get

$$E(\boldsymbol{p}) \;=\; \pm|\boldsymbol{p}|\;, \tag{A.6}$$

and denote the two eigenfunctions leading to positive energy $|\boldsymbol{p}|$ as $u(\boldsymbol{p},s)$, whereas the eigensolutions with negative energy $-|\boldsymbol{p}|$ are referred to as $v(-\boldsymbol{p},s)$. The parameter s introduced in Eq. (A.3) takes the values ± 1. The equation Eq. (A.4) can therefore split up into

$$\boldsymbol{\alpha}\cdot\boldsymbol{p}\,u(\boldsymbol{p},s) \;=\; E(\boldsymbol{p})\,u(\boldsymbol{p},s)\,, \tag{A.7}$$
$$\boldsymbol{\alpha}\cdot\boldsymbol{p}\,v(-\boldsymbol{p},s) \;=\; -E(\boldsymbol{p})\,v(-\boldsymbol{p},s)\,. \tag{A.8}$$

Since $u(\boldsymbol{p},s)$ and $v(-\boldsymbol{p},s)$ are eigenfunctions of the same matrix belonging to different eigenvalues, they must be orthogonal:

$$u^{\dagger}(\boldsymbol{p},s)v(-\boldsymbol{p},s) \;=\; 0\,, \tag{A.9}$$
$$v^{\dagger}(-\boldsymbol{p},s)u(\boldsymbol{p},s) \;=\; 0\,. \tag{A.10}$$

We identify the spinors $u(-\boldsymbol{p},s)$ and $v(\boldsymbol{p},s)$ which solve the eigenvalue equations (A.7), (A.8) with opposite momentum.

A.2 Helicity Spinors

Now we turn to the quantum number s, which was introduced in expression (A.3). It is related to the helicity operator $\boldsymbol{\Sigma}\cdot\boldsymbol{p}$, with the matrix Σ_i defined as

$$\Sigma_i \;=\; \begin{pmatrix} \sigma_i & 0 \\ 0 & \sigma_i \end{pmatrix}\,, \tag{A.11}$$

and σ_i being the Pauli matrices

$$\sigma_1 \;=\; \begin{pmatrix} 0 & 1 \\ 1 & 0 \end{pmatrix}\,, \quad \sigma_2 \;=\; \begin{pmatrix} 0 & -i \\ i & 0 \end{pmatrix}\,, \quad \sigma_3 \;=\; \begin{pmatrix} 1 & 0 \\ 0 & -1 \end{pmatrix}\,. \tag{A.12}$$

Since the helicity operator commutes with the Dirac matrix, i.e., $[\boldsymbol{\Sigma}\cdot\boldsymbol{p},\boldsymbol{\alpha}\cdot\boldsymbol{p}] = 0$, it represents a conserved observable. We therefore use the eigenvectors of the helicity operator to specify the spinor solutions. Note that employing the helicity basis is only one possible way to represent the Dirac spinors u and v, Eqs. (A.7), (A.8) . We solve the following eigenvalue equation

$$\boldsymbol{\sigma}\cdot\hat{\boldsymbol{p}}\;\xi(\boldsymbol{p},s) \;=\; s\;\xi(\boldsymbol{p},s)\,, \tag{A.13}$$

with the unit vector in $\boldsymbol{p}$-direction, i.e., $\hat{\boldsymbol{p}} = \boldsymbol{p}/|\boldsymbol{p}|$. The matrix $\boldsymbol{\sigma}\cdot\hat{\boldsymbol{p}}$ is explicitly given as

$$\boldsymbol{\sigma}\cdot\hat{\boldsymbol{p}} \;=\; \sigma_1\hat{p}_1 + \sigma_2\hat{p}_2 + \sigma_3\hat{p}_3 \;=\; \begin{pmatrix} \hat{p}_3 & \hat{p}_1 - i\hat{p}_2 \\ \hat{p}_1 + i\hat{p}_2 & -\hat{p}_3 \end{pmatrix}\,, \tag{A.14}$$

with the characteristic polynomial

$$\det[\boldsymbol{\sigma}\cdot\hat{\boldsymbol{p}}-\lambda\mathbb{1}] \;=\; \lambda^2-\hat{\boldsymbol{p}}^2=\lambda^2-1\;. \tag{A.15}$$

Hence, the two helicity eigenmodes are $s=\pm1$. The eigenvectors $\xi(\boldsymbol{p},s)$ in Eq. (A.13) are given as

$$\xi(\boldsymbol{p},1) \;=\; \mathcal{N}\begin{pmatrix} 1+\hat{p}_3 \\ \hat{p}_1+i\hat{p}_2 \end{pmatrix}\;,\quad \xi(\boldsymbol{p},-1) \;=\; \mathcal{N}\begin{pmatrix} -\hat{p}_1+i\hat{p}_2 \\ 1+\hat{p}_3 \end{pmatrix}\;, \tag{A.16}$$

with the normalization

$$\mathcal{N} \;=\; \frac{1}{\sqrt{2(1+\hat{p}_3)}}\;. \tag{A.17}$$

We also identify the eigenvalue equation with opposite momentum

$$-\boldsymbol{\sigma}\cdot\hat{\boldsymbol{p}}\;\xi(-\boldsymbol{p},s) \;=\; s\;\xi(-\boldsymbol{p},s)\;, \tag{A.18}$$

and identify $\xi(-\boldsymbol{p},1)$ with negative helicity and $\xi(-\boldsymbol{p},-1)$ with positive helicity. Finally, we list some properties of the helicity solutions

$$\xi^\dagger(\boldsymbol{p},s)\,\xi(\boldsymbol{p},t) \;=\; \delta_{st}\;, \tag{A.19}$$

$$\xi(\boldsymbol{p},s)\,\xi^\dagger(\boldsymbol{p},s) \;=\; \frac{1}{2}\;(\mathbb{1}+s\,\boldsymbol{\sigma}\cdot\hat{\boldsymbol{p}}) \tag{A.20}$$

$$\sum_s \xi(\boldsymbol{p},s)\,\xi^\dagger(\boldsymbol{p},s) \;=\; \mathbb{1}\;, \tag{A.21}$$

$$\sum_s s\,\xi(\boldsymbol{p},s)\,\xi^\dagger(\boldsymbol{p},s) \;=\; \frac{1}{2}\;((\mathbb{1}+\boldsymbol{\sigma}\cdot\hat{\boldsymbol{p}})-(\mathbb{1}-\boldsymbol{\sigma}\cdot\hat{\boldsymbol{p}})) \;=\; \boldsymbol{\sigma}\cdot\hat{\boldsymbol{p}}\;. \tag{A.22}$$

Moreover, the following identities are useful for later applications:

$$\xi^\dagger(\boldsymbol{p},s)\boldsymbol{\sigma}\cdot\hat{\boldsymbol{q}}\xi(\boldsymbol{p},s) \;=\; s\hat{\boldsymbol{p}}\cdot\hat{\boldsymbol{q}}\;, \tag{A.23}$$

$$\sum_s s\,\xi^\dagger(\boldsymbol{p},s)\boldsymbol{\sigma}\cdot\hat{\boldsymbol{q}}\xi(\boldsymbol{p},s) \;=\; 2\,\hat{\boldsymbol{p}}\cdot\hat{\boldsymbol{q}}\;, \tag{A.24}$$

$$\sum_s \xi^\dagger(\boldsymbol{p},s)\boldsymbol{\sigma}\cdot\hat{\boldsymbol{q}}\xi(\boldsymbol{p},s) \;=\; 0\;. \tag{A.25}$$

A.3 Dirac Spinors

Now we have all the ingredients to build up solution vectors to the eigenvalue equations (A.7), (A.8). One possible solution to (A.7) is given as

$$u(\boldsymbol{p},s) \;=\; \sqrt{|\boldsymbol{p}|}\begin{pmatrix} \xi(\boldsymbol{p},s) \\ (\boldsymbol{\sigma}\cdot\hat{\boldsymbol{p}})\,\xi(\boldsymbol{p},s) \end{pmatrix} \;=\; \sqrt{|\boldsymbol{p}|}\begin{pmatrix} \xi(\boldsymbol{p},s) \\ s\xi(\boldsymbol{p},s) \end{pmatrix}\;, \tag{A.26}$$

and the eigenvector $v(-\boldsymbol{p}, s)$, which solves Eq. (A.8) reads

$$v(-\boldsymbol{p}, s) \;=\; \sqrt{|\boldsymbol{p}|}\, \begin{pmatrix} (\boldsymbol{\sigma}\cdot\hat{\boldsymbol{p}})\xi(\boldsymbol{p}, s) \\ -\xi(\boldsymbol{p}, s) \end{pmatrix} \;=\; \sqrt{|\boldsymbol{p}|}\, \begin{pmatrix} s\xi(\boldsymbol{p}, s) \\ -\xi(\boldsymbol{p}, s) \end{pmatrix} . \tag{A.27}$$

For the equations (A.7), (A.8) with opposite momentum, we then have the solutions

$$u(-\boldsymbol{p}, s) \;=\; \sqrt{|\boldsymbol{p}|}\, \begin{pmatrix} \xi(-\boldsymbol{p}, s) \\ s\xi(-\boldsymbol{p}, s) \end{pmatrix} , \quad v(\boldsymbol{p}, s) \;=\; \sqrt{|\boldsymbol{p}|}\, \begin{pmatrix} s\,\xi(-\boldsymbol{p}, s) \\ -\,\xi(-\boldsymbol{p}, s) \end{pmatrix} . \tag{A.28}$$

We summarize important relations for the Dirac spinors, which are of special interest for deriving the energy densities in Appendix C.

1. The normalization condition for the spinors is:

$$u^\dagger(\boldsymbol{p}, s)\, u(\boldsymbol{p}, t) \;=\; |\boldsymbol{p}|\, \left(\xi^\dagger(\boldsymbol{p}, s), s\, \xi^\dagger(\boldsymbol{p}, s)\right) \begin{pmatrix} \xi(\boldsymbol{p}, s) \\ s\, \xi(\boldsymbol{p}, s) \end{pmatrix} \;=\; 2|\boldsymbol{p}|\delta_{st} , \tag{A.29}$$

$$v^\dagger(\boldsymbol{p}, s)\, v(\boldsymbol{p}, t) \;=\; |\boldsymbol{p}|\, \left(s\,\xi^\dagger(-\boldsymbol{p}, s), -\xi^\dagger(-\boldsymbol{p}, s)\right) \begin{pmatrix} s\,\xi(-\boldsymbol{p}, s) \\ -\xi(-\boldsymbol{p}, s) \end{pmatrix} \;=\; 2|\boldsymbol{p}|\delta_{st} . \tag{A.30}$$

   Due to this normalization the pre-factor $\sqrt{2|\boldsymbol{p}|}$ enters the Fourier-decomposition formulae, Eqs. (1.40)-(1.43).

2. The following spinor products vanish for massless fields:

$$\overline{u}(\boldsymbol{p}, s)\, u(\boldsymbol{p}, t) \;=\; |\boldsymbol{p}|\, \left(\xi^\dagger(\boldsymbol{p}, s), -s\, \xi^\dagger(\boldsymbol{p}, s)\right) \begin{pmatrix} \xi(\boldsymbol{p}, s) \\ s\, \xi(\boldsymbol{p}, s) \end{pmatrix} \;=\; 0 , \tag{A.31}$$

$$\overline{v}(\boldsymbol{p}, s)\, v(\boldsymbol{p}, t) \;=\; |\boldsymbol{p}|\, \left(s\, \xi^\dagger(-\boldsymbol{p}, s), \xi^\dagger(-\boldsymbol{p}, s)\right) \begin{pmatrix} s\xi(-\boldsymbol{p}, s) \\ -\xi(-\boldsymbol{p}, s) \end{pmatrix} \;=\; 0 . \tag{A.32}$$

   For massive spinor solutions, these relations would give $\pm 2m\delta_{st}$.

3. We evaluate several spin sums, from which follow the relations (1.47) between the spinor solutions, Eqs. (A.26)-(A.28), and the projection operators $\Lambda_\pm$, Eq. (1.39), projecting to positive and negative energy states

$$\begin{aligned} \sum_s u(\boldsymbol{p}, s)\, \overline{u}(\boldsymbol{p}, s) \;&=\; |\boldsymbol{p}| \sum_s \begin{pmatrix} \xi(\boldsymbol{p}, s) \\ s\, \xi(\boldsymbol{p}, s) \end{pmatrix} \left(\xi^\dagger(\boldsymbol{p}, s), -s\, \xi^\dagger(\boldsymbol{p}, s)\right) \;= \\ &=\; |\boldsymbol{p}| \sum_s \begin{pmatrix} \xi(\boldsymbol{p}, s)\xi^\dagger(\boldsymbol{p}, s) & -s\xi(\boldsymbol{p}, s)\xi^\dagger(\boldsymbol{p}, s) \\ s\,\xi(\boldsymbol{p}, s)\xi^\dagger(\boldsymbol{p}, s) & -\xi(\boldsymbol{p}, s)\xi^\dagger(\boldsymbol{p}, s) \end{pmatrix} \;= \\ &=\; \begin{pmatrix} |\boldsymbol{p}| & -\boldsymbol{\sigma}\cdot\boldsymbol{p} \\ \boldsymbol{\sigma}\cdot\boldsymbol{p} & -|\boldsymbol{p}| \end{pmatrix} \;= \\ &=\; \gamma^0|\boldsymbol{p}| - \boldsymbol{\gamma}\cdot\boldsymbol{p} , \end{aligned} \tag{A.33}$$

and with opposite momentum

$$\sum_s u(-\boldsymbol{p},s)\overline{u}(-\boldsymbol{p},s) \;=\; \gamma^0|\boldsymbol{p}| + \boldsymbol{\gamma}\cdot\boldsymbol{p}\;. \tag{A.34}$$

From these relations we can read off the corresponding relations using the eigenvectors $v(\boldsymbol{p},s)$:

$$\sum_s v(\boldsymbol{p},s)\overline{v}(\boldsymbol{p},s) \;=\; \gamma^0|\boldsymbol{p}| - \boldsymbol{\gamma}\cdot\boldsymbol{p}\;, \tag{A.35}$$

$$\sum_s v(-\boldsymbol{p},s)\overline{v}(-\boldsymbol{p},s) \;=\; \gamma^0|\boldsymbol{p}| + \boldsymbol{\gamma}\cdot\boldsymbol{p}\;. \tag{A.36}$$

4. We show a relation, in which a gamma matrix γ_i appears between a spinor product:

$$\begin{aligned}\overline{u}(\boldsymbol{p},s)\boldsymbol{\gamma}u(\boldsymbol{p},s) \;&=\; |\boldsymbol{p}|\left(\xi^\dagger(\boldsymbol{p},s), -s\,\xi^\dagger(-\boldsymbol{p},s)\right)\begin{pmatrix} 0 & \boldsymbol{\sigma} \\ -\boldsymbol{\sigma} & 0\end{pmatrix}\begin{pmatrix}\xi(\boldsymbol{p},t)\\ t\,\xi(\boldsymbol{p},t)\end{pmatrix} = \\ &=\; s\boldsymbol{p}\,\xi^\dagger(\boldsymbol{p},s)\sigma^i\xi(\boldsymbol{p},t) + t\boldsymbol{p}\,\xi^\dagger(-\boldsymbol{p},s)\xi(-\boldsymbol{p},t) \;= \\ &=\; 2\boldsymbol{p}\,\delta_{st}\;.\end{aligned} \tag{A.37}$$

5. We list a relation, which is used to evaluate Eq. (3.36) from Eq. (3.2):

$$\overline{u}(\boldsymbol{p},s)\,v(-\boldsymbol{p},t) \;=\; |\boldsymbol{p}|\left(\xi^\dagger(\boldsymbol{p},s),\; -s\xi^\dagger(\boldsymbol{p},s)\right)\begin{pmatrix} t\,\xi(\boldsymbol{p},t)\\ -\xi(\boldsymbol{p},t)\end{pmatrix} = 2s|\boldsymbol{p}|\,\delta_{st} \tag{A.38}$$

$$\overline{v}(\boldsymbol{p},s)\,u(-\boldsymbol{p},t) \;=\; |\boldsymbol{p}|\left(s\xi^\dagger(\boldsymbol{p},s),\; \xi^\dagger(\boldsymbol{p},s)\right)\begin{pmatrix} \xi(\boldsymbol{p},t)\\ t\,\xi(\boldsymbol{p},t)\end{pmatrix} = 2s|\boldsymbol{p}|\,\delta_{st} \tag{A.39}$$

6. Finally, we discuss a typical sum of spin products which occurs when evaluating the Coulomb energy density $\langle H_{\rm C}\rangle$, Eq. (5.1),

$$\sum_{s,t} u^\dagger(\boldsymbol{p},s)u(\boldsymbol{q},t)u^\dagger(\boldsymbol{q},t)u(\boldsymbol{p},s)\,. \tag{A.40}$$

With use of Eq. (A.33) we evaluate

$$\sum_t u(\boldsymbol{q},t)\,u^\dagger(\boldsymbol{q},t) \;=\; \mathbb{1}|\boldsymbol{q}| + \boldsymbol{\alpha}\cdot\boldsymbol{q}\;. \tag{A.41}$$

We proceed with

$$\begin{aligned}&\sum_{s,t} u^\dagger(\boldsymbol{p},s)u(\boldsymbol{q},t)u^\dagger(\boldsymbol{q},t)u(\boldsymbol{p},s) = \\ &= \sum_s u^\dagger(\boldsymbol{p},s)|\boldsymbol{q}|u(\boldsymbol{p},s) + \sum_s \overline{u}(\boldsymbol{p},s)\boldsymbol{\gamma}\cdot\boldsymbol{q}u(\boldsymbol{p},s) = \\ &= 4\,|\boldsymbol{q}||\boldsymbol{p}| + 4\,\boldsymbol{q}\cdot\boldsymbol{p}\;,\end{aligned} \tag{A.42}$$

where in the second step we have rewritten the spinor products so, that we can use the identity (A.37).

Appendix B

Quark Wave Functional - Explicit Calculations

In this appendix we explicitly present the computations which were quoted in Chapter 3, namely the evaluation of the fermion generating functional (Section 1), the computation of the gluon loop integral (Section 2), the derivation of the restrictions on the variational kernels (Section 3) and the evaluation of the chiral condensate (Section 4). In Section 5 we determine the dimensions of the variational kernels.

B.1 Evaluating the Generating Functional

In this part of the Appendix we present the derivation of Eq. (3.16) from the key definition of the fermion generating functional (3.15) following Ref. [81]. Summing over repeated color and spin indices and integrating over repeated momentum arguments is implicitly understood, e.g.,

$$\xi^\dagger \xi = \int đ^3 p \sum_{s,a} \xi^{\dagger a}(\boldsymbol{p}, s)\xi^a(\boldsymbol{p}, s) \; . \tag{B.1}$$

Recalling the definition of the generating functional

$$Z[\eta] \equiv Z[\eta_+^*, \eta_-^*; \eta_+, \eta_-] = \mathcal{N}_{\rm F}^2 \langle \phi | e^{\left(\eta_+^* a + \eta_- b\right)} \, e^{\left(a^\dagger \eta_+ + b^\dagger \eta_-^*\right)} | \phi \rangle \; , \tag{B.2}$$

and employing the closure relation of coherent fermion states

$$\mathbb{1} = \int d\mu(\xi) |\xi\rangle\langle\xi| = \int D\xi_+^* D\xi_+ D\xi_- D\xi_-^* \exp\left[-\xi_+^*\xi_+ - \xi_-\xi_-^*\right] \, |\xi\rangle\langle\xi| \; , \tag{B.3}$$

the generating functional (3.15) in the basis of coherent states reads

$$\begin{aligned} Z[\eta] &= |\mathcal{N}_{\rm F}|^2 \int d\mu(\xi) \phi^*(\xi)\phi(\xi) \exp\left[\eta_+^*\xi_+ + \eta_-\xi_-^*\right] \, \exp\left[\xi_+^*\eta_+ + \xi_-\eta_-^*\right] = \\ &= |\mathcal{N}_{\rm F}|^2 \int D\xi_+^* D\xi_+ D\xi_- D\xi_-^* \exp[-\xi_+^*\xi_+ - \xi_-\xi_-^*] \times \\ &\quad \times \exp\left[-\xi_+^* K \xi_- - \xi_-^* \overline{K} \xi_+\right] \exp\left[\eta_+^*\xi_+ + \eta_-\xi_-^* + \xi_+^*\eta_+ + \xi_-\eta_-^*\right] \; . \end{aligned} \tag{B.4}$$

We rewrite the exponent in a compact form introducing the matrix notation

$$\exp\left[-\xi_+^*\mathbb{1}\xi_+ - \xi_+^* K\xi_- - \xi_-^*\overline{K}\xi_+ + \xi_-^*\mathbb{1}\xi_- + \xi_+^*\eta_+ - \xi_-^*\eta_- + \eta_+^*\xi_+ - \eta_-^*\xi_-\right] = \exp\left[-\left(\xi_+^*,\xi_-^*\right)\begin{pmatrix}\mathbb{1} & K\\ \overline{K} & -\mathbb{1}\end{pmatrix}\begin{pmatrix}\xi_+\\ \xi_-\end{pmatrix} + \left(\xi_+^*,\xi_-^*\right)\begin{pmatrix}\eta_+\\ -\eta_-\end{pmatrix} + \left(\eta_+^*,-\eta_-^*\right)\begin{pmatrix}\xi_+\\ \xi_-\end{pmatrix}\right], \tag{B.5}$$

and define

$$\Omega = \begin{pmatrix}\mathbb{1} & K\\ \overline{K} & -\mathbb{1}\end{pmatrix}, \quad \Psi = \begin{pmatrix}\xi_+\\ \xi_-\end{pmatrix}, \quad \Lambda = \begin{pmatrix}\eta_+\\ -\eta_-\end{pmatrix}. \tag{B.6}$$

The generating functional is then easily evaluated applying standard Gaussian integrals for Grassmann fields, yielding

$$\begin{aligned} Z[\eta] &= |\mathcal{N}_{\mathrm{F}}(A)|^2 \int D\Psi^\dagger D\Psi \, \exp\left[-\Psi^\dagger\Omega\Psi + \Psi^\dagger\Lambda + \Lambda^\dagger\Psi\right] = \\ &= |\mathcal{N}_{\mathrm{F}}(A)|^2 \,\mathrm{Det}[\Omega(A)] \, \exp\left[\Lambda^\dagger\Omega^{-1}[A]\Lambda\right] . \end{aligned} \tag{B.7}$$

The normalization is fixed by requiring $|\mathcal{N}_{\mathrm{F}}(A)|^2\,\mathrm{Det}[\Omega] = 1$, see Eq. (3.22). Explicitly inverting the matrix Ω yields

$$\Omega^{-1} = \begin{pmatrix}\left[\mathbb{1} + K\overline{K}\right]^{-1} & \left[\mathbb{1} + K\overline{K}\right]^{-1} K\\ \left[\mathbb{1} + \overline{K}K\right]^{-1}\overline{K} & -\left[\mathbb{1} + \overline{K}K\right]^{-1}\end{pmatrix}, \tag{B.8}$$

and the generating functional can be expressed as

$$\begin{aligned} Z[\eta] = \exp\Big(&\eta_+^*\left[\mathbb{1} + K\overline{K}\right]^{-1}\eta_+ - \eta_-^*\left[\mathbb{1} + \overline{K}K\right]^{-1}\overline{K}\eta_+ \\ &-\eta_+^*\left[\mathbb{1} + K\overline{K}\right]^{-1}K\eta_- - \eta_-^*\left[\mathbb{1} + \overline{K}K\right]^{-1}\eta_-\Big) . \end{aligned} \tag{B.9}$$

We recall that $\overline{K}$ means the complex-conjugated kernel.

We list all occurring fermion two-point functions:

$$\langle a^a(\boldsymbol{p},s)a^{\dagger b}(\boldsymbol{q},t)\,\rangle_{\rm F} = -\frac{\delta^2 Z[\eta]}{\delta\eta_+^{*a}(\boldsymbol{p},s)\,\delta\eta_+^b(\boldsymbol{q},t)}\Big|_{\eta=0} = \left(\left[\mathbb{1}+K\overline{K}\right]^{-1}\right)^{ab}(\boldsymbol{p},s;\boldsymbol{q},t)\,, \tag{B.10}$$

$$\langle a^{\dagger a}(\boldsymbol{p},s)a^b(\boldsymbol{q},t)\,\rangle_{\rm F} = \left(\left[\mathbb{1}+K\overline{K}\right]^{-1}K\overline{K}\right)^{ba}(\boldsymbol{q},t;\boldsymbol{p},s)\,, \tag{B.11}$$

$$\langle b^a(\boldsymbol{p},s)b^{\dagger b}(\boldsymbol{q},t)\,\rangle_{\rm F} = -\frac{\delta^2 Z[\eta]}{\delta\eta_-^a(\boldsymbol{p},s)\,\delta\eta_-^{*b}(\boldsymbol{q},t)}\Big|_{\eta=0} = \left(\left[\mathbb{1}+\overline{K}K\right]^{-1}\right)^{ba}(\boldsymbol{q},t;\boldsymbol{p},s)\,, \tag{B.12}$$

$$\langle b^{\dagger a}(\boldsymbol{p},s)b^b(\boldsymbol{q},t)\,\rangle_{\rm F} = \left(\left[\mathbb{1}+\overline{K}K\right]^{-1}\overline{K}K\right)^{ab}(\boldsymbol{p},s;\boldsymbol{q},t)\,, \tag{B.13}$$

$$\langle a^{\dagger a}(\boldsymbol{p},s)b^{\dagger b}(\boldsymbol{q},t)\,\rangle_{\rm F} = \frac{\delta^2 Z[\eta]}{\delta\eta_+^a(\boldsymbol{p},s)\,\delta\eta_-^{*b}(\boldsymbol{q},t)}\Big|_{\eta=0} = -\left(\left[\mathbb{1}+\overline{K}K\right]^{-1}\overline{K}\right)^{ba}(\boldsymbol{q},t;\boldsymbol{p},s)\,, \tag{B.14}$$

$$\langle a^a(\boldsymbol{p},s)b^b(\boldsymbol{q},t)\rangle_{\rm F} = \frac{\delta^2 Z[\eta]}{\delta\eta_+^{*a}(\boldsymbol{p},s)\,\delta\eta_-^b(\boldsymbol{q},t)}\Big|_{\eta=0} = \left(\left[\mathbb{1}+K\overline{K}\right]^{-1}K\right)^{ab}(\boldsymbol{p},s;\boldsymbol{q},t)\,. \tag{B.15}$$

We note that for the expectations values (B.11) and (B.13) the anti-commutation relations (1.44) and (1.45) were used. Expectation values of the form

$$\langle a^{\dagger a}(\boldsymbol{p},s)b^b(\boldsymbol{q},t)\rangle_{\rm F} = -\frac{\delta^2 Z[\eta]}{\delta\eta_+^a(\boldsymbol{p},s)\,\delta\eta_-^b(\boldsymbol{q},t)}\Big|_{\eta=0} = 0\,, \tag{B.16}$$

as well as

$$\langle a^{\dagger a}(\boldsymbol{p},s)a^{\dagger b}(\boldsymbol{q},t)\rangle_{\rm F} \;=\; -\frac{\delta^2 Z[\eta]}{\delta\eta_+^a(\boldsymbol{p},s)\,\delta\eta_+^b(\boldsymbol{q},t)}\Big|_{\eta=0} = 0\,, \tag{B.17}$$

vanish.

We turn to several properties of the matrices Ω, Eq. (B.6), and Ω^{-1}, Eq. (B.8). The matrix Ω, Eq. (B.6) is obviously Hermitian. For the matrix Ω^{-1}, Eq. (B.8), hermiticity is shown using the relations

$$\begin{aligned}\left[\mathbb{1}+\overline{K}K\right]^{-1}\overline{K} &= \left[\overline{K}\left((\overline{K})^{-1}+K\right)\right]^{-1}\overline{K} = \left[(\overline{K})^{-1}+K\right]^{-1} = \\ &= \left[\left(\mathbb{1}+K\overline{K}\right)(\overline{K})^{-1}\right]^{-1} = \overline{K}\,\left[\mathbb{1}+K\overline{K}\right]^{-1}\,,\end{aligned} \tag{B.18}$$

$$\left[\mathbb{1}+K\overline{K}\right]^{-1}K = K\,\left[\mathbb{1}+\overline{K}K\right]^{-1}\,, \tag{B.19}$$

where in the denominator the kernels K and $\overline{K}$ change order. These relations become especially important when evaluating the expectation value in the gluon sector, see Section B.2. We note that in general $K\overline{K}\neq\overline{K}K$.

At next we compute the normalization $\mathcal{N}_{\rm F}^{-2} = \mathsf{Det}[\Omega]$. From

$$(\mathsf{Det}\Omega)^2 = \mathsf{Det}(1+\overline{K}K)\,\mathsf{Det}(1+K\overline{K})\,, \tag{B.20}$$

and using that there is an overall symmetry between the particles and anti-particles we conclude

$$\mathcal{N}_{\mathrm{F}}^{-2}(A) = \mathrm{Det}\Omega = \mathrm{Det}(1 + \overline{K}K) = \mathrm{Det}(1 + K\overline{K}) \; . \tag{B.21}$$

Limiting the ansatz (3.3) to be of BCS type the fermion normalization becomes

$$\mathrm{Det}[\Omega_0] = \prod_{\boldsymbol{p},s,a} (1 + S^2(\boldsymbol{p})) \; , \tag{B.22}$$

which has been derived in Ref. [80] by means of Bogoliubov-transformations.

B.2 Gluon Loop Integral

At next we explicitly derive the formulae (3.46), (3.47) from the definitions (3.44), (3.45). Using the ansatz (3.37) and (3.39) for the adjoint kernel of the gauge-field dependent part of the vacuum wave functional, Eq. (3.3), the expectation values in the gluonic sector become (using Eq. (1.89))

$$\begin{aligned}
&\left\langle \left(\overline{K}_1 K_1\right)^{ab}(\boldsymbol{p},s;\boldsymbol{q},t)\right\rangle_{\mathrm{G}} = \\
&= \delta^{ab}(2\pi)^3\delta(\boldsymbol{p}-\boldsymbol{q})C_F \int đ^3k\, V^*(\boldsymbol{p},\boldsymbol{k})V(\boldsymbol{k},\boldsymbol{p})\, \frac{1}{2\omega(-\boldsymbol{p}-\boldsymbol{k})}\, \frac{1}{4|\boldsymbol{p}||\boldsymbol{k}|}\times \\
&\times \sum_u t_{ij}(-\boldsymbol{p}-\boldsymbol{k})\, \Gamma_i^\dagger(\boldsymbol{p},s;\boldsymbol{k},u)\Gamma_j(\boldsymbol{k},u;\boldsymbol{p},t)\, ,
\end{aligned} \tag{B.23}$$

$$\begin{aligned}
&\left\langle \left(K_1\overline{K}_1\right)^{ab}(\boldsymbol{p},s;\boldsymbol{q},t)\right\rangle_{\mathrm{G}} = \\
&= \delta^{ab}(2\pi)^3\delta(\boldsymbol{p}-\boldsymbol{q})C_F \int đ^3k\, V(\boldsymbol{p},\boldsymbol{k})V^*(\boldsymbol{k},\boldsymbol{p})\, \frac{1}{2\omega(\boldsymbol{p}+\boldsymbol{k})}\, \frac{1}{4|\boldsymbol{p}||\boldsymbol{k}|}\times \\
&\times \sum_u t_{ij}(\boldsymbol{p}+\boldsymbol{k})\, \Gamma_i(\boldsymbol{p},s;\boldsymbol{k},u)\Gamma_j^\dagger(\boldsymbol{k},u;\boldsymbol{p},t)\, ,
\end{aligned} \tag{B.24}$$

where we have abbreviated

$$\Gamma_i(\boldsymbol{p},s;\boldsymbol{q},t) \; = \; \overline{u}(\boldsymbol{p},s)\gamma_i v(\boldsymbol{q},t) \; . \tag{B.25}$$

The spinor sums in (B.23) and (B.24) coincide

$$\sum_u t_{ij}(-\boldsymbol{p}-\boldsymbol{k})\Gamma_i^\dagger(\boldsymbol{p},s;\boldsymbol{k},u)\Gamma_j(\boldsymbol{k},u;\boldsymbol{p},t) = \sum_u t_{ij}(\boldsymbol{p}+\boldsymbol{k})\Gamma_i(\boldsymbol{p},s;\boldsymbol{k},u)\Gamma_j^\dagger(\boldsymbol{k},u;\boldsymbol{p},t) \; . \tag{B.26}$$

Explicitly we find

$$\sum_u t_{ij}(-\boldsymbol{p}-\boldsymbol{k})\, \Gamma_i^\dagger(\boldsymbol{p},s;\boldsymbol{k},u)\Gamma_j(\boldsymbol{k},u;\boldsymbol{p},t) \; = \; 4\delta_{st}\left(|\boldsymbol{p}||\boldsymbol{k}| - \frac{(p+k)_i(p+k)_j}{(\boldsymbol{p}+\boldsymbol{k})^2}\, p_i k_j\right) \; . \tag{B.27}$$

The expectation values therefore read

$$\left\langle \left(\overline{K}_1 K_1\right)^{ab}(\boldsymbol{p},s;\boldsymbol{q},t)\right\rangle_{\mathrm{G}} = \delta^{ab}\delta_{st}(2\pi)^3\delta(\boldsymbol{p}-\boldsymbol{q})C_F\times$$
$$\times\int đ^3k\, V^*(\boldsymbol{p},\boldsymbol{k})V(\boldsymbol{k},\boldsymbol{p})\,\frac{1}{2\omega(-\boldsymbol{p}-\boldsymbol{k})}\left(1-\frac{(p+k)_i(p+k)_j}{(\boldsymbol{p}+\boldsymbol{k})^2}\frac{p_i}{|\boldsymbol{p}|}\frac{k_j}{|\boldsymbol{k}|}\right)\,, \tag{B.28}$$
$$\left\langle \left(K_1\overline{K}_1\right)^{ab}(\boldsymbol{p},s;\boldsymbol{q},t)\right\rangle_{\mathrm{G}} = \delta^{ab}\delta_{st}(2\pi)^3\delta(\boldsymbol{p}-\boldsymbol{q})C_F\times$$
$$\times\int đ^3k\, V(\boldsymbol{p},\boldsymbol{k})V^*(\boldsymbol{k},\boldsymbol{p})\frac{1}{2\omega(\boldsymbol{p}+\boldsymbol{k})}\left(1-\frac{(p+k)_i(p+k)_j}{(\boldsymbol{p}+\boldsymbol{k})^2}\frac{p_i}{|\boldsymbol{p}|}\frac{k_j}{|\boldsymbol{k}|}\right)\,. \tag{B.29}$$

We abbreviate

$$\left\langle \left(\overline{K}_1 K_1\right)^{ab}(\boldsymbol{p},s;\boldsymbol{q},t)\right\rangle_{\mathrm{G}} = \delta^{ab}\delta_{st}(2\pi)^3\delta(\boldsymbol{p}-\boldsymbol{q})\overline{R}(\boldsymbol{p})\,, \tag{B.30}$$
$$\left\langle \left(K_1\overline{K}_1\right)^{ab}(\boldsymbol{p},s;\boldsymbol{q},t)\right\rangle_{\mathrm{G}} = \delta^{ab}\delta_{st}(2\pi)^3\delta(\boldsymbol{p}-\boldsymbol{q})R(\boldsymbol{p})\,, \tag{B.31}$$

with

$$\overline{R}(\boldsymbol{p}) \;=\; C_F\int đ^3q\, V^*(\boldsymbol{p},\boldsymbol{q})V(\boldsymbol{q},\boldsymbol{p})\,\frac{1}{2\omega(\boldsymbol{p}-\boldsymbol{q})}\left(1+\frac{(p-q)_i(p-q)_j}{(\boldsymbol{p}-\boldsymbol{q})^2}\frac{p_i}{|\boldsymbol{p}|}\frac{q_j}{|\boldsymbol{q}|}\right)\,, \tag{B.32}$$
$$R(\boldsymbol{p}) \;=\; C_F\int đ^3q\, V(\boldsymbol{p},\boldsymbol{q})V^*(\boldsymbol{q},\boldsymbol{p})\,\frac{1}{2\omega(\boldsymbol{p}-\boldsymbol{q})}\left(1+\frac{(p-q)_i(p-q)_j}{(\boldsymbol{p}-\boldsymbol{q})^2}\frac{p_i}{|\boldsymbol{p}|}\frac{q_j}{|\boldsymbol{q}|}\right)\,, \tag{B.33}$$

where we have assumed translational invariance of the kernel $\omega(\boldsymbol{p},\boldsymbol{q})$. The results agree with Eqs. (3.46), (3.47). We remark that in order to make $R(\boldsymbol{p})$ and $\overline{R}(\boldsymbol{p})$ in (B.32) and (B.33) coincide, we have to demand

$$V(\boldsymbol{p},\boldsymbol{q}) \;=\; V(\boldsymbol{q},\boldsymbol{p})\,. \tag{B.34}$$

In the derivation below we will observe that this assumption, in general, will hold true.

B.3 Restrictions of the Variational Kernels

In Eq. (3.50) we have quoted several assumptions. We explicitly show how some of these assumptions arise from the requirement that the relations (B.18), (B.19) also have to hold true for the gluon expectation values, for instance,

$$\left\langle \left[\mathbb{1}+\overline{K}K\right]^{-1}\overline{K}\right\rangle_{\mathrm{G}} = \left\langle \overline{K}\left[\mathbb{1}+K\overline{K}\right]^{-1}\right\rangle_{\mathrm{G}}\,. \tag{B.35}$$

Let us compute the left-hand side of this equation,

$$\begin{aligned}
&\left\langle \left(\left[\mathbb{1} + \overline{K}K\right]^{-1} \overline{K} \right) \right\rangle_{\mathrm{G}}^{ba} (\boldsymbol{q}, t; \boldsymbol{p}, s) = \\
&= \int đ^3 q' \sum_{s'} \left\langle \left[\mathbb{1} + \overline{K}K\right]^{-1} \right\rangle_{\mathrm{G}}^{bb'} (\boldsymbol{q}, t; \boldsymbol{q}', s') \left\langle \overline{K} \right\rangle_{\mathrm{G}}^{b'a} (\boldsymbol{q}', s'; \boldsymbol{p}, s) = \\
&= \int đ^3 q' \sum_{s'} \left(\frac{1}{1 + S^*(\boldsymbol{q}) S(-\boldsymbol{q}) + \overline{R}(\boldsymbol{q})} \delta^{bb'} \delta_{ts'} (2\pi)^3 \, \delta(\boldsymbol{q} - \boldsymbol{q}') \right) \times \\
&\qquad \times \left(s' S^*(\boldsymbol{q}') \delta^{b'a} \delta_{s's} (2\pi)^3 \delta(\boldsymbol{q}' + \boldsymbol{p}) \right) = \\
&= \frac{s S^*(-\boldsymbol{p})}{1 + S^*(\boldsymbol{q}) S(-\boldsymbol{q}) + \overline{R}(\boldsymbol{q})} \delta^{ba} \delta_{t,s} (2\pi)^3 \, \delta(\boldsymbol{q} + \boldsymbol{p})
\end{aligned} \tag{B.36}$$

We proceed with the right-hand side of (B.35)

$$\begin{aligned}
&\left\langle \left(\overline{K} \left[\mathbb{1} + K\overline{K}\right]^{-1} \right) \right\rangle_{\mathrm{G}}^{ba} (\boldsymbol{q}, t; \boldsymbol{p}, s) = \\
&= \int đ^3 q' \sum_{s'} \left\langle \overline{K} \right\rangle_{\mathrm{G}}^{bb'} (\boldsymbol{q}, t; \boldsymbol{q}', s') \left\langle \left[\mathbb{1} + K\overline{K}\right]^{-1} \right\rangle_{\mathrm{G}}^{b'a} (\boldsymbol{q}', s'; \boldsymbol{p}, s) = \\
&= \int đ^3 q' \sum_{s'} \left(t S^*(\boldsymbol{q}) \delta^{bb'} \delta_{ts'} (2\pi)^3 \delta(\boldsymbol{q} + \boldsymbol{q}') \right) \times \\
&\qquad \times \left(\frac{1}{1 + S(\boldsymbol{p}) S^*(-\boldsymbol{p}) + R(\boldsymbol{p})} \delta_{b'a} \delta_{s's} (2\pi)^3 \delta(\boldsymbol{q}' - \boldsymbol{p}) \right) = \\
&= \frac{t S^*(\boldsymbol{q})}{1 + S(\boldsymbol{p}) S^*(-\boldsymbol{p}) + R(\boldsymbol{p})} \delta^{ba} \delta_{t,s} (2\pi)^3 \, \delta(\boldsymbol{q} + \boldsymbol{p}) \, ,
\end{aligned} \tag{B.37}$$

and compare both sides (B.36) and (B.37)

$$\begin{aligned}
&\frac{s S^*(-\boldsymbol{p})}{1 + S^*(\boldsymbol{q}) S(\boldsymbol{q}) + \overline{R}(\boldsymbol{q})} \delta^{ba} \delta_{t,s} (2\pi)^3 \, \delta(\boldsymbol{q} + \boldsymbol{p}) = \\
&\qquad = \frac{t S^*(\boldsymbol{q})}{1 + S(\boldsymbol{p}) S^*(-\boldsymbol{p}) + R(\boldsymbol{p})} \delta^{ba} \delta_{t,s} (2\pi)^3 \, \delta(\boldsymbol{q} + \boldsymbol{p}) \, .
\end{aligned} \tag{B.38}$$

Using $\boldsymbol{q} = -\boldsymbol{p}$ we can identify

$$S(\boldsymbol{q}) \, = \, S(-\boldsymbol{q}) \, , \quad S^*(\boldsymbol{q}) = S^*(-\boldsymbol{q}) \, , \quad R(\boldsymbol{q}) \, = \, \overline{R}(-\boldsymbol{q}) \, . \tag{B.39}$$

Expectation values of the form

$$\left\langle \left[\mathbb{1} + \overline{K}K\right]^{-1} \overline{K} A_i^m(\boldsymbol{k}) \right\rangle_{\mathrm{G}} = \left\langle \overline{K} \left[\mathbb{1} + K\overline{K}\right]^{-1} A_i^m(\boldsymbol{k}) \right\rangle_{\mathrm{G}} \, , \tag{B.40}$$

lead to the additional restriction

$$R(\boldsymbol{q}) = \overline{R}(\boldsymbol{q}) \, , \tag{B.41}$$

from which the symmetry relation (B.34) follows.

B.4 Dimensional Analysis of the Quark Kernels

The kernels K_0, Eq. (3.35), and K_1, Eq. (3.37), are given as

$$K_0^{ab}(\boldsymbol{p},s;\boldsymbol{q},t) = \frac{1}{2\sqrt{|\boldsymbol{p}||\boldsymbol{q}|}} S(\boldsymbol{p})\, u^\dagger(\boldsymbol{p},s)\beta v(\boldsymbol{q},t)(2\pi)^3\delta(\boldsymbol{p}+\boldsymbol{q})\delta_{st}\,\delta^{ab} \tag{B.42}$$

$$K_1^{ab}(\boldsymbol{p},s;\boldsymbol{q},t) = \frac{1}{2\sqrt{|\boldsymbol{p}||\boldsymbol{q}|}} V(\boldsymbol{p},\boldsymbol{q}) u^\dagger(\boldsymbol{p},s)\alpha_i\,(T^m)^{ab}\, v(\boldsymbol{q},t) A_i^m(\boldsymbol{p}+\boldsymbol{q})\ . \tag{B.43}$$

The spinor solutions $u(\boldsymbol{p},s), v(\boldsymbol{p},s)$, Eqs. (A.26)-(A.28), have the dimension

$$[u(\boldsymbol{p},s)] \;=\; \Lambda^{\frac{1}{2}}\ , \tag{B.44}$$

with Λ denoting the dimension of momentum.

The exponential of the vacuum wave functional (3.3) is given as

$$\widetilde{K} \;=\; \int đ^3p \int đ^3q \sum_{s,t} K^{ab}(\boldsymbol{p},s;\boldsymbol{q},t) a^{\dagger a}(\boldsymbol{p},s) b^\dagger(\boldsymbol{q},t)\ . \tag{B.45}$$

Since the kernel $\widetilde{K}$ must be dimensionless, we can compare the dimensions on both sides of the expression,

$$\Lambda^0 \;=\; \Lambda^3\Lambda^3\Lambda^x\Lambda^{-\frac{3}{2}}\Lambda^{-\frac{3}{2}}\ , \tag{B.46}$$

using that $[a^\dagger(\boldsymbol{p},s)] = [b^\dagger(\boldsymbol{p},s)] = \Lambda^{-\frac{3}{2}}$, see Eq. (1.40). We have denoted as x the unknown momentum dimension of the kernel K. Hence, the kernels K_0 and K_1 have the dimension

$$[K_0(\boldsymbol{p},s;\boldsymbol{q},t)] \;=\; [K_1(\boldsymbol{p},s;\boldsymbol{q},t)] \;=\; \Lambda^{-3}\ . \tag{B.47}$$

We now identify the dimensions of the variational functions S and V. Since $[\delta(\boldsymbol{p}+\boldsymbol{q})] = \Lambda^{-3}$ we have

$$[K_0(\boldsymbol{p},s;\boldsymbol{q},t)] \;=\; \Lambda^x\Lambda^{-3}\ , \tag{B.48}$$

with x now denoting the unknown dimension of S. Comparing both sides of Eq. (B.46) we end up with

$$[S(\boldsymbol{p})] \;=\; \Lambda^0\ . \tag{B.49}$$

The scalar variational function $S(\boldsymbol{p})$ is dimensionless.

We turn to the variational function V and use that $[A(\boldsymbol{p})] = \Lambda^{-2}$. The dimension of the interaction kernel K_1, Eq. (B.43), is

$$[K_1(\boldsymbol{p},s;\boldsymbol{q},t)] \;=\; \Lambda^x\Lambda^{-2}\ , \tag{B.50}$$

with x now the dimension of V. Again, comparing both sides of Eq. (B.46) we arrive at

$$[V(\boldsymbol{p})] \;=\; \Lambda^{-1}\;. \tag{B.51}$$

The vector kernel V has dimension of inverse momentum.

Finally, we collect the dimensions of $R(\boldsymbol{p})$, Eq. (3.46), $I_\omega(\boldsymbol{p})$, Eq. (4.12), and $I_{\mathrm{C}}^{(1)}(\boldsymbol{p})$, Eq. (5.14), $I_{\mathrm{C}}^{(2)}(\boldsymbol{p})$, Eq. (5.18),

$$[I(\boldsymbol{p})] = \Lambda^2\;, \tag{B.52}$$

$$[I_C^{(1)}(\boldsymbol{p})] \;=\; [I_C^{(2)}(\boldsymbol{p})] \;=\; [I_\omega(\boldsymbol{p})] \;=\; \Lambda^1\;, \tag{B.53}$$

$$[R(\boldsymbol{p})] \;=\; \Lambda^0\;. \tag{B.54}$$

B.5 Evaluating the Chiral Condensate

We evaluate the expression for the chiral condensate (3.85) in detail. Decomposing the quark fields

$$\begin{aligned}\langle\Phi|\overline{\psi}^a(\boldsymbol{x})\psi^a(\boldsymbol{x})|\Phi\rangle \;=&\langle\Phi|\overline{\psi}^a_+(\boldsymbol{x})\psi^a_+(\boldsymbol{x})|\Phi\rangle + \langle\Phi|\overline{\psi}^a_-(\boldsymbol{x})\psi^a_-(\boldsymbol{x})|\Phi\rangle + \\ &+\langle\Phi|\overline{\psi}^a_+(\boldsymbol{x})\psi^a_-(\boldsymbol{x})|\Phi\rangle + \langle\Phi|\overline{\psi}^a_-(\boldsymbol{x})\psi^a_+(\boldsymbol{x})|\Phi\rangle\;,\end{aligned} \tag{B.55}$$

and expanding in terms of Fourier modes we arrive at four different expectation values

$$\begin{aligned}&\langle\Phi|\overline{\psi}^a_+(\boldsymbol{x})\psi^a_+(\boldsymbol{x})|\Phi\rangle = \\ &= \int đ^3p \int đ^3q \frac{1}{2\sqrt{E(\boldsymbol{p})E(\boldsymbol{q})}} \sum_{s,t} \overline{u}(\boldsymbol{p},s)u(\boldsymbol{q},t)a^{\dagger a}(\boldsymbol{p},s)a(\boldsymbol{q},t)e^{-i\boldsymbol{p}\cdot\boldsymbol{x}}e^{i\boldsymbol{q}\boldsymbol{x}}\;,\end{aligned} \tag{B.56}$$

$$\begin{aligned}&\langle\Phi|\overline{\psi}^a_-(\boldsymbol{x})\psi^a_-(\boldsymbol{x})|\Phi\rangle = \\ &= \int đ^3p \int đ^3q \frac{1}{2\sqrt{E(\boldsymbol{p})E(\boldsymbol{q})}} \sum_{s,t} \overline{v}(\boldsymbol{p},s)v(\boldsymbol{q},t)b^{a}(\boldsymbol{p},s)b^{\dagger a}(\boldsymbol{q},t)e^{i\boldsymbol{p}\cdot\boldsymbol{x}}e^{-i\boldsymbol{q}\boldsymbol{x}}\end{aligned} \tag{B.57}$$

$$\begin{aligned}&\langle\Phi|\overline{\psi}^a_+(\boldsymbol{x})\psi^a_-(\boldsymbol{x})|\Phi\rangle = \\ &= \int đ^3p \int đ^3q \frac{1}{2\sqrt{E(\boldsymbol{p})E(\boldsymbol{q})}} \sum_{s,t} \overline{u}(\boldsymbol{p},s)v(\boldsymbol{q},t)a^{\dagger a}(\boldsymbol{p},s)b^{\dagger a}(\boldsymbol{q},t)e^{-i\boldsymbol{p}\cdot\boldsymbol{x}}e^{-i\boldsymbol{q}\cdot\boldsymbol{x}}\end{aligned} \tag{B.58}$$

$$\begin{aligned}&\langle\Phi|\overline{\psi}^a_-(\boldsymbol{x})\psi^a_+(\boldsymbol{x})|\Phi\rangle = \\ &= \int đ^3p \int đ^3q \frac{1}{2\sqrt{E(\boldsymbol{p})E(\boldsymbol{q})}} \sum_{s,t} \overline{v}(\boldsymbol{p},s)u(\boldsymbol{q},t)b^{a}(\boldsymbol{p},s)a^{a}(\boldsymbol{q},t)e^{i\boldsymbol{p}\cdot\boldsymbol{x}}e^{i\boldsymbol{q}\cdot\boldsymbol{x}}\;.\end{aligned} \tag{B.59}$$

The expectation value of the first term (B.56) gives

$$\begin{aligned}\langle a^{\dagger a}(\boldsymbol{p},s)a^a(\boldsymbol{q},t)\rangle &= \left\langle \left(\left[\mathbb{1} + K\overline{K}\right]^{-1} K\overline{K} \right)^{aa} (\boldsymbol{q},t;\boldsymbol{p},s) \right\rangle_{\mathrm{G}} = \\ &= \frac{S(\boldsymbol{q})S^*(\boldsymbol{q}) + R(\boldsymbol{q})}{1 + S(\boldsymbol{q})S^*(\boldsymbol{q}) + R(\boldsymbol{q})} \delta^{aa}\delta_{ts}(2\pi)^3\delta(\boldsymbol{q}-\boldsymbol{p})\;.\end{aligned} \tag{B.60}$$

However, in the chiral limit this contribution vanishes,

$$\sum_s \overline{u}(\boldsymbol{p},s)u(\boldsymbol{p},s) \;=\; 0\;, \tag{B.61}$$

using Eq. (A.31). The second part has to be normal-ordered, yielding

$$\begin{aligned}-\langle b^{\dagger a}(\boldsymbol{q},t)b^a(\boldsymbol{p},s)\rangle &= \left\langle \left(\left[\mathbb{1}+\overline{K}K\right]^{-1}\overline{K}K\right)^{aa}(\boldsymbol{q},t;\boldsymbol{p},s)\right\rangle_{\mathrm{G}} = \\ &= \frac{S^*(\boldsymbol{q})S(\boldsymbol{q})+R(\boldsymbol{q})}{1+S^*(\boldsymbol{q})S(\boldsymbol{q})+R(\boldsymbol{q})}\delta^{aa}\delta_{ts}(2\pi)^3\delta(\boldsymbol{q}-\boldsymbol{p})\;. \end{aligned} \tag{B.62}$$

This contribution vanishes as well,

$$\sum_s \overline{v}(\boldsymbol{p},s)v(\boldsymbol{p},s) \;=\; 0\;, \tag{B.63}$$

due to Eq. (A.32). The expectation values (B.58) and (B.59) give the non-vanishing contributions. We compute

$$\begin{aligned}\langle a^{\dagger a}(\boldsymbol{p},s)b^{\dagger a}(\boldsymbol{q},t)\rangle &= -\left\langle \left(\left[\mathbb{1}+\overline{K}K\right]^{-1}\overline{K}\right)^{aa}(\boldsymbol{q},t;\boldsymbol{p},s)\right\rangle_{\mathrm{G}} = \\ &= -\frac{tS^*(\boldsymbol{q})}{1+S^*(\boldsymbol{q})S(\boldsymbol{q})+R(\boldsymbol{q})}\delta^{aa}\delta_{ts}(2\pi)^3\delta(\boldsymbol{q}+\boldsymbol{p})\;, \end{aligned} \tag{B.64}$$

employ the spinor relation

$$\sum_t t\,\overline{u}(-\boldsymbol{q},t)v(\boldsymbol{q},t) \;=\; 4|\boldsymbol{q}|\;, \tag{B.65}$$

and obtain

$$\left\langle \Phi|\overline{\psi}^a_+(\boldsymbol{x})\psi^a_-(\boldsymbol{x})|\Phi\right\rangle = -N_{\mathrm{C}}2\int đ^3q\,\frac{S^*(\boldsymbol{q})}{1+S^*(\boldsymbol{q})S(\boldsymbol{q})+R(\boldsymbol{q})}\;. \tag{B.66}$$

The last contribution reads

$$\begin{aligned}\langle b^a(\boldsymbol{p},s)a^a(\boldsymbol{q},t)\rangle &= -\left\langle \left(\left[\mathbb{1}+K\overline{K}\right]^{-1}K\right)^{aa}(\boldsymbol{q},t;\boldsymbol{p},s)\right\rangle_{\mathrm{G}} = \\ &= -\frac{tS(\boldsymbol{q})}{1+S^*(\boldsymbol{q})S(\boldsymbol{q})+R(\boldsymbol{q})}\delta^{aa}\delta_{ts}(2\pi)^3\delta(\boldsymbol{q}+\boldsymbol{p})\;. \end{aligned} \tag{B.67}$$

We use

$$\sum t\,\overline{v}(-\boldsymbol{q},t)u(\boldsymbol{q},t) \;=\; 4\,|\boldsymbol{q}|\;, \tag{B.68}$$

and end up with

$$\left\langle \Phi|\overline{\psi}^a_-(\boldsymbol{x})\psi^a_+(\boldsymbol{x})|\Phi\right\rangle = -N_{\mathrm{C}}2\int đ^3q\,\frac{S(\boldsymbol{q})}{1+S^*(\boldsymbol{q})S(\boldsymbol{q})+R(\boldsymbol{q})}\;. \tag{B.69}$$

Collecting the non-vanishing terms (B.66) and (B.69) we arrive at Eq. (3.85).

Appendix C

Energy Densities Revisited

In this Appendix we present the explicit computation of the energy densities, which lead, after variation with respect to the quark kernels, to the gap equations (5.22), (5.23). In Section 1 we guide through the derivation of the transverse gluon energy density, i.e., from Eq. (4.1) to Eq. (4.8). In the second part we compute the Coulomb energy density and finally arrive at expression (5.9). Throughout this Appendix we make extensive use of the spinor solutions derived in Appendix A. We take into account the properties of the quark variational kernels derived in Appendix B.3.

C.1 Transverse Gluon Energy Density

We evaluate the expectation value of $\langle H_{\rm QGC}\rangle$, Eq. (4.1), describing the interaction of quarks with transverse gluons and explicitly given as

$$\langle H_{\rm QGC}\rangle = \langle\Phi| \int d^3x \, \left(-g\psi^{\dagger a}(\boldsymbol{x})\boldsymbol{\alpha}\cdot\boldsymbol{A}^{ab}(\boldsymbol{x})\psi^b(\boldsymbol{x})\right)|\Phi\rangle \; . \tag{C.1}$$

We split the Hamiltonian $H_{\rm QGC}$, Eq. (4.1), into four parts, expand and normal order it in terms of its Fourier modes, Eqs. (1.40)-(1.43), and end up with four different expectation values

$$H_1 \;=\; -g \int d^3x \, \psi^\dagger_+(\boldsymbol{x}) \, \boldsymbol{\alpha}\cdot\boldsymbol{A}(\boldsymbol{x}) \, \psi_+(\boldsymbol{x}) \; , \tag{C.2}$$

$$H_2 \;=\; -g \int d^3x \, \psi^\dagger_-(\boldsymbol{x}) \, \boldsymbol{\alpha}\cdot\boldsymbol{A}(\boldsymbol{x}) \, \psi_-(\boldsymbol{x}) \; , \tag{C.3}$$

$$H_3 \;=\; -g \int d^3x \, \psi^\dagger_+(\boldsymbol{x}) \, \boldsymbol{\alpha}\cdot\boldsymbol{A}(\boldsymbol{x}) \, \psi_-(\boldsymbol{x}) \; , \tag{C.4}$$

$$H_4 \;=\; -g \int d^3x \, \psi^\dagger_-(\boldsymbol{x}) \, \boldsymbol{\alpha}\cdot\boldsymbol{A}(\boldsymbol{x}) \, \psi_+(\boldsymbol{x}) \; . \tag{C.5}$$

Here the color indices are implicitly understood. Starting with the first term, (C.2), and using for the fermion expectation value Eq. (B.11), we arrive at

$$\langle a^{\dagger a}(\boldsymbol{p},s)a^b(\boldsymbol{q},t)A^l_i(\boldsymbol{k})\rangle = \left\langle \left(\left[\mathbb{1} + K\overline{K}\right]^{-1} K\overline{K} \right)^{ba} (\boldsymbol{q},t;\boldsymbol{p},s) \, A^l_i(\boldsymbol{k}) \right\rangle_{\rm G} \; . \tag{C.6}$$

We use the approximation (3.43) and obtain

$$\left\langle \left(\left[\mathbb{1} + K\overline{K} \right]^{-1} K\overline{K} \right) A \right\rangle_{\mathrm{G}} \approx \left\langle \left[\mathbb{1} + K\overline{K} \right]^{-1} \right\rangle_{\mathrm{G}} \left\langle K\overline{K}A \right\rangle_{\mathrm{G}} \ . \tag{C.7}$$

Splitting up the kernel K into its gauge-field independent (K_0) and gauge-field dependent part ($K_1[A]$), Eq. (3.32), gives two non-vanishing contributions in the numerator of expression (C.7)

$$\left\langle K\overline{K}A \right\rangle_{\mathrm{G}} = \left\langle K_0\overline{K}_1 A \right\rangle_{\mathrm{G}} + \left\langle K_1\overline{K}_0 A \right\rangle_{\mathrm{G}} \ . \tag{C.8}$$

The contributions $\langle K_0\overline{K}_0 A\rangle$, $\langle K_1\overline{K}_1 A\rangle$ vanish, since an odd number of gauge fields occur. The non-vanishing contributions (C.8) are of the form

$$\begin{aligned} &\left\langle \left[K_0\overline{K}_1(\boldsymbol{q},t;\boldsymbol{p},s) \right]^{ba} A_i^l(\boldsymbol{k}) \right\rangle_{\mathrm{G}} = \\ &= \left(T^l\right)^{ba} S(\boldsymbol{q}) V^*(-\boldsymbol{q},\boldsymbol{p}) \frac{(2\pi)^3}{2\omega(\boldsymbol{q}-\boldsymbol{p})} \delta(\boldsymbol{q}-\boldsymbol{p}+\boldsymbol{k})\, \Omega_{1,1}(\boldsymbol{q},\boldsymbol{p}) \ , \end{aligned} \tag{C.9}$$

$$\begin{aligned} &\left\langle \left[K_1\overline{K}_0(\boldsymbol{q},t;\boldsymbol{p},s) \right]^{ba} A_i^l(\boldsymbol{k}) \right\rangle_{\mathrm{G}} = \\ &= \left(T^l\right)^{ba} V(\boldsymbol{q},-\boldsymbol{p}) S^*(-\boldsymbol{p}) \frac{(2\pi)^3}{2\omega(\boldsymbol{q}-\boldsymbol{p})} \delta(\boldsymbol{q}-\boldsymbol{p}+\boldsymbol{k})\, \Omega_{1,2}(\boldsymbol{q},\boldsymbol{p}) \ , \end{aligned} \tag{C.10}$$

where we have defined

$$\Omega_{1,1}(\boldsymbol{q},\boldsymbol{p}) \ = \ \sum_{s,t} \frac{1}{4|\boldsymbol{p}||\boldsymbol{q}|}\, t_{ki}(\boldsymbol{q}-\boldsymbol{p}) t \Gamma_k^\dagger(-\boldsymbol{q},t;\boldsymbol{p},s)\, \overline{u}(\boldsymbol{p},s)\gamma_i\, u(\boldsymbol{q},t) \ , \tag{C.11}$$

$$\Omega_{1,2}(\boldsymbol{q},\boldsymbol{p}) \ = \ \sum_{s,t} \frac{1}{4|\boldsymbol{p}||\boldsymbol{q}|}\, t_{ki}(\boldsymbol{q}-\boldsymbol{p}) s \Gamma_k(\boldsymbol{q},t;-\boldsymbol{p},s) \overline{u}(\boldsymbol{p},s)\gamma_i\, u(\boldsymbol{q},t) \ , \tag{C.12}$$

using the abbreviation $\Gamma_k(\boldsymbol{p},s;\boldsymbol{q},t) = \overline{u}(\boldsymbol{p},s)\gamma_k v(\boldsymbol{q},t)$. With the relations

$$t_{ki}(\boldsymbol{q}-\boldsymbol{p})\gamma_k \left[\gamma_0|\boldsymbol{p}| - \boldsymbol{\gamma}\cdot\boldsymbol{p}\right]\gamma_i \ = \ 2|\boldsymbol{p}|\gamma_0 - 2\widehat{(q-p)}_k \widehat{(q-p)}_i \gamma_k p_i \ , \tag{C.13}$$

$$t_{ki}(\boldsymbol{q}-\boldsymbol{p})\gamma_k \left[-\mathbb{1}|\boldsymbol{p}| + \boldsymbol{\alpha}\cdot\boldsymbol{p}\right]\gamma_i \ = \ 2|\boldsymbol{p}|\mathbb{1} - 2\widehat{(q-p)}_k \widehat{(q-p)}_i \alpha_k p_i \ , \tag{C.14}$$

we find

$$\begin{aligned} \Omega_{1,1}(\boldsymbol{q},\boldsymbol{p}) \ &= \ \sum_{s,t} \frac{1}{4|\boldsymbol{p}||\boldsymbol{q}|}\, t_{ki}(\boldsymbol{q}-\boldsymbol{p}) t \Gamma_k^\dagger(-\boldsymbol{q},t;\boldsymbol{p},s)\, \overline{u}(\boldsymbol{p},s)\gamma_i\, u(\boldsymbol{q},t) \ = \\ &= \sum_{s,t} \frac{1}{4|\boldsymbol{p}||\boldsymbol{q}|}\, t_{ki}(\boldsymbol{q}-\boldsymbol{p}) t\, \overline{v}(-\boldsymbol{q},t)\gamma_k u(\boldsymbol{p},s)\, \overline{u}(\boldsymbol{p},s)\gamma_i\, u(\boldsymbol{q},t) \ = \\ &= \sum_{s,t} \frac{1}{4|\boldsymbol{p}||\boldsymbol{q}|}\, t\, \overline{v}(-\boldsymbol{q},t) \left[2|\boldsymbol{p}|\gamma_0 - 2\widehat{(q-p)}_k \widehat{(q-p)}_i \gamma_k p_i \right] u(\boldsymbol{q},t) \ , \end{aligned} \tag{C.15}$$

where after the third equality sign we have used Eq. (A.33) and Eq. (C.13). Next we evaluate the occurring spin sums with use of Eqs. (A.26), (A.27), yielding

$$\sum_t t\, v^\dagger(-\boldsymbol{q},t)u(\boldsymbol{q},t) \;=\; 0\;, \tag{C.16}$$

$$\sum_t t\, v^\dagger(-\boldsymbol{q},t)\alpha_k\widehat{(q-p)}_k u(\boldsymbol{q},t) \;=\; 0\;. \tag{C.17}$$

We arrive at

$$\Omega_{1,1}(\boldsymbol{q},\boldsymbol{p}) \;=\; 0\;, \tag{C.18}$$

so that the expectation value (C.9) vanishes. We turn to the expectation value (C.10) and compute (C.12), yielding

$$\begin{aligned}\Omega_{1,2}(\boldsymbol{q},\boldsymbol{p}) \;&=\; \sum_{s,t}\frac{1}{4|\boldsymbol{p}||\boldsymbol{q}|}\,t_{ki}(\boldsymbol{q}-\boldsymbol{p})s\Gamma_k(\boldsymbol{q},t;-\boldsymbol{p},s)\overline{u}(\boldsymbol{p},s)\gamma_i\,u(\boldsymbol{q},t) = \\ &= \sum_{s,t}\frac{1}{4|\boldsymbol{p}||\boldsymbol{q}|}\,t_{ki}(\boldsymbol{q}-\boldsymbol{p})\overline{u}(\boldsymbol{q},t)\gamma_k s\,v(-\boldsymbol{p},s)\overline{u}(\boldsymbol{p},s)\gamma_i\,u(\boldsymbol{q},t) = \\ &= \sum_{s,t}\frac{1}{4|\boldsymbol{p}||\boldsymbol{q}|}\,\overline{u}(\boldsymbol{q},t)\left[2|\boldsymbol{p}|\mathbb{1}-2\widehat{(q-p)}_k\widehat{(q-p)}_i\alpha_k p_i\right]u(\boldsymbol{q},t)\;.\end{aligned} \tag{C.19}$$

We have

$$\sum_t \overline{u}(\boldsymbol{q},t)u(\boldsymbol{q},t) \;=\; 0\;, \tag{C.20}$$

$$\sum_t \overline{u}(\boldsymbol{q},t)\alpha_k\widehat{(q-p)}_k u(\boldsymbol{q},t) \;=\; 0\;, \tag{C.21}$$

so that the expectation value (C.10) vanishes as well:

$$\Omega_{1,2}(\boldsymbol{q},\boldsymbol{p}) \;=\; 0\;. \tag{C.22}$$

Therefore, the expectation value H_1, Eq. (C.2), is zero. We turn to the second part in the Hamiltonian, H_2, Eq. (C.3). Using Eqs. (1.41), (1.43) and (B.13) yields

$$-\left\langle b^{\dagger b}(\boldsymbol{q},t)b^a(\boldsymbol{p},s)A_i^l(\boldsymbol{k})\right\rangle = -\left\langle\left(\left[\mathbb{1}+\overline{K}K\right]^{-1}\overline{K}K\right)^{ba}(\boldsymbol{q},t;\boldsymbol{p},s)\,A_i^l(\boldsymbol{k})\right\rangle_{\mathrm{G}}\;, \tag{C.23}$$

where normal ordering leads to the additional minus sign. Two contributions survive after taking the gluon expectation value $\langle\ldots\rangle_{\mathrm{G}}$, namely

$$\begin{aligned}&\left\langle\left[\overline{K}_0K_1(\boldsymbol{q},t;\boldsymbol{p},s)A_i^l(\boldsymbol{k})\right]^{ba}\right\rangle_{\mathrm{G}} = \\ &= \left(T^l\right)^{ba}S^*(\boldsymbol{q})V(-\boldsymbol{q},\boldsymbol{p})\frac{(2\pi)^3}{2\omega(-\boldsymbol{q}+\boldsymbol{p})}\delta(-\boldsymbol{q}+\boldsymbol{p}+\boldsymbol{k})\,\Omega_{2,1}(\boldsymbol{q},\boldsymbol{p})\;,\end{aligned} \tag{C.24}$$

$$\begin{aligned}&\left\langle\left[\overline{K}_1K_0(\boldsymbol{q},t;\boldsymbol{p},s)A_i^l(\boldsymbol{k})\right]^{ba}\right\rangle_{\mathrm{G}} = \\ &= \left(T^l\right)^{ba}V(\boldsymbol{q},-\boldsymbol{p})S(-\boldsymbol{p})\frac{(2\pi)^3}{2\omega(-\boldsymbol{q}+\boldsymbol{p})}\delta(-\boldsymbol{q}+\boldsymbol{p}+\boldsymbol{k})\,\Omega_{2,2}(\boldsymbol{q},\boldsymbol{p})\;,\end{aligned} \tag{C.25}$$

where we have abbreviated

$$\Omega_{2,1}(\boldsymbol{q},\boldsymbol{p}) \;=\; \frac{1}{4|\boldsymbol{q}||\boldsymbol{p}|}\,\sum_{s,t} t_{ki}(-\boldsymbol{q}+\boldsymbol{p})\,t\,\Gamma_k(-\boldsymbol{q},t;\boldsymbol{p},s)\,\overline{v}(\boldsymbol{p},s)\gamma_i v(\boldsymbol{q},t)\;, \tag{C.26}$$

$$\Omega_{2,2}(\boldsymbol{q},\boldsymbol{p}) \;=\; \frac{1}{4|\boldsymbol{q}||\boldsymbol{p}|}\,\sum_{s,t} t_{ki}(-\boldsymbol{q}+\boldsymbol{p})\,s\,\Gamma^{\dagger}_k(\boldsymbol{q},t;-\boldsymbol{p},s)\,\overline{v}(\boldsymbol{p},s)\gamma_i v(\boldsymbol{q},t)\;. \tag{C.27}$$

We start with evaluating the term $\Omega_{2,1}(\boldsymbol{q},\boldsymbol{p})$, Eq. (C.26), which reads

$$\begin{aligned}\Omega_{2,1}(\boldsymbol{q},\boldsymbol{p}) \;&=\; \sum_{s,t}\frac{1}{4|\boldsymbol{p}||\boldsymbol{q}|}\,t_{ki}(-\boldsymbol{q}+\boldsymbol{p})\,t\,\Gamma_k(-\boldsymbol{q},t;\boldsymbol{p},s)\,\overline{v}(\boldsymbol{p},s)\gamma_i v(\boldsymbol{q},t) = \\ &= \sum_{s,t}\frac{1}{4|\boldsymbol{p}||\boldsymbol{q}|}\;\sum_{s,t} t_{ki}(-\boldsymbol{q}+\boldsymbol{p})\,t\,\overline{u}(-\boldsymbol{q},t)\gamma_k v(\boldsymbol{p},s)\,\overline{v}(\boldsymbol{p},s)\gamma_i v(\boldsymbol{q},t) = \\ &= \sum_{s,t}\frac{1}{4|\boldsymbol{p}||\boldsymbol{q}|}\;\sum_{t}\, t\;\overline{u}(-\boldsymbol{q},t)\left[2|\boldsymbol{p}|\gamma_0 - 2\widehat{(q-p)}_k\widehat{(q-p)}_i\gamma_k p_i\right] v(\boldsymbol{q},t)\;,\end{aligned} \tag{C.28}$$

where we have used Eqs. (A.35), (C.13). Performing the spin sums

$$\sum_t\, t\,u^{\dagger}(-\boldsymbol{q},t)v(\boldsymbol{q},t) \;=\; 0\;, \tag{C.29}$$

$$\sum_t\, t\,u^{\dagger}(-\boldsymbol{q},t)\widehat{(q-p)}_k\alpha_k v(\boldsymbol{q},t) \;=\; 0\;, \tag{C.30}$$

the contribution $\Omega_{2,1}(\boldsymbol{q},\boldsymbol{p})$, Eq. (C.26), vanishes, and the expectation value (C.24) is zero. We proceed with $\Omega_{2,2}(\boldsymbol{q},\boldsymbol{p})$, Eq. (C.27). We have

$$\begin{aligned}\Omega_{2,2}(\boldsymbol{q},\boldsymbol{p}) \;&=\; \sum_{s,t}\frac{1}{4|\boldsymbol{q}||\boldsymbol{p}|}\,t_{ki}(-\boldsymbol{q}+\boldsymbol{p})\,s\,\Gamma^{\dagger}_k(\boldsymbol{q},t;-\boldsymbol{p},s)\overline{v}(\boldsymbol{p},s)\gamma_i v(\boldsymbol{q},t) = \\ &= \sum_{s,t}\frac{1}{4|\boldsymbol{q}||\boldsymbol{p}|}\,t_{ki}(-\boldsymbol{q}+\boldsymbol{p})\overline{v}(\boldsymbol{q},t)\gamma_k s\,u(-\boldsymbol{p},s)\overline{v}(\boldsymbol{p},s)\gamma_i\,v(\boldsymbol{q},t) = \\ &= \sum_{s,t}\frac{1}{4|\boldsymbol{q}||\boldsymbol{p}|}\,\overline{v}(\boldsymbol{q},t)\left[2|\boldsymbol{p}|\mathbb{1} - 2\widehat{(q-p)}_k\widehat{(q-p)}_i\alpha_k p_i\right] v(\boldsymbol{q},t)\;.\end{aligned} \tag{C.31}$$

Evaluating the spin sums

$$\sum_t\,\overline{v}(\boldsymbol{q},t)v(\boldsymbol{q},t) \;=\; 0\;, \tag{C.32}$$

$$\sum_t\,\overline{v}(\boldsymbol{q},t)\alpha_k\widehat{(q-p)}_k v(\boldsymbol{q},t) \;=\; 0\;, \tag{C.33}$$

we end up with

$$\Omega_{2,2}(\boldsymbol{q},\boldsymbol{p}) \;=\; 0\;. \tag{C.34}$$

Hence, the first two parts of the Hamiltonian, H_1, Eq. (C.2) and H_2, Eq. (C.3), vanish identically. We note that this is due to the Dirac structure of the kernel V coupling the quarks to the transverse gluons, Eq. (3.35), in the quark vacuum wave functional Eq. (3.3). We go ahead with evaluating the expectation values H_3, Eq. (C.4), and H_4, Eq. (C.5). We start with the expectation value of two creation operators and the gauge field H_3, Eq. (C.4), which reads (using Eqs. (1.41), (1.42) and (B.14))

$$\langle a^{\dagger a}(\boldsymbol{p},s)b^{\dagger b}(\boldsymbol{q},t)A_i^l(\boldsymbol{k})\rangle = \left\langle -\left(\left[\mathbb{1}+\overline{K}K\right]^{-1}\overline{K}\right)^{ba}(\boldsymbol{q},t;\boldsymbol{p},s)\,A_i^l(\boldsymbol{k})\right\rangle_{\mathrm{G}} , \tag{C.35}$$

and the only non-vanishing contribution writes

$$\left\langle \overline{K}_1^{ba}(\boldsymbol{q},t;\boldsymbol{p},s)A_i^l(\boldsymbol{k})\right\rangle_{\mathrm{G}} = \left(T^l\right)^{ba} V^*(\boldsymbol{q},\boldsymbol{p})\frac{(2\pi)^3}{2\omega(-\boldsymbol{q}-\boldsymbol{p})}\delta(-\boldsymbol{q}-\boldsymbol{p}+\boldsymbol{k})\Omega_3(\boldsymbol{q},\boldsymbol{p}) , \tag{C.36}$$

so that we find for the energy density

$$\frac{\langle H_3\rangle}{\delta^3(0)} = gC_FN_{\mathrm{C}}\,(2\pi)^3\int đ^3p\,đ^3q\,\frac{V^*(\boldsymbol{q},\boldsymbol{p})}{1+S^*(\boldsymbol{q})S(\boldsymbol{q})+R(\boldsymbol{q})}\Omega_3(\boldsymbol{q},\boldsymbol{p})\,\frac{1}{2\omega(-\boldsymbol{q}-\boldsymbol{p})} . \tag{C.37}$$

Here we have abbreviated

$$\begin{aligned}\Omega_3(\boldsymbol{q},\boldsymbol{p}) &= \sum_{s,t}\frac{1}{4|\boldsymbol{q}||\boldsymbol{p}|}\,t_{ki}(-\boldsymbol{q}-\boldsymbol{p})\Gamma_k^\dagger(\boldsymbol{q},t;\boldsymbol{p},s)\overline{u}(\boldsymbol{p},s)\gamma_i v(\boldsymbol{q},t) = \\ &= \sum_{s,t}\frac{1}{4|\boldsymbol{q}||\boldsymbol{p}|}t_{ki}(-\boldsymbol{q}-\boldsymbol{p})\Gamma_k^\dagger(\boldsymbol{q},t;\boldsymbol{p},s)\Gamma_i(\boldsymbol{p},s;\boldsymbol{q},t) .\end{aligned} \tag{C.38}$$

Before evaluating this term explicitly we derive the corresponding expectation value of two annihilation operators and the gauge field, H_4, Eq. (C.5). With the use of Eq. (B.15) it reads

$$\langle b^a(\boldsymbol{p},s)\,a^b(\boldsymbol{q},t)A_i^l(\boldsymbol{k})\rangle = \left\langle -\left(\left[\mathbb{1}+K\overline{K}\right]^{-1}K\right)^{ba}(\boldsymbol{q},t;\boldsymbol{p},s)\,A_i^l(\boldsymbol{k})\right\rangle_{\mathrm{G}} . \tag{C.39}$$

We evaluate

$$\left\langle K_1^{ba}(\boldsymbol{q},t;\boldsymbol{p},s)A_i^l(\boldsymbol{k})\right\rangle = \left(T^l\right)^{ba}V(\boldsymbol{q},\boldsymbol{p})\frac{1}{2\omega(\boldsymbol{q}+\boldsymbol{p})}(2\pi)^3\delta(\boldsymbol{q}+\boldsymbol{p}+\boldsymbol{k})\Omega_4(\boldsymbol{q},\boldsymbol{p}) , \tag{C.40}$$

and arrive at

$$\frac{\langle H_4\rangle}{\delta^3(0)} = gN_{\mathrm{C}}C_F\,(2\pi)^3\int đ^3p\,đ^3q\,\frac{V(\boldsymbol{q},\boldsymbol{p})}{1+S(\boldsymbol{q})S^*(\boldsymbol{q})+R(\boldsymbol{q})}\Omega_4(\boldsymbol{q},\boldsymbol{p})\,\frac{1}{2\omega(\boldsymbol{q}+\boldsymbol{p})} , \tag{C.41}$$

where we have identified

$$\Omega_4(\boldsymbol{q},\boldsymbol{p}) \;=\; \frac{1}{4|\boldsymbol{q}||\boldsymbol{p}|}\sum_{s,t} t_{ki}(\boldsymbol{q}+\boldsymbol{p})\Gamma_k(\boldsymbol{q},t;\boldsymbol{p},s)\overline{v}(\boldsymbol{p},s)\gamma_i\, u(\boldsymbol{q},t) \;= \\ =\; \frac{1}{4|\boldsymbol{q}||\boldsymbol{p}|}\sum_{s,t} t_{ki}(\boldsymbol{q}+\boldsymbol{p})\Gamma_k(\boldsymbol{q},t;\boldsymbol{p},s)\Gamma_i^{\dagger}(\boldsymbol{p},s;\boldsymbol{q},t)\;. \tag{C.42}$$

The two contributions (C.37) and (C.41) can be combined since the quantities $\Omega_3(\boldsymbol{q},\boldsymbol{p})$, Eq. (C.38), and $\Omega_4(\boldsymbol{q},\boldsymbol{p})$, Eq. (C.42), coincide. Such quantities were already obtained in (B.27), with the difference that now the spin sum has to be evaluated, which leads to an additional factor of 2:

$$\Omega_3(\boldsymbol{q},\boldsymbol{p}) = \Omega_4(\boldsymbol{q},\boldsymbol{p}) \;=\; \frac{1}{4|\boldsymbol{p}||\boldsymbol{q}|}\sum_{s,t} t_{ki}(\boldsymbol{q}+\boldsymbol{p})\Gamma_k^{\dagger}(\boldsymbol{q},t;\boldsymbol{p},s)\overline{u}(\boldsymbol{p},s)\gamma_i v(\boldsymbol{q},t) = \\ = \frac{1}{4|\boldsymbol{p}||\boldsymbol{q}|}4\cdot 2\left[|\boldsymbol{q}||\boldsymbol{p}| - \widehat{(q+p)}_k\widehat{(q+p)}_i q_k p_i\right] = \\ = 2\left[1 - \widehat{(q+p)}_k\widehat{(q+p)}_i\widehat{q}_k\widehat{p}_i\right] \;=\; 2\left[1 - \frac{(p+k)_k(p+k)_i}{(\boldsymbol{p}+\boldsymbol{k})^2}\,\frac{p_k}{|\boldsymbol{p}|}\,\frac{k_i}{|\boldsymbol{k}|}\right]\;. \tag{C.43}$$

We end up with

$$\frac{\langle H_3+H_4\rangle}{\delta^3(0)} = gN_{\mathrm{C}}C_F\,(2\pi)^3\int đ^3p\, đ^3q\,\frac{V^*(\boldsymbol{p},\boldsymbol{q})+V(\boldsymbol{p},\boldsymbol{q})}{1+S^*(\boldsymbol{q})S(\boldsymbol{q})+R(\boldsymbol{q})}\times \\ \times\;\frac{1}{2\omega(\boldsymbol{q}+\boldsymbol{p})}\,2\,\left(1-((\widehat{\boldsymbol{p}+\boldsymbol{q}})\cdot\hat{\boldsymbol{p}})((\widehat{\boldsymbol{p}+\boldsymbol{q}})\cdot\hat{\boldsymbol{q}})\right)\;. \tag{C.44}$$

Sending $\boldsymbol{q}\to-\boldsymbol{q}$ we eventually obtain

$$\frac{\langle H_{\mathrm{QGC}}\rangle}{\delta^3(0)} = \\ = 2\,g\,N_{\mathrm{C}}\,C_F\,(2\pi)^3\int đ^3p\int đ^3q\frac{V^*(\boldsymbol{p},\boldsymbol{q})+V(\boldsymbol{p},\boldsymbol{q})}{1+S^*(\boldsymbol{p})S(\boldsymbol{p})+R(\boldsymbol{p})}D(\boldsymbol{\ell})\left[1+(\hat{\boldsymbol{p}}\cdot\hat{\boldsymbol{\ell}})(\hat{\boldsymbol{q}}\cdot\hat{\boldsymbol{\ell}})\right]\;, \tag{C.45}$$

where we have used Eq. (B.34) and $\boldsymbol{\ell}=\boldsymbol{p}-\boldsymbol{q}$. This result was used in Eq. (4.8).

Hence, the non-vanishing contributions come from the expectation values H_3, Eq. (C.4) and H_4, Eq. (C.5). We again state that this is due to the form of the variational kernel V in Eq. (3.37).

C.2 Coulomb Energy Density

In this section we explicitly compute the Coulomb energy density, leading from the basic definition, Eq. (5.1), to the result, Eq. (5.9). The first step is to expand the quark fields

in terms of its Fourier modes ($V_{\rm C}(\boldsymbol{k}) = g^2 F(\boldsymbol{k})$ with $F = \langle \hat{F} \rangle$, Eq. (1.82))

$$
\begin{aligned}
H_{\rm C} = \frac{g^2}{2} \int d^3x d^3y \int đ^3p \sum_s & \left(\underbrace{a^{\dagger a}(\boldsymbol{p},s) u^\dagger(\boldsymbol{p},s) e^{-i\boldsymbol{p}\cdot\boldsymbol{x}}}_{1} + \underbrace{b^a(\boldsymbol{p},s) v^\dagger(\boldsymbol{p},s) e^{i\boldsymbol{p}\cdot\boldsymbol{x}}}_{2} \right) \left(T^i\right)^{ab} \\
& \int đ^3p' \sum_{s'} \left(\underbrace{a^b(\boldsymbol{p}',s') u(\boldsymbol{p}',s') e^{i\boldsymbol{p}'\cdot\boldsymbol{x}}}_{1} + \underbrace{b^{\dagger b}(\boldsymbol{p}',s') v(\boldsymbol{p}',s') e^{-i\boldsymbol{p}'\cdot\boldsymbol{x}}}_{2} \right) \\
& \int đ^3k\, F(\boldsymbol{k})\, e^{i\boldsymbol{k}\cdot(\boldsymbol{x}-\boldsymbol{y})} \frac{1}{4|\boldsymbol{p}||\boldsymbol{p}'||\boldsymbol{q}||\boldsymbol{q}'|} \\
& \int đ^3q \sum_t \left(\underbrace{a^{\dagger c}(\boldsymbol{q},t) u^\dagger(\boldsymbol{q},t) e^{-i\boldsymbol{q}\cdot\boldsymbol{y}}}_{1} + \underbrace{b^c(\boldsymbol{q},t) v^\dagger(\boldsymbol{q},t) e^{i\boldsymbol{q}\cdot\boldsymbol{y}}}_{2} \right) \left(T^i\right)^{cd} \\
& \int đ^3q' \sum_{t'} \left(\underbrace{a^d(\boldsymbol{q}',t') u(\boldsymbol{q}',t') e^{i\boldsymbol{q}'\cdot\boldsymbol{y}}}_{1} + \underbrace{b^{\dagger d}(\boldsymbol{q}',t') v(\boldsymbol{q}',t') e^{-i\boldsymbol{q}'\cdot\boldsymbol{y}}}_{2} \right) ,
\end{aligned}
\tag{C.46}
$$

where we have labelled the different terms with $i = 1, 2$ and replaced the Coulomb kernel by its expectation value in the Yang-Mills vacuum, Eq. (5.4). Putting all terms together yields

$$
\begin{aligned}
H_C = & \frac{g^2}{2} \int d^3x\, d^3y \int đ^3p\, đ^3p' \sum_{s,s'} \frac{1}{4|\boldsymbol{p}||\boldsymbol{p}'||\boldsymbol{q}||\boldsymbol{q}'|} \\
& (a^{\dagger a}(\boldsymbol{p},s) u^\dagger(\boldsymbol{p},s) \left(T^i\right)^{ab} a^b(\boldsymbol{p}',s') u(\boldsymbol{p}',s') e^{-i\boldsymbol{p}\cdot\boldsymbol{x}} e^{i\boldsymbol{p}'\cdot\boldsymbol{x}} + \\
& b^a(\boldsymbol{p},s) v^\dagger(\boldsymbol{p},s) \left(T^i\right)^{ab} a^b(\boldsymbol{p}',s') u(\boldsymbol{p}',s') e^{i\boldsymbol{p}\cdot\boldsymbol{x}} e^{i\boldsymbol{p}'\cdot\boldsymbol{x}} + \\
& a^{\dagger a}(\boldsymbol{p},s) u^\dagger(\boldsymbol{p},s) \left(T^i\right)^{ab} b^{\dagger a}(\boldsymbol{p}',s') v(\boldsymbol{p}',s') e^{-i\boldsymbol{p}\cdot\boldsymbol{x}} e^{-i\boldsymbol{p}'\cdot\boldsymbol{x}} + \\
& b^a(\boldsymbol{p},s) v^\dagger(\boldsymbol{p},s) \left(T^i\right)^{ab} b^{\dagger b}(\boldsymbol{p}',s') v(\boldsymbol{p}',s') e^{i\boldsymbol{p}\cdot\boldsymbol{x}} e^{-i\boldsymbol{p}'\cdot\boldsymbol{x}}) \\
& \int đ^3k\, F(\boldsymbol{k}) \int đ^3q\, đ^3q' \sum_{t,t'} \\
& (a^{\dagger c}(\boldsymbol{q},t) u^\dagger(\boldsymbol{q},t) \left(T^i\right)^{cd} a^d(\boldsymbol{q}',t') u(\boldsymbol{q}',t') e^{-i\boldsymbol{q}\cdot\boldsymbol{y}} e^{i\boldsymbol{q}'\cdot\boldsymbol{y}} + \\
& b^c(\boldsymbol{q},t) v^\dagger(\boldsymbol{q},t) \left(T^i\right)^{cd} a^d(\boldsymbol{q}',t') u(\boldsymbol{q}',t') e^{i\boldsymbol{q}\cdot\boldsymbol{y}} e^{i\boldsymbol{q}'\cdot\boldsymbol{y}} + \\
& a^{\dagger c}(\boldsymbol{q},t) u^\dagger(\boldsymbol{q},t) \left(T^i\right)^{cd} b^{\dagger c}(\boldsymbol{q}',t') v(\boldsymbol{q}',t') e^{-i\boldsymbol{q}\cdot\boldsymbol{y}} e^{-i\boldsymbol{q}'\cdot\boldsymbol{y}} + \\
& b^c(\boldsymbol{q},t) v^\dagger(\boldsymbol{q},t) \left(T^i\right)^{cd} b^{\dagger d}(\boldsymbol{q}',t') v(\boldsymbol{q}',t') e^{i\boldsymbol{q}\cdot\boldsymbol{y}} e^{-i\boldsymbol{q}'\cdot\boldsymbol{y}}) \, .
\end{aligned}
\tag{C.47}
$$

With the labels defined in (C.46) we mark the expectation values, for instance

$$
\langle H^{1,1,1,1} \rangle \sim \langle a_A^\dagger a_B a_C^\dagger a_D \rangle \, , \tag{C.48}
$$

where the capital letters $A, B, \ldots$ denote all occurring indices. For the energy density only expectation values with a symmetric number of fermions and anti-fermions contribute, namely

$$\langle H^{1-1-1-1}\rangle, \langle H^{2-2-2-2}\rangle, \langle H^{1-1-2-2}\rangle, \langle H^{2-2-1-1}\rangle, \langle H^{2-1-1-2}\rangle, \langle H^{1-2-2-1}\rangle, \\ \langle H^{2-1-2-1}\rangle, \langle H^{1-2-1-2}\rangle \; . \tag{C.49}$$

For all other terms the spin sums vanish. This will be explicitly shown in the following calculation for the terms $\langle H^{1,1,i,j}\rangle$, with $i, j = 1, 2$. All other contributions follow analogously[1].

Expectation Value $\langle H^{1,1,1,1}\rangle$

We start with the expectation value of four fermion operators

$$\begin{aligned}\langle H_{\mathrm{C}}^{1,1,1,1}\rangle =& \frac{g^2}{2}\left(T^i\right)^{ab}\left(T^i\right)^{cd}\int đ^3[p,p']\int đ^3k\int đ^3[q,q']\,F(\boldsymbol{k})\times \\ &\times\sum_{s,s'}\sum_{t,t'}\langle a^{\dagger a}(\boldsymbol{p},s)a^b(\boldsymbol{p}',s')\,a^{\dagger c}(\boldsymbol{q},t)a^d(\boldsymbol{q}',t')\rangle\times \\ &\times u^\dagger(\boldsymbol{p},s)u(\boldsymbol{p}',s)u^\dagger(\boldsymbol{q},t)u(\boldsymbol{q}',t')\times \\ &\times(2\pi)^3\,\delta(\boldsymbol{k}-\boldsymbol{p}+\boldsymbol{p}')\,(2\pi)^3\delta(-\boldsymbol{k}-\boldsymbol{q}+\boldsymbol{q}')\;. \end{aligned}\tag{C.51}$$

Here we have already evaluated the coordinate space integrals leading to the δ-functions in momentum space. The expectation value is computed applying Wick's Theorem, with only one non-vanishing contribution (for more details see the discussion in Section 5.2 after Eq. (5.7))

$$\langle a_A^\dagger\, a_B\, a_C^\dagger\, a_D\rangle = \langle a_A^\dagger\, a_D\rangle\,\langle a_B a_C^\dagger\,\rangle\;. \tag{C.52}$$

The two remaining expectation values in Eq. (C.51) are then computed as (using the expectation value (B.11))

$$\begin{aligned}&\left\langle a^{\dagger a}(\boldsymbol{p},s)a^d(\boldsymbol{q}',t')\right\rangle\left\langle a^b(\boldsymbol{p}',s')a^{\dagger c}(\boldsymbol{q},t)\right\rangle = \\ &\left\langle\left[\frac{K\overline{K}}{\mathbb{1}+K\overline{K}}\right]^{ad}(\boldsymbol{p},s;\boldsymbol{q}',t')\right\rangle_{\mathrm{G}}\left\langle\left[\frac{\mathbb{1}}{\mathbb{1}+K\overline{K}}\right]^{bc}(\boldsymbol{p}',s';\boldsymbol{q},t)\right\rangle_{\mathrm{G}} = \end{aligned}\tag{C.53}$$

$$\begin{aligned}&= \delta^{ad}\delta_{st'}(2\pi)^3\delta(\boldsymbol{p}-\boldsymbol{q}')\,\frac{S^*(\boldsymbol{p})S(\boldsymbol{p})+R(\boldsymbol{p})}{1+S^*(\boldsymbol{q}')S(\boldsymbol{q}')+R(\boldsymbol{q}')}\times \\ &\quad\times\delta^{bc}\delta_{s't}(2\pi)^3\delta(\boldsymbol{p}'-\boldsymbol{q})\,\frac{1}{1+S^*(\boldsymbol{q})S(\boldsymbol{q})+R(\boldsymbol{q})}\;, \end{aligned}\tag{C.54}$$

[1] From the non-vanishing expectation values the spin sums provide two different terms in (5.9) subsumed as $Y(p,q)$, Eq. (5.10) and $Z(p,q)$, Eq. (5.11). In addition, we note that the occurring expectation values always lead to contributions $\langle K\overline{K}\rangle \sim S^2 + R$ in the numerator, except for the terms

$$\langle H^{1-1-2-2}\rangle, \langle H^{2-2-1-1}\rangle, \langle H^{2-1-2-1}\rangle, \langle H^{1-2-1-2}\rangle\;, \tag{C.50}$$

where only the variational function S appears in the numerator.

and the energy reads

$$\begin{aligned}\langle H_{\mathrm{C}}^{1,1,1,1}\rangle \;=\; & \frac{g^2}{2}\int đ^3[p,p']\int đ^3k\int đ^3[q,q']\sum_{s,s'}\sum_{t,t'}\times \\ & \times \left(T^i\right)^{ac}\left(T^i\right)^{ca}\frac{S^*(\boldsymbol{p})S(\boldsymbol{p})+R(\boldsymbol{p})}{1+S^*(\boldsymbol{q}')S(\boldsymbol{q}')+R(\boldsymbol{q}')}\frac{1}{1+S^*(\boldsymbol{q})S(\boldsymbol{q})+R(\boldsymbol{q})}\times \\ & \times \delta_{st'}\delta_{s't}u^\dagger(\boldsymbol{p},s)u(\boldsymbol{p}',s')u^\dagger(\boldsymbol{q},t)u(\boldsymbol{q}',t')\times \\ & \times (2\pi)^3\delta(\boldsymbol{k}-\boldsymbol{p}+\boldsymbol{p}')(2\pi)^3\delta(-\boldsymbol{k}-\boldsymbol{q}+\boldsymbol{q}') \\ & \times (2\pi)^3\delta(\boldsymbol{p}-\boldsymbol{q}')(2\pi)^3\delta(\boldsymbol{p}'-\boldsymbol{q})\;. \end{aligned} \tag{C.55}$$

Now we perform the δ-function integrals: $\boldsymbol{q}'=\boldsymbol{p}$ and $\boldsymbol{q}=\boldsymbol{p}'$. The spin sum is computed as

$$\sum_{s,s'}u^\dagger(\boldsymbol{p},s)u(\boldsymbol{p}',s')u^\dagger(\boldsymbol{p}',s')u(\boldsymbol{p},s) \;=\; 4|\boldsymbol{p}||\boldsymbol{q}|+4\,\boldsymbol{p}\cdot\boldsymbol{p}'\;, \tag{C.56}$$

which has been explicitly derived in Eq. (A.42). The expectation value $\langle H^{1,1,1,1}\rangle$ becomes

$$\begin{aligned}\langle H_{\mathrm{C}}^{1,1,1,1}\rangle \;=\; & \frac{g^2}{2}\left(T^i\right)^{ac}\left(T^i\right)^{ca}\int đ^3[p,p']\int đ^3k\,F(\boldsymbol{k})\times \\ & \times\frac{S^*(\boldsymbol{p})S(\boldsymbol{p})+R(\boldsymbol{p})}{1+S^*(\boldsymbol{p})S(\boldsymbol{p})+R(\boldsymbol{p})}\frac{1}{1+S^*(\boldsymbol{p}')S(\boldsymbol{p}')+R(\boldsymbol{p}')}\times \\ & \times\left(4\,|\boldsymbol{p}'||\boldsymbol{p}|+4\,\boldsymbol{p}'\cdot\boldsymbol{p}\right)(2\pi)^3\delta(\boldsymbol{k}-\boldsymbol{p}+\boldsymbol{p}')(2\pi)^3\delta(-\boldsymbol{k}-\boldsymbol{p}'+\boldsymbol{p})\;. \end{aligned} \tag{C.57}$$

We use $\boldsymbol{k}=\boldsymbol{p}-\boldsymbol{p}'$ and $(T^i)^{ac}(T^i)^{ca}=\mathrm{Tr}[T^iT^i]=C_FN_{\mathrm{C}}$, Eq. (1.7), and we arrive at

$$\begin{aligned}\frac{\langle H_{\mathrm{C}}^{1,1,1,1}\rangle}{\delta^3(0)} \;=\; & \frac{g^2}{2}N_{\mathrm{C}}\,C_F(2\pi)^3\int đ^3[p,p']\,F(\boldsymbol{p}-\boldsymbol{p}')\times \\ & \times\frac{S^*(\boldsymbol{p})S(\boldsymbol{p})+R(\boldsymbol{p})}{1+S^*(\boldsymbol{p})S(\boldsymbol{p})+R(\boldsymbol{p})}\frac{1}{1+S^*(\boldsymbol{p}')S(\boldsymbol{p}')+R(\boldsymbol{p}')}\left(4\,|\boldsymbol{p}||\boldsymbol{p}'|+4\,(\boldsymbol{p}\cdot\boldsymbol{p}')\right)\;. \end{aligned} \tag{C.58}$$

Expectation Value $\langle H^{1,1,2,1}\rangle$

Here an anti-fermion annihilation operator $b^c(\boldsymbol{p},s)$ is sandwiched between the fermion operators. We will observe, that this term vanishes. We begin with writing down the Hamiltonian

$$\begin{aligned}H_{\mathrm{C}}^{1,1,2,1} \;=\; & \frac{g^2}{2}\left(T^i\right)^{ab}\left(T^i\right)^{cd}\int đ^3[p,p']\int đ^3k\int đ^3[q,q']\sum_{s,s'}\sum_{t,t'}\times \\ & \times\; a^{\dagger a}(\boldsymbol{p},s)a^b(\boldsymbol{p}',s')\,b^c(\boldsymbol{q},t)a^d(\boldsymbol{q}',t')u^\dagger(\boldsymbol{p},s)u(\boldsymbol{p}',s')v^\dagger(\boldsymbol{q},t)u(\boldsymbol{q}',t')F(\boldsymbol{k})\times \\ & \times\,(2\pi)^3\,\delta(\boldsymbol{k}-\boldsymbol{p}+\boldsymbol{p}')\,(2\pi)^3\delta(-\boldsymbol{k}+\boldsymbol{q}+\boldsymbol{q}')\;. \end{aligned} \tag{C.59}$$

We apply Wick's Theorem

$$\langle a_A^\dagger\,a_B\,b_C\,a_D\rangle \;=\; \langle a_A^\dagger\,a_D\rangle\,\langle a_B b_C\,\rangle\;, \tag{C.60}$$

and arrive at

$$\begin{aligned}
&\left\langle a^{\dagger a}(\boldsymbol{p},s)a^{d}(\boldsymbol{q}',t')\right\rangle \left\langle a^{b}(\boldsymbol{p}',s')b^{c}(\boldsymbol{q},t)\right\rangle = \\
&= \left\langle \left[\frac{K\overline{K}}{\mathbb{1}+K\overline{K}}\right]^{ad}(\boldsymbol{p},s;\boldsymbol{q}',t')\right\rangle_{\mathrm{G}} \left\langle \left[\frac{K}{\mathbb{1}+\overline{K}K}\right]^{bc}(\boldsymbol{p}',s';\boldsymbol{q},t)\right\rangle_{\mathrm{G}} = \qquad \text{(C.61)}\\
&= \left(\delta^{ad}\delta_{st'}\,(2\pi)^3\delta(\boldsymbol{p}-\boldsymbol{q}')\frac{S^*(\boldsymbol{p})S(\boldsymbol{p})+R(\boldsymbol{p})}{1+S^*(\boldsymbol{q}')S(\boldsymbol{q}')+R(\boldsymbol{q}')}\right)\times \\
&\quad\times\left(\delta^{bc}\delta_{s't}(2\pi)^3\delta(\boldsymbol{p}'+\boldsymbol{q})\frac{S(\boldsymbol{p}')}{1+S^*(\boldsymbol{q})S(\boldsymbol{q})+R(\boldsymbol{q})}\right), \qquad \text{(C.62)}
\end{aligned}$$

so that the energy becomes

$$\begin{aligned}
\langle H_{\mathrm{C}}^{1,1,2,1}\rangle \;=\; &\frac{g^2}{2}\,\left(T^i\right)^{ac}\left(T^i\right)^{ca}\int đ^3[p,p']\int đ^3k\int đ^3[q,q']\sum_{s,s'}\sum_{t,t'}\times \\
&\times\frac{S^*(\boldsymbol{p})S(\boldsymbol{p})+R(\boldsymbol{p})}{1+S^*(\boldsymbol{p})S(\boldsymbol{p})+R(\boldsymbol{p})}\frac{S(\boldsymbol{p}')}{1+S^*(\boldsymbol{q})S(\boldsymbol{q})+R(\boldsymbol{q})}\times \\
&\times\delta_{st'}\delta_{s't}u^\dagger(\boldsymbol{p},s)u(\boldsymbol{p}',s')v^\dagger(\boldsymbol{q},t)u(\boldsymbol{q}',t')\times \\
&\times(2\pi)^3\delta(\boldsymbol{k}-\boldsymbol{p}+\boldsymbol{p}')\,(2\pi)^3\delta(-\boldsymbol{k}+\boldsymbol{q}+\boldsymbol{q}')\,(2\pi)^3\delta(\boldsymbol{p}-\boldsymbol{q}')(2\pi)^3\delta(\boldsymbol{p}'+\boldsymbol{q})\,. \qquad \text{(C.63)}
\end{aligned}$$

We evaluate the δ-functions: $\boldsymbol{q}'=\boldsymbol{p}$ and $\boldsymbol{q}=-\boldsymbol{p}'$. However, the spin sum becomes zero

$$\sum_{s,t}u^\dagger(\boldsymbol{p},s)u(\boldsymbol{p}',t)v^\dagger(-\boldsymbol{p}',t)u(\boldsymbol{p}',s)\;=\;0\,. \qquad \text{(C.64)}$$

This is explicitly worked out using the spinor eigenstates u, Eq. (A.26), v, Eq. (A.27). We start with

$$\begin{aligned}
&\sum_t u(\boldsymbol{p}',t)v^\dagger(-\boldsymbol{p}',t)=\;|\boldsymbol{p}'|\sum_t\begin{pmatrix}\xi(\boldsymbol{p}',t)\\ t\,\xi(\boldsymbol{p}',t)\end{pmatrix}\left(t\xi^\dagger(\boldsymbol{p}',t),-\xi^\dagger(\boldsymbol{p}',t)\right)\;= \\
&=\;|\boldsymbol{p}'|\sum_t\begin{pmatrix}t\xi(\boldsymbol{p}',t)\xi^\dagger(\boldsymbol{p}',t) & -\xi(\boldsymbol{p}',t)\xi^\dagger(\boldsymbol{p}',t)\\ \xi(\boldsymbol{q},t)\xi^\dagger(\boldsymbol{p}',t) & -t\xi(\boldsymbol{p}',t)\xi^\dagger(\boldsymbol{p}',t)\end{pmatrix} \\
&=\begin{pmatrix}\boldsymbol{\sigma}\cdot\boldsymbol{p}' & -|\boldsymbol{p}'|\mathbb{1}\\ |\boldsymbol{p}'|\mathbb{1} & -\boldsymbol{\sigma}\cdot\boldsymbol{p}'\end{pmatrix}, \qquad \text{(C.65)}
\end{aligned}$$

and arrive at

$$\begin{aligned}
&\sum_s u^\dagger(\boldsymbol{p},s)\begin{pmatrix}\boldsymbol{\sigma}\cdot\boldsymbol{p}' & -|\boldsymbol{p}'|\mathbb{1}\\ |\boldsymbol{p}'|\mathbb{1} & -\boldsymbol{\sigma}\cdot\boldsymbol{p}'\end{pmatrix}u(\boldsymbol{p},s) = \\
=&|\boldsymbol{p}|\sum_s\left(\xi^\dagger(\boldsymbol{p},s), s\,\xi^\dagger(\boldsymbol{p},s)\right)\begin{pmatrix}\boldsymbol{\sigma}\cdot\boldsymbol{p}' & -|\boldsymbol{p}'|\mathbb{1}\\ |\boldsymbol{p}'|\mathbb{1} & -\boldsymbol{\sigma}\cdot\boldsymbol{p}'\end{pmatrix}\begin{pmatrix}\xi(\boldsymbol{p},s)\\ s\,\xi(\boldsymbol{p},s)\end{pmatrix} = \\
=&\,|\boldsymbol{p}|\sum_s\xi^\dagger(\boldsymbol{p},s)\,(\boldsymbol{\sigma}\cdot\boldsymbol{p}')\,\xi(\boldsymbol{p},s) - |\boldsymbol{p}|\sum_s s|\boldsymbol{p}'|\,\xi^\dagger(\boldsymbol{p},s)\xi(\boldsymbol{p},s)\\
&+|\boldsymbol{p}|\sum_s s|\boldsymbol{p}'|\,\xi^\dagger(\boldsymbol{p},s)\xi(\boldsymbol{p},s) - \sum_s\xi^\dagger(\boldsymbol{p},s)\boldsymbol{\sigma}\cdot\boldsymbol{p}'\xi(\boldsymbol{p},s) = \\
=&\,0\,.
\end{aligned} \tag{C.66}$$

This term, like all terms with an unsymmetric number of fermions and anti-fermions, vanishes.

Expectation Value $\langle H^{1,1,1,2}\rangle$
Here an anti-fermion creation operator $b^{\dagger d}(\boldsymbol{q}',t')$ occurs instead of the annihilation operator considered above in Eq. (C.59). We start with

$$\begin{aligned}
H_{\mathrm{C}}^{1,1,1,2} =&\ \frac{g^2}{2}\left(T^i\right)^{ab}\left(T^i\right)^{cd}\int đ^3[p,p']\int đ^3k\int đ^3[q,q']\sum_{s,s'}\sum_{t,t'}F(\boldsymbol{k})\times\\
&\times a^{\dagger a}(\boldsymbol{p},s)a^b(\boldsymbol{p}',s')\,a^{\dagger c}(\boldsymbol{q},t)b^{\dagger d}(\boldsymbol{q}',t')\times\\
&\times u^\dagger(\boldsymbol{p},s)u(\boldsymbol{p}',s)u^\dagger(\boldsymbol{q},t)v(\boldsymbol{q}',t')(2\pi)^3\,\delta(\boldsymbol{k}-\boldsymbol{p}+\boldsymbol{p}')\,(2\pi)^3\delta(-\boldsymbol{k}-\boldsymbol{q}-\boldsymbol{q}')\,,
\end{aligned} \tag{C.67}$$

and apply Wick's Theorem, where only one expectation value survives, namely

$$\begin{aligned}
&\left\langle a^{\dagger a}(\boldsymbol{p},s)b^{\dagger d}(\boldsymbol{q}',t')\right\rangle\left\langle a^b(\boldsymbol{p}',s')a^{\dagger c}(\boldsymbol{q},t)\right\rangle = \\
&\left\langle\left[-\frac{\overline{K}}{\mathbb{1}+K\overline{K}}\right]^{ad}(\boldsymbol{p},s;\boldsymbol{q}',t')\right\rangle_{\mathrm{G}}\left\langle\left[\frac{\mathbb{1}}{\mathbb{1}+K\overline{K}}\right]^{bc}(\boldsymbol{p}',s';\boldsymbol{q},t)\right\rangle_{\mathrm{G}} = \qquad \text{(C.68)}\\
&\left(-\delta^{ad}\delta_{st'}\,(2\pi)^3\delta(-\boldsymbol{p}-\boldsymbol{q}')\frac{S^*(\boldsymbol{p})}{1+S^*(\boldsymbol{q}')S(\boldsymbol{q}')+R(\boldsymbol{q}')}\right)\times\\
&\times\left(\delta^{bc}\delta_{s't}(2\pi)^3\delta(\boldsymbol{p}'-\boldsymbol{q})\frac{1}{1+S^*(\boldsymbol{q})S(\boldsymbol{q})+R(\boldsymbol{q})}\right)\,. \qquad \text{(C.69)}
\end{aligned}$$

The energy density reads

$$\begin{aligned}\langle H_{\mathrm{C}}^{1,1,1,2}\rangle \;=\; & \frac{g^2}{2}\,\left(T^i\right)^{ac}\left(T^i\right)^{ca}\int đ^3[p,p']\int đ^3k\int đ^3[q,q']\sum_{s,s'}\sum_{t,t'}\times\\ & \times\frac{S^*(\boldsymbol{p})}{1+S^*(\boldsymbol{q}')S(\boldsymbol{q}')+R(\boldsymbol{q}')}\frac{1}{1+S^*(\boldsymbol{q})S(\boldsymbol{q})+R(\boldsymbol{q})}\times\\ & \times\delta_{st'}\delta_{s't}u^\dagger(\boldsymbol{p},s)u(\boldsymbol{p}',s')u^\dagger(\boldsymbol{q},t)v(\boldsymbol{q}',t')\times\\ & \times(2\pi)^3\delta(\boldsymbol{k}-\boldsymbol{p}+\boldsymbol{p}')\,(2\pi)^3\delta(-\boldsymbol{k}-\boldsymbol{q}-\boldsymbol{q}')\\ & \times(2\pi)^3\delta(-\boldsymbol{p}-\boldsymbol{q}')(2\pi)^3\delta(\boldsymbol{p}'-\boldsymbol{q})\;, \end{aligned}\tag{C.70}$$

however, again the spin sum vanishes

$$\sum_{s,t}u^\dagger(\boldsymbol{p},s)u(\boldsymbol{p}',t)u^\dagger(\boldsymbol{p}',t)v(-\boldsymbol{p}',s)\;=\;0\;,\tag{C.71}$$

and the contribution $H_{\mathrm{C}}^{1,1,1,2}$, Eq. (C.67) gives zero.

Expectation Value $\langle H^{1,1,2,2}\rangle$

Here two creation and two annihilation operators of particles and anti-particles occur and the term has the form

$$\begin{aligned}H_{\mathrm{C}}^{1,1,2,2}=&\frac{g^2}{2}\,\left(T^i\right)^{ab}\left(T^i\right)^{cd}\int đ^3[p,p']\int đ^3k\int đ^3[q,q']\sum_{s,s'}\sum_{t,t'}\times\\ &\times a^{\dagger a}(\boldsymbol{p},s)a^b(\boldsymbol{p}',s')\,b^c(\boldsymbol{q},t)b^{\dagger d}(\boldsymbol{q}',t')\times\\ &\times u^\dagger(\boldsymbol{p},s)u(\boldsymbol{p}',s')v^\dagger(\boldsymbol{q},t)v(\boldsymbol{q}',t')F(\boldsymbol{k})\times\\ &\times(2\pi)^3\,\delta(\boldsymbol{k}-\boldsymbol{p}+\boldsymbol{p}')\,(2\pi)^3\delta(-\boldsymbol{k}+\boldsymbol{q}-\boldsymbol{q}')\;. \end{aligned}\tag{C.72}$$

The expectation value becomes

$$\begin{aligned}&\left\langle a^{\dagger a}(\boldsymbol{p},s)b^{\dagger d}(\boldsymbol{q}',t')\right\rangle\left\langle a^b(\boldsymbol{p}',s')b^c(\boldsymbol{q},t)\right\rangle=\\ &\left\langle\left[-\frac{\overline{K}}{\mathbb{1}+K\overline{K}}\right]^{ad}(\boldsymbol{p},s;\boldsymbol{q}',t')\right\rangle_{\mathrm{G}}\left\langle\left[\frac{K}{\mathbb{1}+\overline{K}K}\right]^{bc}(\boldsymbol{p}',s';\boldsymbol{q},t)\right\rangle_{\mathrm{G}}=\\ &=\left(-\delta^{ad}\delta_{st'}\,(2\pi)^3\delta(-\boldsymbol{p}-\boldsymbol{q}')\frac{s\,S^*(\boldsymbol{p})}{1+S^*(\boldsymbol{q}')S(\boldsymbol{q}')+R(\boldsymbol{q}')}\right)\times\\ &\quad\times\left(\delta^{bc}\delta_{s't}(2\pi)^3\delta(\boldsymbol{p}'+\boldsymbol{q})\frac{s'\,S(\boldsymbol{p}')}{1+S^*(\boldsymbol{q})S(\boldsymbol{q})+R(\boldsymbol{q})}\right)\;. \end{aligned}\tag{C.73}$$

Here the spin factors s and s' occur. We get for the Hamiltonian

$$\begin{aligned}\langle H_{\mathrm{C}}^{1,1,2,2}\rangle = -\frac{g^2}{2}\,\left(T^i\right)^{ac}\left(T^i\right)^{ca}\int đ^3[p,p']\int đ^3k\int đ^3[q,q']\sum_{s,s'}\sum_{t,t'}F(\boldsymbol{k})\times\\ \times\frac{S^*(\boldsymbol{p})}{1+S^*(\boldsymbol{q}')S(\boldsymbol{q}')+R(\boldsymbol{q}')}\frac{S(\boldsymbol{p}')}{1+S^*(\boldsymbol{q})S(\boldsymbol{q})+R(\boldsymbol{q})}\times\\ \times\, s\,s'\,\delta_{st'}\delta_{s't}u^\dagger(\boldsymbol{p},s)u(\boldsymbol{p}',s')v^\dagger(\boldsymbol{q},t)v(\boldsymbol{q}',t')\times\\ \times\,(2\pi)^3\delta(\boldsymbol{k}-\boldsymbol{p}+\boldsymbol{p}')\times\\ \times\,(2\pi)^3\delta(-\boldsymbol{k}+\boldsymbol{q}+\boldsymbol{q}')(2\pi)^3\delta(\boldsymbol{p}+\boldsymbol{q}')(2\pi)^3\delta(-\boldsymbol{p}'-\boldsymbol{q})\;. \qquad \text{(C.74)}\end{aligned}$$

We resolve the Dirac structure. The spin sum gives

$$\sum_{s,t}s\,t\,u^\dagger(\boldsymbol{p},s)u(\boldsymbol{p}',t)v^\dagger(-\boldsymbol{p}',t)v(-\boldsymbol{p},s)\;=\;4pq+4\boldsymbol{p}\cdot\boldsymbol{q}\;. \qquad \text{(C.75)}$$

We get

$$\begin{aligned}\frac{\langle H_{\mathrm{C}}^{1,1,2,2}\rangle}{\delta^3(0)}\;=\;-\frac{g^2}{2}\,C_F N_{\mathrm{C}}(2\pi)^3\int đ^3[p,p']\,F(\boldsymbol{p}-\boldsymbol{p}')\times \qquad \text{(C.76)}\\ \times\frac{S^*(\boldsymbol{p})}{1+S^*(\boldsymbol{p})S(\boldsymbol{p})+R(\boldsymbol{p})}\frac{S(\boldsymbol{p}')}{1+S^*(\boldsymbol{p}')S(\boldsymbol{p}')+R(\boldsymbol{p}')}\times\\ \times\,(4pq+4\boldsymbol{p}\cdot\boldsymbol{q})\;. \qquad \text{(C.77)}\end{aligned}$$

Putting both non-vanishing contributions $H_{\mathrm{C}}^{1,1,1,1}$, Eq. (C.58) and $H_{\mathrm{C}}^{1,1,2,2}$, Eq. (C.76), together, we end up with

$$\begin{aligned}\frac{\langle H_{\mathrm{C}}^{1,1,2,2}\rangle}{\delta^3(0)}\;=\frac{g^2}{2}\,C_F\,N_{\mathrm{C}}\,(2\pi)^3\int đ^3[p,p']\,F(\boldsymbol{p}-\boldsymbol{p}')\,(4\,|\boldsymbol{p}||\boldsymbol{p}'|+4\boldsymbol{p}\cdot\boldsymbol{p}')\\ \Big(\frac{S^*(\boldsymbol{p})S(\boldsymbol{p})+R(\boldsymbol{p})}{1+S^*(\boldsymbol{p})S(\boldsymbol{p})+R(\boldsymbol{p})}\frac{1}{1+S^*(\boldsymbol{p}')S(\boldsymbol{p}')+R(\boldsymbol{p}')}-\\ -\frac{S^*(\boldsymbol{p})}{1+S^*(\boldsymbol{p})S(\boldsymbol{p})+R(\boldsymbol{p})}\frac{S(\boldsymbol{p}')}{1+S^*(\boldsymbol{p}')S(\boldsymbol{p}')+R(\boldsymbol{p}')}\Big)\;. \qquad \text{(C.78)}\end{aligned}$$

All other contributions follow the same working prescription and we end up with the result (5.9).

Appendix D

Solving Integral Equations

The every-day skills of a lattice practitioner are matrix computations, e.g., inverting huge matrices. In continuum QCD we are mostly confronted with solving integral equations. In Chapters 4 and 5 we have derived such integral equations, and in this Appendix we give the prescription how to solve them by iteration.

In Section 1 we show how to discretize a general non-linear integral equation, replacing the integration with an n-point Gaussian quadrature and the solution function with a finite expansion in terms of Chebyshev polynomials. In Section 2 we present the iteration scheme used for solving the integral equation and a so-called relaxation method which enhances the convergence of the iteration process. Finally, we present the organization of the programming code.

D.1 Discretization

The integral equations (5.22), (5.23), which are solved in Chapter 5 have the general structure

$$S(\boldsymbol{k}) = \int đ^3 q \, K(|\boldsymbol{k}-\boldsymbol{q}|, S(\boldsymbol{k}), S(\boldsymbol{q})) \; , \tag{D.1}$$

with $S(\boldsymbol{k})$ the solution function and K the integral kernel. The equation is non-linear, i.e., the integral kernel depends non-linearly on the unknown solution function S. It is a convenient feature of the gap equations (5.22), (5.23), that the integral kernel does *not* depend on the sum or difference of the solution functions, i.e., $S(\boldsymbol{k} \pm \boldsymbol{q})$. Hence, we do not need extrapolation prescriptions for the solution function S. Moreover, the gap equations (5.22), (5.23) are coupled, i.e., the integral kernel K also depends on a second unknown solution function V. However, this does not change the prescription of how to solve such equations and we therefore present for simplicity the strategy only for the uncoupled integral equation (D.1).

As a first step, we go over to spherical coordinates, i.e, $(q_1, q_2, q_3) \to (\varphi, \theta, q)$ and evaluate the φ-integral analytically, so that we have

$$S(k) = \frac{1}{(2\pi)^2} \int_0^\pi d\theta \sin\theta \int_0^\infty q^2 \, K(k, q, \theta, S(k), S(q)) \; , \tag{D.2}$$

where we have assumed that the $S(\boldsymbol{k})$ only depends on the norm of the momentum, i.e., $S(\boldsymbol{k}) = S(|\boldsymbol{k}|)$. In the gap equations (5.22), (5.23) the integral kernel K can be split up in

$$K(k, q, \theta, S(k), S(q)) = V_{\mathrm{C}}(k, q, \theta)\widetilde{K}(S(k), S(q)), \tag{D.3}$$

where $V_{\mathrm{C}}(k, q, \theta)$ is here a general function. In the gap equations (5.22), (5.23) it is identified with the non-Abelian color Coulomb potential V_{C}, Eq. (5.6). The θ-integral can be performed analytically as well, leading to Eqs. (5.30), (5.31). The kernel K, Eq. (D.3), therefore simplifies to

$$\widetilde{V}_{\mathrm{C}}(k, q)\widetilde{K}(S(k), S(q)) \; . \tag{D.4}$$

The remaining integral in Eq. (D.2), which has to be evaluated numerically, is the q-integral. The integrand is evaluated at a finite set of integration points using an n-point Gaussian quadrature formula, as implemented in Ref. [131]. The q-integral in Eq. (D.2) is approximated by a weighted sum of these values,

$$S(k) = \frac{1}{(2\pi)^2} \sum_{j=1}^{N} w_j \, q_j^2 \, \left(\widetilde{V}_{\mathrm{C}}(k, q_j)\widetilde{K}(S(k), S(q_j)) \right) \; , \tag{D.5}$$

with q_j the N nodes of the orthogonal polynomial and w_j the weight factors. A commonly used set of abscissas and weights is the so-called Gauss-Legendre quadrature and is implemented in a standard routine of Ref. [131]. It returns the abscissas q_j and weights w_j of the Gauss-Legendre quadrature formula for given lower and upper limit a and b of the integral and given order N. For the q-integration in the interval $[0, \infty]$, Eq. (D.2), we use a logarithmic transformation

$$y = \log q \qquad \Longrightarrow \qquad dq = e^y dy \; , \tag{D.6}$$

so that

$$\begin{aligned} \int_0^\infty dq \, q^2 \, \widetilde{V}_{\mathrm{C}}(k, q)\widetilde{K}(S(k), S(q)) \approx \int_{\Lambda_{\mathrm{IR}}}^{\Lambda_{\mathrm{UV}}} dq \, q^2 \, \widetilde{V}_{\mathrm{C}}(k, q)\widetilde{K}(S(k), S(q)) = \\ = \int_{\log[\Lambda_{\mathrm{IR}}]}^{\log[\Lambda_{\mathrm{UV}}]} dy e^{3y} \, \widetilde{V}_{\mathrm{C}}(k, e^y)\widetilde{K}(S(k), S(e^y)) \, , \end{aligned} \tag{D.7}$$

with Λ_{IR} and Λ_{UV} the limits of the integration range. It is important to take care of possible singularities in the integrand. (Note, however, that the singularity must be integrable.) Since in our case the quantity $\widetilde{V}_{\mathrm{C}}$, Eq. (5.26), is indeed divergent at $k = p$, we split the range of integration in Eq. (D.7) into

$$\int_{\log[\Lambda_{\mathrm{IR}}]}^{\log[\Lambda_{\mathrm{UV}}]} = \int_{\log[\Lambda_{\mathrm{IR}}]}^{\log[k-\varepsilon]} + \int_{\log[k-\varepsilon]}^{\log[k]} + \int_{\log[k]}^{\log[k+\varepsilon]} + \int_{\log[k+\varepsilon]}^{\log[\Lambda_{\mathrm{UV}}]} \; , \tag{D.8}$$

where ε is a small region around the singularity. In this procedure many nodes appear in the vicinity of the singularity, which makes a high precision evaluation of the integral in this region possible. We emphasize that in any evaluation of the integral equation, Eq. (D.2), we have to enlarge the interval of integration $[\Lambda_{\rm IR}, \Lambda_{\rm UV}]$ and correspondingly the number of nodes q_j and check that the solution function $S(k)$ does not change by this extension.

Up to now we have taken the loop momentum q on a finite grid of Gauss-Legendre nodes q_j. Next we replace the external momentum k by a finite set of Chebyshev nodes k_i, given by

$$k_i = \cos\left(\frac{\pi(i-\frac{1}{2})}{l}\right), \qquad i = 1, 2, \ldots, l\ . \tag{D.9}$$

The Chebyshev polynomial $T_l(x)$, defined in the interval $[-1, 1]$ by the formula

$$T_l(k) = \cos(l \arccos k)\ , \tag{D.10}$$

has l zeroes. The function $S(q)$ in Eq. (D.5), which has to be evaluated in every iteration step, is then replaced by a finite expansion in Chebyshev polynomials

$$S(q_j) \approx \sum_{l=1}^{L} c_l T_{l-1}(q_j) - \frac{1}{2}c_1, \qquad j = 1, \ldots, N\ , \tag{D.11}$$

where $T_l(q_j)$ are the Chebyshev polynomials (D.10) evaluated at the Gauss-Legendre nodes q_j and c_l the expansion coefficients. These coefficients c_l are calculated from the function $S(q)$, which has to be evaluated. In Eq. (D.11) we have used that $T_0(q_i) = 1$. The standard routines implementing the Chebyshev formula (D.11) are found in Ref. [131].

We emphasize that the sets of quadrature sample points q_j and interpolation points k_i are, in general, disjoint. Formula (D.11) is exact for $q_j = k_i$, where k_i is equal to all of the l zeros of $T_l(k_i)$. Among all approximating polynomials of the same degree the Chebyshev approximation (D.11) has the advantage that it has the smallest maximum difference from the function to be approximated [131].

We are interested in $S(k)$ over a wide range of magnitudes, i.e., for small momenta ($\Lambda_{\rm IR} \approx 10^{-6}$) and large momenta ($\Lambda_{\rm UV} \approx 10^{6}$). We therefore make use of a logarithmic transformation according to Eq. (D.6) for the Chebyshev abscissas k_i, i.e.,

$$x_i = \log k_i \qquad \Longrightarrow \qquad k_i = e^{x_i}\ . \tag{D.12}$$

Now we face a problem. The analytic results, Eq. (5.45), show that the solution function $S(k)$ will have a power law behavior for large momenta, i.e., $S(k \to \infty) \sim 1/k^5$. However, on a logarithmic scale power laws turn into exponentials, i.e., $1/k^5 \to 1/(e^{5x})$. The Chebyshev basis functions T_l, Eq. (D.10), are polynomials and therefore not suited to approximate exponential behavior. To overcome this problem, we use a logarithmic scale for the function values as well:

$$\ln S(e^x) = \widetilde{S}(e^x)\ . \tag{D.13}$$

For this double-logarithmic solution function $\widetilde{S}$ power laws become linear functions and therefore the transformed function $\widetilde{S}$ is well approximated by Chebyshev polynomials T_l, Eq. (D.10). In total, the resulting dicrete analogue to Eq. (D.1) takes the form (using the definitions (D.4), (D.5), (D.6), (D.9), (D.11), (D.12))

$$S(e^{x_i}) = \frac{1}{(2\pi)^2} \sum_{j=1}^{N} \omega_j e^{3y_j}\, \widetilde{V}_{\mathrm{C}}(e^{x_i}, e^{y_j}) \widetilde{K}\Big(S(e^{x_i}), \underbrace{\exp\big(\sum_{k=1}^{L} c_l T_{l-1}(y_j) - \frac{1}{2}c_1\big)}_{S(e^{y_j})} \Big) \,. \tag{D.14}$$

D.2 Iterative Procedure

The iteration scheme for the non-linear integral equation of the form (D.5) is given by

$$S^{(n)}(k) = \int dq\, q^2\, \widetilde{V}_{\mathrm{C}}(k,q) \widetilde{K}(S^{(n-1)}(k), S^{(n-1)}(q)) \,, \tag{D.15}$$

with $n-1$ and n denoting the iteration steps. Here we have used, for convenience, continuous momenta k, q. For the convergence of the iteration process we use the criterion

$$\Big| \frac{S^{(n)}(k) - S^{(n-1)}(k)}{S^{(n-1)}(k)} \Big| < \varepsilon_{\mathrm{TOL}} \qquad \forall k \,, \tag{D.16}$$

with $\varepsilon_{\mathrm{TOL}}$ being the tolerance of the procedure, which usually takes values of about $\varepsilon_{\mathrm{TOL}} \approx 10^{-5} - 10^{-8}$. With a given start function $S^{(0)}(k)$ the program iterates the equation (D.15) until a self-consistent solution $S(k)$ via the convergence criterion (D.16) is achieved. Due to the asymptotic analysis of the integral equation the general shape of the solution $S(k)$ is known, so that a reasonably good start function $S^{(0)}(k)$ can be chosen. Here a comment is in order: If the procedure converges, then the function $S^{(n)}(k)$ is a solution function. However, from the non-convergence we cannot conclude that there does not exist a solution $S^{(n)}(k)$.

In order to improve the convergence of the procedure we use a so-called relaxation method, which is for the n-th iteration step given by

$$r S^{(n)}(k) + [1-r] S^{(n-1)}(k) \to S^{(n)}(k) \,. \tag{D.17}$$

This relaxation prescription mixes the function values $S^{(n-1)}(k)$ evaluated in the $(n-1)$-th iteration step with the new values $S^{(n)}(k)$ evaluated in the n-th iteration step. The so-called adiabatic factor r lies between 0 and 1 and is varied depending on how much the solution function changes from one step to the next. Typical values lie between $r = 0.2 - 0.5$. For all integral equations evaluating $S(k)$ such a relaxation prescription was used, however, to solve the dynamical mass equation (5.42) no such relaxation was necessary.

Let us, in the end, collect all the steps to derive a self-consistent solution $S(k)$ to the equation (D.1) and present the corresponding algorithm:

1. Initialize Chebyshev nodes k_i, Eq. (D.9), on the logarithmic scale $[\log \Lambda_{\mathrm{IR}}, \log \Lambda_{\mathrm{UV}}]$
2. Start the iteration process:
   a) For the first iteration choose a starting function on the logarithmic scale $S^{(n=0)}(k)$, Eq. (D.13). We conveniently choose a constant starting function $S^{(n=0)}(k)$ or a function which shows the correct asymptotic behavior. For the scalar variational function S solving the equation (5.22) it reads

$$S^{(n=0)}(k) = \frac{1}{1+k^5} \, . \tag{D.18}$$

   b) For all other iterations transform the solution function $S^{(n\neq 0)}(k)$ on a logarithmic scale, Eq. (D.13).
3. Compute Chebyshev coefficients c_l, Eq. (D.11), of the function $S^{(n)}(k)$
4. Start the integral routine using the Gaussian quadrature formula, Eq. (D.5):

```
Define integration range
Initialize Gauss-Legendre routine
Loop i:for the external momenta k
Loop j: for the integration momenta q
Evaluate Chebyshev fits
Compute integrands on logarithmic scale
Evaluate integral
End Loop j
End Loop i
```

5. Compute the new solution function $S^{(n+1)}$ according to Eq. (D.14) and use the relaxation formula, Eq. (D.17) if necessary
6. Compute the tolerance according to Eq. (D.16). If the error is smaller than the tolerance $\varepsilon_{\mathrm{TOL}}$ then a self-consistent solution is achieved and the iteration process stops. Otherwise perform the next iteration step by returning to 2.b).

Appendix E

Schrödinger Potential

The Schrödinger equation (6.45) with the potential $U(r)$ given in Eq. (6.46) has to be solved for the lowest eigenvalue $\Omega_0(L)$ in order to extract the static quark potential $V_{\mathrm{W}}(L)$, Eq. 6.49. The potential $U(r)$, Eq. (6.46), is essentially the transverse gluon propagator in coordinate space contracted with the two temporal paths of the Wilson loop. Below we derive this quantity for transverse gluon propagators in arbitrary dimensions d.

In Section 1 we parameterize the temporal trapezoidal Wilson loop. In Section 2 we derive the expression for the contracted gluon propagator. In Section 3 we discuss the asymptotic behavior of the contracted gluon propagator with the Gribov solution as input. In Section 4 we present the numerical procedure to evaluate the lowest eigenvalue of a general one-dimensional Schrödinger equation, known as the shooting method.

E.1 Parameterization of the Wilson Loop

We want to derive the quantity (6.28), explicitly given as

$$D\left((x(s)-x(t))^2\right) = \dot{x}_\mu^-(s) D_{\mu\nu}\left(x(s),x(t)\right)\dot{x}_\nu^+(t)\;. \tag{E.1}$$

We consider a planar temporal Wilson loop in the $0-1$ plane in d dimensions. The paths along the Wilson lines are parameterized as (see Fig. 6.1)

$$\boldsymbol{x}^-(s) = \begin{pmatrix} s \\ 0 \\ 0 \\ \vdots \\ 0 \end{pmatrix}, \qquad \boldsymbol{x}^+(t) = \begin{pmatrix} t \\ L \\ 0 \\ \vdots \\ 0 \end{pmatrix}, \tag{E.2}$$

with $s \in [S,0]$ and $t \in [0,T]$. The unit vector along the Wilson line is

$$\dot{\boldsymbol{x}}^\pm(s) \equiv \hat{\boldsymbol{e}} = \begin{pmatrix} 1 \\ 0 \\ 0 \\ \vdots \\ 0 \end{pmatrix}. \tag{E.3}$$

The difference vector $\boldsymbol{x} = \boldsymbol{x}^-(s) - \boldsymbol{x}^+(t)$ is given as

$$\boldsymbol{x}(s-t) \;=\; \boldsymbol{x}(r) \;=\; L \begin{pmatrix} \frac{s-t}{L} \\ -1 \\ 0 \\ \vdots \\ 0 \end{pmatrix} \;=\; L \begin{pmatrix} r \\ -1 \\ 0 \\ \vdots \\ 0 \end{pmatrix} \;, \tag{E.4}$$

where we have used the dimensionless variables r and R defined in Eq. (6.39). After normalization the difference vector becomes

$$\hat{\boldsymbol{x}}(r) \;=\; \frac{1}{\sqrt{1+r^2}} \begin{pmatrix} r \\ -1 \\ 0 \\ \vdots \\ 0 \end{pmatrix} \;. \tag{E.5}$$

We compute for later use

$$(\hat{\boldsymbol{x}} \cdot \hat{\boldsymbol{e}})^2 = \frac{r^2}{1+r^2} \;. \tag{E.6}$$

E.2 Gluon Propagator Contracted with the Temporal Paths

We compute the Fourier-transform of the translationally invariant transverse gluon propagator

$$D_{\mu\nu}(x) = \int \frac{d^dk}{(2\pi)^d} \left[\delta_{\mu\nu} - \hat{k}_\mu \hat{k}_\nu\right] \bar{D}(k^2)\, e^{i\boldsymbol{k}\cdot\boldsymbol{x}} \;, \tag{E.7}$$

where $\hat{k}_\mu = k_\mu/\sqrt{k^2}$ and $\bar{D}\,(k^2)$ is a function of $\boldsymbol{k}^2 = k_\mu k_\mu$ only. We can split the gluon propagator into two parts

$$D_{\mu\nu}(x) \;=\; \delta_{\mu\nu} I(x) - I_{\mu\nu}(x) \;, \tag{E.8}$$

with

$$I_{\mu\nu}(x) \;=\; \int \frac{d^dk}{(2\pi)^d}\, \bar{D}(\boldsymbol{k}^2)\, e^{i\boldsymbol{k}\cdot\boldsymbol{x}}\, \hat{k}_\mu \hat{k}_\nu \;. \tag{E.9}$$

In Eq. (E.8) we have defined $I(x) = I_{\mu\mu}(x)$. The quantity $I_{\mu\nu}(x)$ can be decomposed in two Lorentz tensor components, namely

$$I_{\mu\nu}(x) = \delta_{\mu\nu} f_1(x) + \hat{x}_\mu \hat{x}_\nu f_2(x) \;, \tag{E.10}$$

where we have introduced the two unknown functions $f_1(x), f_2(x)$ and $\hat{x}_\mu = x_\mu/\sqrt{x^2}$. Multiplying equation (E.10) with $\delta_{\mu\nu}$ yields

$$I(x) \;=\; d\, f_1(x) + f_2(x)\;, \tag{E.11}$$

and multiplying equation (E.10) with $\hat{x}_\mu \hat{x}_\nu$ gives

$$\hat{x}_\mu\, I_{\mu\nu}\, \hat{x}_\nu \;=\; f_1(x) + f_2(x)\;. \tag{E.12}$$

We abbreviate $\overline{I}(x) \equiv \hat{x}_\mu\, I_{\mu\nu}(x) \hat{x}_\nu$. We have gained two equations (E.11) and (E.12), from which we can derive the unknown functions $f_1(x), f_2(x)$ as

$$f_1(x)\,(d-1) \;=\; I(x) - \hat{x}_\mu\, I_{\mu\nu}(x)\, \hat{x}_\nu\;, \tag{E.13}$$
$$f_2(x)\,(d-1) \;=\; d\,\hat{x}_\mu\, I_{\mu\nu}(x)\, \hat{x}_\nu - I(x)\;. \tag{E.14}$$

Plugging in the functions $f_1(x), f_2(x)$ in Eq. (E.10) we get for the quantity $I_{\mu\nu}$ the relation

$$I_{\mu\nu}(x) \;=\; \frac{1}{d-1}\left(\delta_{\mu\nu}\left[I(x) - \overline{I}(x)\right] + \hat{x}_\mu \hat{x}_\nu \left[d\overline{I}(x) - I(x)\right]\right)\;, \tag{E.15}$$

and for the transverse gluon propagator, Eq. (E.8),

$$D_{\mu\nu}(x) = \frac{1}{d-1}\delta_{\mu\nu}\left[(d-2)I(x) + \overline{I}(x)\right] - \hat{x}_\mu\hat{x}_\nu[d\overline{I}(x) - I(x)]\;. \tag{E.16}$$

The propagator $D_{\mu\nu}(x)$ is explicitly given as

$$\begin{aligned} D_{\mu\nu}(x) \;=& \frac{1}{d-1}\delta_{\mu\nu}\int \frac{d^dk}{(2\pi)^d}\, e^{i\boldsymbol{k}\cdot\boldsymbol{x}}\, \bar{D}(\boldsymbol{k}^2)\, \left[(d-2) + \left(\hat{\boldsymbol{x}}\cdot\hat{\boldsymbol{k}}\right)^2\right] - \\ & - \frac{1}{d-1}\hat{x}_\mu\hat{x}_\nu \int \frac{d^dk}{(2\pi)^d}\, e^{i\boldsymbol{k}\cdot\boldsymbol{x}}\, \bar{D}(\boldsymbol{k}^2)\, \left[d\left(\hat{\boldsymbol{x}}\cdot\hat{\boldsymbol{k}}\right)^2 - 1\right]\;. \end{aligned} \tag{E.17}$$

We proceed with evaluating Eq. (E.1) and arrive at

$$D(x^2) \;=\; \hat{e}_\mu\, D_{\mu\nu}(x)\, \hat{e}_\nu \;=\; \hat{e}_\mu\, \delta_{\mu\nu}\, \hat{e}_\nu I(x) - \hat{e}_\mu\, \hat{x}_\mu\, \hat{x}_\nu\, \hat{e}_\nu\, I_{\mu\nu}(x)\;, \tag{E.18}$$

We use $\hat{e}_\mu\, \delta_{\mu\nu}\, \hat{e}_\nu = 1$ and Eq. (E.6) so that we end up with

$$\begin{aligned} D(x^2) \;=& \frac{1}{d-1}\int \frac{d^dk}{(2\pi)^d}\, e^{i\boldsymbol{k}\cdot\boldsymbol{x}}\, D(\boldsymbol{k}^2)\, \left[(d-2) + \left(\hat{\boldsymbol{x}}\cdot\hat{\boldsymbol{k}}\right)^2\right] - \\ & - \frac{1}{d-1}\frac{r^2}{1+r^2}\int \frac{d^dk}{(2\pi)^d}\, e^{i\boldsymbol{k}\cdot\boldsymbol{x}}\, D(\boldsymbol{k}^2)\, \left[d\left(\hat{\boldsymbol{x}}\cdot\hat{\boldsymbol{k}}\right)^2 - 1\right]\;. \end{aligned} \tag{E.19}$$

E.3 Spherical Integrals

For the integrals

$$\begin{Bmatrix} I(x^2) \\ \bar{I}(x^2) \end{Bmatrix} = \int \frac{d^dk}{(2\pi)^d} e^{i\boldsymbol{k}\cdot\boldsymbol{x}} \overline{D}(\boldsymbol{k}^2) \begin{Bmatrix} 1 \\ (\hat{\boldsymbol{k}}\cdot\hat{\boldsymbol{x}})^2 \end{Bmatrix} \tag{E.20}$$

the angular integrals are worked out in the standard fashion using spherical coordinates in k-space and putting the d-axis of k-space parallel to $\hat{x}$. We define the angle between the vectors $\hat{\boldsymbol{x}}, \hat{\boldsymbol{k}}$ as

$$\hat{\boldsymbol{x}}\cdot\hat{\boldsymbol{k}} = \cos\theta \; . \tag{E.21}$$

The integrals over the first $d-2$ angles are trivial yielding the volume of the unit sphere S_{d-2} in $d-1$ dimensions

$$\int_{S_{d-2}} = \frac{(d-1)\pi^{\frac{d-1}{2}}}{\Gamma\left(\frac{d+1}{2}\right)} \; . \tag{E.22}$$

The integrals over the last angle yield (with substituting $z = \cos\theta$)

$$\int_{-1}^{1} dz\, e^{izkx} = 2\,\frac{\sin kx}{kx} \; , \tag{E.23}$$

$$\int_{-1}^{1} dz\, z^2 e^{izkx} = 2\,\frac{\sin kx}{kx} + \frac{4}{k^2x^2}\left(\cos kx - \frac{\sin kx}{kx}\right) \; . \tag{E.24}$$

Inserting these results into (E.20) we obtain

$$I(x) = 2\,C_d \int_0^\infty dk k^{d-1}\, \bar{D}(k^2)\, \frac{\sin kx}{kx} \tag{E.25}$$

$$\overline{I}(x) = 2\,C_d \int_0^\infty dk k^{d-1}\, \bar{D}(k^2) \left[\frac{\sin kx}{kx} + \frac{2}{k^2x^2}\left(\cos kx - \frac{\sin kx}{kx}\right)\right] \; , \tag{E.26}$$

where

$$C_d = \frac{(d-1)\pi^{\frac{d-1}{2}}}{(2\pi)^d \Gamma\left(\frac{d+1}{2}\right)} \; . \tag{E.27}$$

E.4 Contracted Gluon Propagator in $d = 3$ Dimensions

For $d = 3$ dimensions we get in Eq. (E.19)

$$\begin{aligned} D(x^2) = \frac{1}{2}\int \frac{d^3k}{(2\pi)^3} e^{i\boldsymbol{k}\cdot\boldsymbol{x}}\, \bar{D}(k^2) \left[1 + \left(\hat{\boldsymbol{x}}\cdot\hat{\boldsymbol{k}}\right)^2\right] - \\ - \frac{1}{2}\frac{r^2}{1+r^2}\int \frac{d^3k}{(2\pi)^3} e^{i\boldsymbol{k}\cdot\boldsymbol{x}}\, \bar{D}(k^2) \left[3\left(\hat{\boldsymbol{x}}\cdot\hat{\boldsymbol{k}}\right)^2 - 1\right] \; . \end{aligned} \tag{E.28}$$

We use (E.23), (E.24) for the integrals

$$\int dz e^{ikxz} \left[1 + z^2\right] = \frac{4\sin kx}{kx} + \frac{4\cos kx}{k^2x^2} - \frac{4\sin kx}{k^3x^3} , \tag{E.29}$$

$$\int dz e^{ikxz} \left[3z^2 - 1\right] = \frac{4\sin kx}{kx} + \frac{12\cos kx}{k^2x^2} - \frac{12\sin kx}{k^3x^3} , \tag{E.30}$$

and end up with

$$D(x^2) = \frac{1}{2}\frac{1}{2}\frac{1}{(2\pi)^2}\int dk\, k^2\omega^{-1}(k)\left(\left[\frac{4\sin kx}{kx} + \frac{4\cos kx}{k^2x^2} - \frac{4\sin kx}{k^3x^3}\right] - \frac{r^2}{1+r^2}\left[\frac{4\sin kx}{kx} + \frac{12\cos kx}{k^2x^2} - \frac{12\sin kx}{k^3x^3}\right]\right) . \tag{E.31}$$

The factor 2π comes from the integration of $S_2 = \int d\Omega_2$. The additional factor $1/2$ comes from the definition of the propagator

$$D(k) = \frac{1}{2}\,\omega^{-1}(k) . \tag{E.32}$$

We use for the (inverse) propagator the Gribov parametrization, Eq. (1.95), given as

$$\omega^{-1}(k) = \sqrt{\frac{k^2}{k^4 + M_{\rm G}^4}} , \tag{E.33}$$

with $M_{\rm G}$ the Gribov mass scale, Eq. (1.96). We now analyze the asymptotic regions of the integral (E.31). In the IR region the inverse gluon propagator behaves as

$$\omega^{-1}(k) \sim k . \tag{E.34}$$

The leading term in the integrand of Eq. (E.31) goes as $1/k^3$, so that

$$D(x^2) \sim \int dk\, k^2\, k\, \frac{\sin kx}{k^3x^3} , \tag{E.35}$$

which is a convergent expression, since $\int_0^{\Lambda_{\rm UV}} dk \sin kx = \frac{1}{x}\left(1 - \cos[\Lambda_{\rm UV}x]\right)$, where $\Lambda_{\rm UV}$ is some ultraviolet cutoff. In the UV region the inverse gluon propagator behaves as

$$\omega^{-1}(k) \sim \frac{1}{k} . \tag{E.36}$$

Here the leading contribution in Eq. (E.31) comes from the term proportional to $1/k$ and we have

$$D(x^2) \sim \int k^2\, \frac{1}{k}\, \frac{\sin kx}{kx} . \tag{E.37}$$

However, the integral

$$\int_{\Lambda_{\rm IR}}^{\Lambda_{\rm UV}} \sin kx , \tag{E.38}$$

is not defined for $\Lambda_{\rm UV} \to \infty$. To overcome this problem we introduce for the gluon propagator the UV anomalous dimension, see Eq. (6.51). We point out, that this procedure only alters the UV-region, but the IR-modes are not affected.

E.5 Shooting Method

To evaluate the lowest eigenvalue $\Omega_0(L)$ in the Schrödinger equation (6.45) for the potentials $U(r)$, Eq. (6.46), shown in Fig. (6.5) we make use of the shooting method as implemented in Ref. [131]. The shooting method can be applied to essentially any quantum well problem in one dimension with a symmetric potential. The basic idea is to convert the boundary-value problem into an initial-value problem and then to solve the latter. We review the method for a general problem of the form

$$\frac{d^2\varphi}{dx^2} + (2E - V(x))\varphi = 0 \; . \tag{E.39}$$

The solution must satisfy $\varphi(x = \pm\infty) \to 0$. This is implemented for some finite distance L, so that $\varphi(-L) = \varphi(L) = 0$. The distance L should be well away from the classical turning point x_{turn}, where $V(x_{\text{turn}}) = E$. We note that it is necessary to increase this distance L to get the higher energy levels accurately. Next we rewrite the Schrödinger equation (E.39) as

$$\frac{d\varphi}{dx} = \varphi', \qquad \frac{d\varphi'}{dx} = (V(x) - 2E)\varphi \; . \tag{E.40}$$

We choose the initial conditions

$$\varphi(-L) = 0, \qquad \varphi'(-L) = 1 \; . \tag{E.41}$$

The iterative process to solve the Schrödinger equation (E.39) alters the initial guess for $\varphi'(-L)$ until the solution on the right-hand side of the interval $\varphi(L) = 0$ is found. The procedure is repeated with different values for the energy eigenvalue E. Note that it is convenient to "shoot" to an intermediate point, mostly chosen to be a classical turning point x_{turn} and then to match continuity conditions at this point. The lowest eigenvalue is found by requiring that $\varphi'(0) = 0$. For the odd parity solution we have to demand the wave function φ to vanish at the origin $\varphi(0) = 0$.

Bibliography

[1] M. H. Seymour, "Quantum chromodynamics," arXiv:hep-ph/0505192 [hep-ph].

[2] P. Skands, "Introduction to QCD," arXiv:1207.2389 [hep-ph].

[3] A. S. Kronfeld, "Twenty-first Century Lattice Gauge Theory: Results from the QCD Lagrangian," arXiv:1203.1204 [hep-lat]. invited review for Annual Reviews of Nuclear and Particle Science (2012)/ 21 pp., 4 tables, 6 figures.

[4] C. D. Roberts, "Strong QCD and Dyson-Schwinger Equations," arXiv:1203.5341 [nucl-th].

[5] A. P. Szczepaniak and E. S. Swanson, "Coulomb gauge QCD, confinement, and the constituent representation," *Phys.Rev.* **D65** (2002) 025012, arXiv:hep-ph/0107078 [hep-ph].

[6] A. P. Szczepaniak, "Confinement and gluon propagator in Coulomb gauge QCD," *Phys.Rev.* **D69** (2004) 074031, arXiv:hep-ph/0306030 [hep-ph].

[7] C. Feuchter and H. Reinhardt, "Variational solution of the Yang-Mills Schrodinger equation in Coulomb gauge," *Phys.Rev.* **D70** (2004) 105021, arXiv:hep-th/0408236 [hep-th].

[8] D. Epple, H. Reinhardt, and W. Schleifenbaum, "Confining Solution of the Dyson-Schwinger Equations in Coulomb Gauge," *Phys.Rev.* **D75** (2007) 045011, arXiv:hep-th/0612241 [hep-th].

[9] C. Itzykson and J.-B. Zuber, *Quantum Field Theory*. McGraw-Hill, 1980.

[10] A. Duncan, H. Meyer-Ortmanns, and R. Roskies, "VARIATIONAL METHODS IN SUPERSYMMETRIC LATTICE FIELD THEORY. 1. THE VACUUM SECTOR," *Phys.Rev.* **D36** (1987) 3788.

[11] R. Floreanini and R. Jackiw, "FUNCTIONAL REPRESENTATION FOR FERMIONIC QUANTUM FIELDS," *Phys.Rev.* **D37** (1988) 2206.

[12] J. Greensite, H. Matevosyan, S. Olejnik, M. Quandt, H. Reinhardt, *et al.*, "Testing Proposals for the Yang-Mills Vacuum Wavefunctional by Measurement of the Vacuum," *Phys.Rev.* **D83** (2011) 114509, arXiv:1102.3941 [hep-lat].

[13] L. Faddeev and V. Popov, "Feynman Diagrams for the Yang-Mills Field," *Phys.Lett.* **B25** (1967) 29–30.

[14] D. R. Campagnari, *The Yang-Mills Vacuum Wave Functional in Coulomb Gauge*. PhD thesis, Universität Tübingen, 2010.

[15] C. Feuchter, *The Yang-Mills Vacuum Wave Functional in Coulomb Gauge*. PhD thesis, Universität Tübingen, 2006.

[16] N. Christ and T. Lee, "Operator Ordering and Feynman Rules in Gauge Theories," *Phys.Rev.* **D22** (1980) 939.

[17] N. Vandersickel and D. Zwanziger, "The Gribov problem and QCD dynamics," arXiv:1202.1491 [hep-th].

[18] R. A. Bertlmann, *Anomalies in Quantum Field Theory*. Oxford University Press Inc., New York, 1996.

[19] V. Gribov, "Quantization of Nonabelian Gauge Theories," *Nucl.Phys.* **B139** (1978) 1.

[20] P. van Baal, "More (thoughts on) Gribov copies," *Nucl.Phys.* **B369** (1992) 259–275.

[21] H. Reinhardt and C. Feuchter, "On the Yang-Mills wave functional in Coulomb gauge," *Phys.Rev.* **D71** (2005) 105002, arXiv:hep-th/0408237 [hep-th].

[22] D. Zwanziger, "Fundamental modular region, Boltzmann factor, and area law in lattice theory," *Nucl.Phys.Proc.Suppl.* **34** (1994) 198–200.

[23] J. Greensite, S. Olejnik, and D. Zwanziger, "Coulomb energy, remnant symmetry, and the phases of nonAbelian gauge theories," *Phys.Rev.* **D69** (2004) 074506, arXiv:hep-lat/0401003 [hep-lat].

[24] J. Greensite, S. Olejnik, and D. Zwanziger, "Center vortices and the Gribov horizon," *JHEP* **0505** (2005) 070, arXiv:hep-lat/0407032 [hep-lat].

[25] D. R. Campagnari and H. Reinhardt, "Non-Gaussian wave functionals in Coulomb gauge Yang–Mills theory," *Phys.Rev.* **D82** (2010) 105021, arXiv:1009.4599 [hep-th].

[26] W. Schleifenbaum, M. Leder, and H. Reinhardt, "Infrared analysis of propagators and vertices of Yang-Mills theory in Landau and Coulomb gauge," *Phys.Rev.* **D73** (2006) 125019, arXiv:hep-th/0605115 [hep-th].

[27] D. Epple, H. Reinhardt, W. Schleifenbaum, and A. Szczepaniak, "Subcritical solution of the Yang-Mills Schroedinger equation in the Coulomb gauge," *Phys.Rev.* **D77** (2008) 085007, arXiv:0712.3694 [hep-th].

[28] D. Zwanziger, "No confinement without Coulomb confinement," *Phys.Rev.Lett.* **90** (2003) 102001, arXiv:hep-lat/0209105 [hep-lat].

[29] K. Langfeld and L. Moyaerts, "Propagators in Coulomb gauge from SU(2) lattice gauge theory," *Phys.Rev.* **D70** (2004) 074507, arXiv:hep-lat/0406024 [hep-lat].

[30] A. Voigt, E.-M. Ilgenfritz, M. Muller-Preussker, and A. Sternbeck, "The Effective Coulomb potential in SU(3) lattice Yang-Mills theory," *Phys.Rev.* **D78** (2008) 014501, arXiv:0803.2307 [hep-lat].

[31] Y. Nakagawa, A. Nakamura, T. Saito, and H. Toki, "Scaling study of the gluon propagator in Coulomb gauge QCD on isotropic and anisotropic lattices," *Phys.Rev.* **D83** (2011) 114503, arXiv:1105.6185 [hep-lat].

[32] J. Greensite and S. Olejnik, "Coulomb energy, vortices, and confinement," *Phys.Rev.* **D67** (2003) 094503, arXiv:hep-lat/0302018 [hep-lat].

[33] A. Cucchieri and D. Zwanziger, "Renormalization group calculation of color Coulomb potential," *Phys.Rev.* **D65** (2001) 014002, arXiv:hep-th/0008248 [hep-th].

[34] P. Watson and H. Reinhardt, "Leading order infrared quantum chromodynamics in Coulomb gauge," *Phys.Rev.* **D85** (2012) 025014, arXiv:1111.6078 [hep-ph]. 27 pages, 11 figures.

[35] L. Giusti, M. Paciello, C. Parrinello, S. Petrarca, and B. Taglienti, "Problems on lattice gauge fixing," *Int.J.Mod.Phys.* **A16** (2001) 3487–3534, arXiv:hep-lat/0104012 [hep-lat].

[36] G. Burgio, M. Quandt, and H. Reinhardt, "Coulomb gauge gluon propagator and the Gribov formula," *Phys.Rev.Lett.* **102** (2009) 032002, arXiv:0807.3291 [hep-lat].

[37] H. Reinhardt, D. Epple, and W. Schleifenbaum, "Hamiltonian approach to Yang-Mills theory in Coulomb gauge," *AIP Conf.Proc.* **892** (2007) 93–99, arXiv:hep-th/0610324 [hep-th].

[38] H. Reinhardt, W. Schleifenbaum, D. Epple, and C. Feuchter, "Hamiltonian approach to Coulomb gauge Yang-Mills Theory," *PoS* **LAT2007** (2007) 326, arXiv:0710.0316 [hep-th].

[39] H. Reinhardt, D. Campagnari, D. Epple, M. Leder, M. Pak, *et al.*, "Coulomb gauge Yang-Mills theory in the Hamiltonian approach," arXiv:0807.4635 [hep-th].

[40] H. Reinhardt and D. Epple, "The 't Hooft loop in the Hamiltonian approach to Yang-Mills theory in Coulomb gauge," *Phys.Rev.* **D76** (2007) 065015, arXiv:0706.0175 [hep-th].

[41] H. Reinhardt, "The Dielectric function of the QCD vacuum," *Phys.Rev.Lett.* **101** (2008) 061602, arXiv:0803.0504 [hep-th].

[42] D. R. Campagnari and H. Reinhardt, "Topological susceptibility in SU(2) Yang-Mills theory in the Hamiltonian approach in Coulomb gauge," *Phys.Rev.* **D78** (2008) 085001, arXiv:0807.1195 [hep-th].

[43] H. Reinhardt, D. Campagnari, and A. Szczepaniak, "Variational approach to Yang-Mills theory at finite temperatures," *Phys.Rev.* **D84** (2011) 045006, arXiv:1107.3389 [hep-th]. 11 pages, 6 eps figures.

[44] H. Reinhardt, D. R. Campagnari, J. Heffner, and M. Pak, "Hamilton Approach to QCD in Coulomb Gauge: Finite Temperatures and Chiral Symmetry Breaking," *PoS* **QCD-TNT-II** (2011) 038, arXiv:1111.7141 [hep-th]. 12 pages, 14 figures, talk given by H. Reinhardt at the 'II International Workshop on QCD Green's Functions, Confinement and Phenomenology', Trento, Italy, September 2011. Submitted to the proceedings.

[45] C. Feuchter and H. Reinhardt, "The Yang-Mills vacuum in Coulomb gauge in D=2+1 dimensions," *Phys.Rev.* **D77** (2008) 085023, arXiv:0711.2452 [hep-th].

[46] H. Reinhardt and W. Schleifenbaum, "Hamiltonian Approach to 1+1 dimensional Yang-Mills theory in Coulomb gauge," *Annals Phys.* **324** (2009) 735–786, arXiv:0809.1764 [hep-th].

[47] P. Watson and H. Reinhardt, "Propagator Dyson-Schwinger Equations of Coulomb Gauge Yang-Mills Theory Within the First Order Formalism," *Phys.Rev.* **D75** (2007) 045021, arXiv:hep-th/0612114 [hep-th].

[48] P. Watson and H. Reinhardt, "Slavnov-Taylor identities in Coulomb gauge Yang-Mills theory," *Eur.Phys.J.* **C65** (2010) 567–585, arXiv:0812.1989 [hep-th].

[49] H. Reinhardt and P. Watson, "Resolving temporal Gribov copies in Coulomb gauge Yang-Mills theory," *Phys.Rev.* **D79** (2009) 045013, arXiv:0808.2436 [hep-th].

[50] C. Popovici, P. Watson, and H. Reinhardt, "Three-quark confinement potential from the Faddeev equation," *Phys.Rev.* **D83** (2011) 025013, arXiv:1010.4254 [hep-ph].

[51] C. Popovici, P. Watson, and H. Reinhardt, "Coulomb gauge confinement in the heavy quark limit," *Phys.Rev.* **D81** (2010) 105011, arXiv:1003.3863 [hep-th].

[52] C. Popovici, P. Watson, and H. Reinhardt, "Higher order heavy quark Green's functions in Coulomb gauge," *Phys.Rev.* **D83** (2011) 125018, arXiv:1103.4786 [hep-ph].

[53] P. Watson and H. Reinhardt, "Perturbation Theory of Coulomb Gauge Yang-Mills Theory Within the First Order Formalism," *Phys.Rev.* **D76** (2007) 125016, arXiv:0709.0140 [hep-th].

[54] P. Watson and H. Reinhardt, "Two-point functions of Coulomb gauge Yang-Mills theory," *Phys.Rev.* **D77** (2008) 025030, arXiv:0709.3963 [hep-th].

[55] C. Popovici, P. Watson, and H. Reinhardt, "Quarks in Coulomb gauge perturbation theory," *Phys.Rev.* **D79** (2009) 045006, arXiv:0810.4887 [hep-th].

[56] C. Wetterich, "Exact evolution equation for the effective potential," *Phys.Lett.* **B301** (1993) 90–94.

[57] M. Leder, *Renormalization Group Flows of Hamiltonian QCD in Coulomb Gauge*. PhD thesis, Universität Tübingen, 2011.

[58] M. Leder, J. M. Pawlowski, H. Reinhardt, and A. Weber, "Hamiltonian Flow in Coulomb Gauge Yang-Mills Theory," *Phys.Rev.* **D83** (2011) 025010, arXiv:1006.5710 [hep-th].

[59] M. Leder, H. Reinhardt, A. Weber, and J. M. Pawlowski, "Color Coulomb Potential in Yang-Mills Theory from Hamiltonian Flows," arXiv:1105.0800 [hep-th].

[60] M. Quandt, G. Burgio, S. Chimchinda, and H. Reinhardt, "Coulomb gauge ghost propagator and the Coulomb potential," *PoS* **CONFINEMENT8** (2008) 066, arXiv:0812.3842 [hep-th].

[61] M. Quandt, H. Reinhardt, and G. Burgio, "The role of center vortices in Gribov's confinement scenario," *Phys.Rev.* **D81** (2010) 065016, arXiv:1001.3699 [hep-lat].

[62] G. Burgio, M. Quandt, M. Schrock, and H. Reinhardt, "Propagators in lattice Coulomb gauge and confinement mechanisms," *PoS* **LATTICE2010** (2010) 272, arXiv:1011.0560 [hep-lat].

[63] **Particle Data Group** Collaboration, K. Nakamura *et al.*, "Review of particle physics," *J.Phys.G* **G37** (2010) 075021.

[64] M. Pennington, "QCD down under: Building bridges," *Nucl.Phys.Proc.Suppl.* **141** (2005) 1–8, arXiv:hep-ph/0409156 [hep-ph].

[65] A. Bashir, L. Chang, I. C. Cloet, B. El-Bennich, Y.-x. Liu, *et al.*, "Collective perspective on advances in Dyson-Schwinger Equation QCD," arXiv:1201.3366 [nucl-th].

[66] M. Pennington and D. Walsh, "Masses from nothing: A Nonperturbative study of QED in three-dimensions," *Phys.Lett.* **B253** (1991) 246–251.

[67] K. Fujikawa, "Path Integral Measure for Gauge Invariant Fermion Theories," *Phys.Rev.Lett.* **42** (1979) 1195.

[68] R. Williams, C. Fischer, and M. Pennington, "Anti-q q condensate for light quarks beyond the chiral limit," *Phys.Lett.* **B645** (2007) 167–172, arXiv:hep-ph/0612061 [hep-ph].

[69] T. Banks and A. Casher, "Chiral Symmetry Breaking in Confining Theories," *Nucl.Phys.* **B169** (1980) 103.

[70] T. DeGrand, Z. Liu, and S. Schaefer, "Quark condensate in two-flavor QCD," *Phys.Rev.* **D74** (2006) 094504, arXiv:hep-lat/0608019 [hep-lat].

[71] **JLQCD collaboration** Collaboration, H. Fukaya *et al.*, "Determination of the chiral condensate from 2+1-flavor lattice QCD," *Phys.Rev.Lett.* **104** (2010) 122002, arXiv:0911.5555 [hep-lat].

[72] **JLQCD and TWQCD collaborations** Collaboration, H. Fukaya *et al.*, "Determination of the chiral condensate from QCD Dirac spectrum on the lattice," *Phys.Rev.* **D83** (2011) 074501, arXiv:1012.4052 [hep-lat].

[73] C. Vafa and E. Witten, "Restrictions on Symmetry Breaking in Vector-Like Gauge Theories," *Nucl.Phys.* **B234** (1984) 173.

[74] M. Pak and H. Reinhardt, "Chiral symmetry breaking in Hamiltonian QCD in Coulomb gauge," *Phys.Lett.* **B707** (2012) 566–569, arXiv:1107.5263 [hep-ph].

[75] P. S. Peter Ring, *The Nuclear Many-Body Problem*. Springer-Verlag New York, 1980.

[76] Y. Nambu and G. Jona-Lasinio, "Dynamical Model of Elementary Particles Based on an Analogy with Superconductivity. 1.," *Phys.Rev.* **122** (1961) 345–358.

[77] Y. Nambu and G. Jona-Lasinio, "DYNAMICAL MODEL OF ELEMENTARY PARTICLES BASED ON AN ANALOGY WITH SUPERCONDUCTIVITY. II," *Phys.Rev.* **124** (1961) 246–254.

[78] J. R. Finger and J. E. Mandula, "Quark Pair Condensation and Chiral Symmetry Breaking in QCD," *Nucl.Phys.* **B199** (1982) 168.

[79] A. Le Yaouanc, L. Oliver, O. Pene, and J. Raynal, "Spontaneous Breaking of Chiral Symmetry for Confining Potentials," *Phys.Rev.* **D29** (1984) 1233.

[80] S. L. Adler and A. Davis, "Chiral Symmetry Breaking in Coulomb Gauge QCD," *Nucl.Phys.* **B244** (1984) 469.

[81] H. Reinhardt, Lecture Notes, unpublished.

[82] C. Gattringer and C. B. Lang, "Quantum chromodynamics on the lattice," *Lect.Notes Phys.* **788** (2010) 1–211.

[83] C. S. Fischer, "Infrared properties of QCD from Dyson-Schwinger equations," *J.Phys.G* **G32** (2006) R253–R291, arXiv:hep-ph/0605173 [hep-ph].

[84] C. Fischer, P. Watson, and W. Cassing, "Probing unquenching effects in the gluon polarisation in light mesons," *Phys.Rev.* **D72** (2005) 094025, arXiv:hep-ph/0509213 [hep-ph].

[85] A. Kizilersu and M. Pennington, "Building the Full Fermion-Photon Vertex of QED by Imposing Multiplicative Renormalizability of the Schwinger-Dyson Equations for the Fermion and Photon Propagators," *Phys.Rev.* **D79** (2009) 125020, arXiv:0904.3483 [hep-th].

[86] P. Watson, W. Cassing, and P. Tandy, "Bethe-Salpeter meson masses beyond ladder approximation," *Few Body Syst.* **35** (2004) 129–153, arXiv:hep-ph/0406340 [hep-ph].

[87] C. D. Roberts and A. G. Williams, "Dyson-Schwinger equations and their application to hadronic physics," *Prog.Part.Nucl.Phys.* **33** (1994) 477–575, arXiv:hep-ph/9403224 [hep-ph].

[88] G. Burgio, M. Schrock, H. Reinhardt, and M. Quandt, "Running mass, effective energy and confinement: the lattice quark propagator in Coulomb gauge," arXiv:1204.0716 [hep-lat].

[89] R. Alkofer and P. Amundsen, "CHIRAL SYMMETRY BREAKING IN AN INSTANTANEOUS APPROXIMATION TO COULOMB GAUGE QCD," *Nucl.Phys.* **B306** (1988) 305–342.

[90] K. Langfeld, "Chiral symmetry breaking in strongly coupled QED?," arXiv:hep-ph/9508307 [hep-ph].

[91] D. Atkinson, J. C. Bloch, V. Gusynin, M. Pennington, and M. Reenders, "Strong QED with weak gauge dependence: Critical coupling and anomalous dimension," *Phys.Lett.* **B329** (1994) 117–122.

[92] A. Bashir and M. Pennington, "Gauge independent chiral symmetry breaking in quenched QED," *Phys.Rev.* **D50** (1994) 7679–7689, arXiv:hep-ph/9407350 [hep-ph].

[93] J. C. Bloch and M. Pennington, "Numerical cancellation of photon quadratic divergence in the study of the Schwinger-Dyson equations in strong coupling QED," *Mod.Phys.Lett.* **A10** (1995) 1225–1233, arXiv:hep-ph/9501411 [hep-ph].

[94] D. Curtis, M. Pennington, and D. Walsh, "Dynamical mass generation in QED in three-dimensions and the 1/N expansion," *Phys.Lett.* **B295** (1992) 313–319.

[95] D. Curtis and M. Pennington, "Generating fermion mass in quenched QED in four-dimensions," *Phys.Rev.* **D46** (1992) 2663–2667.

[96] A. Trzupek, "Chiral Symmetry Breaking in the Pairing Model of QCD with the Coulomb Potential," *Acta Phys.Polon.* **B20** (1989) 93.

[97] A. Swift, "SELFCONSISTENT MODEL OF CONFINEMENT," *Phys.Rev.* **D38** (1988) 668–691.

[98] A. P. Szczepaniak and E. S. Swanson, "On the Dirac structure of confinement," *Phys.Rev.* **D55** (1997) 3987–3993, arXiv:hep-ph/9611310 [hep-ph].

[99] A. Davis and A. Matheson, "CHIRAL SYMMETRY BREAKING AT FINITE TEMPERATURE IN COULOMB GAUGE QCD," *Nucl.Phys.* **B246** (1984) 203.

[100] A. Kocic, "CHIRAL SYMMETRY RESTORATION AT FINITE DENSITIES IN COULOMB GAUGE QCD," *Phys.Rev.* **D33** (1986) 1785.

[101] J. Govaerts, J. Mandula, and J. Weyers, "A MODEL FOR CHIRAL SYMMETRY BREAKING IN QCD," *Nucl.Phys.* **B237** (1984) 59.

[102] R. Alkofer, M. Kloker, A. Krassnigg, and R. Wagenbrunn, "Aspects of the confinement mechanism in Coulomb-gauge QCD," *Phys.Rev.Lett.* **96** (2006) 022001, arXiv:hep-ph/0510028 [hep-ph].

[103] S. L. Adler, "GAP EQUATION MODELS FOR CHIRAL SYMMETRY BREAKING," *Prog.Theor.Phys.Suppl.* **86** (1986) 12. Dedicated to Prof. Y. Nambu on his 65th birthday.

[104] F. J. Llanes-Estrada, S. R. Cotanch, A. P. Szczepaniak, and E. S. Swanson, "Hyperfine meson splittings: Chiral symmetry versus transverse gluon exchange," *Phys.Rev.* **C70** (2004) 035202, arXiv:hep-ph/0402253 [hep-ph].

[105] A. P. Szczepaniak and P. Krupinski, "Spontaneous chiral symmetry breaking in the linked cluster expansion," *Phys.Rev.* **D66** (2002) 096006, arXiv:hep-ph/0204249 [hep-ph].

[106] M. Pak and H. Reinhardt, "The Wilson loop from a Dyson equation," *Phys.Rev.* **D80** (2009) 125022, arXiv:0910.2916 [hep-th].

[107] H. Reinhardt, G. Burgio, D. Campagnari, D. Epple, C. Feuchter, *et al.*, "Hamiltonian approach to Yang-Mills theory in Coulomb gauge," *PoS* **QCD-TNT09** (2009) 038, arXiv:0911.0613 [hep-th].

[108] J. Greensite, "The Confinement problem in lattice gauge theory," *Prog.Part.Nucl.Phys.* **51** (2003) 1, arXiv:hep-lat/0301023 [hep-lat].

[109] B. Bolder, T. Struckmann, G. S. Bali, N. Eicker, T. Lippert, *et al.*, "A High precision study of the Q anti-Q potential from Wilson loops in the regime of string breaking," *Phys.Rev.* **D63** (2001) 074504, arXiv:hep-lat/0005018 [hep-lat].

[110] G. Bali, T. Dussel, T. Lippert, H. Neff, Z. Prkacin, *et al.*, "String breaking with dynamical Wilson fermions," *Nucl.Phys.Proc.Suppl.* **140** (2005) 609–611, arXiv:hep-lat/0409137 [hep-lat].

[111] **SESAM Collaboration** Collaboration, G. S. Bali, H. Neff, T. Duessel, T. Lippert, and K. Schilling, "Observation of string breaking in QCD," *Phys.Rev.* **D71** (2005) 114513, arXiv:hep-lat/0505012 [hep-lat].

[112] H. J. Rothe, *Lattice Gauge Theories: An Introduction*. World Scientific Publishing Co.Ptd.Ltd., 2005.

[113] G. S. Bali, "QCD forces and heavy quark bound states," *Phys.Rept.* **343** (2001) 1–136, arXiv:hep-ph/0001312 [hep-ph]. massive review article (145 pages), v2: typos corrected, minor errors removed, potentially misleading statements reformulated, references updated Report-no: HUB-EP-99/67.

[114] R. Alkofer and J. Greensite, "Quark Confinement: The Hard Problem of Hadron Physics," *J.Phys.G* **G34** (2007) S3, arXiv:hep-ph/0610365 [hep-ph].

[115] H. Reinhardt, M. Quandt, and G. Burgio, "On the temporal Wilson loop in the Hamiltonian approach in Coulomb gauge," *Phys.Rev.* **D85** (2012) 025001, arXiv:1110.2927 [hep-th]. 24 pages, 4 eps-figures; new version matches published one.

[116] J. Erickson, G. Semenoff, R. Szabo, and K. Zarembo, "Static potential in N=4 supersymmetric Yang-Mills theory," *Phys.Rev.* **D61** (2000) 105006, arXiv:hep-th/9911088 [hep-th].

[117] J. Erickson, G. Semenoff, and K. Zarembo, "Wilson loops in N=4 supersymmetric Yang-Mills theory," *Nucl.Phys.* **B582** (2000) 155–175, arXiv:hep-th/0003055 [hep-th].

[118] A. Zayakin and J. Rafelski, "The Confinement Property in SU(3) Gauge Theory," *Phys.Rev.* **D80** (2009) 034024, arXiv:0905.2317 [hep-ph].

[119] J. B. Kogut, "An Introduction to Lattice Gauge Theory and Spin Systems," *Rev.Mod.Phys.* **51** (1979) 659.

[120] J. Greensite, "CALCULATION OF THE YANG-MILLS VACUUM WAVE FUNCTIONAL," *Nucl.Phys.* **B158** (1979) 469.

[121] P. Olesen, "CONFINEMENT AND RANDOM FIELDS," *Nucl.Phys.* **B200** (1982) 381.

[122] C. Piccioni, "Casimir scaling in SU(2) lattice gauge theory," *Phys.Rev.* **D73** (2006) 114509, arXiv:hep-lat/0503021 [hep-lat].

[123] S. Deldar, "Static SU(3) potentials for sources in various representations," *Phys.Rev.* **D62** (2000) 034509, arXiv:hep-lat/9911008 [hep-lat].

[124] G. S. Bali, "Casimir scaling of SU(3) static potentials," *Phys.Rev.* **D62** (2000) 114503, arXiv:hep-lat/0006022 [hep-lat].

[125] L. Del Debbio, M. Faber, J. Greensite, and S. Olejnik, "Casimir scaling versus Abelian dominance in QCD string formation," *Phys.Rev.* **D53** (1996) 5891–5897, arXiv:hep-lat/9510028 [hep-lat].

[126] D. Zwanziger, "Renormalization in the Coulomb gauge and order parameter for confinement in QCD," *Nucl.Phys.* **B518** (1998) 237–272.

[127] W. Schleifenbaum, "Nonperturbative aspects of Yang-Mills theory," arXiv:0809.1339 [hep-th].

[128] **HPQCD Collaboration, UKQCD Collaboration, MILC Collaboration, Fermilab Lattice Collaboration** Collaboration, C. Davies *et al.*, "High precision lattice QCD confronts experiment," *Phys.Rev.Lett.* **92** (2004) 022001, arXiv:hep-lat/0304004 [hep-lat].

[129] K. Lichtenegger, *Aspects of Confinement in a Functional Approach to Coulomb Gauge QCD*. PhD thesis, Karl-Franzens Universität Graz, 2010.

[130] K. Novoselov, A. Geim, S. Morozov, D. Jiang, M. Katsnelson, *et al.*, "Two-dimensional gas of massless Dirac fermions in graphene," *Nature* **438** (2005) 197, arXiv:cond-mat/0509330 [cond-mat.mes-hall].

[131] W. Press, B. Flannery, S. A. Teukolsky, and W. Vetterling, *Numerical Recipes in Fortran 77: The Art of Scientific Computing*. Cambridge University Press, 1992.